This dissertation was submitted to fulfill the requirements for the degree of Doctor in Medical Sciences.

Promoter

Prof. Natzi Sakalihasan, University of Liège, Faculty of Medicine

President of the examining committee

Prof. Jean-Olivier Defraigne, University of Liège, Faculty of Medicine

Local examining committee

Prof. Vincenzo D'Orio, University of Liège, Faculty of Medicine
Prof. Roland Hustinx, University of Liège, Faculty of Medicine
Prof. Patrizio Lancellotti, University of Liège, Faculty of Medicine

External examining committee

Prof. Eric Allaire, Chair of the UMR 7054 unit of the C.N.R.S., France.
Prof. Frank Vermassen, University of Gand, Faculty of Medicine

PREAMBLE

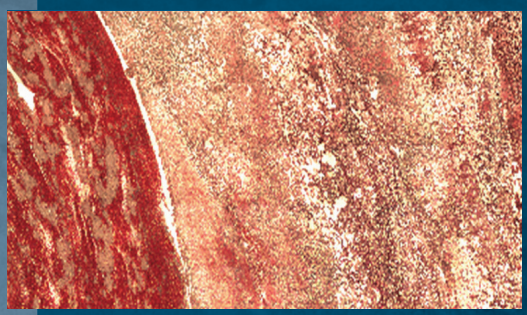
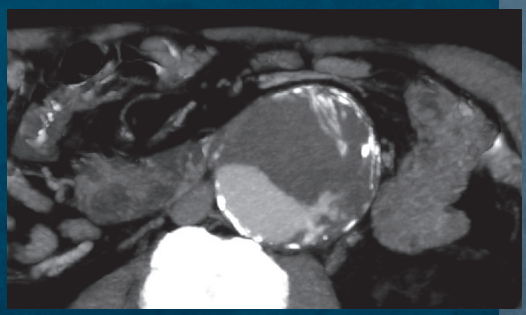
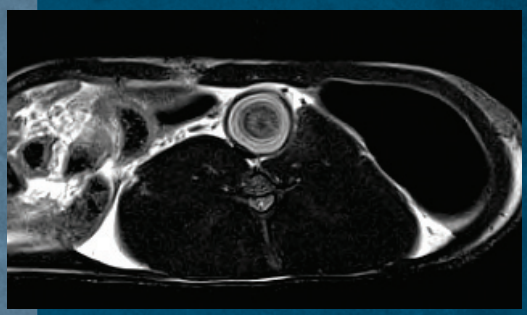
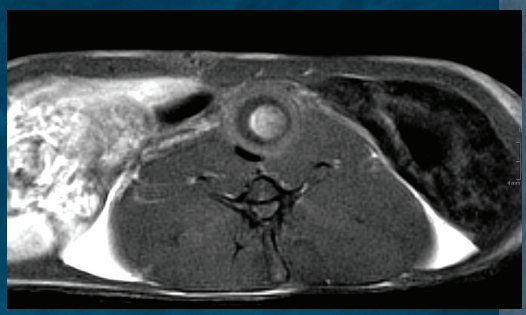

To Bruno, Jeremy and David.

This work is, though significant, only part of a much bigger picture that started a long time ago with the promise of your -then a little boy- dad to his grandmother Joséphine † 1988.

My proud musketeers, may you take every life step with the sense of strength infused by your own promises to the likes of Françoise, Christine, Justine and Carole.

Acknowledgements

The journey through this doctoral thesis has been a passionate human and scientific adventure for which I would like to thank all people who let me neither down nor walking alone; citing them is the guarantee of embarrassingly forgetting many. So, first of all, thanks to the anonymous, the missing and the forgotten, who anyhow have been source of support at anytime.
My educational continuum started in late seventies in a wondeful family; not only about dad, mum, Sandrine, Nadège, Paul Patrick and Patricia, but also about uncles, aunts, nephews and nieces who all believed in me and instilled me the ambition to achieve the highest degrees. My educators from the basic school through my master degree, all made a sensational job preparing me to the doctoral school. My last teacher and Professor of radiology Robert Dondelinger has been a source of inspiration, so did my ex-boss, Doctor Paul Magotteaux. I just feel fortunate and thank each for sharing pieces of lifetime with me.

While working on this thesis, I have been a part of several institutions including the CHC and the University Hospital of Liège where. I'm indebted the personnel and my colleagues gave me support and time to get ready.

I kindly thank the President of my Jury, Professor Jean-Olivier Defraigne, the members of my jury, Professors Eric Allaire, Vincent D'Orio, Roland Hustinx and Frank Vermassen, for their support, constructive criticism and patience. Among those, Professor Patrizio Lancellotti, a long lasting friend and example deserves a special attention. So do Professor Natzi Sakalihasan who is not only the man without whom this work has never been done, not only my thesis promoter, not only a tremendous friend; much more than that. I thank him for being the big brother I missed. Grazie amico! Teşekkürler değerli arkadaşım!

Many thanks to Professor Betty Nusgens for her reading prowess, Doctor Benoît Meunier for pieces of artwork, and all the co-authors who energetically worked on the papers supporting this dissertation.

A deserved attention to Catherine Voll, Isabelle Mancini, Cécile Wegria and Charlemagne Noukoua who did not co-authored my works, but meanwhile shared most of my diaries, stood by my side and never stopped trusting me.

Lastly, I have no words to express my deepest gratitude and consideration to my whole and big family, especially to my loving spouse Carole, and sons for all the sacrifices they have endured for years with pride.

Table of contents

Acknowledgements ... 2
Glossary ... 5
Abstract ... 6
Prologue ... 8
General Introduction ... 11
1. Definitions ... 12
1.1. Normal aorta ... 12
1.2. Aneurysmal aorta ... 13
2. Natural history of AAA ... 15
3. Factors involved in the genesis and rupture of AAA ... 16
3.1. Extracellular matrix remodeling ... 16
3.2. Protective mechanisms and circumstances ... 16
3.3. Deleterious mechanisms ... 18
4. General principles of imaging in AAA ... 19
4.1. Conventional imaging techniques ... 19
4.2. Tissue composition imaging ... 19
4.3. Calcifications ... 20
4.4. Fat ... 21
4.5. Hemorrhage ... 21
5. Metabolic imaging – Molecular imaging ... 23
5.1. Radionuclide imaging ... 23
5.2. Diffusion–weighed imaging ... 23
Goal and work plan ... 25
Part one:
Clinical value of FDG PET and imaging-derived biomechanical estimates in patients with AAA ... 27
Introduction to biomechanical estimates from imaging data:
geometry-based models and simulations ... 28
1. Publication N°1: High levels of 18F-FDG uptake in aortic
aneurysm wall are associated with high wall stress ... 30
1.1. Introduction ... 30
1.2. Findings summary ... 30
1.3. Conclusions ... 30
1.4. Reassessment summary/opportunities ... 30
2. Publication N°2: A novel strategy to translate the biomechanical rupture risk of abdominal
aortic aneurysms to their equivalent diameter risk: Method and retrospective validation ... 44
2.1. Introduction ... 44
2.2. Findings summary ... 44
2.3. Conclusions ... 44
2.4. Reassessment summary/opportunities ... 44

3. Publication N° 3. Multifactorial Relationship Between
F-Fluoro-Deoxy-Glucose Positron Emission Tomography Signaling
and Biomechanical Properties in Unruptured Aortic Aneurysms 59
3.1. Introduction 59
3.2. Findings summary 59
3.3. Conclusions 60
3.4. Reassessment summary/opportunities 60
Part Two: New and promising concepts for biological process imaging in AAAs 83
Introduction to the structure and the activities of the intraluminal thrombus 84
1. Publication N°4. MR imaging of iron phagocytosis in intraluminal
thrombi of abdominal aortic aneurysms in humans 85
1.1. Introduction 85
1.2. Findings summary 85
1.3. Conclusions 85
1.4. Reassessment summary/opportunities 85
2. Publication N°5 (submitted). Assessment of the deleterious role
of the intraluminal thrombus and its iron content with multimodality imaging,
in a rat model of abdominal aortic aneurysm 105
2.1. Introduction 105
2.2. Findings summary 105
2.3. Conclusions 105
General Discussion 127
Conclusion and Perspectives 132
Epilogue 133
Bibliography 134
Annexes 143
Résumé (FR) 169
Curriculum vitae 172

Glossary

TERMS	ABBREVIATIONS
Abdominal aortic aneurysm	AAA
Apparent Diffusion Coefficient	ADC
Computed tomography	CT
Diffusion-weighted	DW
Extracellular Matrix	ECM
^{18}F-Fluoro-deoxy-glucose	^{18}F-FDG, FDG
Field-of-view	FOV
Finite element simulation	FES
Free induction decay transverse relaxation time	T2*
General Linear Mixed Model	GLMM
International Society for Cardio-Vascular Surgery	ISCVS
Intraluminal thrombus	ILT
Longitudinal relaxation time	T1
Low-density lipoprotein	LDL
Magnetic Resonance Imaging	MRI
Matrix Metalloproteinase	MMP
Peak Wall Rupture Index	PWRI
Peak Wall Rupture Risk	PWRR
Peak Wall Stress	PWS
Positron emission tomography	PET
Region-Of-Interest	ROI
Reticuloendothelial system	RES
Ribonucleic acid	RNA
Signal Intensity	SI
Single Photon Emission Computed Tomography	SPECT
Smooth muscle cell	SMC
Society for Vascular Surgery	SVS
Standardized Uptake Value	SUV
Superparamagnetic iron oxide	SPIO
T1-weighted	T1W
T2*-weighted	T2*W
T2-weighted	T2W
Thoracic aortic aneurysm	TAA
Thromboxane A2	TXA2
Tissue inhibitor of Matrix Metalloproteinase	TIMP
Transverse relaxation time	T2
Ultrasmall superparamagnetic iron oxide	USPIO
Ultrasonography	US

Abstract

Introduction

The general context of this dissertation is to evaluate patient-specific approaches to the risk of rupture of abdominal aortic aneurysm (AAA), using imaging techniques with ability to assess biological processes. Following a thorough description of available imaging techniques, our work is divided in two main research objectives, namely: (i) to provide greater clinical value to existing but unproven imaging concepts, and (ii) to suggest new concepts for improved AAA risk of rupture assessment.

Methods

The first research objective evaluated how far imaging biological activities using 18F-Fluorodeoxyglucose (FDG) Positron Emission Tomography (PET) and modeling wall stress using finite element simulations (FES) may help clinical decision-making in patients with AAA, and what would be their incremental value as compared to diameter-based patient management algorithms. On a patient basis, clinical outcomes were evaluated with regard to FDG PET and FES signaling. Further, the concept of AAA risk-equivalent diameter using FES was described and retrospectively validated using data from large multicenter trials. The second research objective included the assessment of the biological activities of the intraluminal thrombus (ILT) and the demonstration of its deleterious role in AAA using multimodality imaging. A special emphasis was put on the ability of magnetic resonance imaging (MRI) to monitor the biological activities of ILT without exogenous contrast, by evaluating its iron content.

Results

Increased FDG uptake was a diameter-independent marker of AAA-related events over 2 years. Missing dichotomy prevented such a finding for increased wall stress, although its correlation with increased FDG uptake indicates a potentially comparable value in terms of risk management. Wall metabolism is influenced by patient-specific susceptibility factors, indicating hereditary or acquired alteration of the biological responses to wall stress.

The concept of risk-equivalent diameters on FES links biomechanical estimates to basic conclusions drawn from large diameter-based clinical AAA trials. Our retrospective and diameter-adjusted validation analysis verified that biomechanical risk indicators are higher in ruptured than non-ruptured AAAs. Part of the FDG uptake is associated with biological activity along the luminal surface of the ILT, where we experimentally demonstrated phagocytosis of superparamagnetic iron oxide on MRI , both ex vivo and in vivo. This phagocytosis is correlated with the abundance of leukocytes and proteolytic activity. In addition, unenhanced MRI appearances resulting from the endogenous iron distribution within ILT also relate to these biological activities. Lastly, multimodality imaging was used to confirm the concept of the deleterious role of the ILT in AAA growth in a model of AAA by infusion of elastase in the rat.

Conclusion

MRI and FDG PET are capable of evidencing and quantifying in vivo some of the notoriously deleterious biological processes taking place in the aneurysmal sac, especially related to the entrapped phagocytes and red blood cells in ILT and the periadventitial inflammatory response.

The central role played by ILT and its biological activities was demonstrated in vivo using several imaging techniques. The clinical value of imaging these biological activities is epitomized by a diameter-independent 2-year increased risk of event in AAA with increased wall metabolism.

Prologue

Rupture of abdominal aortic aneurysm (AAA) represents a significant cause of mortality potentially preventable in economically developed countries. In the current state of knowledge, only the maximal aneurismal diameter and its derivatives, such as growth rate, are significantly associated with risk of rupture on a population basis. The subsequent diameter-based management algorithm of patients with AAA saves more lives and money than no recommendation at all, but raises patient-specific concerns, as it implies that an "acceptable" range of patients are either undertreated or overtreated. This dissertation assumes a change of this paradigm, with a patient-specific approach to AAA rupture risk assessment. It appeals for a thorough assessment of available imaging techniques, both to provide greater clinical value to existing but unproven imaging concepts and to suggest new concepts for AAA risk of rupture assessment.

AAA rupture occurs when the internal force (stress) exceeds the strength of the wall. This biomechanical view has driven efforts to determine experimentally the tearing properties of aortic tissue fragments and to evaluate the wall stress in vivo, using tridimensional imaging data to compute finite element simulations (FES). Though helpful, this approach is unsatisfactory in terms of risk-management, because aneurysm rupture is a discrete time-point to which the following understatement applies: "before the aneurysm is ruptured, it is not". Actually, AAA rupture is a complex process that can be simplistically summarized as a loss of balance between biological destructive and healing processes. Therefore, special emphasis has been put on: how to evaluate and quantify biological processes in AAA? How to correlate these processes to non-biological parameters, such as wall stress, or patient outcomes?

After a review of imaging techniques used to evaluate AAA, our dissertation is divided into two personal contributions including: clinically-oriented (Part 1) and experimental (Part 2) investigations. Part 1 aims at determining how far imaging biological activities may help clinical decision-making in patients with AAA and what would be its incremental value, as compared to the diameter-based patient management algorithm. To extend our alternative approach, we included biomechanical imaging, in order to evaluate the clinical usefulness of a further distinct approach to the diameter-based rupture risk-assessment. Indeed, establishing the clinical value of one type of imaging could serve by transitivity another correlating imaging technique. The experimental part of our work aims at finding new promising imaging concepts for the assessment of biological processes in AAAs.

With the rising ability to evaluate biological activities in vivo using 18F-fluorodeoxy-glucose (FDG) positron emission tomography (PET), the unexplored point from where we conducted a pilot study (5 patients) was: "is there any correlation between wall stress and biological activity in AAAs?" (Publication N°1). A practical challenge was the difference in reporting options between PET and FES: How could we translate the myriad of finite elements into a single score or state, that represents a marker of the risk of rupture for a given patient and vice-versa? While we could easily figure out defining a PET-positive or a PET-negative examination, such as in use in oncology, it seemed almost

impossible to conceptualize a similar dichotomization with wall stress. We therefore tried to improve the clinical value of FES by evaluating directly how it could alter the diameter-based rupture risk-assessment algorithm (Publication N° 2). In other words, how do estimates of wall stress or stress/strength distribution affect the risk of rupture assigned to an AAA considering its maximal diameter? Finally, we included 53 patients with a wide range of aortic aneurysm type (abdominal, thoracic), shape and diameter in a study, to evaluate the outcomes and the correlations between FDG PET and FES signaling (Publication N°3).

Assessment of ILT properties and content as potential markers of its biological activities has received only little attention so far. Yet, a significant part of the biological activities and metabolism in AAA can be attributed to phagocytic cells entrapped in ILT, a nearly ubiquitous component in AAA that also biomechanically impacts the wall properties. We used the reticuloendothelial system (RES) specificity of superparamagnetic iron oxide (SPIO) contrast agents for magnetic resonance imaging (MRI) to evaluate in vivo the phagocytic properties of ILT (Publication N° 4). We evaluated the MRI signal properties of ILT before and after SPIO, the ILT densities of macrophages and neutrophils determined by histology, and its level of expression and activation of proteolytic enzymes by zymography. In addition, SPIO phagocytosis was tested by ex vivo experiments on ILT fragments.

How the deleterious role of ILT on AAA can be shown by imaging? How far the endogenous iron content in ILT can be measured using MRI? Could this be helpful in determining the level of biological activities of ILT? These were remaining unanswered questions behind of a proof-of-concept study we conducted in rat models of AAA by aortic infusion of elastase before and after anti-platelet aggregation treatment using a thromboxane A2 (TXA2) antagonist (Publication N°5, in progress).

GENERAL INTRODUCTION

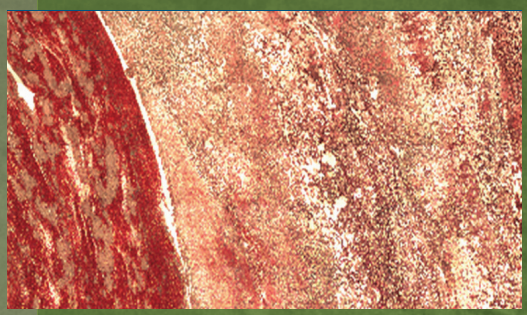
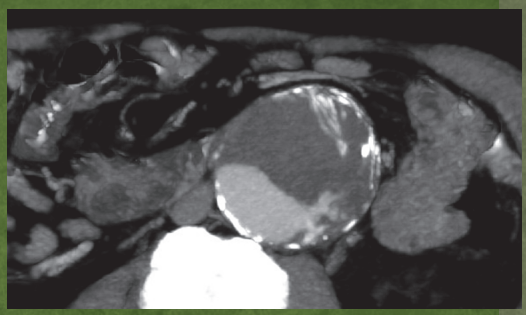
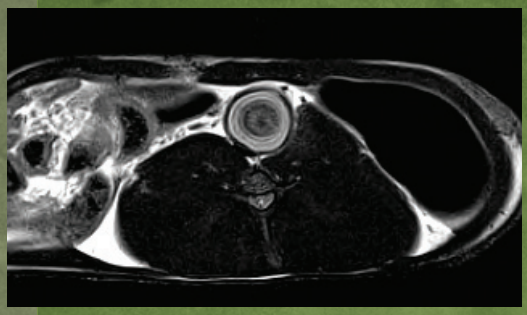
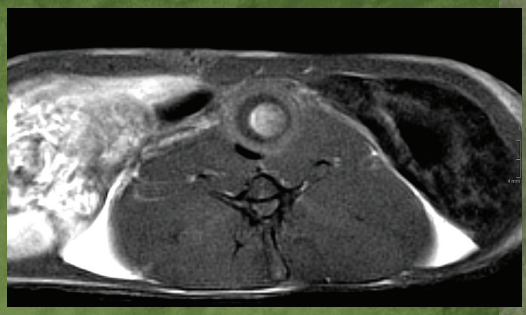

"There is no disease more conductive to clinical humility than aneurysm of the aorta."

Sir William Osler
Professor of Medicine 1849-1919

1. Definitions

1.1. Normal aorta

Structurally, the aortic wall is constituted by three layers: intima, media and adventitia, from its inner to the outer limit (Figure 1). The most luminal component of the intima is the endothelium, lying on a layer of connective tissue, the basement membrane. The intima is separated from the media by an internal elastic lamina. The media is constituted by concentric lamellae containing fibers of collagen elastin and a variety of glycoproteins, along with smooth muscle cells. It is separated from the adventitia by the external elastic lamina. The adventitia is a loose connective tissue containing mainly collagen and some elastic fibers. It also contains vasa vasorum, nerve fibers of the sympathetic and parasympathetic nervous system and lymphoid follicles.

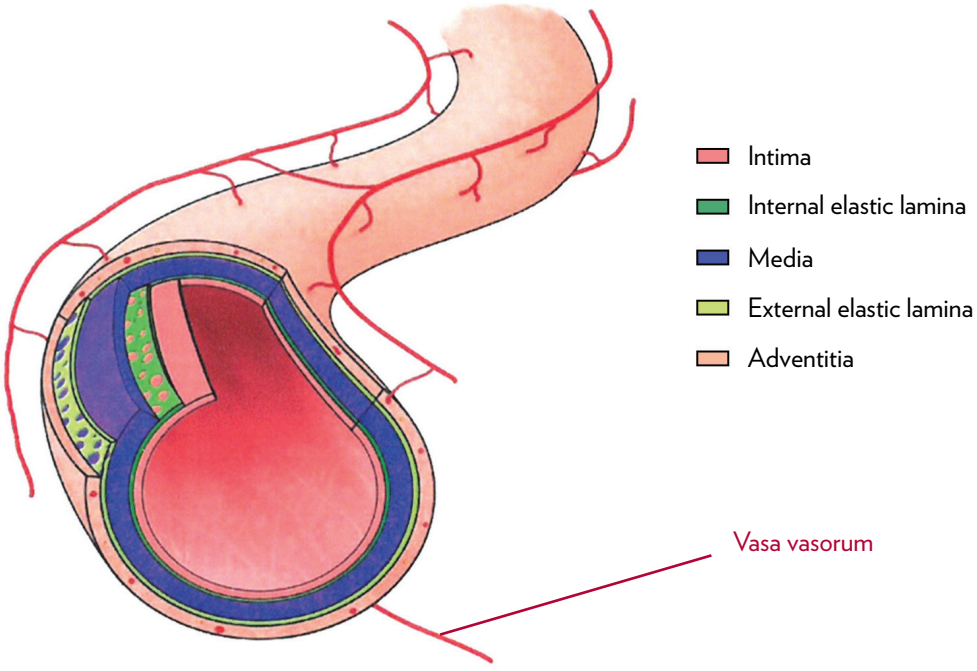

Figure 1 : Schematic representation of the aortic wall layers.

A critical component of the aortic wall is the extracellular matrix (ECM) that accounts 20% of collagen. Twenty-eight different types of collagen have been identified, several are present in blood vessel wall and can be divided into two groups according to their ability to form fibrils. In the aorta, the most important collagens are fibrillar type I and III. The type I/III collagen ratio is 3/1 in average, but is heterogeneous and tends to be higher with aging, or at distance to the heart[1]. Type III collagens are most often in contact with elastin fibers. Type IV collagens are much less abundant than the fibrillar collagens, but play an important role as components of the basement membrane[2].

Elastin fibers are other major component of the aortic media. The molecular structure of elastin is unique, alternating hydrophobic and basic domains that allow it to stretch to almost the double length and quickly return to normal. Elastin polymers are insoluble and extremely stable[2]. Elastin is deposited on a microfibrillar scaffold including fibrillin-1, fibrillin-2 and related proteins. Other components of the ECM act on structure and cross-linking, hydration, cell-cell and cell-ECM interactions, including proteoglycans, hyaluronic acid and several glycoproteins including fibronectin, vibronectin, laminin, entactin, tenascin and thrombospondin-1. In general, the macromolecules of the ECM are synthesized by smooth muscle cells (SMCs) in the media and fibroblasts in the adventitia.

1.2. Aneurysmal aorta

Currently, aneurysm defines a permanent and irreversible vascular segment dilatation, involving all three wall layers. This pathological definition differentiates aneurysms from pseudoaneurysms, where expansion affects a lower number of layers (Figure 2). Some individuals may have diffusely larger arteries, but because of the non-segmental nature of this expansion, this state refers to arteriomegaly. Even within a normal range, significant interindividual variations of the arterial diameter apply. Indeed, arteries are larger in the elderly[3] and in men[4]. In addition, the diameter of the aorta narrows considerably from the valve down to the iliac bifurcation. To define abdominal aortic aneurysm, we use the simple criterion of an aortic diameter > 30 mm, although other criteria have been proposed to improve the specificity and sensitivity for the diagnosis of AAA, taking into account gender, ethnicity and suprarenal aortic diameter [5-8] (Table1). Aortic dilatations with a lower diameter may be referred to as "incipient aneurysms"[9].

Author	Infrarenal aortic diameter threshold value for AAA
Mc Gregor et al.[10]	≥ 30 mm
Sterpetti et al.[11]	≥ 1.5 x suprarenal aortic diameter
Collin et al. [4]	≥ 40 mm or 5 mm > to the suprarenal aortic diameter
ISCVS/SVS[5]	≥ 1.5 x expected normal diameter
Wanhainen et al.[6]	Men: ≥ 30 mm and/or ≥ 1.1 x suprarenal aortic diameter Women: ≥ 27 mm and/or ≥ 1.0 x suprarenal aortic diameter
* International Society of Cardiovascular Surgery / Society of Vascular Surgery	

Table 1 : Proposed definitions for abdominal aortic aneurysm.

Morphologically, two types of aneurysms can be distinguished: fusiform aneurysms, in which the entire circumference of the vessel is dilated; and saccular aneurysms, in which only a portion of the vascular circumference is involved, resulting into the formation of a sac alongside the mainstream (Figure 2).

Aorta is the most common site for aneurysms development. Most of the aortic aneurysms are located in the infrarenal portion of the abdominal aorta[12]; the so-called abdominal aortic aneurysm (AAA), that constitute the main scope of this dissertation. Arterial aneurysms may be multiple and involve several arteries; to this regard, there is a strong association between AAA and thoracic aortic aneurysm (TAA)[13].

The ratio between AAA and TAA decreases with age from 1/2 to 1/6[14]. Other arteries frequently involved by aneurysms are intracranial arteries that have an estimated prevalence of 1-2%[15], peripheral arteries (common and internal iliac, femoral and popliteal) that have an estimated prevalence <8/100,000[16] and visceral abdominal arteries (splenic, hepatic, and renal).

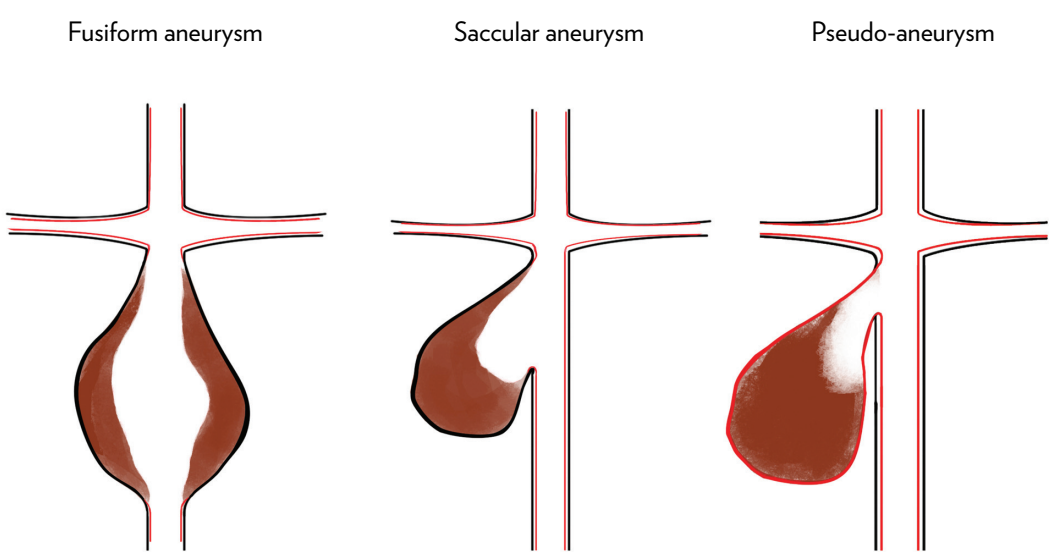

Figure 2 : Coronal plane schematic representations of types of infrarenal aortic dilatation, with intraluminal thrombus.

2. Natural history of AAA

Aortic aneurysm prevalence increases with age to reach 5-10% of the population over 65 years of age[17-18]. AAA is a slow disease process, often asymptomatic until occurrence of rupture, its most common complication. Less frequent complications include peri-adventitial inflammation, thrombosis and peripheral embolization. Rupture-related symptoms may be serious and lead to death before admission in nearly half of the patients, and another half of those operated[19]. The natural history of aortic aneurysms is incompletely elucidated for several reasons. The first is the hypothetical nature of the events occurring before diagnosis. Second, the putative risk of rupture of larger aneurysms is the cause for preventive interventions. Finally, many co-morbidity factors are present in patients with aortic aneurysm. This chapter focuses on the description of related clinical events that may occur in a patient with aortic aneurysm.

The annual rate of aneurysmal rupture in people denying surgery is estimated at 8%, 10% and 20% respectively for aneurysms of 55-59mm, 60-69mm and >70mm[20]. Further, several studies have shown that the annual risk for AAA rupture statistically exceeds operative risk at the critical diameter of 55 mm in men and 50 mm in women[21-25]. The initial diameter of AAA is therefore one but not the sole critical parameter for risk assessment. Indeed, it has been shown that the growth of aortic aneurysms is not linear but may progress very diversely. Growth rate is independent of the diameter[26], and sometimes has exponential, quadratic, or plateau shapes[27-28]. Longitudinal AAA studies in the UK have shown that the rupture rate is not negligible in aneurysms below the aforementioned thresholds of preventive surgery[27,29], while unruptured aneurysm beyond these thresholds is not uncommon at autopsy[20]. These facts imply that a secondary prevention of rupture and death strategy in patients with AAA could be the precise assessment (or anticipation) of the growth rate acceleration (Figure 3).

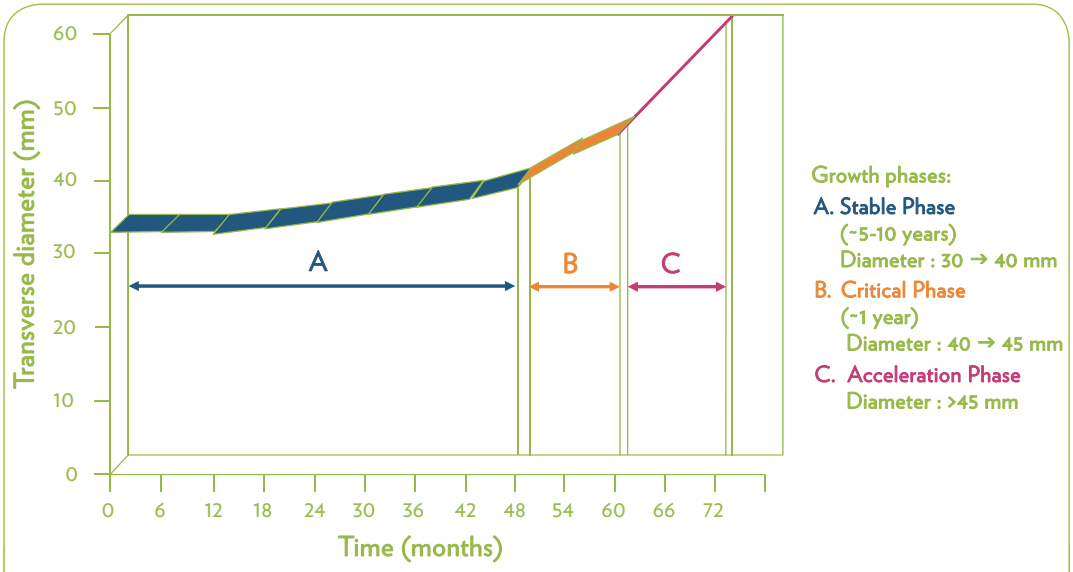

Figure 3 : The typical growth rate of an aortic aneurysm exhibits a quiescent or stable phase in which the maximal growth rate is 2-3 mm/year (30), separated by a critical curve inflexion from an acceleration phase in which the growth rate may exceed 10 mm/year (27).

3. Factors involved in the genesis and rupture of AAA

It is commonly admitted that both genetic and environmental risk factors (table 2) are associated with genesis of AAA through a common pathway that result in the proteolytic depletion of the extracellular matrix (ECM), resulting in a structural imbalance[31].

3.1. Extracellular matrix remodeling

Busuttil et al. first reported the involvement of proteolytic enzymes in AAA, by identifying a collagenase activity in AAA tissue[32]. Later, involvement of elastases were reported, but the respective roles of elastases and collagenases in the AAA advent and rupture was clarified by the experiment of Dobrin et al. who infused carotid arteries by solutions of elastase or collagenase and observed that the subsequent specimen inflation resulted respectively in expansion and rupture[33]. It was later clarified that the process of aneurismal expansion is characterized in its early phases by a loss of elastins, while collagen content remain unchanged[34]. Although other enzymes, such as cathepsins, have also been identified in AAA tissues, degradation of ECM proteins in vivo is mediated by matrix metalloproteinases (MMPs) or serum proteases[35]. Twenty-three MMPs are identified in mammalians and classified into eight groups according to their structural and functional properties[36]. Among these, eight have been identified in AAAs, including MMP-1, MMP-2, MMP-3, MMP-8, MMP-9, MMP-12, MMP-13 and MMP-14, produced by different sources including fibroblasts, SMC, macrophages, neutrophils, platelets, T-cells and endothelial cells[37]. Although less effective in the degradation of ECM than MMPs, plasmin and plasminogen activators are also involved in the initiation and progression of AAA, as they specifically activate MMPs. Activation of the latent MMP generally requires the proteolytic cleavage of the pro-domain inactivating the catalytic site associated with the cation Zn^{++}. The MMP activity is modulated by nonspecific (α2-macroglobulin) and specific tissue inhibitors (TIMP), also present in the ECM and secreted by SMC and macrophages or provided exogenously (tetracyclines, statins)[38].

3.2. Protective mechanisms and circumstances

ECM fibrosis through fibroblast colonization and macromolecules crosslinking is the main, but poorly investigated protective mechanism in AAA[40]. Calcifications theoretically provide a biomechanical protective effect, by decreasing elasticity and increasing stiffness of the vessel wall subject to a substantial loss of elastin[41]. It is well established that arterial calcification is actively deposited under the control of osteoblast-like cells derived from SMCs[42-43]. Calcification is a marker of atherosclerosis severity and cardiovascular mortality[44]. As such, it is almost ubiquitous in AAA. However correlation between calcification severity and clinical outcomes is debated[45-46]. This may be related to the specific site of calcification in consideration. Calcification can be deposited in the intima, the ILT and the media, just beneath the adventitia. In atherosclerotic plaques, intimal calcifications are associated with instability[47], while medial calcification is present in elderly, diabetes and renal failure and seems to result from a different mechanism[48] that does not denote plaque instability, although overlaps exist between both sites of calcification. In AAA, medial (sub-adventitial) calcifications are thinner and smaller than in age, gender and risk factors for cardiovascular disease-matched undilated aortas[49].

POPULATION				
Variables	Without AAA (N=3.033.009)	With AAA (N=23.446)	p-value	Relative- Risk
Gender				
Women	65.07%	20.66%	<0.001	0.23-0.31
Men	34.93%	79.34%	<0.001	
Mean age (years) (95% confidence interval)	62.98 (62.97-92.99)	71.10 (71.08-71.20)	<0.001	1.10-1.16
Race/ethnicity				
Caucasian	86.78%	90.73%	<0.001	
Other	13.21%	9.27%	<0.001	
Marital state				
Married	68.52%	69.53%	0.0009	
Alone	8.08%	6.48%	<0.001	
Divorced	8.78%	6.99%	<0.001	
Widow	11.83%	14.02%	<0.001	
Smokers				
	42.47%	80.23%	<0.001	2.48-3.10
Active	10.68%	28.09%	<0.001	
Past	31.79%	52.14%	<0.001	
Arterial hypertension	65.02%	81.51%	<0.001	1.24-1.46
Controlled	19.49%	22.86%	<0.001	
Uncontrolled	27.09%	38.61%	<0.001	
Unaware	18.44%	20.05%	<0.001	
Hypercholesterolemia	53.89%	68.06%	<0.001	1.26-1.49
Coronary disease	6.72%	26.69%	<0.001	1.68-2.02
Carotid atherosclerosis	2.48%	9.76%	<0.001	
History of transient ischemic attack	5.47%	13.32%	<0.001	
Lower limb atherosclerosis	2.96%	12.56%	<0.001	
Diabetes	10.69%	13.83%	<0.001	
Familial history				
Carotid atherosclerosis	17.66%	22.52%	<0.001	
Transient ischemic attack	9.38%	10.01%	0.0009	
AAA	2.48%	7.95%	<0.00	
Lower limb atherosclerosis	2.91%	3.01%	0.3350	
Body mass index				
Underweight <20	1.18%	1.20%	0.8260	
Normal 20-25	30.20%	23.87%	**<0.001**	
Obese >25	66.73%	73.30%	**<0.001**	

Table 2 : Epidemiological factors influencing the AAA rate adapted from Kent et al. (39).

With regard to protection against AAA, diabetes deserves a special comment. Although it has been recently reported as a risk factor for AAA, probably owing to its association with other significant risk factors[39], it actually exerts a protective effect[17, 50], probably related to the induction of: (i) ECM protein modifications preventing their degradation, (ii) a dysfunction of the molecules involved in this degradation, or (iii) malfunction of the adventitial nerve fibers of the autonomic nervous system.

3.3. Deleterious mechanisms

Biomechanically, aneurysm rupture occurs when the internal force per area (stress) exceeds the wall strength. The generic term "wall stress" sums an infinity of force vectors exerting in different directions of space[51], to which superimpose shear forces generated by the blood flow at the inner wall interface. As such, the net wall stress strongly depends on arterial pressure. Theoretically, the law of Laplace ($\sigma = (P \times r)/t$) defines the relationship between wall tension (σ), its thickness (t) and the radius (r) of a cylinder in which a fluid flows at a given pressure (P). Nevertheless, this can apply imperfectly to blood flow in a compliant and biologically active vessel after the initiation of aneurysmal dilatation. Biological activities in response to the biomechanical stimuli increase the complexity of the relationship between wall stress, arterial pressure and vessel diameter.

The wall remodeling due to stress is hypertrophic, resulting into vascular enlargement, elongation and change of shape[52-53]. The contralateral curvature of the aneurysm in amputated war survivors with AAA, thought to result from asymmetry of the blood flow-related stress provides a nice illustration to this process[54]. Wall stress and low shear stress also cause platelet activation with apposition of an intraluminal thrombus (ILT)[55]. The biomechanical effect of ILT is protective. Unfortunately, ILT triggers many biological activities including *de novo* platelet adhesion[56-57]; fibrinolytic cascade[58] and complement activation[59]; trapping and activation of leukocytes[60-61] that release serine proteases and matrix metalloproteases (MMPs), and lastly; trapping of red blood cells (RBCs). The net effect of ILT is therefore deleterious, as it causes wall weakening[53, 62-63]and eventually aneurysm enlargement[64]. Excess oxidative stress can result into AAA destabilization[65], triggering rupture. Specific causes for oxidative stress are multiple and include smoking[66], hemagglutination (iron mediated oxidation) and infection. Infection or immune dysfunction in the context of chronic inflammation contributes to the destabilization of AAA [67]. Further, *Chlamydia Pneumoniae* infection has been reported in patients with ruptured AAA[68-69]. The possible involvement of weak pathogens recently came under discussion, since oral bacteria including *Actinobacillus Actinomicetemcomitans* and *Porphyromonas Gingivalis* have been identified in aneurysmal tissues[70-71].

Increased microvasculature in response to pro-angiogenic cytokines plays a role in AAA destabilization and progression towards rupture[72-74]. Indeed, neovessels are relevant sources of intimal inflammatory and immune cell activities, causing increased MMP activity and decreasing the wall strength[75].

Finally, female gender and a genetic susceptibility for AAA rupture have been described in several series[76-78].

4. General principles of imaging in AAA

4.1. Conventional imaging techniques

AAA morphology can be evaluated by plain films, angiography, ultrasonography (US), computed tomography (CT) and magnetic resonance imaging (MRI). With the advent of cross-sectional techniques, plain films and angiography are being progressively abandoned because of their low information yield. US is harmless and as such, useful in AAA screening programs. Description of these imaging techniques was published as a book chapter annexed at the end of this thesis (see additional Publication N° 1). Briefly, US is based on the ability of the tissues to change the properties of an ultrasound beam, while X-ray techniques such as plain films, angiography and CT are based on the ability of the tissues to attenuate an X-ray beam that is proportional to the constituting atomic numbers. MRI is based on the electromagnetic properties (magnetization recovery or spoiling) of nuclei under the effect of an oscillating magnetic field. This is typically obtained by applying brief radiofrequency (RF) pulses at the appropriate resonant frequency to tissues beforehand magnetized by an external magnetic field (B_0). The contrast between tissues is determined by the rate at which excited atoms return to the equilibrium state. A given nuclei relaxation time has longitudinal (T1) and transverse (T2 and T2*) components that strongly depend on its electromagnetic environment. On the other hand, functional imaging is a growing concept that refers to the assessment of one or several pathophysiological pathways involved in AAA. As such, it includes tissue composition, metabolic and molecular imaging.

4.2. Tissue composition imaging

Imaging techniques using X-rays have the ability to distinguish certain natural contrasts such as calcium, water, fat and air. However, tissue characterization by imaging became a refined concept with the advent of MRI, owing to the wider range of the nuclear electromagnetic environment in human tissues. Some of the tissue components identifiable with imaging within the aortic wall and the underlying thrombus are potentially of special interest in terms of risk stratification for AAA (Table 3).

Tissue of interest	Imaging properties				
	T1W MRI SI	T2W MRI SI	T2*W MRI SI	CT attenuation	Enhancement*
Fat	High	High	High	Low	None
Acute hemorrhage (Iron)	Variable	Low	Low	High	None
Calcium	None	None	Low	Very High	None
Inflammation (edema, neovascularization)	Low	High	NA	Low	Yes

Table 3 : Imaging properties of components involved in AAA (*denotes the tissue properties after intravenous contrast agent administration).

4.3. Calcifications

Calcifications are easily detectable on X-ray-based imaging techniques (plain films, CT). Those located within ILT are of special interest, because the calcification mechanism involving perivascular deposit implies that intra-thrombus former or current vascular channels should be present, both macroscopically (Figure 4) and microscopically (Figure 5).

This unreported finding provides a potential explanation to how factors located deeper in the ILT can be exposed to the circulating blood cells.

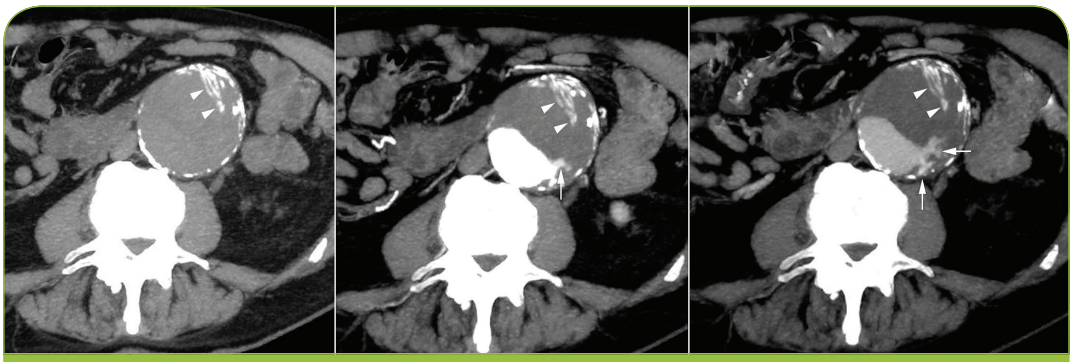

Figure 4 : Transverse maximum intensity projection thick-slabs CT of a large AAA obtained before (left panel), and on arterial (centre panel) and portal (right panel) phases after intravenous injection of iodine contrast agent, showing both calcifications (arrowheads) and progressively enhancing vascular channels inside ILT (arrows) (Unpublished data).

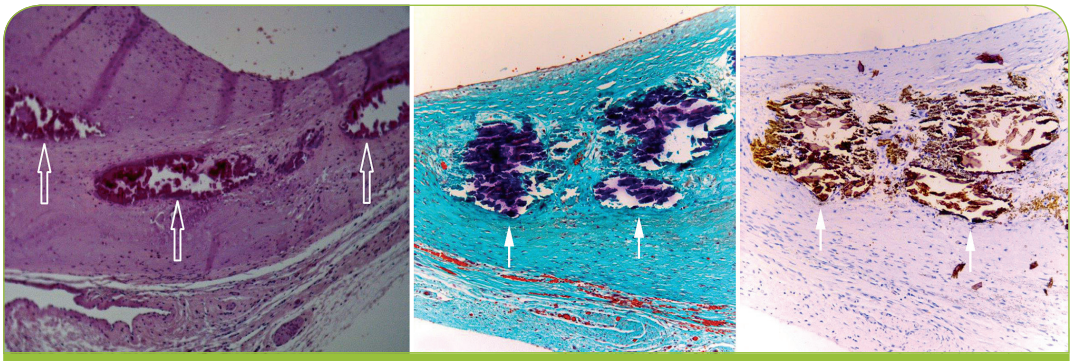

Figure 5 : Hematoxylin-eosin staining (left panel) section of the aortic wall in a model of AAA by infusion of elastase in the rat, showing channels containing RBC within the ILT at early stages (open arrow). On older aneurysms, Masson Trichrome and Von Kossa staining (resp. center and right panels) show clusters of calcifications on similar locations (arrows) (Unpublished data).

4.4. Fat

Fatty replacement (lipomatous metaplasia) is a rare and unreported feature of AAA. It may represent a cause of biomechanical weakening of the wall[79], but mainly a marker of stabilization as in other cardiovascular disease[80], although it has not been specifically evaluated so far.

Fat is detected as low attenuation tissue relative to water on X-ray techniques. It has a high signal on T1- and T2-weighted MRI. The decrease of its signal on MRI after a pulse or spectral fat suppression further helps fat identification (Figure 6).

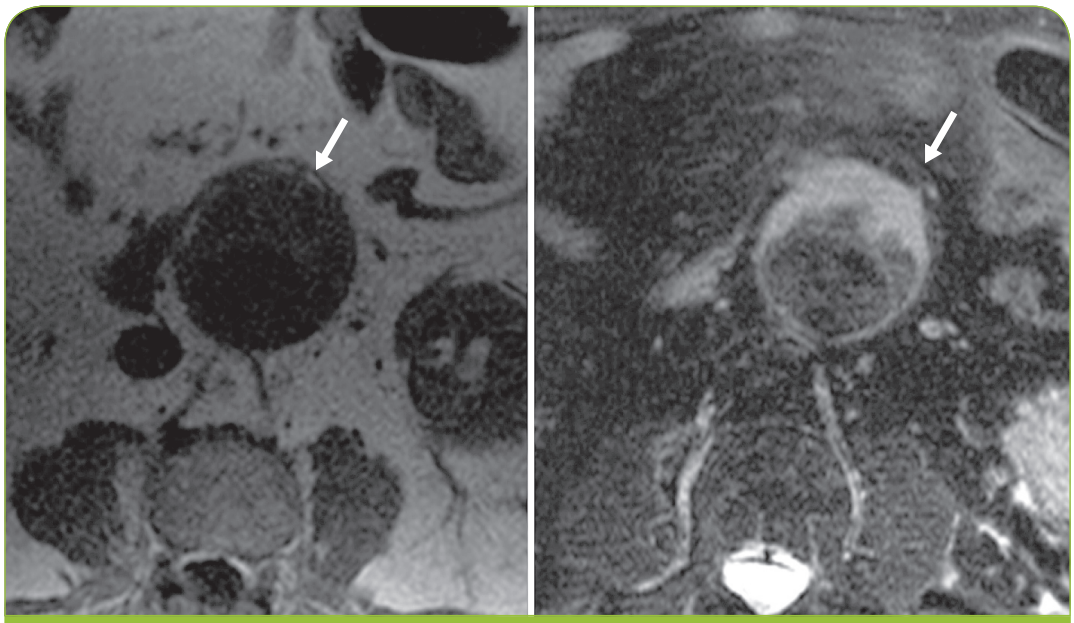

Figure 6 : Transverse MRI of a large but stable AAA using a T1-weighted (left panel) and a T2-weighted image with fat saturation (right panel) in which the fat appears respectively with high and very-low signal (arrows) (Unpublished data).

4.5.Hemorrhage

Emergency aneurysm repair is advised when acute hemorrhage within ILT or the surrounding tissues is detected, especially in association with clinical symptoms. The classic sign of acute hemorrhage is a semi-lunar high attenuation layer within ILT on CT; the so-called «crescent sign»[81-82] (Figure 7).

Nevertheless, AAA symptoms are not necessarily correlated with histological abnormalities[83]. It is not uncommon to find chronic foci of hemorrhage inside thrombus. On MRI, the signal of hemorrhage is influenced by its composition, and thus its age. A simplistic but reasonably accurate approach is to consider that the high signal intensity on T1W MRI is associated with the presence of methemoglobin (intra- or extra-cellular)[84].

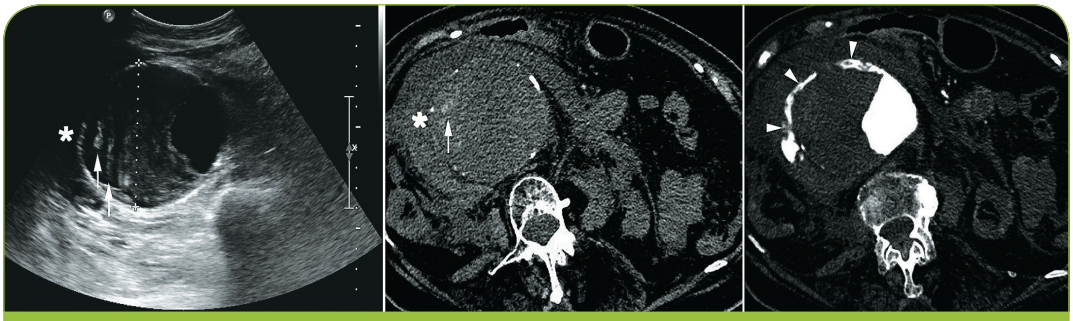

Figure 7 : Transverse ultrasound (left panel) in an 89 year-old female admitted with shock showed a 11 cm AAA with a heterogeneous ILT, exhibiting an external hypoechoic crescent containing thick hyperechoic lines (arrows). Another hypoechoic structure surrounds the aorta (asterisk) suggesting a retroperitoneal hematoma. These intra-thrombus and retroperitoneal hematomas are confirmed by high attenuation (50-70 Hounsfield Units) on unenhanced CT (centre panel). Contrast-enhanced CT (right panel) shows luminal contrast leaking into the periaortic hematoma through a channel dissecting the external ILT (arrowheads) (Unpublished data).

In foci of chronic hemorrhage, a low T2*W signal indicates the presence of hemosiderin, whatever the T1W signal. Of note, the low T2*W SI caused by hemosiderin is virtually indistinguishable from that caused by calcification (Figure 8).

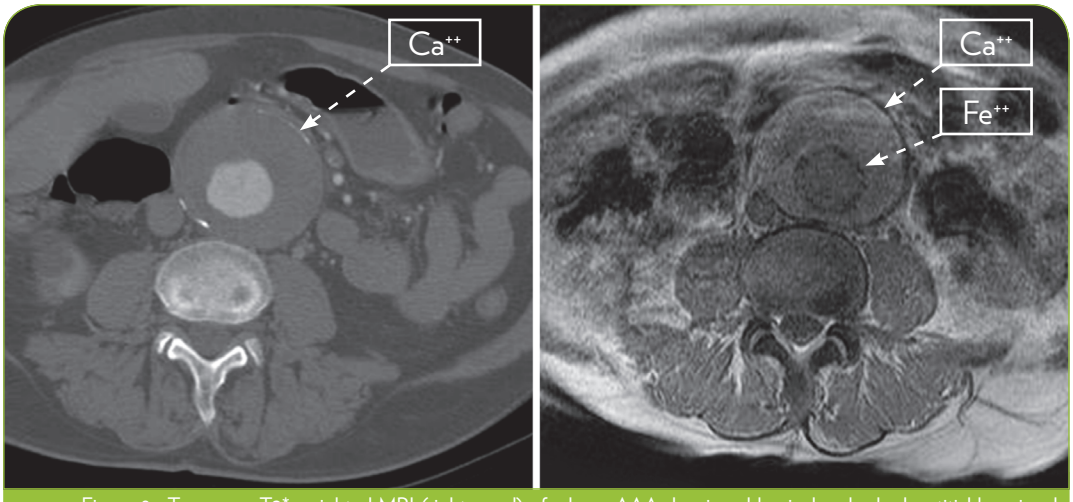

Figure 8 : Transverse T2*-weighted MRI (right panel) of a large AAA showing abluminal and subadventitial low signal rings. The corresponding contrast-enhanced CT transver se slice (left panel) shows subadventitial hyperdense calcifications (Ca^{++}) but fails to replicate this finding around the aortic lumen, as CT is less sensitive to low iron (Fe^{++}) concentrations than T2*-weighted MRI (Unpublished data).

A single or repeated hemorrhage within ILT is biologically pejorative. Indeed, iron released by lysed RBC induces oxidation through the Fenton reaction[85] , resulting amongst others, into proteolysis and increased platelet aggregation[56-61].

5. Metabolic imaging – Molecular imaging

5.1. Radionuclide imaging

Single Photon Emission Computed Tomography (SPECT) is designed to evaluate the internal distribution of a radionuclide using a photon sensitive camera rotating around the patient. Inversely, Positron Emission Tomography (PET) produces images from an internal source, by detecting the two opposite (coincident) photons resulting from positron annihilation, after disintegration of a radionuclide. The first human whole-body PET was commercialized in 1978 and the first hybrid PET-CT and PET-MRI scanners, respectively in 2000 and 2011. Improved spatial resolution down to 4-7 mm, availability of cyclotrons[86] and radio-pharmaceuticals suited to this type of imaging[87] allowed PET and its variants to be established as cornerstones of molecular imaging. FDG is one of the most popular radionuclide.

Similarly to glucose, FDG enters cells using the same membrane transporter (GLUT) and undergoes phosphorylation by hexokinase to get metabolized as FDG-6-phosphate. As the latter cannot enter glycolysis (the cycle of hexoses), it accumulates into cells[88]. As such, FDG is a glucose analog, and its accumulation identifies sites of increased uptake (glycolysis). In aortic aneurysm wall, FDG uptake is correlated with inflammatory and phagocytic cells infiltrates[89-92], activated matrix metalloproteases[93] and risk of rupture[94-95]. FDG uptake is quantifiable.

Assuming a 1g/ml constant body volumetric mass, the standardized uptake value (SUV) of a region-of-interest (ROI) relates the uptake in a given tissue to the total dose injected to the patient. SUV_{ROI} = [FDG $uptake_{ROI}$ (MBq/g) x body weight (g)] / injected activity (MBq).

To compensate for background noise, SUV_{ROI} is often normalized by the vascular SUV or the liver SUV that are sensitive to most input or output bias. Even so, use of SUV remains subject to bias, although it is the most common quantitative uptake descriptor in clinical practice[96]. Lastly, partial volume effects also have to be considered and if necessary corrected, especially when the objects' size are less than 2 times the full width at half maximum resolution in x-y and z directors (Nyquist limit).

5.2. Diffusion–weighed imaging

The concept of molecular imaging also belongs to MRI, with sequences evaluating the movement of water molecules (diffusion) in tissues; the so-called (DW-MRI)[97]. In short, on DW-MRI a regular magnetic field inhomogeneity (so-called gradient) is generated for a defined duration and intensity. It results into a shift of the proton precession within the magnetic field. After a few milliseconds, a second magnetic gradient with the same intensity and duration than the first is applied in the opposite direction. The intensity of the resulting magnetization (and hence of the signal) (S) equals the signal before application of the first gradient (S_0), minus intensity related to the spins that have moved off-plane in-between the two gradients.

The relationship between these signals and the apparent diffusion coefficient is given by the equation: S/S0 = exp (-b x ADC), where b is the diffusion factor, which depends on acquisition parameters (field strength, gradient duration...) and ADC is the Apparent Diffusion Coefficient.

As water diffusion is a multidirectional process, ADC in all planes can be calculated by obtaining images with two or more b-values: ADC (x,y,z) = ln [S2 (x,y,z)/ S1 (x,y,z)]/(b1-b2). ADC is directly proportional to the diffusion within the milieu and therefore on the latter's molecular and cellular density. DW-MRI is an emerging technique for clinically important applications such as acute stroke, white matter tract assessment, diagnosis and therapeutic responses in tumors and inflammatory diseases[98-99]. DW-MRI necessitates no ionizing radiation and the actual causes of signaling differ from those of FDG-PET, but are similarly sensitive to the cellular density.

Furthermore, the composite nature of DW-MRI signaling makes it sensitive to perfusion effects at low b-values, the so-called intravoxel incoherent motion, that reflect other important biological process, such as edema, and angiogenesis. Because of an inherently low vascular background signal, DW-MRI may theoretically supplant FDG-PET in the detection of cellular infiltrates. Despite these potential advantages, the DW-MRI findings have, to our knowledge, never been evaluated in aortic aneurysms. Our personal contribution to this debate are reported in the appendix section and consisted: (i) in a figure showing a significant correlation between the aortic wall maximal FDG uptake (SUV) and the minimal ADC values in 5 AAAs; and (ii) a case-report describing DW-MRI findings and clinical outcome in a patient with FDG-avid aortic aneurysm (see additional Publication N° 2).

On both PET and MRI, the development of contrast agents and tracers with organ and/or physiological process-specific affinity support the concept of molecular imaging. The future of molecular imaging lies in combining almost all contrast agents and radiotracers to specific ligands, such as membrane components of macrophages, platelets, oxidized low-density lipoproteins (LDL), and activated endothelia[100-101].

GOAL AND WORK PLAN

AAA: (i) result from imbalance between synthesis and destruction of the ECM as a consequence of polygenic predisposition and exposure to risk factors, (ii) its quiescence or slow growth indicate that the protective mechanisms tend to balance those destroying the ECM, (iii) its growth acceleration and rupture result from a breakdown of this equilibrium towards degradation and weakening, in relation with an internal or an external trigger. Imaging is currently the cornerstone of the secondary prevention of AAA rupture, owing to its ability to detect and evaluate accurately and noninvasively the aneurysm diameter and its growth rate. Given the unpredictable behavior of AAA on a patient basis, we hypothesized that the ability of imaging techniques to assess quantitatively and qualitatively biological mechanisms involved in AAA rupture may provide clues for improved patient-specific risk assessment. Specifically, this dissertation involves two parts:

The part one aims at determining how far imaging biological activities and biomechanical constraints may help clinical decision-making in patients with AAA, and what would be the incremental value versus the diameter-based management. This part includes: The description of FDG uptake and wall stress patterns in AAAs (Publication N°1), translation of the biomechanical risk of rupture into diameter-equivalent and its validation using a large database registry (Publication N°2) and assessment of the correlation between imaging-derived biomechanical estimates and FDG uptake and it determinants, as well as patient outcomes with regard to imaging findings (Publication N°3).

The part two aims at finding new and promising imaging concepts for the assessment of biological processes in AAAs. This part includes: Description of MRI features of AAA, with emphasis on ILT appearance, iron content and its phagocytic and proteolytic activities (Publication N°4), determination of growth rates in a rat model of AAA after aortic infusion of elastase to emphasize the concept of the deleterious role of ILT and the ability of MRI to evaluate its biological activities via iron content assessment (Publication N°5, submitted).

PART ONE: Clinical value of FDG PET and imaging-derived biomechanical estimates in patients with AAA

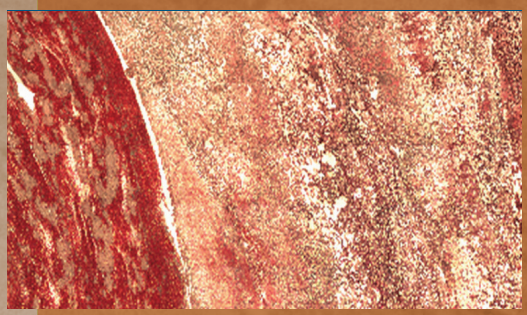
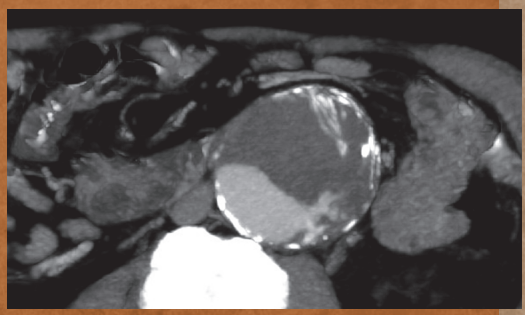
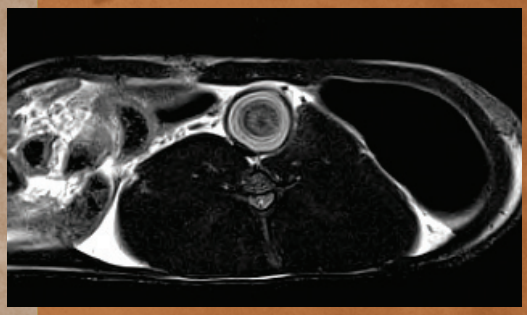
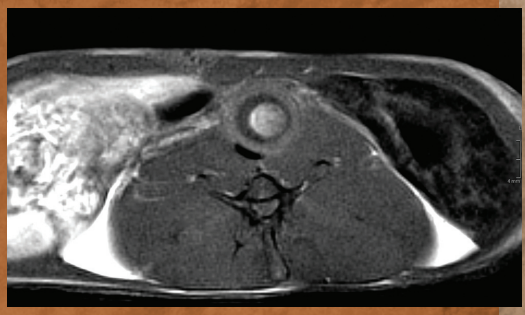

"Progress means getting nearer to the place you want to be. And if you have taken a wrong turning, then to go forward does not get you any nearer..."

Clive Staples Lewis
Novelist, Poet and Professor of Literature 1898-1963

..."But sometimes, the unexpected awaits you, while persisting in heresy"

Robert F Dondelinger
Professor of Radiology

Introduction to biomechanical estimates from imaging data: geometry-based models and simulations

Contrast-enhanced tridimensional cross-sectional imaging is increasingly used to estimate the biomechanical forces that exert on the arterial wall components. Imaging-based simulations aim at estimating, amongst other, the wall stress (ie: unit of force per unit area, N/cm^2). Wall stress estimate accounts for vessel geometry, fluid dynamics and elastic/rupture properties of the vessel wall components studied ex vivo. Considering that vessel rupture occurs when the wall stress exceeds its strength, these estimates provide unique and valuable information regarding risk stratification in AAA[51]. The computations providing biomechanical estimates are detailed in the appendix section of publication N°2. They include several steps that can be summarized as follows: (i) definition of the model and its various components (ie: circulating channel, ILT, wall outer limit) using three-dimensional representation of the vessel segment (Figure 9). A theoretical thickness is assigned to the wall covered by ILT, as it is generally not visible. (ii) the geometry described is divided into a high number of finite elements[102], (iii) this hypothetical and deformable model[103] is then pressurized by the mean arterial pressure (1/3 of systolic blood pressure + 2/3 diastolic pressure), and (iv) the longitudinal, axial and circumferential forces on each of the elements are estimated and summed into one force vector, the so-called Von Mises stress. Currently, these analyses cannot be performed on all multimodality imaging platforms, but the generated reports can be stored on picture archive communicating systems, along other patient's data files (Figure 10).

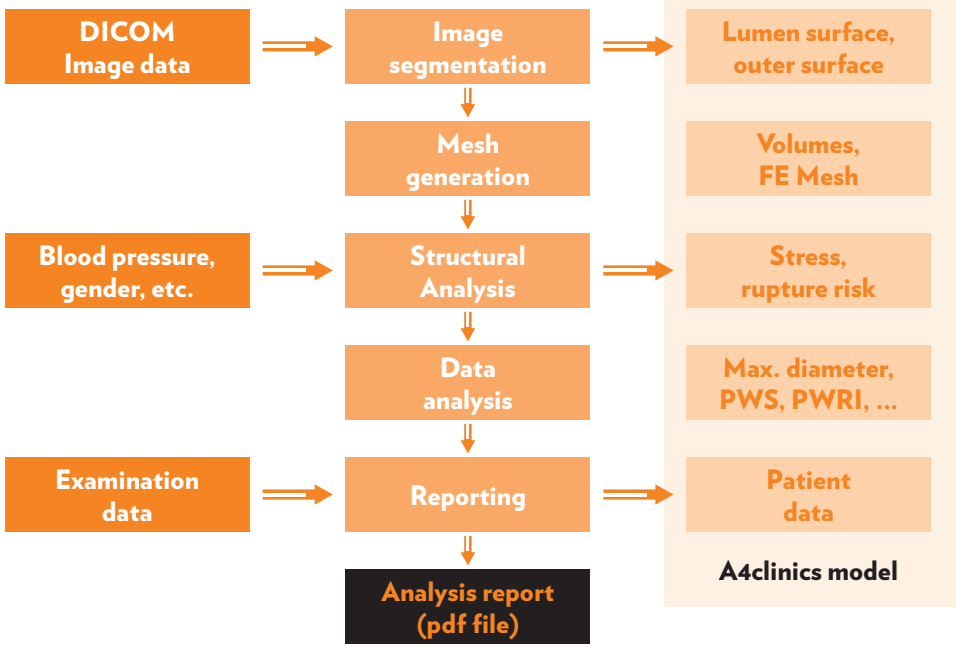

Figure 9 : Graph analysis of patient-specific finite element analysis and reporting steps (Unpublished data).

Shear stress from flowing blood is another important component of the wall stress, as it plays a role in platelet activation and convection[104-105]. Nevertheless it is often analyzed separately from Von Mises stress, because its estimation requires inflow data that are not available on tridimensional CT or MRI.

Lastly, wall stress should not be confused with wall compliance, which is directly proportional to its elastic properties and a measure of the propensity of the wall to expand under the pressure (ie: inverse pressure; $mmHg^{-1}$). Technically, the compliance is studied by synchronizing continuous imaging with electrocardiogram and pressure measurement.

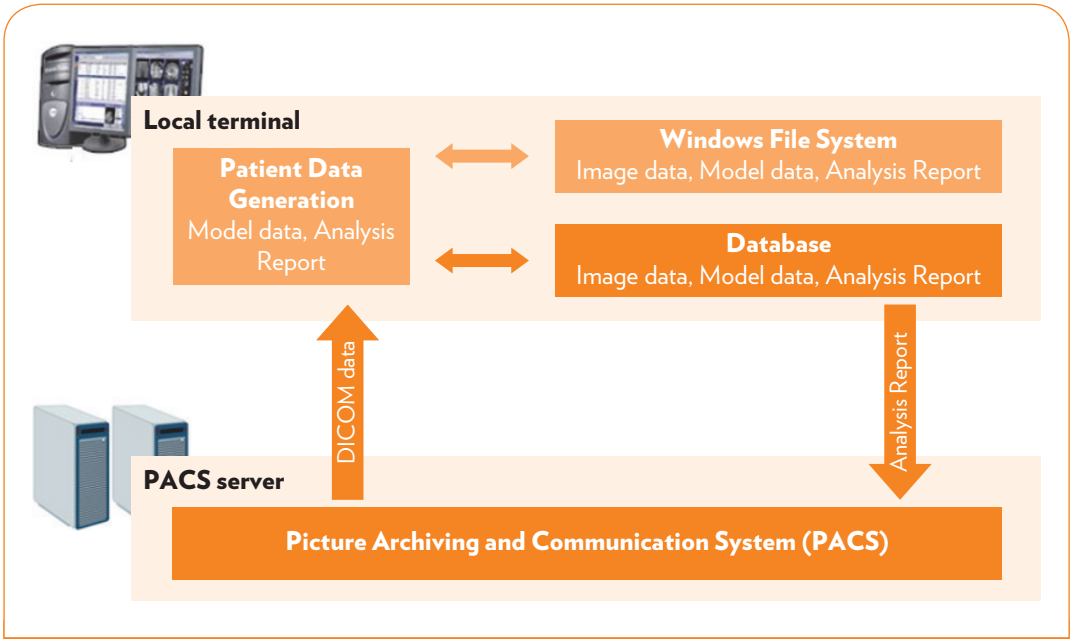

Figure 10 : Graph integration of finite element analysis report to picture archiving communication system (Unpublished data).

1. Publication N°1: High levels of 18F-FDG uptake in aortic aneurysm wall are associated with high wall stress

1.1. Introduction

Both wall stress and biological activities are major players, increasingly recognized as hallmarks of AAA progression. They can be evaluated respectively using FES and FDG PET. We aimed at investigating their respective distribution with respect to the clinical outcomes. Five aortic aneurysms (3 TAAs and 2 AAAs) with foci of increased FDG uptake on PET were evaluated by FES. Areas of maximum aortic wall stress and high FDG uptake were localized by co-registration to CT using anatomical landmarks.

1.2. Findings summary

The aneurysm diameter range was 46-60 mm. The study showed that the wall stress is non-uniform in aortic aneurysms. In all cases, areas of high FDG uptake corresponded to those displaying increased wall stress. During the follow-up, three patients had aneurysm-related events including death, dissection and emergency surgery. The originating site for these events corresponded topographically to areas of increased FDG uptake and wall stress.

1.3. Conclusions

The so-called "hot spots" on both FDG PET and FES tend to co-localize, and to be associated with poor outcomes. This warrants further studies with larger samples.

1.4. Reassessment summary/opportunities

Establishing a correlation between FDG uptake and wall stress is possible on ROI basis. However, wall stress imaging may not be able to dictate patient management by providing a dichotomous ("positive/negative") report such as FDG PET. Causes for the intra-individual heterogeneities in the distribution of wall stress and FDG uptake should be investigated, especially to determine the effect of the ILT that has theoretically impact on both.

Publication N° 1

This subchapter has been published as:

High levels of 18F-FDG uptake in aortic aneurysm wall are associated with high wall stress

X.Y. Xu, A. Borghi, A. Nchimi, J. Leung, P. Gomez, Z. Cheng, J.O. Defraigne, N.Sakalihasan

European Journal of Vascular and Endovascular Surgery, 2010 (39), 295-301

Eur J Vasc Endovasc Surg (2010) **39**, 295–301

High Levels of 18F-FDG Uptake in Aortic Aneurysm Wall are Associated with High Wall Stress

X.Y. Xu [a], A. Borghi [a], A. Nchimi [b], J. Leung [a], P. Gomez [c], Z. Cheng [a], J.O. Defraigne [d], N. Sakalihasan [d,*]

[a] *Department of Chemical Engineering, Imperial College London, UK*
[b] *Department of Radiology, CHC, Liege, Belgium*
[c] *Department of Nuclear Medicine, CHC, Liege, Belgium*
[d] *Department of Cardiovascular Surgery, University Hospital of Liege, Liege, Belgium*

Submitted 28 June 2009; accepted 20 October 2009
Available online 18 November 2009

KEYWORDS
Aneurysm;
Aorta;
Wall stress;
PET-CT examination

Abstract *Background:* Functional imaging using positron emission tomography (PET) showed increased metabolic activities in the aneurysm wall prior to rupture, whereas separate studies using finite element analysis techniques found the presence of high wall stresses in aneurysms that subsequently ruptured. This case series aimed to evaluate the association between wall stress and levels of metabolic activities in aneurysms of the descending thoracic and abdominal aorta.
Methods: Five patients with aneurysms in the descending thoracic aorta or abdominal aorta were examined using positron emission tomography–computed tomography (PET-CT). Patient-specific models of the aortic aneurysms were reconstructed from CT scans, and wall tensile stresses at peak blood pressure were calculated using the finite element method. Predicted wall stresses were qualitatively compared with measured levels of 18F-fluoro-2-deoxy-glucose (18F-FDG) uptakes in the aneurysm wall.
Results: The distribution of wall stress in the aneurysm wall was highly non-uniform depending on the individual geometry. Predicted high wall stress regions co-localised with areas of positive 18F-FDG uptake in all five patients examined. In the two ruptured cases, the locations of rupture corresponded well with regions of elevated metabolic activity and high wall stress.
Conclusions: These preliminary observations point to a potential link between high wall stress and accelerated metabolism in aortic aneurysm wall and warrant further large population-based studies.

* Corresponding author. Tel.: +32 436 67163; fax: +32 4366 7164.
E-mail address: nsaka@chu.ulg.ac.be (N. Sakalihasan).

1078-5884/$36
doi:10.1016/j.ejvs.2009.10.016

Abdominal aortic aneurysm (AAA) is an important cause of deaths in Western society, especially among elderly patients. Rupture of AAA is responsible for approximately 1.3% of all deaths in men.[1] The fact that not all AAA would eventually rupture has created a dilemma for surgeons with regard to treatment choice: Is it necessary to operate on all patients, or should we reserve prophylactic surgery only for a subgroup where factors indicative of a probable rupture could be identified? Diameter of the aneurysm is the most important factor in the decision to repair an aneurysm, but rate of enlargement is usually taken into account where watchful surveillance is employed for sub-surgical cases.2

On the one hand, although the size of the aneurysm still remains the most widely accepted predictor of rupture, small AAAs may also rupture. In their preliminary study, Sakalihasan et al.[3] by means of combined positron emission tomography and computed tomography (PET-CT) examination, observed positive correlation between clinically unstable AAA and positive uptake of 18F-fluoro-2-deoxyglucose (FDG) in the aneurysm wall. Elevated FDG uptake was also related to the presence of a high density of inflammatory cells (e.g. macrophages and lymphocytes) in the aneurysmal aortic wall.[4] These observations have been confirmed by recent clinical and fundamental studies on in vivo demonstration of inflammatory cells using PET-CT.[5-6]

On the other hand, recent biomechanics studies using finite element analysis and patient-specific geometries of AAAs derived from CT scans have demonstrated that peak wall stress could be a better indicator of rupture than diameter.[7-10]

The role of biomechanical forces in the formation, propagation and ultimate rupture of aortic aneurysms has received some attention and is beginning to be better understood. Certain key mechanisms can be outlined. The initial change in the formation of an aneurysm is structural and results from a degenerative process in the vascular wall. As the morphology changes, related changes occur in the blood flow pattern, with consequential modification of fluid stresses and their interaction with the mechanical stresses within the arterial wall. The objective of this study was to investigate the role of increased metabolism in aneurysm rupture and whether this is linked with mechanical forces experienced by the affected aorta, by a combination of function imaging using PET and finite element stress analysis based on patient-specific data.

Materials and Methods

Patients

Since the first pilot study by Sakalihasan et al.[3] PET-CT examination has been performed routinely on almost all patients referred to the Department of Cardiovascular Surgery at the University Hospital of Liege, with known aortic aneurysms diagnosed initially by CT scans. Among 131 patients, the first three patients with thoracic aortic aneurysms (TAAs) in the descending aorta and two patients

with abdominal aortic aneurysms (AAAs) with high FDG uptakes were included in this study. All patients had the first PET-CT examination within 2 weeks from the initial diagnostic contrast-enhanced CT scan. Thereafter, they were monitored by follow-up CT or PET-CT examinations or underwent surgical repair. The study protocol was approved by the University Hospital of Liege local ethics review board and a written informed consent and authorisation to use the images for research were obtained from the patients or their relatives.

PET-CT imaging

The PET-CT examination was performed by following the procedure described by Burger et al.[11] After a minimum of 6-h fasting, 3.7 mBq F18-FDG per kilogram body weight was injected through a peripheral vein catheter. The patient was placed in a quiet room and instructed not to move. One hour after injection of the tracer, static whole-body examination was performed with a PET-CT scanner (Discovery LS, GE Healthcare). The CT component of this scanner can acquire eight slices per X-ray tube rotation. After scout views, continuous CT was performed from the skull base to the femoral necks with the following parameters: 5 mm collimation, 50 x 50 cm field-of-view (FOV), 140 mA and 140 kVp, pitch of 1.5:1 and gantry rotation cycle of 0.8 s. The patients were asked to breath shallowly during CT data acquisition.

Emission and transmission images were recorded 60 min after the F18-FDG injection, at each couch position for 4-5 and 2-3 min, respectively. PET data were acquired as six consecutive coronal 4.25-mm-slice-thickness 2D scans in all patients, overlapping from 15-30% PET raw data, were reconstructed by means of ordered subset expectation maximisation (pixel matrix of 128 x 128 and FOV of 50 cm), with 5.86 mm full width at half maximum (FWHM) post filter and 3.91 mm FWHM loop filter model-based scatter correction (convolution subtraction) and normalisation correction. Additional attenuation correction was performed on PET data, using the CT raw data.[11] Attenuationcorrected PET and reformatted CT data were fused on a dedicated workstation (Advantage Windows, release 4.4.07, GE Healthcare). Both uncorrected and attenuationcorrected images were assessed to identify potential artifacts. The FDG uptake was defined as high when the maximum Standardised Uptake Value (SUV max) was greater than 2.5.

3D geometry reconstruction

The contrast-enhanced CT images were processed using our in-house MATLAB-based image processing toolkit, which has been tested extensively for accuracy and reproducibility. [12-13] The lumen boundary was segmented semiautomatically by using the region growing method (RGM),[14] which traces the perimeter of the lumen by seeking pixels of a selected range of intensities.

Before applying the RGM, images were pre-processed by using a Gaussian filter to reduce the noise and improve image clarity. The segmented lumen contours were then assembled in 3D, and the lumenal surface was constructed by using cubic B splines. Similar procedures were followed

for the segmentation and reconstruction of the outer wall surface. Since all patients included in this study presented intra-luminal thrombus (ILT) in their aneurysms, ILT was also reconstructed and included in the finite element stress analysis model. Owing to the low contrast between arterial wall and ILT in CT images, it was not possible to distinguish the wall from thrombus; therefore, the inner wall boundary was generated by shrinking the outer wall boundary by a constant thickness, which was determined using an average value of 12 measurements made at sections where wall thickness was clearly defined (usually in the region where the thrombus was not present).

Finite element stress analysis

Stress analysis was performed for all the reconstructed aneurysm models by using a finite element method code ADINA 8.2 (Automatic Dynamic Incremental Nonlinear Analysis, Watertown, MA, USA). Since arterial walls exhibit non-linear behaviour and undergo large strains, a finite strain constitutive equation was employed.

This was based on the two-parameter hyper-elastic constitutive model derived by Raghavan and Vorp,[15] specifically suited for aortic aneurysms with corresponding material properties obtained from uniaxial tensile testing carried out on aneurysm tissue specimens. Each aneurysm model consisted of the arterial wall domain, including both wall and thrombus, where present. The thrombus was treated in a similar way to the aortic wall but with different material properties, as reported by Wang et al.[16] A uniform load (corresponding to the peak systolic pressure) was applied on the inner surface of the aneurysm models in the direction normal to the surface.

Suitable boundary conditions were applied at the two ends, where rotations and translations were constrained to simulate the tethering to the rest of the aorta. For the wallethrombus boundary, the same number of elements was used; therefore the displacement was continuous across the two domains.

Patient	Sex	Age (years)	Localisation of aneurysm	Inital Diameter[a] (mm)	Follow-up (months)	Last Diameter (mm)	Outcome
1	male	75	thoracic	46	8	70	Died from rupture
2	female	73	thoraco-abdominal	48	30	56	Type B dissection
3	female	74	thoraco-abdominal	46	36	49	Died unrelated causes
4	male	70	abdominal	67	1	67	Elective surgery
5	male	87	abdominal	60	7	60	Surgery for ruptured AAA

[a] Diameter at the time of the PET/CT examination.

Table 1 The characteristics and outcome of the patients.

Results

PET-CT examinations

The characteristics and outcome of the patients are summarised in Table 1. Patient 1 with a TAA (initial diameter 46 mm) declined any surgical treatment despite having a high FDG uptake in the terminal segment of the descending thoracic aorta, which was also rapidly expanding. Six months later, the patient was admitted to hospital with dorso-lumbar pain. CT examination performed immediately revealed a markedly larger and ruptured terminal thoracic aorta (Fig. 1).

Patient 2 was monitored over 2 years with regular PETCT examinations for TAA. Intermediate PET-CT revealed high FDG uptake and an increasing aneurysm diameter (56 mm) of the descending thoracic aorta. Despite the proposal of endovascular repair, this patient refused any treatment. Unfortunately, she presented Type B dissection diagnosed by PET–CT examination.

Patient 3 was followed up for 3 years with diffusemoderate uptake of the FDG at the level of the descending thoracic aorta. She died from unrelated causes.

Patient 4 underwent resection of a large inflammatory abdominal aortic aneurysm (IAAA) with increased uptake of FDG at the neck of the aneurismal sac (Fig. 2).

The last patient (patient 5) having a diffuse pattern of FDG uptake at the edge of intra-luminal thrombus on the anterior wall, and the junction between the neck and AAA sac on the posterior wall, refused any operation. Seven months later, he was admitted to the emergency department with back pain. A CT examination performed immediately confirmed the suspected clinical diagnosis of early stage AAA rupture (leaking) at the junction between the neck and AAA sac on the posterior wall (Fig. 3). Expanded retro-peritoneal haematoma was observed during surgery.

Wall stress patterns

Our finite element analysis of wall stress shows that the stress distribution is highly dependent on the 3D geometric features of the aneurysms, and that areas of maximum stress do not occur at the maximum diameter. In the case of patient 1 (Fig. 1A(b)), there are two concentrated regions of elevated wall stress, but the peakwall stresswas found in the distal part of the aorta (marked by a black triangle). In patient 4 (Figs. 2A(c) and 2B(a)), the maximum stress is located approximately 5 mm below the renal arteries, in the anterior aspect of the aneurysm neck, but the overall stress levels are low owing to the thick thrombus. In patient 5, high wall stress can be seen in the anterior aspect of the aneurysm neck (Fig. 3(e)) and local stress concentration at the junction between the neck and aneurysm sac in the posterior side (not shown here) where fluid wall shear stress was found to be high (Fig. 3(f)).

Comparison with PET images

Since the finite element models were constructed from contract-enhanced CT images, matching the wall stress analysis results and the corresponding PET-CT images has to be performed carefully. This was achieved with the aid of anatomical landmarks, such as the renal arteries or the aortic bifurcation. The vertical distance to or from the anatomical landmarks were calculated and used to find the correspondence between the two data sets. It can be seen from Figs. 1A and 1B where wall stress contours in a vertical section (1A(b)) and a horizontal section (1B(b)) of the TAA in patient 1 are compared with the corresponding PET-CT images. It is clear that there was a high level of FDG uptake in the terminal aorta. Rapid expansion of the TAA at this location was confirmed by subsequent scans and the aneurysm eventually ruptured at approximately the same location. It is interesting to note that levels of wall stress were also high in this region (shown in red). The horizontal plot further demonstrates that the location of high wall stress at this section correlates well with the site of high FDG uptake shown by the PET-CT fusion image (Fig. 1B(a)). CT scan performed 6 months after the PET-CT examination revealed covered rupture of the TAA and a much enlarged terminal aorta (93 mm) at the same site as shown in Fig. 1B(c). And the finite element model (based on the geometry 6 months prior to rupture) predicted high levels of wall stress at the location of rupture.

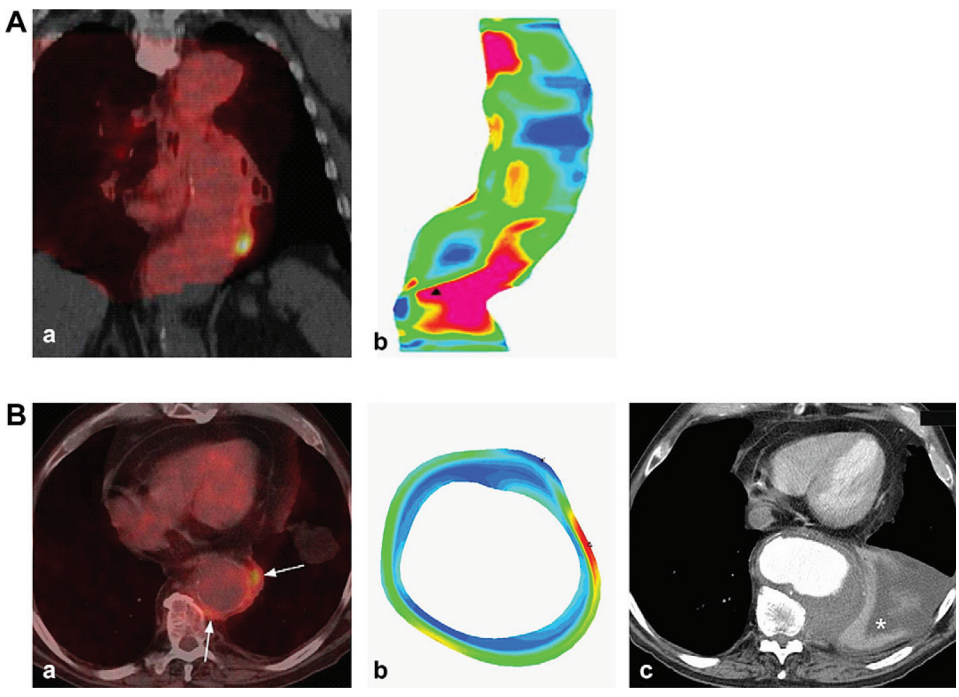

Figure 1 A. PET-CT fusion image of the TAA in patient 1 (a) showing positive 18-FDG uptake in the terminal aorta, and the corresponding wall stress contours (b). The location of peak wall stress is indicated with a black triangle. B. Transverse images of fused PET-CT in the terminal thoracic aorta of patient 1 at initial examination (a), predicted wall stress contours at the same location (b), and contrast-enhanced CT acquired 6 months later (c) showing a markedly larger and ruptured descending aorta, associated with left pleural effusion (white asterisk).

Similar correspondence between areas of high wall stress and sites of elevated FDG uptake has also been found for the other patients examined. Figs. 2A and 2B show the comparison of high wall stress region in the aneurysm neck of patient 4 and the corresponding PET-CT image revealing elevated FDG uptake at the same location. This observation has significant clinical importance since the FDG uptake and high wall stress region was close to the renal arteries and the proximal suture following aneurysm resection of this patient was placed just below the renal arteries but at the top of this region.

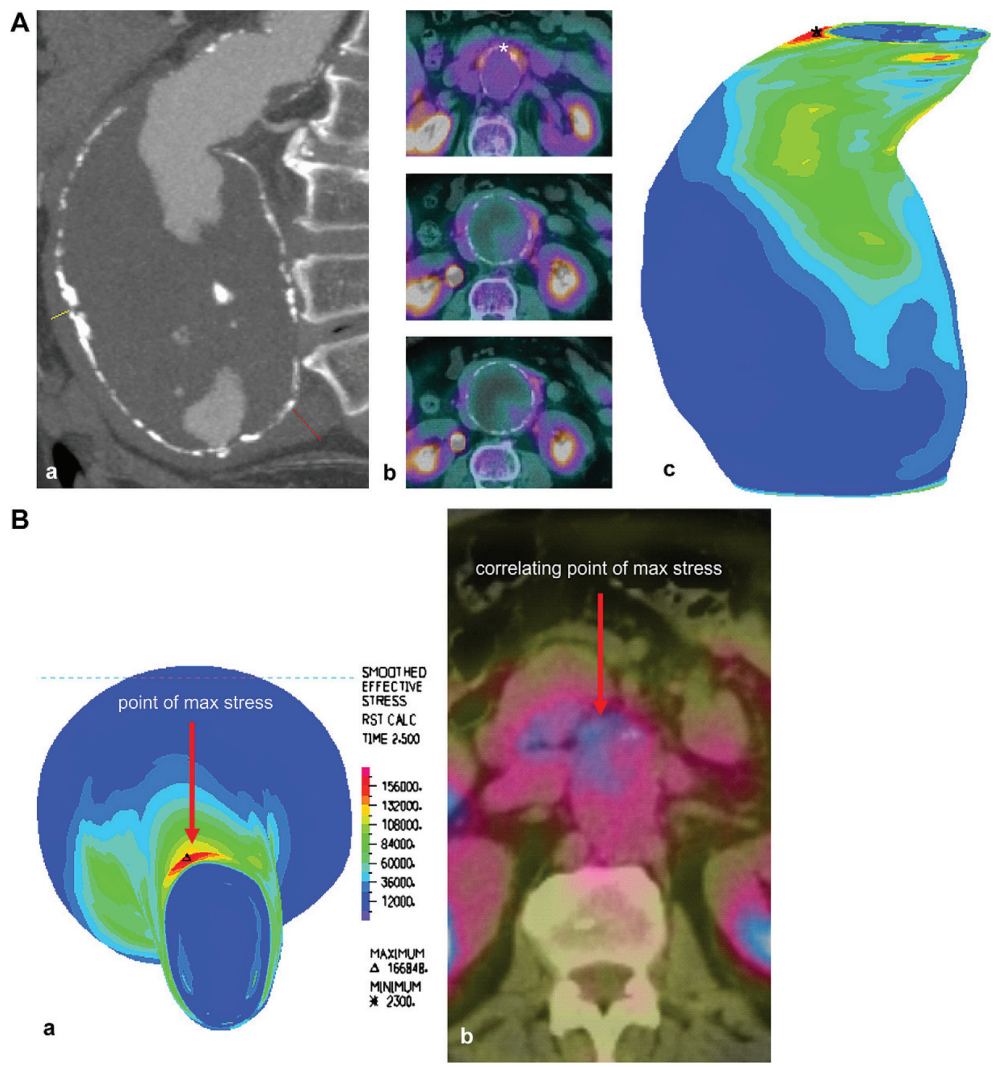

Figure 2 A. CTimage of the inflammatory AAA in patient 4 (a), transverse images of fused PET-CT (b) showing positive 18-FDG update in the aneurysm neck, and the predicted wall stress (c). B. Top view of the predicted wall stress in the AAA of patient 4 (a) and the corresponding PET image (b) showing good correspondence between locations of high wall stress and positive 18-FDG uptake.

If the suture was performed lower (i.e. closer to the level of increased metabolism identified by PET-CT), the risk of recurrent AAA or false aneurysm at the level of the suture would be higher. This was reinforced by the finite element analysis, although wall stress results were not available at the time of resection.

In patient 5, maximum wall stress (Fig. 3(e)) was found to correlate with one of the regions showing positive FDG uptake on initial PET-CT scan (Fig. 3(a)). A suspected early rupture of AAA on the posterior wall was confirmed on subsequent CT examinations performed 6 months after the initial PET-CT scan. As shown in Figs. 3(b) and (c), the AAA started leaking (early sign of rupture) at the junction between its neck and sac where both wall stress concentration and fluid shear stress (shown in Fig. 3(f)) were relatively high. The AAA neck was found to have expanded from 40 mm to 42 mm during the 6-month period.

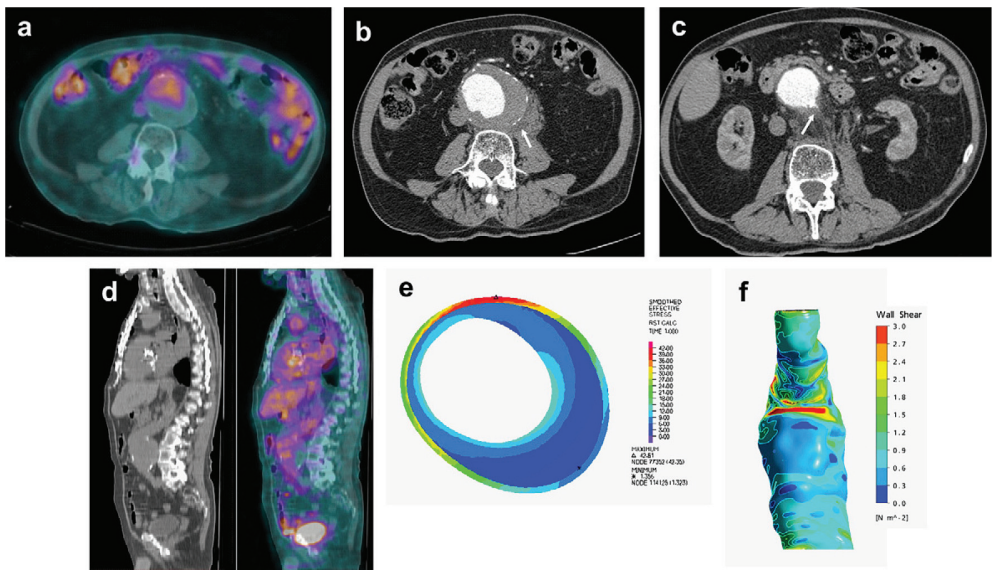

Figure 3 PET-CT images of the AAA in patient 5 (a) and (d) acquired at initial examination, and contrast-enhanced CT images acquired 6 months later showing early stage of rupture (white arrow) at the junction between the neck and AAA sac on the posterior wall (b), and at a distal section (c) showing peritoneal haematoma (white arrow). Predicted wall stress based on initial CT images is shown in (e) for a transverse section corresponding to the same location as (a), and predicted wall shear stress contours (f).

Discussion

Inflammation and media cell death are important biological activities involved in aneurysm growth. PET can help locate and measure metabolic activity of cells: PET is a technique that can produce image maps of functional processes in the body. It is based on the use of a short-lived radioactive tracer isotope, which has been chemically incorporated into a metabolically active molecule and injected into a living subject through the blood circulation.

The radioactive tracer decays by emitting a positron; the most commonly used molecule for this purpose is fluorodeoxyglucose (FDG). This technique is usually used for the detection of tumours, since FDG uptake into malignant cells is enhanced by an increased expression of glucose transport molecules on the tumour cell surface. However, FDG uptake is not specific for tumours. FDG-PET can also be positive in inflammatory disease and atherosclerotic lesions,[17] as part of FDG is taken by macrophages and other blood cells. The macrophage glycolisis generates the signal that reaches the scanner.

In a previous study, we investigated the clinical use of PET for detecting increased metabolic activity in the aneurysm wall and concluded that PET imaging has the capacity to assess increased metabolic activity within the aneurysm wall.[3] A subset of aneurysms showed increased 18-FDG uptakes, suggestive of a focally accelerated metabolism. This FDG uptake in the aneurysm wall probably reflects the presence of a high density of inflammatory cells (e.g. macrophages and lymphocytes) in the adventitia, as previously described. The activated inflammatory cells might correspond to the increased metabolic activity seen on PET imaging.[4] These preliminary observations have been confirmed recently by a study performed by Reeps et al.[5] In their study, increased FDG uptake was found in patients with a very high macrophage activity and symptomatic AAA.

However, in agreement with the reports of Sakalihasan and Truijers et al.[3, 6] these authors failed to find a correlation between maximum standard uptake value (SUV) and maximum cross-sectional infrarenal AAA diameter, which may predispose to rapid growth and/or imminent rupture. In the present study, five patients with expanding aneurysms were detected by PET-CT, and the expansion was found at the level of the aorta where elevated metabolic activity of the aortic wall was present. The corresponding CT images were processed separately and blindly to construct patient-specific models for finite element wall stress analyses. Our computational results showed highly non-uniform distribution of stress in the aneurysm walls due to their complex geometry.

Moreover, the predicted high wall stress zones co-localised with the sites of positive FDG uptake in all five patients examined, and the location of rupture (for patient 1 and 5), and dissection (for patient 3). This observation reinforced our hypothesis that there exists a possible correlation between 18-FDG uptake by the aneurysm wall and the triggering processes leading to aortic aneurysm rupture. PET imaging, combined with biomechanical analysis, could potentially help us make more reliable decisions on the need for surgical repair of aortic aneurysms.

Conclusion

The main conclusions that can be drawn from our investigation on a small number of patients are as follows: (1) there is a potential link between accelerated metabolism in aortic aneurysm wall and high mechanical stresses experienced by the wall; and (2) PET imaging combined with wall stress analysis could potentially give more reliable predictions of the risk of aneurysm rupture. Moreover, PET-CT scan and finite element analysis are able to monitor the development and evolution of AAA. However, further large population-based studies are needed to confirm our preliminary findings. Conflict of Interest The authors have no conflict of interest. Acknowledgements This study was partially supported by a grant from the University of Liege 'Crédit d'impulsion.' The cardiovascular surgery department in Liège is supported by the European Union integrated project "FightingAneurysmal Disease"(FAD, http://www.fighting-aneurysm.org/).

Conflict of Interest

The authors have no conflict of interest.

Acknowledgements

This study was partially supported by a grant from the University of Liege 'Crédit d'impulsion.' The cardiovascular surgery department in Liège is supported by the European Union integrated project "FightingAneurysmal Disease"(FAD, http://www.fighting-aneurysm.org/).

References

1. Sakalihasan N, Limet R, Defawe OD. Abdominal aortic aneurysm. Lancet 2005;365(9470):1577-89.
2. Brewster DC, Cronenwett JL, Hallett Jr JW, Johnston KW, Krupski WC, Matsumura JS. Guidelines for the treatment of abdominal aortic aneurysms. Report of a subcommittee of the Joint Council of the American Association for Vascular Surgery and Society for Vascular Surgery. J Vasc Surg 2003;37:1106-17.
3. Sakalihasan N, Van Damme H, Gomez P, Rigo P, Lapiere CM, Nusgens B, Limet R. Positron emission tomography (PET) evaluation of abdominal aortic aneurysm (AAA). Eur J Vasc Endovasc Surg 2002;23:431-6.
4. Defawe OD, Hustinx R, Defraigne JO, Limet R, Sakalihasan N. Distribution of F-18 fluorodeoxyglucose (F-18 FDG) in abdominal aortic aneurysm: high accumulation in macrophages seen on PET imaging and immunohistology. Clin Nucl Med 2005 May; 30(5):340-1.
5. Reeps Ch, Essler M, Pelisek J, Seidl S, Eckstein HH, Krause BJ. Increased 18F-fluorodeoxyglucose uptake in abdominal aortic aneurysms in positron emission/computed tomography is associated with inflammation, aortic wall instability, and acute symptoms. J Vasc Surg 2008;48(2):417-23.
6. Truijers M, Kurvers HA, Bredie SJ, Oyen WJ, Blankensteijn JD. In vivo imaging of abdominal aortic aneurysms; increased FDG uptake suggests inflammation in the aneurysmal wall. J Endovasc Ther 2008;15(4):462e7.
7. Thubrikar MJ, Al-Soudi J, Robicsek F. Wall stress studies of the abdominal aortic aneurysm in a clinical model. Ann Vasc Surg 2001;15:355-66.
8. Venkatasubramaniam AK, Fagan MJ, Mehta T, Mylankal KJ, Ray B, Kuhan G, et al. A comparative study of aortic wall stress using finite element analysis for ruptured and non-ruptured abdominal aortic aneurysms. Eur J Vasc Endovasc Surg 2004;28: 168-76.
9. Fillinger MF, Marra SP, Raghavan ML, Kennedy FE. Prediction of rupture risk in abdominal aortic aneurysm during observation: wall stress versus diameter. J Vasc Surg 2003;37:724-32.
10. Fillinger MF, Raghavan ML, Marra SP, Cronenwett JL, Kennedy FE. In vivo analysis of mechanical wall stress and abdominal aortic aneurysm rupture risk. J Vasc Surg 2002;36:589-97.
11. Burger C, Goerres G, Schoenes S, Buck A, Lonn AHR, von Schultess GK. PET attenuation coefficients from CT images: experimental evaluation of the transformation of CT into PET 511-keV attenuation coefficients. Eur J NuclMed2002;29:922-7.
12. Leung JH. Determination of flow patterns and stresses in patient-specific models of abdominal aortic aneurysm. PhD thesis, Imperial College London;2006.
13. Leung JH, Wright AR, Cheshire N, Crane J, Thom SA, Hughes AD, et al. Fluid structure interaction of patient specific abdominal aortic aneurysms: a comparison with solid stress models. BioMed Eng Online 2006;5:33.
14. Gonzalez RC, Woods RE. Digital image processing. Upper Saddle River, New Jersey: Prentice-Hall Inc; 2002.

15. Raghavan ML, Vorp DA. Toward a biomechanical tool to evaluate rupture potential of abdominal aortic aneurysm: identification of a finite strain constitutive model and evaluation of its applicability. J Biomech 2000;33:475-82.
16. Wang DH, Makaroun M, Webster MW, Vorp DA. Mechanical properties and microstructure of intraluminal thrombus from abdominal aortic aneurysm. J Biomech Eng 2001;123:536-9.
17. Tawakol A, Migrino RQ. Noninvasive in vivo measurement of vascular inflammation with F-18 fluorodeoxyglucose positron emission tomography. J Nucl Cardiol 2005;12:294-301.

2. Publication N°2: A novel strategy to translate the biomechanical rupture risk of abdominal aortic aneurysms to their equivalent diameter risk: Method and retrospective validation

2.1. Introduction

AAA rupture risk management is based on the maximum diameter; a diameter of 55 mm or more is generally accepted as an indication for repair in males, although other risk factors exist. Peak Wall Stress (PWS) and Peak Wall Rupture Index (PWRI) discriminate better ruptured and non-ruptured aneurysms than the maximum diameter. Specifically, the PWRI relates mechanical stress to the strength of the aneurysm wall. It incorporates risk factors associated with aneurysm wall weakening, such as female gender and ILT thickness. No clinical trial, however, has investigated threshold values of these parameters for AAA repair. Consequently they have limited clinical relevance. Using 203 and 40 CT datasets, respectively from non-ruptured and ruptured AAAs, we evaluated the concept of risk-equivalent diameters. Risk-equivalent diameters result from the translation of the estimates of biomechanical rupture risk to a diameter of an "average aneurysm patient" with a similar risk of rupture, defined as the mean PWRI-diameter response of our non-ruptured patient cohort, weighted by the gender ratio of the UK small aneurysm trial.

2.2. Findings summary

With respect to the maximum AAA diameter, PWS increased linearly while PWRI increased exponentially. The latter finding reflects the known nonlinear increase of the annual risk of rupture with increasing aneurysm size. A size-adjusted analysis showed that PWS-equivalent and PWRI-equivalent diameters were significantly increased in ruptured cases when compared to non-ruptured controls, respectively. In non-ruptured cases the PWRI-equivalent diameters were significantly increased in females as compared to males.

2.3. Conclusions

The concept of equivalent diameters links biomechanical estimates to basic conclusions drawn from large diameter-based clinical AAA trials, and hence supports a sound clinical interpretation of biomechanical stimulations. Finally, our retrospective and size-adjusted validation analysis verified that biomechanical risk indicators are higher in ruptured than non-ruptured cases.

2.4. Reassessment summary/opportunities

PWRI-equivalent diameter facilitates a straightforward interpretation of biomechanical analyses and connects to diameter-based guidelines for AAA repair indication. PWRI-equivalent diameter reflects an additional diagnostic parameter that may provide more accurate data for AAA repair indication. The impact of the equivalent-diameter biomechanical parameters on clinical decision-making should therefore be assessed through (a) randomized trial(s).

Publication N° 2

This subchapter has been published as:

A novel strategy to translate the biomechanical rupture risk of abdominal aortic aneurysm to their equivalent diameter risk: method and retrospective validation

T.C. Gasser, A. Nchimi, J. Swedenborg, J. Roy, N. Sakalihasan, D. Böckler, A. Hyhlik-Dürr

European Journal of Vascular and Endovascular Surgery, 2014 (3):288-95

A Novel Strategy to Translate the Biomechanical Rupture Risk of Abdominal Aortic Aneurysms to their Equivalent Diameter Risk: Method and Retrospective Validation

T.C. Gasser [a,*], A. Nchimi [b], J. Swedenborg [c], J. Roy [c], N. Sakalihasan [b,d], D. Böckler [e], A. Hyhlik-Dürr [e]

[a] Department of Solid Mechanics, Royal Institute of Technology (KTH), Stockholm, Sweden
[b] Department of Vascular Surgery, University Hospital of Liège, Liège, Belgium
[c] Department of Vascular Surgery, Karolinska University Hospital and Institute, Stockholm, Sweden
[d] St Joseph Hospital, Department of Medical Imaging, Liège, Belgium
[e] Department of Vascular Surgery, University of Heidelberg, Heidelberg, Germany

WHAT THIS PAPER ADDS

Reported biomechanical abdominal aortic aneurysm (AAA) rupture risk assessment studies suffer from severe limitations such as high operator variability, small sample sizes, and clinically difficult interpretation of the results. The present paper used a gender-specific computational method of low operator variability and tested the biomechanical rupture risk assessment on the largest patient cohort so far. The concept of equivalent diameters relates biomechanical results to basic conclusions drawn from large clinical AAA trials, and hence supports a sound clinical interpretation of biomechanical results. Finally, the retrospective and size-adjusted analysis verified that biomechanical risk indicators are higher in ruptured than non-ruptured cases.

Objective: To translate the individual abdominal aortic aneurysm (AAA) patient's biomechanical rupture risk profile to risk-equivalent diameters, and to retrospectively test their predictability in ruptured and non-ruptured aneurysms.

Methods: Biomechanical parameters of ruptured and non-ruptured AAAs were retrospectively evaluated in a multicenter study. General patient data and high resolution computer tomography angiography (CTA) images from 203 non-ruptured and 40 ruptured aneurysmal infrarenal aortas. Three-dimensional AAA geometries were semi-automatically derived from CTA images. Finite element (FE) models were used to predict peak wall stress (PWS) and peak wall rupture index (PWRI) according to the individual anatomy, gender, blood pressure, intraluminal thrombus (ILT) morphology, and relative aneurysm expansion. Average PWS diameter and PWRI diameter responses were evaluated, which allowed for the PWS equivalent and PWRI equivalent diameters for any individual aneurysm to be defined.

Results: PWS increased linearly and PWRI exponentially with respect to maximum AAA diameter. A size-adjusted analysis showed that PWS equivalent and PWRI equivalent diameters were increased by 7.5 mm ($p = .013$) and 14.0 mm ($p < .001$) in ruptured cases when compared to non-ruptured controls, respectively. In non-ruptured cases the PWRI equivalent diameters were increased by 13.2 mm ($p < .001$) in females when compared with males.

Conclusions: Biomechanical parameters like PWS and PWRI allow for a highly individualized analysis by integrating factors that influence the risk of AAA rupture like geometry (degree of asymmetry, ILT morphology, etc.) and patient characteristics (gender, family history, blood pressure, etc.). PWRI and the reported annual risk of rupture increase similarly with the diameter. PWRI equivalent diameter expresses the PWRI through the diameter of the average AAA that has the same PWRI, i.e. is at the same biomechanical risk of rupture. Consequently, PWRI equivalent diameter facilitates a straightforward interpretation of biomechanical analysis and connects to diameter-based guidelines for AAA repair indication. PWRI equivalent diameter reflects an additional diagnostic parameter that may provide more accurate clinical data for AAA repair indication.

Article history: Received 25 September 2013, Accepted 11 December 2013, Available online 20 January 2014

Keywords: Aneurysms rupture, Biomechanical analysis, Aneurysm repair indication, Computer-based model, Risk assessment

* Corresponding author. T.C. Gasser, KTH Solid Mechanics, Teknikringen 8, SE-100 44 Stockholm, Sweden.
E-mail address: gasser@kth.se (T.C. Gasser).

1078-5884/$ – see front matter © 2013 European Society for Vascular Surgery. Published by Elsevier Ltd. All rights reserved.
http://dx.doi.org/10.1016/j.ejvs.2013.12.018

Introduction

The natural history of abdominal aortic aneurysms (AAAs) is determined by proteolytic degradation of elastin and collagen in the aortic wall resulting in dilatation and eventual rupture. AAA rupture has a total mortality between 75% and 90%, and death from ruptured AAAs ranks among the 10th leading cause of death in men above the age of 65.[1]

The indication for elective AAA repair is determined by the likelihood of rupture.[2] Consequently an accurate evaluation of rupture risk is of vital importance in reducing aneurysm related mortality, without substantially increasing the rate of elective AAA repair.

Data on AAA rupture risk has been provided from different sources.[3] According to the current clinical view, AAA rupture risk is based on the maximum diameter; a diameter of 55 mm or more is a generally accepted as indication for repair in males.[3,4] This kind of rupture risk assessment is, however, undergoing discussions,[5, 6] since AAAs with a diameter less than 55 mm may rupture[7,8] whereas many aneurysms larger than 55 mm may never rupture.[8]

Large AAA diameter is not the only risk factor, and rupture has also been associated with shape,[9] female gender,[10-13] family susceptibility,[14-16] high mean arterial pressure (MAP), smoking,[9, 17] and fludeoxyglucose (FDG) uptake on positron emission tomography (PET).[18] Nearly all large AAAs have intraluminal thrombus (ILT),[19] which is associated with a weaker[20] and thinner[21] underlying aneurysm wall, and ILT growth has been associated with risk of rupture.[22] Consequently, the diameter criterion has clear limitations.

According to the biomechanical rupture risk hypothesis, an aneurysm ruptures if wall stress overcomes wall strength at a certain location in the wall.[6] A biomechanical analysis is typically based on finite element (FE) predictions and such studies showed that peak wall stress (PWS)[23-24] and peak wall rupture index (PWRI)[25-26] discriminate better between ruptured and non-ruptured aneurysms than the maximum diameter.

Specifically, the PWRI relates mechanical stress and strength of the aneurysm wall, and incorporates risk factors associated with aneurysm wall weakening including female gender, ILT thickness and large relative expansion with respect to the normal infrarenal diameter.[27] No clinical trial, however, has investigated threshold values of these parameters for AAA repair, consequently they have limited clinical relevance.

The present study used the concept of risk-equivalent diameters, i.e. where biomechanical rupture risk values are translated to equivalent diameters of the average aneurysm patient. Specifically, the average patient is defined as the mean response of our non-ruptured patient cohort weighted by the gender ratio of the UK small aneurysm trial.[3] Retrospectively collected ruptured and non-ruptured cases were used to test to what extent biomechanical indices can discriminate among the groups.

Methods

Patient cohort and data acquisition

Data from 40 ruptured and 203 non-ruptured aneurysmal infrarenal aortas from 229 patients (179 male and 50 female) were retrospectively considered for this study (Table 1). Patients underwent contrast-enhanced computed tomography angiography (CTA) of the aorta at Karolinska University Hospital and Sankt Göran Hospital in Stockholm, University Hospital and St Joseph Hospital of Liege, and University Hospital in Heidelberg at typical image resolutions (in-plane, from 0.39 mm to 0.8 mm; slice thickness, from 1.0 mm to 5.0 mm). A considerable portion of our cohort is not in the diameter range of primary clinical importance, 50 mm to 60 mm say, but investigating a larger diameter spectrum might help to identify reasons why some small AAA rupture whereas many large cases do not. Prior to CTA, patient data were recorded for non-ruptured cases, and for the ruptured cases blood pressure at the last admission before rupture was used. If this information was not available, blood pressure of 140/80 mmHg was considered. No gender differences for age and systolic/diastolic pressure among the different groups were recorded (Table 1). The female-male ratio was lower in the ruptured (6/34) than in the non-ruptured (44/159) group. CTA scans recorded with strongly inhomogeneous lumen intensity were a priori rejected to minimize user interactions to build the computational models. The collection and use of anonymized data from human subjects was approved by the local ethics committees.

	Non-ruptured							
	n	Age (years)	Systolic/diastolic pressure (mmHg)	Diam. (mm)	PWS (kPa)	PWRI	D_{PWS} (mm)	D_{PWRI} (mm)
Female	44	72 (SD 9)	144/81 (SD 22/10)	53 (SD 14)	196 (SD 66)	0.59 (SD 0.29)	51 (SD 18)	63 (SD 23)
Male	159	72 (SD 8)	142/80 (SD 22/13)	56 (SD 17)	212 (SD 78)	0.46 (SD 0.23)	55 (SD 21)	52 (SD 18)
All	203	72 (SD 8)	143/80 (SD 22/12)	55 (SD 16)	208 (SD 76)	0.49 (SD 0.24)	55 (SD 20)	55 (SD 19)
	Ruptured							
	n[a]	Age (years)	Systolic/diastolic pressure (mmHg)	Diam. (mm)	PWS (kPa)	PWRI	D_{PWS} (mm)	D_{PWRI} (mm)
Female	6 (1)	80 (SD 17)	143/79 (SD 42/4)	71 (SD 12)	285 (SD 66)	1.07 (SD 0.30)	75 (SD 18)	100 (SD 21)
Male	34 (13)	74 (SD 8)	141/81 (SD 15/9)	82 (SD 18)	334 (SD 105)	0.99 (SD 0.46)	88 (SD 28)	92 (SD 29)
All	40 (14)	74 (SD 10)	141/81 (SD 19/8)	82 (SD 18)	336 (SD 107)	1.03 (SD 0.44)	89 (SD 29)	96 (SD 28)

a The number of cases where blood pressure measurements could not be taken from the last admission before rupture is given in brackets.

Table 1. Mean and standard deviation (SD) of age, blood pressure, maximum diameter, Peak Wall Stress (PWS), Peak Wall Rupture Risk Index (PWRI), PWS-equivalent diameter (D_{PWS}) and PWRI-equivalent diameter (D_{PWRI}) of non-ruptured and ruptured cases. The number of cases in the different groups is denoted by n.

Image reconstruction and biomechanical analysis

Aneurysms were reconstructed and analyzed with the diagnostic system A4clinics (VASCOPS GmbH, Graz, Austria). The reconstruction process used deformable image segmentation models and required minimal user interactions dependent on the complexity of the aneurysm and the quality of the image data. Centerline-based maximum diameter, PWS, and PWRI were calculated automatically. FE models that specifically account for the ILT, and the thinning of the aneurysm wall covered by it, were used; all modeling details have been reported elsewhere.[21,25,28] The FE method is an established numerical concept that divides any geometry into a large number of small finite elements, which together define a (hypothetical) biomechanical model of the aneurysm. The hypothetical model (FE model) was pressurized by the mean arterial pressure (MAP; 1/3 systolic pressure + 2/3 diastolic pressure), which in turn predicted the mechanical stress (force per area) in the wall of the aneurysm. Apart from geometry and arterial pressure, a FE model requires constitutive descriptions for the wall and the ILT. A constitutive description is a mathematical model of biomechanical properties, which relates stress and strain (deformation) and/or describes the strength of the tissue. The FE models used in the present analysis considered isotropic constitutive descriptions for the ILT and the aneurysm wall. An isotropic constitutive model is a common approximation for aneurysm tissue and assumes that the tissue's mechanical properties do not depend on the orientation, i.e. the stressestrain responses of circumferential and longitudinal strips of tissue are identical. The strength of the aneurysm wall is inhomogeneous and the applied FE models consider a wall strength model that accounts for local wall weakening influenced by the ILT, gender, family history, and the ratio between the local diameter and the normal infrarenal aortic diameter.[27] Further details regarding the biomechanical AAA rupture risk assessment and specific modeling assumptions used by A4clinics are given elsewhere.[25,28] A typical image showing the distribution of the rupture risk index (stress-strength ratio) in the aneurysm wall is illustrated in Fig. 1, and further details regarding the reproducibility of the analysis are reported elsewhere.[29,30]

Data analysis

To quantify the change in PWS and PWRI between the different patient groups independently from the diameter, we introduced the mean population PWS and PWRI curve for non-ruptured AAAs thought to reflect the average (nonruptured) patient. Here, "average" is understood in a purely mathematical sense. For this definition we considered a female percentage of 17, such that our average patient reflects the gender ratio of the UK small aneurysm trial.[3] Specifically, the mean population PWS and PWRI curves as functions of the maximal diameter (i.e. which reflect the average patient) were generated by weighting female and male regression curves by 0.17 and 0.83, respectively, based on several clinical studies[3] and served as reference for the average patient curve. In order to compare with clinical studies, PWRI regression curves of ruptured and non-ruptured aneurysms were weighted according to the rupture prevalence[2] and plotted with respect to the diameter. Statistical data analysis was performed with Mathematica (Wolfram Research Inc., Champaign, IL, USA). Normal distribution of the variables was tested using the Kolmogorov-Smirnov test. For hypothesis testing Welch's t test with the one-sided significance level of $p < .05$ was used.

Results

General cohort characteristics

Maximum diameter (82 mm vs. 55 mm; $p < .001$), PWS (336 kPa vs. 208 kPa; $p < .001$), and PWRI (1.03 vs. 0.49; $p < .001$) were larger in the ruptured than in the nonruptured cases. This was also seen in male and female subgroups, and further details are listed in Tables 1 and 2. The Kolmogorov-Smirnov test showed that the diameter was normally distributed in the ruptured groups (female, $p = .754$; male, $p = .749$; all, $p = .938$), whereas this was not the case for all non-ruptured groups ($p < .01$) (Table 3).

Relation between biomechanical indices and the maximum diameter

In all groups PWS and PWRI were scattered and increased with diameter, underlining the fact that the size is recognized by these biomechanical indices. A non-linear regression analysis demonstrated that PWS increases linearly and PWRI exponentially with diameter and had similar relative mean square errors in females and males (PWS regression, female/male = 0.046/0.045; PWRI regression, female/ male = 0.091/0.067). Simplified theoretical considerations that assume linearly increasing wall stress and linearly decreasing wall strength with relative expansion also point towards an exponential increase of PWRI with respect to the diameter. For the non-ruptured aortas, male and female regression curves are shown in Fig. 2, indicating that PWS is similar, whereas PWRI differs between men and women. Indeed, PWRI increases faster in females than in males with respect to diameter; similar observations were made for the ruptured cases.

	Female	Male	All
Age	.282	.105	.078
Systolic/diastolic pressure	.474/.270	.313/.330	.309/.387
Diameter D	.115	<.001	<.001
Peak wall stress (PWS)	.009	<.001	<.001
Peak wall rupture index (PWRI)	.004	<.001	<.001
PWS-equivalent diameter D_{PWS}	.009	<.001	<.001
PWRI-equivalent diameter D_{PWRI}	.003	<.001	<.001

Table 2. Value for p from difference testing (Welch's t test) between non-ruptured and ruptured cases.

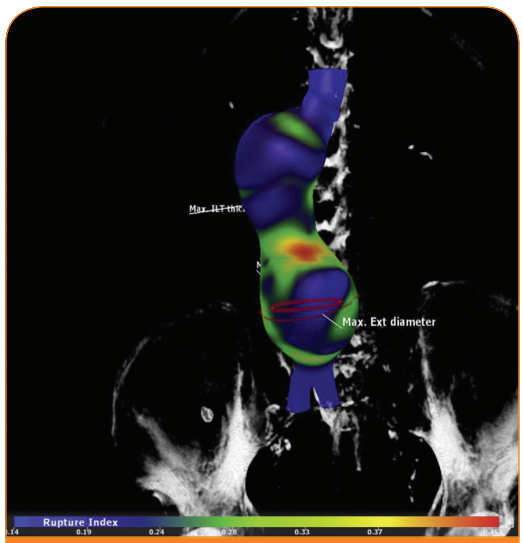

Figure 1. Color coded illustration of the rupture risk index distributed over the abdominal aortic aneurysm (AAA) wall. The peak wall rupture index (PWRI) represents the highest rupture index over the entire AAA wall between renal arteries and aortic bifurcation. 290 T.C. Gasser et al

Relation between PWRI and the annual risk of rupture

The predicted progressive increase in the average patient's PWRI with diameter using our biomechanical model has the similar exponential appearance as the progressive increase in annual AAA rupture risk with diameter. Upper and lower estimates of the annual rupture risk were estimated by Brewster et al.[2] (based on several clinical studies), and are illustrated by the thin solid lines in Fig. 3, whereas the thick line represents the PWRI that were computed from the biomechanical analysis of our patient cohort. Note that the representation is also a translation from the PWRI to an estimated annual risk of rupture, for example a PWRI of 0.39, 0.53, 0.68, 0.95, and 1.23 corresponds to an annual rupture risk of 3.6%, 9.8%, 16.8%, 28.7%, and 41.4%, respectively.

Biomechanical estimates among patient groups

In order to compare biomechanical estimates among the different patient groups, the PWS- and PWRI-equivalent diameters, D_{PWS} and D_{PWRI} say, were introduced (Fig. 4). These diameters reflect the size of the average aneurysm that experiences the same estimates as the individual case. Subtracting the maximum diameter D from D_{PWS} or D_{PWRI} gives a risk measure $\Delta D_{PWS} = D_{PWS} - D$ or $\Delta D_{PWRI} = D_{PWRI} - D$ (Fig. 4) that can be used to compare among patient groups independently of the diameter (size) effect.

ΔD_{PWS} was similar in males and females (non-ruptured $p = .251$; ruptured $p = .358$) but was elevated by 7.5 mm ($p = .013$) in ruptured patients compared with the nonruptured cases (Fig. 5A). This difference remained statistical significant in male (ΔD_{PWS} = 6.8 mm; $p = .032$) but not in female (ΔD_{PWS} = 5.4 mm; $p = .231$) subgroups. The relation between PWRI and D_{PWRI} for the average patient is shown in Table 4, where a PWRI of 0.48 corresponds to a D_{PWRI} of 55 mm, the generally accepted indication for AAA repair in males. ΔD_{PWRI} was 13.2 mm ($p < .001$) and 17.9 mm ($p = 0.014$) higher in females than males for the non-ruptured and ruptured groups, respectively. Most important, ΔD_{PWRI} was elevated by 14.0 mm ($p < .001$) in ruptured patients when compared with the non-ruptured cases (Fig. 5B). This difference

Significance level (p-value)	Non-ruptured			Ruptured		
	Female	Male	All	Female	Male	All
Diameter D	.004	<.001	<.001	.754	.749	.938
PWS-equivalent diameter D_{PWS}	.245	<.001	<.001	.639	.442	.245
PWRI-equivalent diameter D_{PWRI}	.077	<.001	<.001	.821	.174	.406
$\Delta D_{PWS} = D_{PWS} - D$	.006	.084	.021	.220	.236	.097
$\Delta D_{PWRI} = D_{PWRI} - D$	732	.519	.008	.268	.773	.706

Table 3. Kolmogorov-Smirnov testing the normal distribution of parameters.

remained statistically significant in male (D_{PWRI} = 14.1 mm; $p < .001$) and female (ΔD_{PWRI} = 18.8 mm; $p = .012$) subgroups. Finally, in order verify that these results are not biased by the difference in size of ruptured and non-ruptured groups more homogeneous (but still not diameter-matched) groups were tested. Specifically, non-ruptured cases that were smaller than 60 mm were excluded, which led to a subgroup analysis that contained 53 non-ruptured and 40 ruptured cases. Here, ΔD_{PWS} was elevated by 9.2 mm ($p = .003$) in the ruptured group (males 8.9 mm, $p = .011$; females 9.3, $p = .045$). Similarly, D_{PWRI} was elevated by 20.0 mm ($p < .001$) in the ruptured group (males 17.3 mm, $p < .001$; females 21.2, $p = .118$).

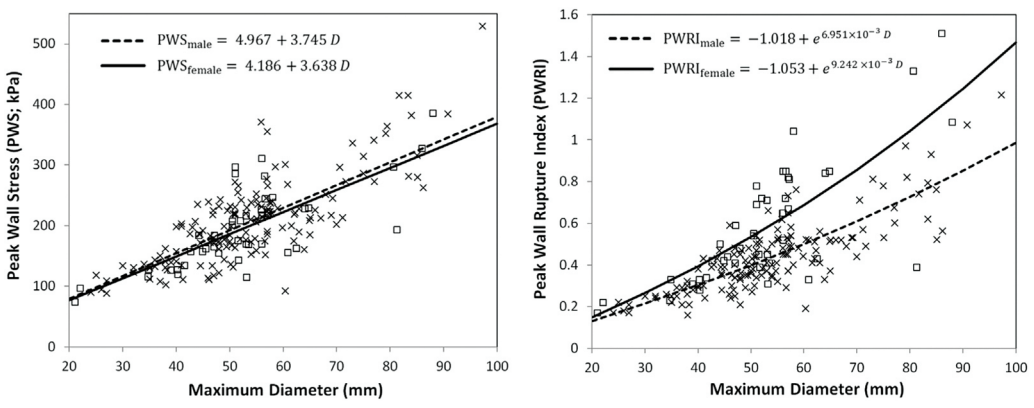

Figure 2. Development of peak wall stress (PWS) and peak wall rupture index (PWRI) with respect to the maximum diameter of nonruptured abdominal aortic aneurysms (AAAs). Squares denote female and crosses male patients. Solid lines (female) and dashed lines (male) denote regression curves.

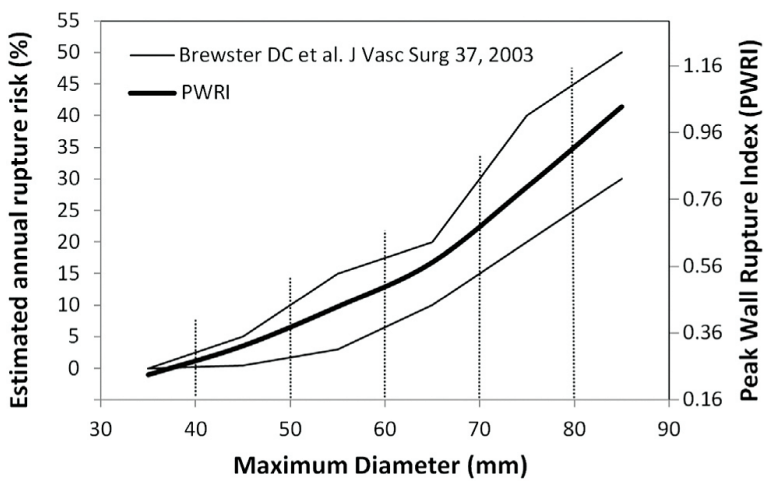

Figure 3. Progressive increase of annual rupture risk of abdominal aortic aneurysm (AAA) with respect to the maximum diameter. Thin solid lines represent upper and lower estimates[2] based on reported data. The thick solid line denotes peak wall rupture index (PWRI) based on a regression analysis of our patient cohort. PWRI has been adjusted for ruptured AAAs, i.e. regression curves for ruptured and non-ruptured cases were weighted according to reported rupture prevalence.[2]

Discussion

Biomechanically analyzing a large patient cohort illustrated that PWS increases linearly whereas PWRI increases exponentially with the maximal diameter. These average trends were expected, since simpler biomechanical models like the inflated tube or sphere already predict a linear increase of PWS, whereas the wall weakening properties that are incorporated by PWRI explain the progressive increase of this index with diameter. The average trend curves were in turn used to introduce D_{PWS} and D_{PWRI}, that is equivalent maximum diameters of an average aneurysm that experiences the same PWS and PWRI, respectively.

A size-adjusted analysis showed that D_{PWS} and D_{PWRI} were increased by 7.5 mm and 14.0 mm respectively in ruptured cases when compared with non-ruptured controls. Although comparison was statistically significant, a large overlap between ruptured and non-ruptured cases was observed. Aneurysm rupture is to some extent a stochastic event, which, even in cases at relatively low risk of rupture, can be triggered by a high peak in blood pressure. The present study agrees with previous ones showing that PWRI (or PWRI-based indices[27]) discriminates better between ruptured and non-ruptured cases than PWS.[25, 26] Most important, however, D_{PWRI} links an individualized biomechanical rupture risk assessment with conclusions drawn from earlier clinical studies.

PWRI was higher in females than in males, which is a direct consequence of the lower strength of the female aneurysm wall, and a borderline increase of PWRI in females has been reported from a FE study in a small cohort.[31] The present analysis used a larger number of patients and PWRI could significantly discriminate between males and females. In addition, the data predicted by our FE models suggested that a 50-mm AAA in females has the equivalent risk of rupture as a 63-mm aneurysm in males. This finding agrees with an earlier study suggesting that 50 mm in females compares with 60 mm in males.[8] The present study has some limitations. FE models introduce numerous modeling assumptions and cannot com-

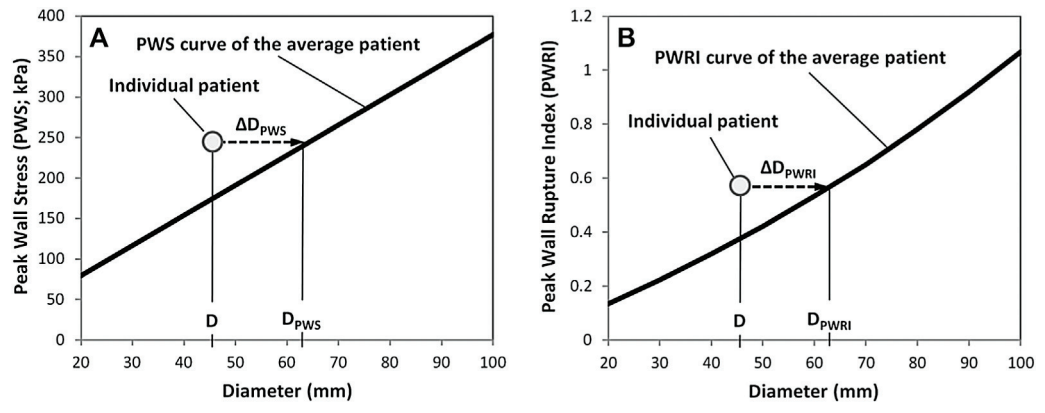

Figure 4. Definition of equivalent diameters for an individual abdominal aortic aneurysm (AAA) patient. (A) Peak wall stress (PWS) equivalent diameter D_{PWS} denotes the diameter of an average AAA that experiences the same PWS. (B) The peak wall rupture index (PWRI) equivalent diameter D_{PWRI} denotes the diameter of an average AAA that experiences the same PWRI.

pletely reflect the biomechanics of the real aneurysm. In the present study, the constitution of aneurysm tissue including wall and ILT was captured by mean population data, but patient-specific elastic properties would have increased the accuracy of the stress prediction. Likewise, the present study considers an isotropic wall model, although it is known that the AAA wall exhibits mild anisotropy, which can influence PWS predictions.[5] Constitutive data used by our, and by other, FE models of aneurysms is based on in vitro testing of the anterior wall, which may differ from the posterior wall, where aneurysm rupture is frequently observed.[32] Finally, calcifications of the aneurysm wall were not specifically considered by our FE models.

Although some attempts on integrating calcifications in FE models are reported in the literature, no consistent and reliable approach that accounts for the multiple influences of calcification on the aneurysm wall is known. With respect to the above-mentioned simplifications of our FE model, previous studies showed that stress predictions in aneurysms are relatively insensitive to changes in constitutive properties of the wall and the ILT,[33] and consequently the geometry seems to be the most critical property for wall stress estimates. Finally, it needs to be emphasized that potential modeling improvements do not necessarily improve the clinical benefit of the biomechanical AAA rupture risk assessment. Wall strength and thickness are other major determinants in FE model-based risk assessment. Even though the present study could not consider a patient-specific wall thickness, at least the reported thinning behind a thicker ILT[21] was implemented. It is also noted that failure tension (strength times wall thickness) remains almost constant in the AAA wall,[34] such that the computation of PWRI is much more insensitive to the local (and unknown) wall thickness than the PWS. It should be emphasized that in contrast to diameter measurements that do not depend to a large extent on different methods, different model assumptions of the FE model can cause severely different predictions.[35] Consequently, the presented data in this study must always be seen in relation to the specific modeling assumptions. Clinical studies have demonstrated that growth of the aneurysm[36] or the ILT[22]

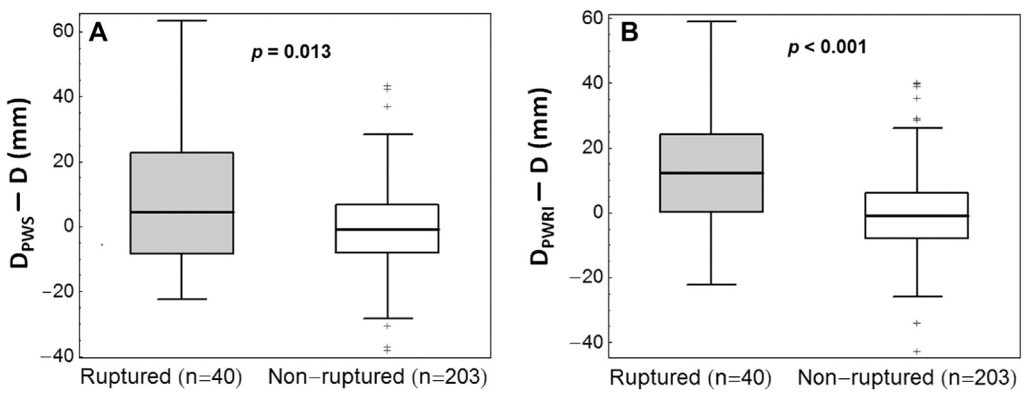

Figure 5. Difference between abdominal aortic aneurysm (AAA) maximum diameter D and their biomechanical equivalent diameters for ruptured (grey) and non-ruptured (white) cases. (A) Maximum diameter subtracted from the peak wall stress (PWS) equivalent diameter ($\Delta D_{PWS} = D_{PWS} - D$). (B) Maximum diameter subtracted from the peak wall rupture index (PWRI) equivalent diameter ($\Delta D_{PWRI} = D_{PWRI} - D$). The number of aneurysms for the different groups is given by n, and p denotes the one-sided p-value, respectively.

PWRI	0.24	0.32	0.40	0.48	0.56	0.64	0.72	0.80	0.88	0.96
D_{PWRI} (mm)	32	40	48	55	62	69	75	81	87	93

Table 4. Relation between peak wall rupture index (PWRI) and the PWRI-equivalent diameter D_{PWRI}. The D_{PWRI} reflects the maximum diameter of the average abdominal aortic aneurysm (AAA) patient experiencing the same PWRI, see also Fig. 4B for its definition.

might indicate an increased rupture risk, but the present study did not account for these types of risk. In addition, our FE models did not consider ILT fissures; although it is known that, if they involve a large volume or reach the aneurysm wall, wall stress is significantly elevated.[37] The applied retrospective grouping in ruptured and nonruptured cases has drawbacks. For example AAA patients in the non-ruptured group could have ruptured after a short time if they would not have been repaired, while ruptured case would have ended up in the non-ruptured group if treated shortly before rupture.

Conclusions

The biomechanical rupture risk assessment quantitatively integrates many known risk factors, and hence supports a highly individualized risk assessment. The biomechanical risk for rupture is best expressed by the PWRI-equivalent diameter, which relates the individual case to the size of an average aneurysm at the same biomechanical risk for rupture. The PWRI-equivalent diameter allows for a sizeindependent discrimination between ruptured and nonruptured aneurysms. Consequently, the PWRI-equivalent diameter should be included as an additional indication for elective AAA repair.

Acknowledgements

We acknowledge the assistance of Martin Auer, Fausto Labruto, Emma Larsson, Giampaolo Martufi, Tim Krieger, and Thomas Able who substantially contributed to the work by collecting data.

Conflict of interest

T.C. Gasser, J. Swedenborg and D. Böckler are members of the scientific advisory board of VASCOPS GmbH.

Funding

Financial support for this research was provided by Young Faculty Grant “Integrated Biomechanical Diagnosis of AAAs” No. 2006-7568 from the Swedish Research Council, VINNOVA, and the Swedish Foundation for Strategic Research, as well as the EC Seventh Framework Programme “Fighting Aneurysmal Disease (FAD-200647)”.

References

1. Fleming C, Whitlock EP, Beil TL, Lederle FA. Screening for abdominal aortic aneurysm: a best-evidence systematic review for the U.S. Preventive Services Task Force. Ann Intern Med 2005;142:203-11.
2. Brewster DC, Cronenwett JL, Hallett JW, Johnston KW, Krupski WC, Matsumura JS. Guidelines for the treatment of abdominal aortic aneurysms. Report of a subcommittee of the Joint Council of the American Association for Vascular Surgery and Society for Vascular Surgery. J Vasc Surg 2003;37:1106-17.
3. The UK Small Aneurysm Trial Participants. Mortality results for randomised controlled trial of early elective surgery or ultrasonographic surveillance for small abdominal aortic aneurysms. Lancet 1998;352:1649-55.
4. Lederle FA, Wilson SE, Johnson GR, Reinke DB, Littooy FN, Acher CW, et alfor the Aneurysm Detection and Management (ADAM) Veterans Affairs Cooperative Study Group. Immediate repair compared with surveillance of small abdominal aortic aneurysms. N Engl J Med 2002;346:1437-44.
5. Vorp DA. Biomechanics of the abdominal aortic aneurysm. J Biomech 2007;40:1887-902.
6. Fillinger MF. Who should we operate on and how do we decide: predicting rupture and survival in patients with aortic aneurysm. Semin Vasc Surg 2007;20:121-7.
7. Nicholls SC, Gardner JB, Meissner MH, Johansen HK. Rupture in small abdominal aortic aneurysms. J Vasc Surg 1998;28:884-8.
8. Darling RC, Messina CR, Brewster DC, Ottinger LW. Autopsy study of unoperated abdominal aortic aneurysms. Circulation 1977;56(Suppl. II):161-4.
9. Vorp DA, Raghavan ML, Webster MW. Mechanical wall stress in abdominal aortic aneurysm: influence of diameter and asymmetry. J Vasc Surg 1998;27:632-9.
10. Heikkinen M, Salenius J, Zeitlin R, Saarinen J, Suominen V, Metsanoja R, et al. The fate of AAA patients referred electively to vascular surgical unit. Scand J Surg 2002;91:345-52.
11. Brown PM, Zelt DT, Sobolev B. The risk of rupture in untreated aneurysms: the impact of size, gender, and expansion rate. J Vasc Surg 2003;37:280-4.
12. Wilson KA, Lee AJ, Hoskins PR, Fowkes FG, Ruckley CV, Bradbury AW. The relationship between aortic wall distensibility and rupture of infrarenal abdominal aortic aneurysm. J Vasc Surg 2003;37:112-7.
13. Derubertis BG, Trocciola SM, Ryer EJ, Pieracci FM, McKinsey JF, Faries PL, et al. Abdominal aortic aneurysm in women: prevalence, risk factors, and implications for screening. J Vasc Surg 2007;46:630-5.
14. Darling 3rd RC, Brewster DC, Darling RC, LaMuraglia GM, Moncure AC, Cambria RP, et al. Are familial abdominal aortic aneurysms different? J Vasc Surg 1989;10:39-43.
15. Verloes A, Sakalihasan N, Koulischer L, Limet R. Aneurysms of the abdominal aorta: familial and genetic aspects in three hundred thirteen pedigrees. J Vasc Surg 1995;21:646-55.
16. Larsson E, Granath F, Swedenborg J, Hultgren R. A populationbased case-control study of the familial risk of abdominal aortic aneurysm. J Vasc Surg 2009;49:47-50.

17. Powell JT, Worrell P, MacSweeney ST, Franks PJ, Greenhalgh RM. Smoking as a risk factor for abdominal aortic aneurysm. Ann N Y Acad Sci 1996;800:246-8.
18. Sakalihasan N, Van Damme H, Gomez P, Rigo P, Lapiere CM, Nusgens B, et al. Positron emission tomography (PET) evaluation of abdominal aortic aneurysm (AAA). Eur J Vasc Endovasc Surg 2002;23(5):431-6.
19. Hans SS, Jareunpoon O, Balasubramaniam B, Zelenock GB. Size and location of thrombus in intact and ruptured abdominal aortic aneurysms. J Vasc Surg 2005;41:584-8.
20. Vorp DA, Lee PC, Wang DH, Makaroun MS, Nemoto EM, Ogawa S, et al. Association of intraluminal thrombus in abdominal aortic aneurysm with local hypoxia and wall weakening. J Vasc Surg 2001;34:291-9.
21. Kazi M, Thyberg J, Religa P, Roy J, Eriksson P, Hedin U, et al. Influence of intraluminal thrombus on structural and cellular composition of abdominal aortic aneurysm wall. J Vasc Surg 2003;38:1283-92.
22. Stenbaek J, Kalin B, Swedenborg J. Growth of thrombus may be a better predictor of rupture than diameter in patients with abdominal aortic aneurysms. Eur J Vasc Endovasc Surg 2000;20:466-99.
23. Fillinger MF, Raghavan ML, Marra SP, Cronenwett J-L, Kennedy FE. In vivo analysis of mechanical wall stress and abdominal aortic aneurysm rupture risk. J Vasc Surg 2002;36: 589-97.
24. Venkatasubramaniam AK, Fagan MJ, Mehta T, Mylankal KJ, Ray B, Kuhan G, et al. A comparative study of aortic wall stress using finite element analysis for ruptured and non-ruptured abdominal aortic aneurysms. Eur J Vasc Surg 2004;28:168-76.
25. Gasser TC, Auer M, Labruto F, Swedenborg J, Roy J. Biomechanical rupture risk assessment of abdominal aortic aneurysms: model complexity versus predictability of finite element simulations. Eur J Vasc Endovasc Surg 2010;40:176-85.
26. Maier A, Gee MW, Reeps C, Pongratz J, Eckstein HH, Wall WA. A comparison of diameter, wall stress, and rupture potential index for abdominal aortic aneurysm rupture risk prediction. Ann Biomed Eng 2010;38:3124-34.
27. Vande Geest JP, Di Martino ES, Bohra A, Makaroun MS, Vorp DA. A biomechanics-based rupture potential index for abdominal aortic aneurysm risk assessment: demonstrative application. Ann N Y Acad Sci 2006;1085:11-21.
28. Martufi G, Gasser TC. Review: the role of biomechanical modeling in the rupture risk assessment for abdominal aortic aneurysms. J Biomech Eng 2013;135:021010 [1-10].
29. Hyhlik-Dürr A, Krieger T, Geisbüsch P, Kotelis D, Able T, Böckler D. Reproducibility of aortic diameter, volume, peak wall stress, and peak rupture risk index using semiautomatic finite element analyses of infrarenal aortic aneurysms. J Endovasc Ther 2011;18:289-98.
30. Teutelink A, Cancrinus E, van de Heuvel D, Moll F, de Vries JP. Preliminary intraobserver and interobserver variability in wall stress and rupture risk assessment of abdominal aortic aneurysms using a semiautomatic finite element model. J Vasc Surg 2012;55:326-30.
31. Larsson E, Labruto F, Gasser TC, Swedenborg J, Hultgren R. Analysis of aortic wall stress and rupture risk in AAA patients with a gender perspective. J Vasc Surg 2011;54:295-9.

32. Roy J, Labruto F, Beckman MO, Danielson J, Johansson G, Swedenborg J. Bleeding into the thrombus e a possible sign of threatening rupture of infrarenal aortic aneurysms. J Vasc Surg 2008;48:1108-13.
33. DiMartino ES, Vorp DA. Effect of variation in intraluminal thrombus constitutive properties on abdominal aortic wall stress. Ann Biomed Eng 2003;31:804-9.
34. Raghavan ML, Hanaoka M, Kratzberg J, de Lourdes Higuchi M, da Silva E. Biomechanical failure properties and microstructural content of ruptured and unruptured abdominal aortic aneurysms. J Biomech 2011;44(13):2501-7.
35. Reeps C, Gee M, Maier A, Gurdan M, Eckstein HH, Wall WA. The impact of model assumptions on results of computational mechanics in abdominal aortic aneurysm. J Vasc Surg 2010;51: 679-88.
36. Sakalihasan N, Delvenne P, Nusgens BV, Limet R, Lapiere CM. Activated forms of MMP2 and MMP9 in abdominal aortic aneurysms. J Vasc Surg 1996;24:127-33.
37. Polzer S, Gasser TC, Swedenborg J, Bursa J. The impact of intraluminal thrombus failure on the mechanical stress in the wall of abdominal aortic aneurysms. Eur J Vasc Endovasc Surg 2011;41:467-73.

3. Publication N° 3: Multifactorial Relationship Between F-Fluoro-Deoxy-Glucose Positron Emission Tomography Signaling and Biomechanical Properties in Unruptured Aortic Aneurysms

3.1. Introduction

We aimed at investigating the correlations between biological activities and the estimates of wall stress, their main determinants and their clinical outcomes.

We enrolled 53 patients (45 men) with a mean age of 72 years. A total of 68 combined FDG PET-CT examinations were performed. Visual and SUV analyzes of FDG uptake were performed and correlated with estimates of wall stress. An average follow-up of 11 months was observed and significant clinical events, defined by: (i) diameter growth> 1 cm/year, (ii) dissection and (iii) rupture or urgent surgery, were recorded.

Finally, we evaluated the effect of several variables on FDG uptake and wall stress estimates using general linear mixed models (GLMM).

This regression analysis included the technique of investigation (PET-CT vs. FES), biomechanical and morphometric parameters (stress, stress/strength, maximum aortic diameter and thickness of the ILT), aneurysm type (TAA vs. AAA) and patient-specific properties (age, gender, smoking, presence of other arterial aneurysms, diabetes, arterial hypertension, hyperlipidemia, chronic obstructive pulmonary disease, history of stroke, angina, myocardial infarction, claudication, renal insufficiency and family history of aneurysm).

3.2. Findings summary

The study showed a higher rate of increased FDG uptake areas per examination in TAA (18/11) than in AAA (14/57). Similarly, the co-localization rate between increased FDG uptake and increased wall stress was higher in TAA (6/11) than in AAA (1/57). The occurrence of clinical events during follow-up was higher in patients with high FDG uptake than in patients with no uptake (71.4% vs. 23.3%, $p = 0.04$). FDG uptake was therefore associated with a significant decrease of the event-free survival at 30 months; this outcome prediction was independent of the aneurysm diameter.

Quantitatively the FDG uptake was positively correlated with wall stress estimates. It was also significantly higher depending on the location of the aneurysm (thoracic > abdominal), in patients with other arterial aneurysms, a family history of aortic aneurysm and a personal history of angina.

However, claudication and COPD were negative determinants of FDG uptake. In short, FDG uptake is at least partially related to genetic or acquired alterations of the arterial wall response to stress.

3.3. Conclusions

Increased FDG uptake was a diameter-independent marker of poor outcome over 2 years, supporting the possible use of FDG PET to determine the risk of rupture in patients with aortic aneurysms. No such finding was found for FES estimates that are inherently not thresholded. The observed correlation between elevated wall metabolic activity and wall stress indicates a potentially comparable value for risk management. Nevertheless, FDG uptake (wall metabolism) is influenced by patient's specific genetic or acquired alterations of the biological responses to wall stress. It therefore appeals for an integrated patient-specific risk assessment strategy that would include all or most of these imaging, personal and heritable factors.

3.4. Reassessment summary/opportunities

Increased FDG uptake is relatively infrequent in AAA. Therefore, the statistical power of our outcome analysis was low, which would require larger and randomized clinical trials to determine the role of FDG PET imaging in the decision-making in patients with AAA. Interestingly, the heritable conditions associated with increased FDG uptake may provide clues for the known prohibitive risk of rupture in familial aneurysms.

Publication N° 3

This subchapter has been published as:

Multifactorial relationship between F-Fluoro-Deoxy-Glucose Positron Emission Tomography signaling and biomechanical properties in unruptured aortic aneurysms

A. Nchimi, JP. Cheramy-Bien, T. C. Gasser, G. Namur, P. Gomez, L. Seidel, A. Albert, JO. Defraigne, N. Labropoulos, N. Sakalihasan

Circulation: Cardiovascular Imaging, 2014 (7) : 82-91

Circulation
Cardiovascular Imaging

American Heart Association®

Multifactorial Relationship Between ^{18}F-Fluoro-Deoxy-Glucose Positron Emission Tomography Signaling and Biomechanical Properties in Unruptured Aortic Aneurysms

Alain Nchimi, Jean-Paul Cheramy-Bien, T. Christian Gasser, Gauthier Namur, Pierre Gomez, Laurence Seidel, Adelin Albert, Jean-Olivier Defraigne, Nicos Labropoulos and Natzi Sakalihasan

Circ Cardiovasc Imaging. 2014;7:82-91; originally published online November 4, 2013;
doi: 10.1161/CIRCIMAGING.112.000415
Circulation: Cardiovascular Imaging is published by the American Heart Association, 7272 Greenville Avenue, Dallas, TX 75231

Print ISSN: 1941-9651. Online ISSN: 1942-0080

Multifactorial Relationship Between ^{18}F-Fluoro-Deoxy-Glucose Positron Emission Tomography Signaling and Biomechanical Properties in Unruptured Aortic Aneurysms

Alain Nchimi, MD; Jean-Paul Cheramy-Bien, MLT; T. Christian Gasser, PhD; Gauthier Namur, MD; Pierre Gomez, MD; Laurence Seidel, MSc; Adelin Albert, PhD; Jean-Olivier Defraigne, MD, PhD; Nicos Labropoulos, MD, PhD; Natzi Sakalihasan, MD, PhD

Background—The relationship between biomechanical properties and biological activities in aortic aneurysms was investigated with finite element simulations and ^{18}F-fluoro-deoxy-glucose (^{18}F-FDG) positron emission tomography.

Methods and Results—The study included 53 patients (45 men) with aortic aneurysms, 47 infrarenal (abdominal aortic) and 6 thoracic (thoracic aortic), who had ≥1 ^{18}F-FDG positron emission tomography/computed tomography. During a 30-month period, more clinical events occurred in patients with increased ^{18}F-FDG uptake on their last examination than in those without (5 of 18 [28%] versus 2 of 35 [6%]; P=0.03). Wall stress and stress/strength index computed by finite element simulations and ^{18}F-FDG uptake were evaluated in a total of 68 examinations. Twenty-five (38%) examinations demonstrated ≥1 aneurysm wall area of increased ^{18}F-FDG uptake. The mean number of these areas per examination was 1.6 (18 of 11) in thoracic aortic aneurysms versus 0.25 (14 of 57) in abdominal aortic aneurysms, whereas the mean number of increased uptake areas colocalizing with highest wall stress and stress/strength index areas was 0.55 (6 of 11) and 0.02 (1 of 57), respectively. Quantitatively, ^{18}F-FDG positron emission tomographic uptake correlated positively with both wall stress and stress/strength index (P<0.05). ^{18}F-FDG uptake was particularly high in subjects with personal history of angina pectoris and familial aneurysm.

Conclusions—Increased ^{18}F-FDG positron emission tomographic uptake in aortic aneurysms is strongly related to aneurysm location, wall stress as derived by finite element simulations, and patient risk factors such as acquired and inherited susceptibilities. **(*Circ Cardiovasc Imaging*. 2014;7:82-91.)**

Key Words: aneurysm ■ aorta ■ tomography

Aneurysms are permanent vascular dilatations that involve the aorta in ≤10% of subjects >65 years of age, with more than half localized in the infrarenal aorta.[1,2] Their rupture causes death in ≤90% of cases,[2,3] and according to recent trials, the operative mortality does not exceed 5%.[4] The aneurysm maximal diameter identifies the time point when the risk of rupture exceeds that of repair, hence indicating a preventive intervention in asymptomatic patients.[5–7] Research, however, has been driven toward more patient-specific risk assessment because aneurysms above the critical diameter thresholds may never rupture, whereas smaller aneurysms will.[8–10]

Rupture occurs when the wall stress exceeds the wall strength. Aortic geometry can be used for finite element simulations (FES)[11,12] providing, among other estimates, wall stress. Before rupture occurs, wall stress is involved in aneurysmal expansion and remodeling; the latter triggers and amplifies numerous biological mechanisms that may result in apposition of an intraluminal thrombus with its own biomechanical[13] and biological characteristics.[14–17] The biological activity of the aortic wall can be evaluated indirectly through energy consumption using ^{18}F-fluoro-deoxy-glucose (^{18}F-FDG) as a tracer for positron emission tomographic (PET) imaging.[18] ^{18}F-FDG uptake is not uncommon in aortic aneurysms[19,20] and has been shown to correlate with the amount of inflammatory cells, proteolytic activity, and risk of rupture.[21–23] Xu et al[24] previously evidenced associations among biological activity, wall stress estimates, and rupture in 3 patients with aortic aneurysms. The actual relationship between biomechanical parameters and biological activity, however, has never been studied in large series.

Our study was designed to assess the relationship and the independent determinants between biomechanical estimates of wall stress and ^{18}F-FDG uptake in unruptured aortic aneurysms.

Received November 28, 2012; accepted October 16, 2013.

From the Departments of Cardiovascular and Thoracic Imaging (A.N.) and Cardiovascular and Thoracic Surgery (J.-P.C.-B., J.O.D., N.S.), University Hospital, Liège, Belgium; Department of Solid Mechanics, Royal Institute of Technology (KTH), Stockholm, Sweden (T.C.G.); Department of Nuclear Medicine, Centre Hospitalier Chrétien St Joseph, Liège, Belgium (G.N., P.G.); Medical Informatics and Biostatistics, University of Liège, Liège, Belgium (L.S., A.A.); and Stony Brook University Medical Center, NY (N.L.).

The Data Supplement is available at http://circimaging.ahajournals.org/lookup/suppl/doi:10.1161/CIRCIMAGING.112.000415/-/DC1.

Correspondence to Alain Nchimi, MD, Department of Cardiovascular and Thoracic Imaging, University Hospital Sart Tilman B35, Liège 4000, Belgium. E-mail anchimi@chu.ulg.ac.be

Circ Cardiovasc Imaging **is available at http://circimaging.ahajournals.org** **DOI: 10.1161/CIRCIMAGING.112.000415**

Methods

Study Patients This study is part of a larger trial aiming to determine the role of ^{18}F-FDG PET in aortic aneurysm rupture risk assessment as approved by the institutional review board.[25] It included 53 patients (45 men) with aortic aneurysm who underwent ≥1 whole-body ^{18}F-FDG PET examination using contrast-enhanced computed tomography (CT) for attenuation correction in a single center within a 5-year period. All patients provided written informed consent.

Patients with aneurysm of the ascending thoracic aorta were excluded to avoid pathophysiology clustering. There were 47 patients with aneurysms involving the infrarenal aorta (abdominal aortic aneurysm [AAA]) and 6 the thoracic aorta (thoracic aortic aneurysm [TAA]), including arch (n=1), descending thoracic aorta (n=2), and thoracoabdominal aortic aneurysms, with the largest diameter at the level of the thoracic aorta (n=3). Between 1 and 5 ^{18}F-FDG PET examinations were performed on 44, 6, 1, 1, and 1 patients, respectively, resulting in a total of 68 examinations (11 in TAAs and 57 in AAAs).

The average interscan duration among patients was 7.2±5.9 months. Based on clinical and imaging followup, significant events related to the aortic disease were defined as an aneurysm growth of >1 cm per year, dissection, rupture, or emergency surgery. ^{18}F-FDG PET CT and FES imaging data acquisition procedures are detailed in Method I in the Data Supplement. Visual Image Analysis Experts with ≥6 years of experience in nuclear imaging examined all 68 tests. Increased ^{18}F-FDG uptake in the aortic aneurysm wall was documented by identifying any area with >1 cm of increased signaling compared with the intra-arterial background and distant aortic wall segments. Examinations were declared positive when ≥1 such area was noted. Clinical reports were also carefully analyzed to describe ^{18}F-FDG uptake as diffuse, monofocal, or plurifocal and to identify and localize uptake areas on the corresponding CT images using predefined anatomic landmarks. Specifically, this required the readers to identify the center of the area relative to a vascular or a vertebral landmark cranio-caudally and then to localize the main quadrant of the area relative to sagittal and coronal lines across the aortic center.

In a second step, a radiologist with >5 years of experience in vascular imaging analyzed the 68 examinations by the FES method using the A4clinics software system (VASCOPS GmbH; Graz, Austria)[26] set on read-only mode that did not allow any modification of the aortic segmentation and geometry. The radiologist determined the maximal values of wall stress, stress/strength index, and thrombus thickness in all 68 examinations. The same radiologist verified whether the area containing the highest values of either wall stress or stress/strength index estimates colocalized with an area of increased ^{18}F-FDG uptake as described in the clinical reports.

For visual analyses, maximal wall stress and stress/strength index were expressed as relative intensity in areas with ^{18}F-FDG uptake to compensate for interpatient variability (Method II in the Data Supplement).

Quantitative Image Analysis

Two other observers with >5 years of experience in vascular imaging and vascular surgery, respectively, were asked to determine in consensus the areas of interest for the quantitative analysis and the topographical correspondences between wall stress and ^{18}F-FDG PET.

Multiplanar and volumetric analyses of CT, ^{18}F-FDG PET, and fused ^{18}F-FDG PET/CT images (all had similar spatial coordinates) were performed on a dedicated workstation (Advantage Windows, release 4.3; GE Healthcare).

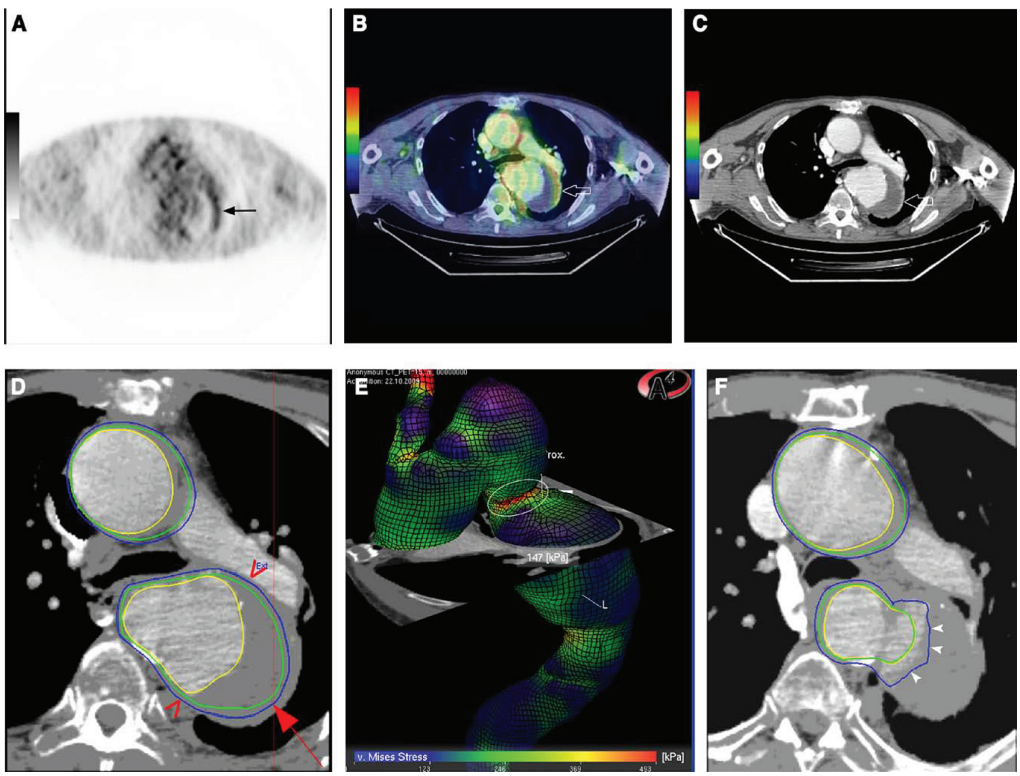

Figure 1. 18F-fluoro-deoxy-glucose (^{18}F-FDG) uptake and wall stress estimates in a 79-year-old man with a descending thoracic aortic aneurysm. An area of increased ^{18}F-FDG uptake (arrows) is identified on axial positron emission tomographic (PET; A), fused PET computed tomographic (CT; B), and then on CT (C) images. Reconstruction of a model using CT image, magnified at the same level (red arrow, D), including external and luminal aortic boundaries (blue and yellow lines) and hypothetical wall limit paralleling the external contour (green line), allows diameter (between brackets) and thrombus (between yellow and green lines) assessment. E, Color-coded 3-dimensional wall stress map of the aorta after pressurization of this model, where the axial slice in the area of interest has been inserted, showing the wall stress estimate (147 kPa). By convention, color code represents intensity scale ranging from deep blue to red. An artifact located >1 cm proximally in the aorta, exhibiting a red spot of increased wall stress (E, circled area), is excluded for analysis and explained in F by failure of the aortic contour reconstruction (arrowheads on blue line). The patient denied surgery and experienced acute dissection 5 months after this examination. The intimal tear was located around previously increased 18F-FDG uptake area. The patient eventually died 1 week after this complication.

^{18}F-Fluoro-Deoxy-Glucose PET

On CT images, a volume of interest (VOI) was automatically selected to include the aorta using the high intravascular attenuation (mean, 214 [range, 70–335] Hounsfield units). Structures that were included in the volume because of similar attenuation values were manually deleted, and the remaining VOI was copied and pasted on ^{18}F-FDG PET images. If needed (eg, because of a slight patient position change between CT and PET images), the pasted VOI was slightly adjusted to include the whole intraluminal thrombus and match the anatomic contours. Then, the mean and SD of the ^{18}F-FDG uptake in the VOI were estimated quantitatively using standardized uptake value (SUV) as shown in Method III in the Data Supplement. Within this VOI, the observers selected all clusters of >10 voxels with SUV above the threshold of mean+2SD of the whole volume. Using fused ^{18}F-FDG PET-CT images, they excluded the areas belonging to structures surrounding the aorta (eg, vertebra, ureter, duodenum; n=7) or to the aortic lumen (n=19). Another VOI was drawn manually to include the right hepatic lobe and the retrohepatic inferior vena cava and to determine their maximal SUVs. Then, to compensate for contrast-enhanced CT overcorrection and patient variability, the aortic wall maximal SUVs were normalized as SUV-to-liver (SUV_{RL}) and SUV-to-venous background (SUV_{RV}) ratios.

Finite Element Simulations

FES image displays (A4clinics) were set to highlight clusters of >10 elements exhibiting values of wall stress and stress/strength index estimates of ≥mean of whole aorta+2SD. The geometry of these areas was checked on CT to exclude reconstruction failures (n=20; eg, complex geometry, kinking, bifurcations), as shown in Figure 1.

Patient Characteristic	n (%)	Mean±SD	Patient Characteristic	n (%)	Mean±SD
Age, y		72.0±8.2	COPD	15 (28)	
Sex (male)	45 (85)		Stroke	9 (17)	
Current smoking	24 (45)		Peripheral artery disease	20 (38)	
Stopped smoking	19 (36)		Angina pectoris	15 (28)	
Aneurysm location (TAA)	6 (11)		Renal insufficiency†	8 (15)	
Other arterial aneurysms	13 (24)		Acute myocardial infarction	22 (41)	
Diabetes mellitus	11 (21)		Familial aneurysm	6 (12)	
Arterial hypertension	32 (60)		Follow-up duration, mo		11.4±8.6
Dyslipidemia*	36 (69)		Adverse event	7 (13)	

COPD indicates chronic obstructive pulmonary disease; and TAA, descending thoracic aortic aneurysm.
*Increased serum levels of triglycerides, low-density lipoprotein cholesterol, or both
†Clearance of creatinine <60 mL/min.

Table 1. Patient Demographics and Risk Factors for Aortic Aneurysms (n=53)

Topographical Matching of ^{18}F-FDG PET and FES

In all selected areas, intraluminal thrombus thickness, aortic diameter, and maximal values of SUV_{RL}, SUV_{RV}, wall stress, and stress/ strength index were recorded. Each observer instructed the other to derive ^{18}F-FDG uptake and FES estimates on selected areas. The areas were topographically matched using CT images, with the rule that any part of one intersects the other by ≤1 cm to its center (Figure 1).

Statistical Methods

Statistics were mainly descriptive. Quantitative data were summarized by mean and SD, whereas numbers and percentages were used for categorical findings. Correlations were calculated to assess the relationships between SUV_{RL} and SUV_{RV} values and the corresponding wall stress and stress/ strength index estimates. Event-free survival curves were compared using the log-rank test.

The general linear mixed model, which accounts for repeated measurements within subjects, was used to compare AAAs versus TAAs with respect to imaging and FES in areas of interest and to assess the relationship between SUV_{RV} and biomechanical parameters, aneurysm location, and patient-specific factors. Results were significant at the 5% critical level ($P<0.05$). All statistical calculations were performed with SAS (version 9.3 for Windows).

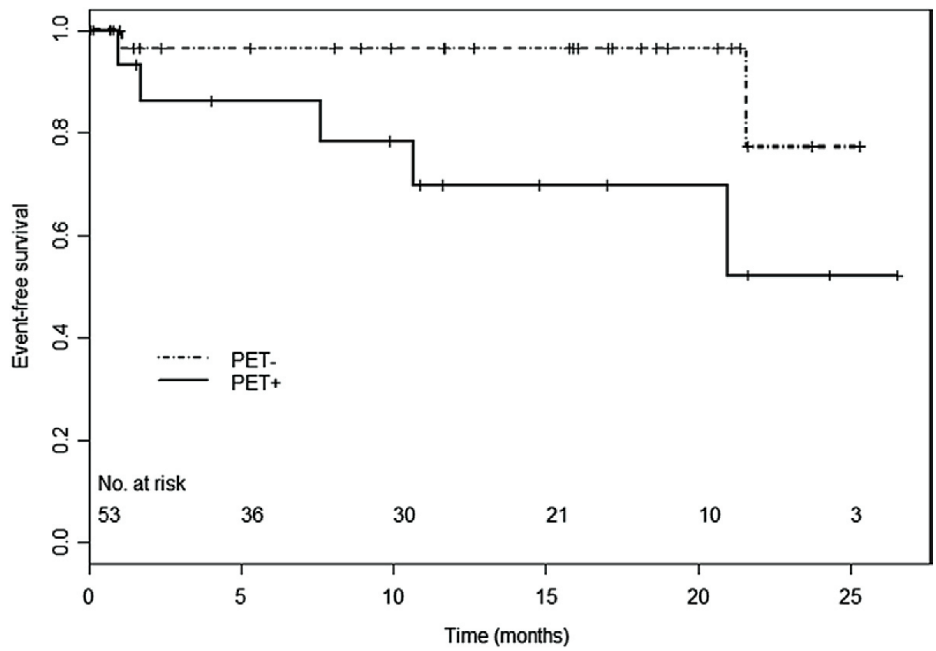

Figure 2. Thirty-month event-free survival curves in positron emission tomography (PET)–positive and PET-negative patients according to increased ^{18}F-fluoro-deoxy-glucose uptake at the last examination.

Results

Patient Characteristics

Patient characteristics are described in Table 1. Five of the 6 patients (83%) with TAA were above the rupture risk threshold of 55 mm, whereas only 24 of the 47 patients (51%) with AAA were higher than the corresponding 50-mm threshold. During the follow-up period, adverse clinical events occurred in 7 (13%) patients. The outcomes of all patients after the last examination with regard to ^{18}F-FDG PET uptake and colocalization with maximal FES estimates are given in Table I in the Data Supplement. Among the 53 patients, 18 (34%) were ^{18}F-FDG PET positive (ie, with increased ^{18}F-FDG uptake on their last examination), and 35 were ^{18}F-FDG PET negative. The proportion of clinical events was higher (28% versus 6%; P=0.03), and the 30-month event-free survival was worse in the former group (log-rank test: P=0.040; Figure 2).

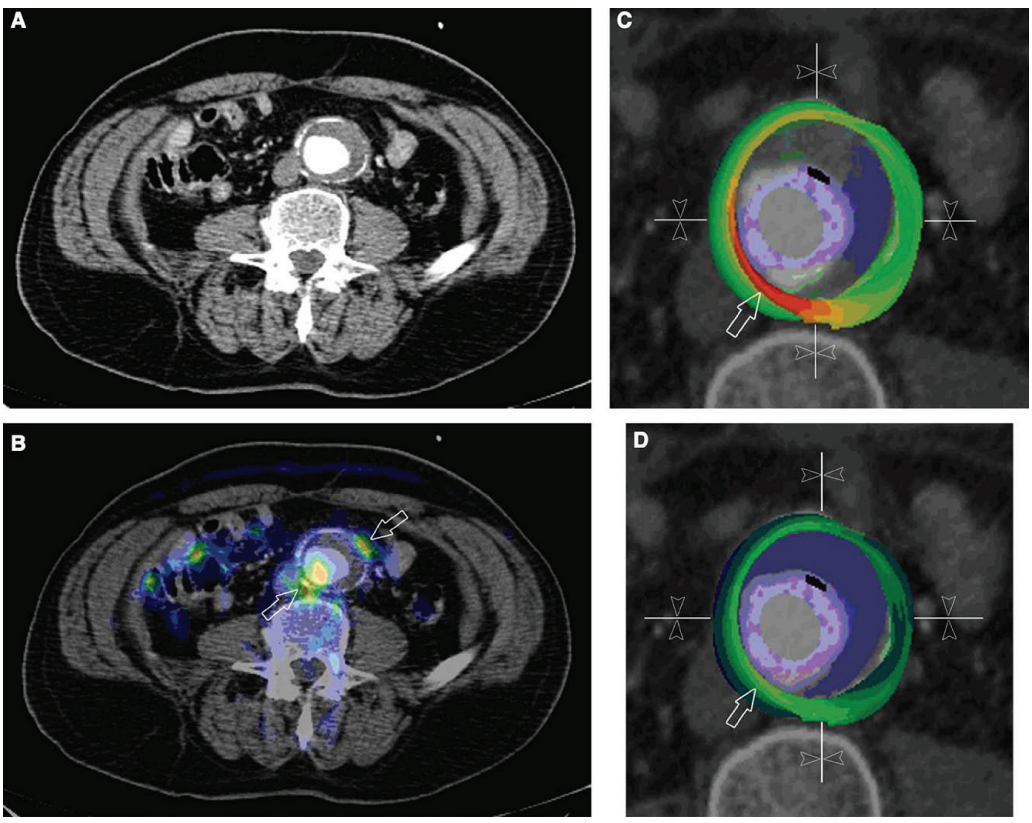

Figure 3. Partial coincidence between positron emission tomographic (PET) imaging findings and finite element simulation (FES) estimates in an 80-year-old man with abdominal aortic aneurysm (A). After fusion with 18F-fluoro-deoxy-glucose (18F-FDG) PET imaging (B), 2 distinct aortic areas of 18F-FDG uptake are seen (arrows): one in the left anterior and the other in the right posterior quadrants. On FES, these areas show, respectively, average and increased (arrows) wall stress (C; wall stress=161 kPa) and stress/strength index (D; stress/ strength index=0.34). By convention, color code represents intensity scale ranging from deep blue to red. The patient's last follow-up computed tomography showed no aneurysm enlargement after 1 year. He eventually died shortly after from lung cancer.

Visual Analyses at Segment Level

Among the 68 ^{18}F-FDG PET examinations, there were 25 (38%) with visually increased aortic uptake. These uptakes were diffuse, monofocal, bifocal, and trifocal, respectively, in 1, 18, 5, and 1 examinations, yielding a total of 32 areas. Of these areas, 18 (56%) were in TAAs and 14 (44%) in AAAs. For wall stress, the mean relative intensity was 55±45% for all examinations (76±38% in TAAs versus 31±41% in AAAs). The stress/strength index equaled 57±48% for all examinations (77±37% in TAAs versus 33±49% in AAAs). The mean number of uptake areas per examination was 1.6 (18 of 11) in TAAs versus 0.25 (14 of 57) in AAAs, whereas the mean number of uptake areas colocalizing with highest wall stress and stress/ strength index areas was, respectively, 0.55 (6 of 11) in TAAs and 0.02 (1 of 57) in AAAs. Examples for PET imaging findings and FES estimates are shown in Figures 3 and 4.

Quantitative Analyses

On the entire set of examinations, 163 areas were selected: 54 areas based on ^{18}F-FDG PET (mean: 1.46±0.69 areas per patient) and 109 on FES (mean: 1.85±0.85 areas per patient; P=0.0019). Wall stress (P=0.017) and wall stress/strength index (P=0.011) estimates were significantly higher in TAAs than in AAAs, unlike SUV_{RL} (P=0.068), SUV_{RV} (P=0.12), local aortic diameter (P=0.21), and thrombus thickness (P=0.39; Table 2). A strong correlation (r=0.71; P<0.0001) was found between SUV_{RL} and SUV_{RV} (Figure 5). Positive correlations were observed between ^{18}F-FDG uptake and both wall stress and stress/strength index (Figures 6 and 7), but these were lower in FES-selected areas (r=0.28 for wall stress and r=0.30 for stress/strength index) than in 18F-FDG PET-selected areas (r=0.36 for wall stress and r=0.37 for wall stress/strength index using SUVRV, and r=0.44 for both wall stress and wall stress/strength index using SUV_{RL}; all P<0.05). A general linear mixed model was fitted to SUV_{RV} values to assess potential associations with FES-related characteristics and patient-related risk factors while accounting for repeated scans within patients (Table 3). As a result, SUV_{RV} values were significantly higher in TAA- than in AAA-selected areas (P=0.027) in subjects with a personal history of angina pectoris (P=0.012) and in patients with familial aneurysm (P=0.0065); no other parameter was significant.

Variable	AAA n=131 Areas	TAA n=32 Areas	P Value*
SUV_{RL}	0.68±0.15	0.86±0.24	0.068
SUV^{RV}	1.22±0.28	1.53±0.46	0.12
Wall stress, kPa	174±60.5	320±161	0.017
Stress/strength index	0.38±0.15	0.81±0.33	0.011
Local diameter, mm	42.6±10.3	47.3±19.0	0.21
Thrombus thickness, mm	2.01±2.08	2.53±3.74	0.39

Table 2. Values of Selected Areas of 18F-FDG Uptake, FES Estimates, Aortic Diameter, and Thrombus Thickness According to the Aneurysm Location

Discussion

There are only a few case studies in the literature that correlate wall stress estimates to ^{18}F-FDG uptake, often with opposite findings.[24,27] In the present hypothesis-generating work, we first evaluated such correlations visually and patient outcome. We observed differences between TAAs and AAAs on both the properties of imaging techniques and their rates of colocalization. This may be because of known structural differences between TAAs and AAAs: a larger intraluminal thrombus is a well-documented characteristic of AAA. However, inclusion of follow-up examinations, even after TAA dissection and false lumen thrombosis, did not support this explanation but, to the contrary, caused a larger dispersion of thrombus thickness in TAAs than in AAAs (2.53±3.74 versus 2.01±2.08 mm). However, the wall strength is better anticipated in the absence of extensive calcifications[28] or

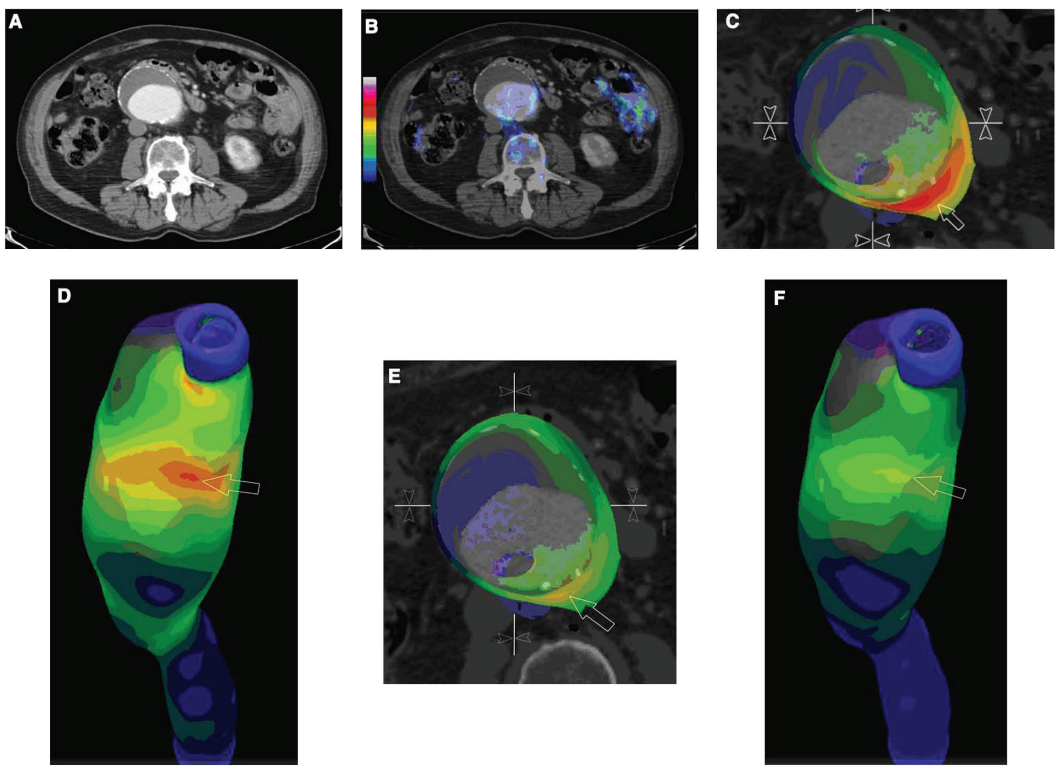

Figure 4. Absence of coincidence between positron emission tomographic (PET) imaging findings and finite element simulation estimates in a 72-year-old man with abdominal aortic aneurysm (A). After fusion with 18F-fluoro-deoxy-glucose (18F-FDG) PET imaging (B), no area of 18F-FDG uptake is seen, whereas coronal and axial projections of the aortic geometry show a large area (arrows) of increased wall stress (C and D; wall stress=315 kPa) and stress/strength index (E and F; stress/strength index=0.75) in the left posterior quadrant of the aorta. By convention, color code represents intensity scale ranging from deep blue to red. The patient's aneurysm was surgically repaired without delay because of the aneurysm diameter.

large intraluminal thrombus such as in AAAs.15,[29-31] Despite this, only minor differences were observed between the magnitudes of wall stress and stress/strength index, meaning that FES estimates were actually largely weighted by wall stress compared with wall strength. Therefore, further adjustments in wall strength assumptions are needed to increase correlations between ^{18}F-FDG uptake and stress/strength index, especially in AAAs.

When it comes to outcome prediction, Fillinger et al[32] and Sakalihasan et al[21] first suggested that wall stress estimates and ^{18}F-FDG uptake may perform better than the maximal aneurysm diameter. It is unknown whether biomechanical stress generates biological activity or, inversely, but the 2 imaging methods assess the pathophysiological activities involved in aneurysm rupture, which include aortic wall injury, inflammatory cell recruitment, and imbalance between elastin and collagen turnover.[14-15, 33] Our study was underpowered because only 7 events occurred during followup. Further, because most patients were close to having an intervention, they did not have a longer follow-up that would have increased longitudinal testing and more correlations among the tests and the event rate.

Despite this, there was a poorer 30-month clinical outcome prediction for patients with aneurysms with increased ^{18}F-FDG PET uptake. This suggests that yearly ^{18}F-FDG PET examination may be a reliable diameter-independent tool for clinical decision making in aortic aneurysms. Unfortunately, a similar dichotomization of FES based on an empirical value was not possible because of the heterogeneity of the study group. Nevertheless, the correlation levels between ^{18}F-FDG PET uptake and FES estimates indicate that similar outcome predictions could be expected from qualitative FES.

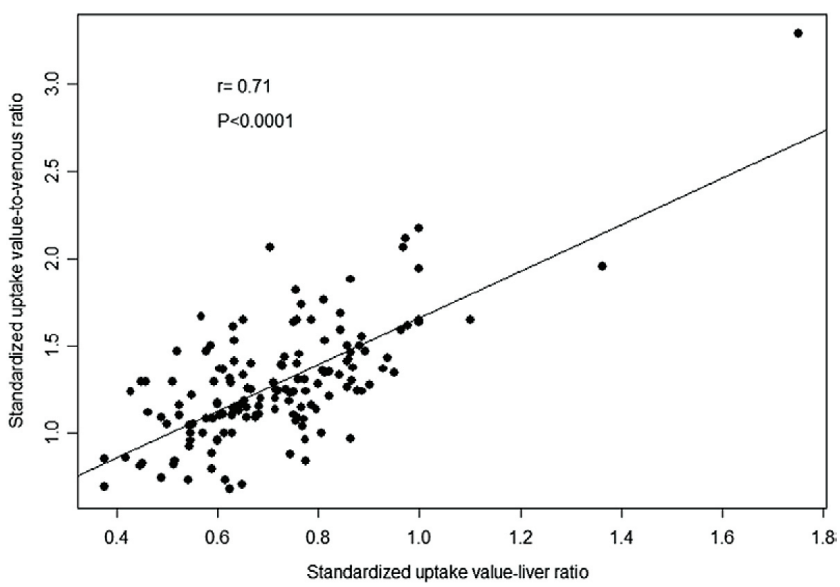

Figure 5. Scatter plot showing a significant positive correlation between quantitative 18F-fluoro-deoxyglucose uptake, normalized by the liver and the venous background in all patients.

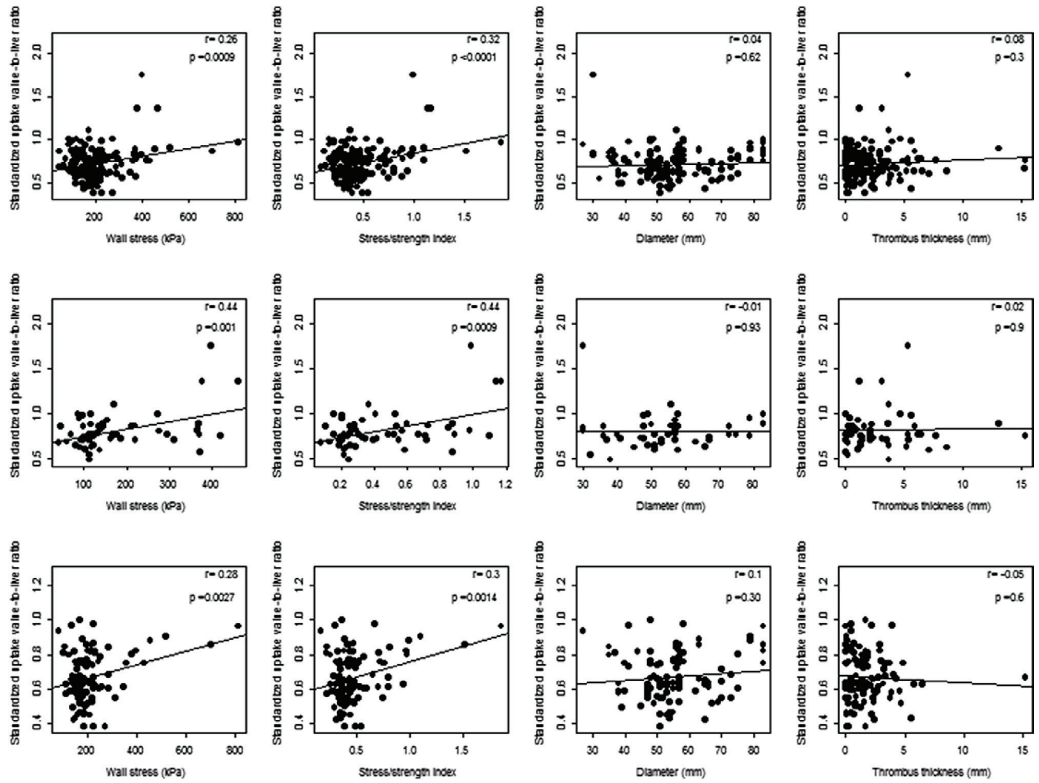

Figure 6. Scatter plots of standardized uptake value-to-liver ratio (SUV_{RL}) vs (from left to right rows) wall stress, wall stress/strength index, maximal diameter, and local thrombus thickness, respectively, for the whole areas (top line), those selected on ^{18}F-fluoro-deoxy-glucose positron emission tomographic imaging (middle line), and those selected on finite element simulation (bottom line). In all groups, a positive correlation is found between SUV_{RL} and both wall stress and wall stress/strength index estimates. No other variable is significantly correlated to SUV_{RL}.

FES and ^{18}F-FDG PET imaging are fully quantifiable methods. However, evaluating their correlation is technically challenging, mainly because the effect of partial volume and vessel background signaling on both modalities is different. Using a semiquantitative selection of areas of interest, we found modest positive linear relationships between 18F-FDG uptake and FES estimates (correlation range, 0.28–0.44). Our study is the first reporting FES geometry reconstruction without user interaction, obviously resulting in imprecision. We have also identified several determinants for these correlations, including technical factors that can affect the analysis.

The correlations with FES parameters were better using a liver rather than a venous-to-background correction, despite a strong correlation between both normalizers. Further, PET scanners have a finite spatial resolution of 5 to 8 mm, causing a low sensitivity to small focus of ^{18}F-FDG uptake, which may account for the mean number of area selection in each examination being lower based on ^{18}F-FDG PET than on FES (1.46±0.69 versus 1.85±0.85 areas per patient). Angina pectoris and

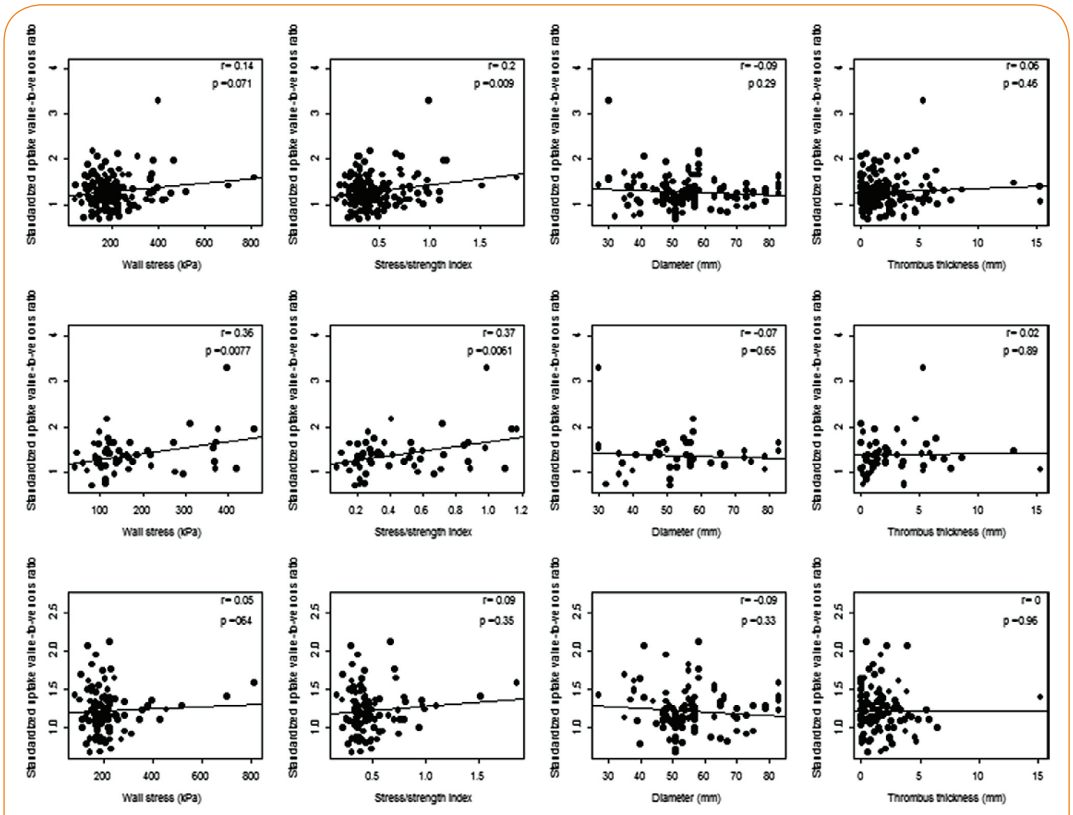

Figure 7. Scatter plots of standardized uptake value-to-venous ratio (SUV_{RV}) vs (from left to right rows) wall stress, wall stress/strength index, maximal diameter, and local thrombus thickness, respectively, for the whole areas (top line), those selected on ^{18}F-fluoro-deoxyglucose (^{18}F-FDG) positron emission tomographic (PET) imaging (middle line), and those selected on finite element simulation (bottom line). In all areas, a positive correlation is found between SUV_{RV} and wall stress and stress/strength index estimate. In ^{18}FDG PET selected areas, a positive correlation is found between SUV_{RV} and both wall stress and wall stress/strength index estimates. No other variable is significantly correlated to SUV_{RV}.

familial aneurysms had a significant effect on the relationship between ^{18}F-FDG uptake and FES estimates.[34] Previously, Verloes et al[35] found that the likelihood of aortic aneurysm rupture is strongly linked to the family history and gene susceptibility. These observations may be related to an alteration in the aortic wall response to stress.

Other factors, beyond the scope of the present study, may theoretically influence the relationship between ^{18}F-FDG uptake and wall stress estimates. Wall stress elevation does not necessarily imply increased ^{18}F-FDG uptake. This is illustrated by the fact that in normal and dilated aortas, the magnitude of blood flow velocity decreases gradually from proximal to distal, whereas ^{18}F-FDG uptake does not change in the same magnitude.[19] Finally, it has been reported that an inflammatory reaction related to nonspecific injuries, such as thrombus apposition and calcifications, may result in increased ^{18}F-FDG uptake without wall stress increase.[36]

Study Limitations

The current study has several limitations. Heterogeneity in aneurysm size introduced a potential bias by the lack of previous evidence that both ^{18}F-FDG uptake and wall stress profiles are similar in small and large aneurysms. AAAs largely outnumbered TAAs, although this reflects their relative proportions in the general population. It obviously resulted in comparison bias between aortic aneurysm types. This study was designed for a time point correlation between variables obtained from a single examination. The fact that most of the AAAs and TAAs were, respectively, >50 and >55 mm in diameter did not allow sufficient follow-up data because most patients were readily eligible for repair. Further, ^{18}F-FDG activity may change over time, whereas wall stress is unlikely to change in the same manner. However, these changes over time have never been studied. This was difficult in our study because of limited follow- up examinations dictated by the time scale and entry-point heterogeneities.

The isotropic model, which assumes that wall stress is the same in all directions, has been used here because it is easier to estimate, whereas an anisotropic model would have been more realistic and would allow for more accurate correlations. As in other studies, wall thickness assumption was independent of the underlying intraluminal thrombus. Although both are strongly related,[30] there is no valid way to measure the wall thickness (therefore, inappropriately the same wall thickness is used throughout the aneurysm) of aneurysmal aorta containing intraluminal thrombus and atherosclerotic changes. Despite all these assumptions, the FES model used in the present study has been validated in the sense that it retrospectively discriminated ruptured and intact AAAs.[37] Finally, low wall shear stress because of blood flow might also be related to metabolic activity by inducing inflammatory responses.[38] Nevertheless, wall shear stress predictions would have required computational fluid dynamics simulations, which are known to be sensitive to inflow conditions (ie, aortic blood flow velocity at the level of the renal arteries), that were unfortunately not available.

Variable	Regression Coefficient±SE	P Value*	Patient Characteristic	Regression Coefficient±SE	P Value*
Area selection technique (FES)	−0.04±0.071	0.57	Current smoking	−0.15±0.10	0.15
Maximal aortic diameter	−0.004±0.004	0.26	Stopped smoking	−0.19±0.10	0.061
Wall stress, kPa	0.0010±0.002	0.54	COPD	−0.11±0.078	0.17
Wall stress/strength	−0.48±0.62	0.43	Stroke	−0.062±0.092	0.51
Local diameter	0.0007±0.003	0.83	Peripheral artery disease	−0.029±0.077	0.71
Thrombus thickness	0.024±0.016	0.15	Angina pectoris	0.23±0.087	0.012
Aneurysm location (AAA)	−0.30±0.13	0.027	Renal insufficiency	−0.12±0.095	0.20
Age	0.006±0.005	0.29	Acute myocardial infarction	−0.069±0.078	0.38
Sex (male)	−0.060±0.12	0.63	Familial aneurysm	0.37±0.13	0.0065

Table 3. Evaluation of SUV_{RV} as a Function of Area Selection Method, Imaging and FES Parameters, and Subjects' Risk Factors (n=163)

Conclusions

^{18}F-FDG uptake and estimates of wall stress and stress/strength index, using the data from a single examination, showed better positive correlations in TAAs than in AAAs. The signaling relationships are related to the properties of both imaging techniques and become more complex by the influence of patient-specific risk factors such as inherited susceptibilities.

The findings of this study warrant further investigations in larger trials with prospective long-term data to identify patients at risk for clinical events and to better determine the relationships among wall biomechanics, blood flow interaction, wall remodeling, and inflammation.

Acknowledgments

We thank Cécile Wégria and Isabelle Mancini for article handling, editing, and management; Martin Auer for A4clinics software support; and Roland Hustinx, MD, PhD, for technical advice in 18F-fluoro-deoxy-glucose positron emission tomography imaging data interpretation. Sources of Funding The study was supported by the European Union Seventh Framework Programme (FP7) Fighting Aneurysmal Diseases No. 20064725 and a grant of impulsion from University of Liège.

Disclosures

None.

Clinical perspective

The maximal diameter remains the only validated criterion for preventive repair in asymptomatic aortic aneurysm. Because aortic aneurysm is an aging disease, the operative risk has to account for comorbidities that often make clinical decisions difficult. We compared 2 alternative approaches to assess the clinical risk associated with aortic aneurysm using 18F fluorodeoxyglucose positron emission tomography and finite element simulations. Our study revealed that increased fluoro-deoxy-glucose uptake in aortic aneurysm was associated with a higher risk of clinical event. Provided this finding is replicated in larger series, fluoro-deoxy-glucose uptake could serve as an additional independent factor in the management of patients with aortic aneurysms. Fluoro-deoxy-glucose uptake and wall stress were positively correlated and were both higher in thoracic than in abdominal aortic aneurysms. The strength of association, however, may strongly depend on technical and patient-specific factors, probably related to the ability of the aneurysmal wall to respond appropriately to wall stress.

References

1. Gillum RF. Epidemiology of aortic aneurysm in the United States. J Clin Epidemiol. 1995;48:1289–1298.
2. Bengtsson H, Sonesson B, Bergqvist D. Incidence and prevalence of abdominal aortic aneurysms, estimated by necropsy studies and population screening by ultrasound. Ann N Y Acad Sci. 1996;800:1–24.
3. Dillavou ED, Muluk SC, Makaroun MS. Improving aneurysm-related outcomes: nationwide benefits of endovascular repair. J Vasc Surg. 2006;43:446–451; discussion 451.
4. Greenhalgh RM, Brown LC, Powell JT, Thompson SG, Epstein D, Sculpher MJ; United Kingdom EVAR Trial Investigators. Endovascular versus open repair of abdominal aortic aneurysm. N Engl J Med. 2010;362:1863–1871.
5. Brady AR, Thompson SG, Fowkes FG, Greenhalgh RM, Powell JT; UK Small Aneurysm Trial Participants. Abdominal aortic aneurysm expansion: risk factors and time intervals for surveillance. Circulation. 2004;110:16–21.
6. Elefteriades JA. Natural history of thoracic aortic aneurysms: indications for surgery, and surgical versus nonsurgical risks. Ann Thorac Surg. 2002;74:S1877–S1880; discussion S1892.
7. Brewster DC, Cronenwett JL, Hallett JW Jr, Johnston KW, Krupski WC, Matsumura JS; Joint Council of the American Association for Vascular Surgery and Society for Vascular Surgery. Guidelines for the treatment of abdominal aortic aneurysms. Report of a subcommittee of the Joint Council of the American Association for Vascular Surgery and Society for Vascular Surgery. J Vasc Surg. 2003;37:1106–1117.
8. Darling RC, Messina CR, Brewster DC, Ottinger LW. Autopsy study of unoperated abdominal aortic aneurysms. The case for early resection. Circulation. 1977;56(3 Suppl):II161–II164.
9. Nicholls SC, Gardner JB, Meissner MH, Johansen HK. Rupture in small abdominal aortic aneurysms. J Vasc Surg. 1998;28:884–888.
10. Brown LC, Powell JT. Risk factors for aneurysm rupture in patients kept under ultrasound surveillance. UK Small Aneurysm Trial Participants. Ann Surg. 1999;230:289–296; discussion 296.
11. Zienkiewicz OC, Taylor R.L., J.Z. Zhu. The Finite Elements Method. The Basis. 5th ed. Oxford, United Kingdom: Butterworth-Heinemann; 2000.
12. Raghavan ML, Hanaoka MM, Kratzberg JA, de Lourdes Higuchi M, da Silva ES. Biomechanical failure properties and microstructural content of ruptured and unruptured abdominal aortic aneurysms. J Biomech. 2011;44:2501–2507.
13. Gasser TC, Görgülü G, Folkesson M, Swedenborg J. Failure properties of intraluminal thrombus in abdominal aortic aneurysm under static and pulsating mechanical loads. J Vasc Surg. 2008;48:179–188.
14. Michel JB, Thaunat O, Houard X, Meilhac O, Caligiuri G, Nicoletti A. Topological determinants and consequences of adventitial responses to arterial wall injury. Arterioscler Thromb Vasc Biol. 2007;27:1259–1268.
15. Fontaine V, Jacob MP, Houard X, Rossignol P, Plissonnier D, Angles- Cano E, Michel JB. Involvement of the mural thrombus as a site of protease release and activation in human aortic aneurysms. Am J Pathol. 2002;161:1701–1710.

16. Houard X, Rouzet F, Touat Z, Philippe M, Dominguez M, Fontaine V, Sarda-Mantel L, Meulemans A, Le Guludec D, Meilhac O, Michel JB. Topology of the fibrinolytic system within the mural thrombus of human abdominal aortic aneurysms. J Pathol. 2007;212:20–28.
17. Defawe OD, Colige A, Lambert CA, Munaut C, Delvenne P, Lapière CM, Limet R, Nusgens BV, Sakalihasan N. TIMP-2 and PAI-1 mRNA levels are lower in aneurysmal as compared to athero-occlusive abdominal aortas. Cardiovasc Res. 2003;60:205–213.
18. Sakalihasan N, Michel JB. Functional imaging of atherosclerosis to advance vascular biology. Eur J Vasc Endovasc Surg. 2009;37:728–734.
19. Truijers M, Kurvers HA, Bredie SJ, Oyen WJ, Blankensteijn JD. In vivo imaging of abdominal aortic aneurysms: increased FDG uptake suggests inflammation in the aneurysm wall. J Endovasc Ther. 2008;15:462–467.
20. Kotze CW, Menezes LJ, Endozo R, Groves AM, Ell PJ, Yusuf SW. Increased metabolic activity in abdominal aortic aneurysm detected by 18F-fluorodeoxyglucose (18F-FDG) positron emission tomography/computed tomography (PET/CT). Eur J Vasc Endovasc Surg. 2009;38:93–99.
21. Sakalihasan N, Hustinx R, Limet R. Contribution of PET scanning to the evaluation of abdominal aortic aneurysm. Semin Vasc Surg. 2004;17:144–153.
22. Defawe OD, Hustinx R, Defraigne JO, Limet R, Sakalihasan N. Distribution of F-18 fluorodeoxyglucose (F-18 FDG) in abdominal aortic aneurysm: high accumulation in macrophages seen on PET imaging and immunohistology. Clin Nucl Med. 2005;30:340–341.
23. Reeps C, Essler M, Pelisek J, Seidl S, Eckstein HH, Krause BJ. Increased 18F-fluorodeoxyglucose uptake in abdominal aortic aneurysms in positron emission/computed tomography is associated with inflammation, aortic wall instability, and acute symptoms. J Vasc Surg. 2008;48:417–423; discussion 424.
24. Xu XY, Borghi A, Nchimi A, Leung J, Gomez P, Cheng Z, Defraigne JO, Sakalihasan N. High levels of 18F-FDG uptake in aortic aneurysm wall are associated with high wall stress. Eur J Vasc Endovasc Surg. 2010;39:295–301.
25. http://ec.europa.eu/research/health/medical-research/cardiovascular-diseases/projects/fad_en.html. Accessed November 25, 2013.
26. A4clinics User Manual vers. 3.0 VG. A4clinics, Vascops GmbH, Graz, Austria.
27. Reeps C, Gee MW, Maier A, Pelisek J, Gurdan M, Wall W, Mariss J, Eckstein HH, Essler M. Glucose metabolism in the vessel wall correlates with mechanical instability and inflammatory changes in a patient with a growing aneurysm of the abdominal aorta. Circ Cardiovasc Imaging. 2009;2:507–509.
28. Maier A, Gee MW, Reeps C, Eckstein HH, Wall WA. Impact of calcifications on patient-specific wall stress analysis of abdominal aortic aneurysms. Biomech Model Mechanobiol. 2010;9:511–521.
29. Wang DH, Makaroun MS, Webster MW, Vorp DA. Effect of intraluminal thrombus on wall stress in patient-specific models of abdominal aortic aneurysm. J Vasc Surg. 2002;36:598–604.
30. Kazi M, Thyberg J, Religa P, Roy J, Eriksson P, Hedin U, Swedenborg J. Influence of intraluminal thrombus on structural and cellular composition of abdominal aortic aneurysm wall. J Vasc Surg. 2003;38:1283–1292.

31. Dobrin PB. Pathophysiology and pathogenesis of aortic aneurysms. Current concepts. Surg Clin North Am. 1989;69:687–703.
32. Fillinger MF, Marra SP, Raghavan ML, Kennedy FE. Prediction of rupture risk in abdominal aortic aneurysm during observation: wall stress versus diameter. J Vasc Surg. 2003;37:724–732.
33. Sakalihasan N, Limet R, Defawe OD. Abdominal aortic aneurysm. Lancet. 2005;365:1577–1589.
34. Nordon IM, Hinchliffe RJ, Loftus IM, Thompson MM. Pathophysiology and epidemiology of abdominal aortic aneurysms. Nat Rev Cardiol. 2011;8:92–102.
35. Verloes A, Sakalihasan N, Koulischer L, Limet R. Aneurysms of the abdominal aorta: familial and genetic aspects in three hundred thirteen pedigrees. J Vasc Surg. 1995;21:646–655.
36. Georgakarakos E, Ioannou CV, Papaharilaou Y, Kostas T, Tsetis D, Katsamouris AN. Peak wall stress does not necessarily predict the location of rupture in abdominal aortic aneurysms. Eur J Vasc Endovasc Surg. 2010;39:302–304.
37. Gasser TC, Auer M, Labruto F, Swedenborg J, Roy J. Biomechanical rupture risk assessment of abdominal aortic aneurysms: model complexity versus predictability of finite element simulations. Eur J Vasc Endovasc Surg. 2010;40:176–185.
38. Cecchi E, Giglioli C, Valente S, Lazzeri C, Gensini GF, Abbate R, Mannini L. Role of hemodynamic shear stress in cardiovascular disease. Atherosclerosis. 2011;214:249–256.

Supplemental material

Supplementary method 1

^{18}F-FDG PET CT imaging

All patients underwent the same image acquisition protocol. After a minimum of 6h fasting, 3.7 MBq ^{18}F-FDG/Kg body weight (mean activity/patient: 277 MBq, range: 202-394 MBq) was injected through a peripheral vein catheter. The patient was placed into a quiet room and instructed not to move. All patients had glucose serum levels below the threshold of 200 mg/dl, except one (292 mg/dl). Approximately 1h (mean: 69 min, range: 54-100 min) after injection of ^{18}F-FDG, static whole-body examination was performed with a PET-CT scanner Discovery LS (General Electrics Healthcare, Milwaukee, WI). The CT component of this scanner (LightSpeed Ultra) can acquire 4 slices per X-ray tube rotation. After scout views, CT was performed from the skull base to the femoral necks 50 seconds after the start of intravenous injection of 120 ml of an iodinated contrast agent (Omnipaque 350 mg of I/ml, General Electrics Healthcare, Diegem, Belgium) into an antecubital vein, at a rate of 2 ml/s. CT parameters were: 5 mm collimation, 50 x 50 cm field-of-view (FOV), 120 kVp, pitch of 1.5:1, gantry rotation cycle of 0.8 s, and automatic adaptation of the amperage at each tube rotation, optimized with indications provided by the scout views. During CT data acquisition, the patients were asked to hold breath at an average lung volume as long as they can, and if necessary, to breath shallowly until the end of acquisition. Thereafter, emission images were recorded at each bed position for 4 minutes. PET raw data were reconstructed as coronal 4.25 mm slice-thickness overlapping from 15-30%, by mean of ordered subset expectation maximization (OSEM) reconstruction algorithm performed with 2 iterations and 21 ordered subsets (pixel matrix of 128 x 128 and FOV of 50 cm), with 5.86 mm full width at mid-height (FWHM) post filter and 3.91 mm FWHM loop filter, model-based scatter correction (convolution subtraction) and normalization correction. To decrease the total radiation dose, PET data attenuation correction was performed using contrast-enhanced CT raw data that cause a 20-40% overcorrection [1-3].

FES

Aneurysms were reconstructed off-line from the CT images by an experienced operator blinded to patient and ^{18}F-FDG PET data, with the diagnostic system A4clinics (VASCOPS GmbH, Graz, Austria)[4]. The reconstruction was based on deformable models [5], which require minimal user interactions and provide operator insensitive results [6]. The finite element method [7] is an established numerical concept that divides any geometry into a large number of small finite elements, which together define a structural model of the aneurysm including a hypothetical wall-thrombus limit paralleling the external aortic contour (Figure 1). The hypothetical finite element model is pressurized by the mean arterial pressure (1/3 systolic pressure + 2/3 diastolic pressure). The applied models considered isotropic constitutive descriptions for the intraluminal thrombus [8] and the aneurysm wall [9]. An isotropic constitutive model is thought to be an acceptable approximation and assumes that the tissue's mechanical properties do not depend on the orientation, i.e. the stress-strain responses of circumferential and longitudinal strips of tissue are identical. In this study, the same wall thickness assumptions were applied to TAAs and AAAs. Finite element models used in this study specifically adjust the wall thickness inversely proportional to the amount of intraluminal thrombus[10], as this is required for accurate stress predictions [11]. Further details regarding the concept and assumptions used by A4clinics are given elsewhere [4-5].

For each aneurysm, the detailed FES predicted the distribution of the wall stress all over the aorta. Specifically, the von Mises stress $\sigma_M = \{[(\sigma_1 - \sigma_2)^2 + \sigma_1^2 + \sigma_2^2]/2\}^{0.5}$ *was used to represent the biaxial stress state by a single stress value. Here,* σ_1 *and* σ_2 *denote respectively the principal stress components, i.e. the circumferential and axial stresses in the wall. Relating this stress to estimated wall strength defines a stress/strength index. The used wall strength model was based on in-vitro failure tests of AAA wall samples [12]. The applied model considered heterogeneous wall strength that accounted for local wall weakening influenced by the ILT, gender, family history and the ratio between the local diameter and the normal infrarenal aortic diameter [12].*

Supplementary method 2

Relative intensity of a Finite Element Simulation (FES) estimate = [(recorded maximal value – mean value of the whole aorta)/(maximal value of the whole aorta – mean value of the whole aorta)] x100.

Supplementary method 3

^{18}F-FDG Standardized Uptake Value (SUV) allows inter-subject comparisons by removing most of the differences due to body weight and injected dose, using the following formula:
SUV = [^{18}F-FDG uptake (MBq/g) x patient weight (g)] / injected activity (MBq).

	Unoperated		*Operated*	*Other causes of follow-up termination*	
	Uneventful follow-up	*Death from unrelated cause*	*Oversized*	*Growth (> 1cm/year)*	*Acute rupture/ dissection*
Patients (n = 53)	*24*	*7 (2)*	*15 (1)*	*4*	*(3) (3)*
Follow-up duration (months)	*15.4±6.6*	*9.3±8.0*	*5.7±8.5*	*10.8±11.8*	*6.0±4.6*
Initial aneurysm diameter (mm)	*41.7±6.5*	*47.8±8.5*	*56,5±9.4*	*48.4±5.5*	*65.3±12.9*
PET-(n = 35)	*19*	*5 (1)*	*9*	*2*	*0*
PET+(n = 18)	*5*	*2 (1)*	*6 (1)*	*2*	*1*
FES Co-localization	*2*	*1 (1)*	*0*	*0*	*1*

Terminated follow-up are on darker background and significant clinical events right to the orange vertical line.
Between parentheses are the patients with TAAs.
PET = Positron Emission Tomography, ^{18}F-FDG = 18-fluoro-deoxy-glucose, FES = Finite Element Simulation.
PET+ are patients with aortic area of ^{18}F-FDG uptake on PET images, and PET- refers to no uptake.
FES co-localization (between parentheses) refers to the subgroup of PET+ patients in areas co-localized with a maximal value of a FES estimate.

Supplementary table1: Detailed clinical outcomes after the first examination

References

1. A4clinics User Manual vers. 3.0 VG.
2. Mawlawi O, Erasmus JJ, Pan T, Cody DD, Campbell R, Lonn AH, Kohlmyer S, Macapinlac HA, Podoloff DA. Truncation artifact on pet/ct: Impact on measurements of activity concentration and assessment of a correction algorithm. AJR. American journal of roentgenology. 2006;186:1458-1467.
3. Vera P, Ouvrier MJ, Hapdey S, Thillays M, Pesquet AS, Diologent B, Callonec F, Hitzel A, Edet-Sanson A, Menard JF, Jardin F, Tilly H. Does chemotherapy influence the quantification of suv when contrast-enhanced ct is used in pet/ct in lymphoma? European journal of nuclear medicine and molecular imaging. 2007;34:1943-1952.
4. Kotze CW, Groves AM, Menezes LJ, Harvey R, Endozo R, Kayani IA, Ell PJ, Yusuf SW. What is the relationship between (1)(8)f-fdg aortic aneurysm uptake on pet/ct and future growth rate? European journal of nuclear medicine and molecular imaging. 2011;38:1493-1499.
5. Auer M, Gasser TC. Reconstruction and finite element mesh generation of abdominal aortic aneurysms from computerized tomography angiography data with minimal user interactions. IEEE transactions on medical imaging. 2010;29:1022-1028.
6. Hyhlik-Durr A, Krieger T, Geisbusch P, Kotelis D, Able T, Bockler D. Reproducibility of deriving parameters of aaa rupture risk from patient-specific 3d finite element models. Journal of endovascular therapy : an official journal of the International Society of Endovascular Specialists. 2011;18:289-298.
7. Zienkiewicz OC TR e. The finite elements method. The basis. 5th edition ed. Oxford:Butterworth heinemann; n°1. 2000 Version révisée Page 6 of 6.
8. Gasser TC, Gorgulu G, Folkesson M, Swedenborg J. Failure properties of intraluminal thrombus in abdominal aortic aneurysm under static and pulsating mechanical loads. Journal of vascular surgery. 2008;48:179-188.
9. Raghavan ML, Vorp DA. Toward a biomechanical tool to evaluate rupture potential of abdominal aortic aneurysm: Identification of a finite strain constitutive model and evaluation of its applicability. Journal of biomechanics. 2000;33:475-482.
10. Kazi M, Thyberg J, Religa P, Roy J, Eriksson P, Hedin U, Swedenborg J. Influence of intraluminal thrombus on structural and cellular composition of abdominal aortic aneurysm wall. Journal of vascular surgery. 2003;38:1283-1292.
11. Gasser TC, Auer M, Labruto F, Swedenborg J, Roy J. Biomechanical rupture risk assessment of abdominal aortic aneurysms: Model complexity versus predictability of finite element simulations. European journal of vascular and endovascular surgery : the official journal of the European Society for Vascular Surgery. 2010;40:176-185.
12. Vande Geest JP, Wang DH, Wisniewski SR, Makaroun MS, Vorp DA. Towards a noninvasive method for determination of patient-specific wall strength distribution in abdominal aortic aneurysms. Annals of biomedical engineering. 2006;34:1098-1106.

PART TWO: New and promising concepts for biological process imaging in AAAs

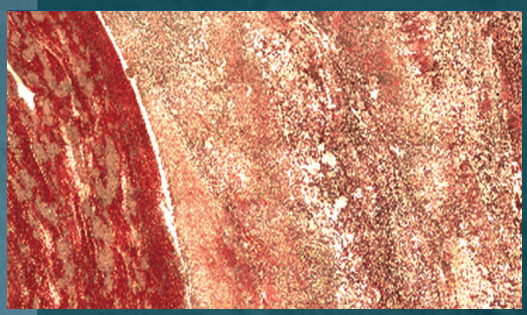
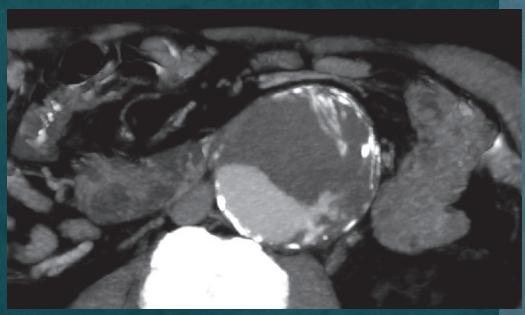
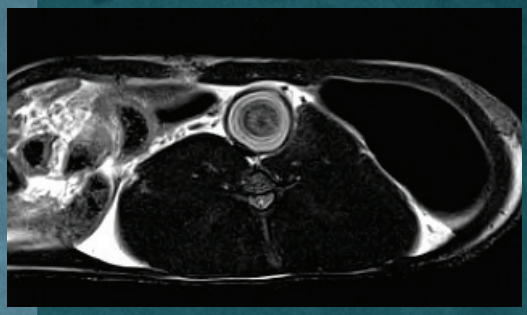
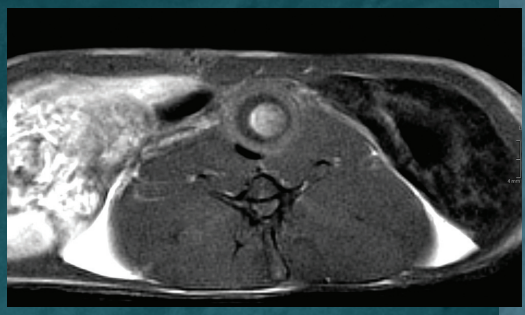

"The time will come when diligent research over long periods will bring to light things which now lie hidden..."

Seneca
Roman Stoic Philosopher (4BC –AD65)

Introduction to the appearance and the activities of the intraluminal thrombus

ILT is a parietal coagulum, almost ubiquitously part of the wall remodeling in human AAA and acting biomechanically as a damper against wall stress. Although ILT may contain patent vascular channels, calcifications or fat (see General Introduction), its typical macrospopic appearance represent a shade of colors from a carmine luminal layer towards a grayer red abluminal layer (Figure 11).

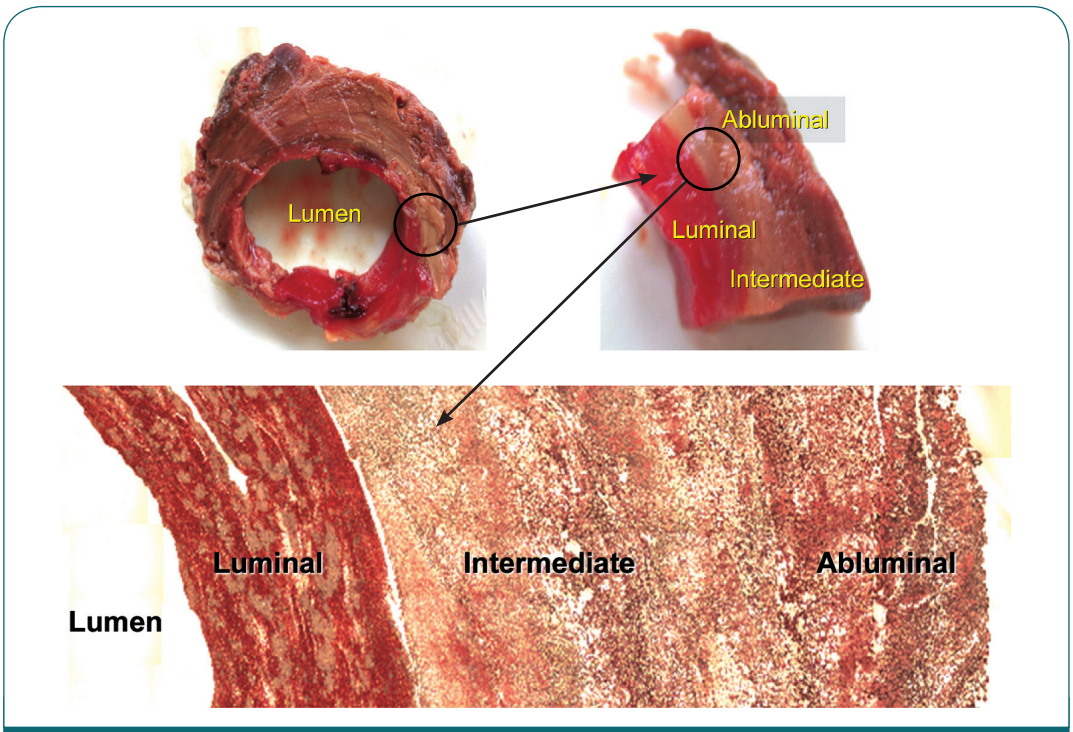

Figure 11 : Photograph of an ILT excised from human AAA, showing its color shades from a carmine luminal layer towards grayer abluminal layers.[31]

This appearance relates to the apposition with time of successive layers of thrombus from the lumen. It denotes a decrease of RBC content from the lumen towards the adventitia, and therefore refers to at least one of the ILT activities, namely RBC entrapment[106]. This gradient of RBC creates an oxidative gradient though the release of oxidant iron species. It should be stressed that not all of the ILT activities can be inferred of its appearance. Indeed, ex vivo and in vivo experiments have shown that ILT has the ability to activate platelets[56-57], initiate the fibrinolytic cascade[58, 107], activate the complement[59] and trap and activate leukocytes[60-61, 108]. Lastly, the structural organization of ILT makes it partially and heterogeneously permeable, ensuring pathways of communication between the lumen and the adventitia (inside-out) and vice versa (outside-in). The first is related to the convection of ILT activities from the lumen towards the adventitia[31], and the second to those of the periadventitial immune system through the lumen[72-74, 79].

1. Publication N°4: MR imaging of iron phagocytosis in intraluminal thrombi of abdominal aortic aneurysms in humans

1.1. Introduction

Biomechanical stress causes platelet activation and deposition of ILT in AAA. Biological activities associated with ILT are involved into rupture of aneurysms, including aggregation and activation of leukocytes that are responsible for the release of ECM proteases. These leukocytes have also phagocytic properties, capable of endocyting multiple particles such as superparamagnetic iron oxides (SPIO), which provide an opportunity for in vivo assessment of ILT biological activities. We conducted a study to assess the feasibility of such prospect in 15 patients who underwent T1W, T2W and pre- and post-SPIO T2*W MRI within 2 weeks before aneurysm repair. The T2*W signal changes of ILT after SPIO injection were quantified and correlated to the histological and immunohistological analysis of the collected fragments, as well as measurement of MMP2 and MMP9 mRNA level and activity by zymography. Finally, in-vivo findings were validated by ex-vivo scanning of ILT fragments, before and after incubation into solutions of SPIO.

1.2. Findings summary

Most of the patients were actually experiencing transient or constant clinical symptoms in relation with the aneurysm, such as back pain. Relevant morphological appearances of ILT on MRI were a high signal on T1W images (7/15) and a multilayered appearance (12/15) on T2W images, respectively resulting from unique or several intra-thrombus hemorrhages. A lower T2*W signal of the luminal layer of ILT, which reflects iron concentration, was the hallmark of unenhanced imaging. After injection of SPIO, the T2*W signal further decreased significantly along the luminal surface of ILT. There was a significant linear correlation between the magnitude of this signal drop and the density of phagocytic cells, as well as with the mRNA level of MMP9 and its activation. Further, the expression of this enzyme was associated in decreasing order of frequency to the following appearances of ILT: pluristratification, high T1W SI and monostratification.

1.3. Conclusions

MRI allows in vivo demonstration of phagocytosis along the luminal surface of ILT. SPIO phagocytosis is correlated with the abundance of leukocytes and proteolytic (MMP) activity. In addition, some appearances of ILT on MRI are also related to its biological activities, including thrombus stratification and subacute hemorrhage.

1.4. Reassessment summary/opportunities

The adventitial part of the thrombus was not affected by the signal changes related to the injection of SPIO, leaving no option for the assessment of this critical area where neo-angiogenesis and rupture eventually occur. The association between pre-contrast appearances of ILT and its iron content should be stressed, quantitatively evaluated and correlated with other biological activities.

Publication N° 4

This subchapter has been published as:

MR imaging of iron phagocytosis in intraluminal thrombi of abdominal aortic aneurysms in humans

A. Nchimi, O. Defawe, D. Brisbois, TK. Broussaud, JO. Defraigne, P. Magotteaux, B. Massart, JM. Serfaty, X. Houard, JB Michel, N. Sakalihasan

Radiology, 2010; (3): 973-81

MR Imaging of Iron Phagocytosis in Intraluminal Thrombi of Abdominal Aortic Aneurysms in Humans[1]

Alain Nchimi, MD
Olivier Defawe, MSc
Denis Brisbois, MD
Thomas K. Y. Broussaud, MSc
Jean-Olivier Defraigne, MD, PhD
Paul Magotteaux, MD
Brigitte Massart, MD
Jean-Michel Serfaty, MD
Xavier Houard, MD
Jean-Baptiste Michel, PhD
Natzi Sakalihasan, MD, PhD

Purpose: To prospectively determine if superparamagnetic iron oxide (SPIO)-enhanced magnetic resonance (MR) imaging could help visualize leukocyte phagocytic activities in human abdominal aortic aneurysms (AAAs).

Materials and Methods: This study was approved by the institutional ethics committee; all patients gave informed consent. Preoperative MR imaging data, including unenhanced and SPIO-enhanced T1-, T2*-, and T2-weighted transverse images of the entire AAA, obtained 1 hour after contrast enhancement from 15 patients (mean age, 72.7 years ± 8.2; range, 60–83 years), 10 men (mean age, 73.5 years ± 7.9; range, 60–83 years) and five women (mean age, 71.2 years ± 9.4; range 60–82), were retrospectively evaluated. Morphologic appearance and semiquantitative and contrast-to-noise ratio (CNR) analyses of the thrombi were performed. Thrombi were analyzed semiquantitatively at microscopy after staining with hematoxylin-eosin, CD68, and CD66b. Levels of promatrix metalloproteinase (pro-MMP)-2 and pro-MMP-9, MMP-2 and MMP-9, and their mRNA located in the thrombus were assessed by using zymography and quantitative reverse transcriptase polymerase chain reaction analysis. Nonparametric statistics of the Spearman rank correlation were calculated to evaluate correlations between the aneurysm thrombus signal level decrease after SPIO and the levels of $CD68^+$, $CD66b^+$ cells, pro-MMP-2 and pro-MMP-9, MMP-2 and MMP-9, and MMP-9 mRNA.

Results: The pre-SPIO CNRs in the luminal sublayer of the thrombus and the deeper thrombus were -10.20 ± 12.69 and -5.68 ± 10.38, respectively. After SPIO, the CNRs decreased to -21.34 ± 13.07 ($P < .001$) and -12.44 ± 14.56, respectively ($P < .012$). There was a significant linear correlation between the thrombus signal level decrease and the levels of $CD68^+$ and $CD66b^+$ cells, pro-MMP-9, and MMP-9 mRNA ($P < .05$).

Conclusion: MR imaging allows in vivo demonstration of SPIO uptake at the luminal interface of the thrombus. This uptake is correlated to the abundance of leukocytes.

Supplemental material: *http://radiology.rsna.org/lookup/suppl/doi:10.1148/radiol.09090657/-/DC1*

[1] From the Departments of Medical Imaging (A.N., D.B., T.K.Y.B., P.M.) and Pathology (B.M.), Centre Hospitalier Chrétien, Rue de Hesbaye, 75, B-4000 Liège, Belgium; Department of Cardiovascular Surgery, CHU Liège, University of Liège, Liège, Belgium (O.D., J.O.D., N.S.); and INSERM and Paris 7 University, Paris, France (J.M.S., X.H., J.B.M.). Received April 15, 2009; revision requested June 3; revision received July 20; accepted September 23; final version accepted October 5. Supported in part by the European Union integrated project, Fighting Aneurysmal Disease (*http://www.fighting-aneurysm.org*) and a grant from the University of Liege "Crédit de l'impulsion."
Address correspondence to A.N. (e-mail: *alain.nchimi@chc.be*).

Abdominal aortic aneurysm (AAA) complications are important causes of preventable deaths in the Western world[1]. Macroscopically, an AAA is fi lled to a varying extent with a parietal thrombus (the intraluminal thrombus), which decreases aneurysm wall stress[2]. Commonly, an aneurysm thrombus is a multilayered tissue that includes a luminal red blood cell (RBC)-rich sublayer and deeper RBCpoor sublayers.

The luminal sublayer interfaces the circulating blood components[3] and is biologically active[4-6], which may infl uence the evolution of the aneurysm. These biologic activities include (a) platelet activation[7-8], (b) the initiation of the fi brinolytic cascade[9-10], (c) the trapping of lysed RBC and the release of free iron, and (d) the trapping and activation of leukocytes that release matrix metalloproteinases (MMPs)[11-13] and other serine proteases. Therefore, it is of interest to help image leukocyte trapping. These leukocytes are professional phagocytic cells, capable of endocytosis of numerous microparticles, including iron microparticles[14].

Superparamagnetic iron oxide (SPIO) particles, which are contrast agents used for magnetic resonance (MR) imaging, and endogenous hemosiderin, both have a known affi nity for leukocytes. It has been suggested that macromolecular SPIO particles of a diameter similar to those of low-density lipoproteins (15–25 nm) and RBC-derived hemosiderin[15] enter and accumulate in atherosclerotic plaques with high macrophage content[16]. This prospective study was undertaken to determine if SPIO-enhanced MR imaging could allow visualization of leukocyte phagocytic activities in human AAA.

Materials and Methods

Patients

The institutional review board of the Centre Hospitalier Chrétien (Liège, Belgium) approved our study. All additional tissue samples used for the ex vivo experiments were obtained with the approval of the institutional ethics committee of the Hôpital Cochin. Between December 2003 and December 2005, we enrolled all patients who were referred for MR evaluation of an AAA and who did not have a contraindication to MR imaging or SPIO- or gadolinium-based contrast agent injection. During this period, 21 consecutive patients met the inclusion criteria and gave written informed consent. The indications for surgery and the clinical status of each patient included in our study were recorded and summarized online (Tables E1, E2) and in Table 1.

The following exclusion criteria were applied to our study group: failure to complete the MR protocol because of claustrophobia (n = 1), anaphylactic adverse reaction to the intravenous administration of SPIO (n = 1), and no surgery performed within two weeks of imaging (n = 4). Thus, complete preoperative MR imaging and postoperative histopathologic data obtained from 15 patients (mean age, 72.7 years ± 8.2 [standard deviation]; range, 60–83 years), 10 men (mean age, 73.5 years 6 7.9; range, 60–83 years) and fi ve women (mean age, 71.2 years 6 9.4; range, 60–82 years), who comprised our study group.

In Vivo MR Imaging Protocol

MR was performed with a 1.5-T imager (Magnetom Avanto; Siemens Medical Solutions, Erlangen, Germany) with an eight-element phased-array coil placed around the abdomen. After scout imaging was carried out, baseline sequences were performed, consisting of turbo spin-echo T2- and gradient-echo T2*- and T1-weighted imaging of the entire abdominal cavity in the axial plane. Non-breath-hold T2-weighted images were acquired by using a variable repetition time of at least 1800 msec, equaling a respiratory cycle, and an echo time of 101 msec. Then, T2*-weighted (repetition time msec/echo time msec, 146/10; flip angle, 65°) and T1-weighted (74/2.38; flip angle, 70°) imaging were performed in the same imaging planes with breath holds of less than 30 seconds.

All sequences were performed with the following parameters: section thickness, 6 mm; matrix size, 384 x 288; and field of view, 340 mm. Following baseline imaging, the patients received a slow intravenous infusion of ferumoxide SPIO (Endorem; Guerbet, Aulnay-sous-bois, France) of 0.075 mL per kilogram of body weight added to 500 mL of a 5% glucose solution over approximately a 30-minute period. One hour after the beginning of the infusion of the SPIO agent, the same pulse sequences were repeated. Thereafter, MR angiography of the abdominal aorta was performed and processed as previously described (17) to provide landmarks for tissue sampling and obtain relevant preoperative measurements. To evaluate the late postcontrast changes, we repeated the baseline pulse sequences 24 hours after SPIO administration on the first three patients enrolled in our study.

We proceeded to an intermediate analysis of late (24-hour) follow-up post-SPIO image data in this subset of patients, which revealed similar appearances to baseline images. Therefore, we decided to cancel late follow-up imaging and to analyze only early (1-hour) follow-up post-SPIO imaging data in all patients.

Qualitative Analysis of in Vivo MR Imaging

Two radiologists (A.N. and D.B., with 5 and 7 years experience in vascular MR, respectively) analyzed the preoperative imaging findings in consensus. For the morphologic evaluation of the AAAs, the aneurysm thrombus was considered to extend from the outer limit of the blood pool to the outer aortic contour on T2-weighted images.

The reviewers were asked to (a) categorize the thrombus appearance as homogenous, multilayered, or neither; (b) identify areas of low signal intensity (SI) on T2*-weighted images and areas of high SI on T1-weighted images, as compared with the paravertebral muscle; (c) identify the luminal sublayer (defined as the part of the thrombus adjacent to the blood pool and exhibiting a homogenous signal that is different from the blood pool signal) and the deeper thrombus (defined as the remaining part of the thrombus) on T2-weighted images; and (d) describe the SI of the blood pool as lower, higher, or unchanged after the SPIO injection.

Semiquantitative and Quantitative Analysis of in Vivo MR Imaging

The pre- and post-SPIO T2*-weighted images were compared at all section locations and the maximal SI decrease after SPIO at the level of the thrombus was semiquantitatively assessed by using a five-point scale: A score of 0 indicated null SI; 1, low SI; 2, moderate SI; 3, high SI; and 4, very high SI. After thrombus identification on each pre-SPIO T2-weighted image, the readers were asked to measure the maximal thickness of the whole thrombus, as well as the maximal thickness of its luminal sublayer, by using electronic calipers. SI values were averaged on three circular regions of interest (ROIs; range, 1–2 mm in diameter) at the levels of the luminal sublayer and the deeper thrombus (distance from the lumen of at least one-half of the thrombus thickness).

These ROIs were placed on the corresponding pre- and post-SPIO T2*-weighted images. If necessary, the ROIs were slightly corrected to match the targeted structures. Subsequently, ROIs of similar size were drawn on T2*-weighted images at the level of the paravertebral muscle and the air. For all analyses, the adventitial parts of the aortic wall were excluded because of possible signal variations related to the presence of calcifi cation and chemicalshift artifacts.

In addition, we evaluated (a) the SNR of the luminal sublayer of the thrombus, the deeper thrombus, and the muscle before and after SPIO by dividing their mean SI by the standard deviation of the air SI; and (b) the SI changes after SPIO injection by calculating the CNR relative to the muscle for the luminal sublayer and the deeper thrombus on pre- and post-SPIO T2* images. CNR was measured as the mean SI minus the mean SI of the muscle divided by the standard deviation of the SI of the air.

Parameter	Ratios	P Value	Parameter	Ratios	P Value
Pre-SPIO SNR			Post-SPIO SNR		
Luminal sublayer of the thrombus	28.60±19.24	.081	Luminal sublayer of the thrombus	30.60±16.07	.019 *
Deeper thrombus	37.10±26.12		Deeper thrombus	40.18±20.66	
Muscle	47.66±21.94		Muscle	51.95±22.39	
Pre-SPIO CNR			Post-SPIO CNR †		
Luminal sublayer of the thrombus	10.20±12.69	Not applicable	Luminal sublayer of the thrombus	21.34±13.07	Not applicable
Deeper thrombus	5.68±10.38		Deeper thrombus	12.44±14.56	

Note.—Data are the mean ± standard deviation for 15 AAAs. P values are analyses of variance. CNR = contrast-to-noise ratio, SNR = signal-to-noise ratio.
* Significant for thrombus vs muscle (P = .016).
† Wilcoxon matched-pair signed-rank test vs pre-SPIO CNR is P < .001 for thrombus and P < .012 for deeper thrombus.

Table 1. Quantitative MR Characteristics of AAAs

Collection of Specimens

For identification of the luminal sublayer and the deeper thrombus, the sections exhibiting the largest CNR decrease from pre- to post-SPIO imaging were identifi ed relative to an anatomic landmark (eg, a renal artery ostium) seen on preoperative maximum intensity projection MR angiograms displayed in the cephalocaudal axis. The area of interest was further identified, in degrees, relative to the anterior midline (ie, the largest sagittal diameter) of the infrarenal aorta. Prior to surgery, the section position displays were printed and given to the surgeon who was asked to collect fragments of full-thickness aortic wall in the preoperatively defined areas.

Ex Vivo MR Examination Protocol

To better evaluate the correlation between aneurysm thrombus signal and structure at MR imaging and pathologic findings, fresh well-conserved aneurysm thrombi were obtained from a human tissue bank (from five subjects) and were evaluated ex vivo by using MR. Thrombi were placed in a petri dish at the center of the 1.5-T MR imager between two four-element coils that measured 105 x 60 mm. Transverse T2*-weighted (650/27; flip angle 30°), T1-weighted (350/9.1; flip angle 180°), and T2-weighted (2500/81; flip angle, 150°) sequences were obtained by using the following parameters: section thickness, 2 mm; intersection gap, 0.2 mm; matrix, 256 x 256; and field of view, 80 mm. Thrombi were then fixed in 1% formol, embedded in paraffin, and cut in 5- μm sections.

Histologic and Immunohistochemical Analysis

Fragments of aortic tissue were fixed in 10% saline-buffered formaldehyde and processed with standard techniques for paraffin embedding. Tinctorial staining, including hematoxilin-eosin, Prussian blue

SI Level Scored	Score Total (n = 15)	r Value	P Value
Post-SPIO SI decrease of the luminal sublayer of the thrombus	27	Not applicable	Not applicable
CD68	29	0.731	.002
CD66b	30	0.646	.009
pro-MMP-2	32	0.396	.144
MMP-2	14	0.204	.465
mRNA MMP-9	29	0.582	.022
pro-MMP-9	43	0.614	.014
MMP-9	21	0.333	.225

Note.—Scores are for the post-SPIO SI loss of the luminal sublayer of the thrombus and the levels of immunohistologic, zymographic, and of reverse transcriptase polymerase chain reaction components.

Table 2. Correlation between Semiquantitative Scores

staining, and Masson Trichrome, as well as immunostaining for macrophages (CD68) and polymorphonuclears (CD66b) were used to evaluate the density, localization, and nature of the leukocytes in the thrombus. Sections for immunochemical analysis were pretreated with 0.1 mol/L of pepsin and subsequently incubated with monoclonal CD68 and CD66b mouse antibody (at a 1:100 solution; Dako, Glostrup, Denmark), biotinylated swine antimouse antibody (at a 1:250 solution; Amersham Life Science, Arlington Heights, Ill), and alkaline phosphatasecoupled ABC reagent (at a 1:200 solution; Dako). The sections were counterstained with hematoxylin-eosin. An abundance of CD68 + and CD66b + cells at the luminal surface of the thrombus was independently assessed by a pathologist (B.M., with 20 years experience), who was blinded to the clinical and image data, by using a five-point scale: A score of 0 indicated no cells; 1, barely any cells; 2, some cells; 3, many cells; and 4, high concentration of cells.

Zymography and Quantitative Reverse

Transcriptase Polymerase Chain Reaction From a thrombus sample dissected from the aortic wall in all specimens, equal amounts of proteins were loaded on sodium dodecyl sulfate gelatin polyacrylamide gels, and zymography was performed as described elsewhere[18]. After isolation, RNA concentration was measured from a similar sample by using a fl uorimetric assay (SpectraMax, Gemini-XS; MDS Analytical Technologies, Toronto, Canada). The steady-state mRNA levels of the proteolytic enzymes MMP-2 and MMP-9, as well as their inactive forms (pro-MMP-2 and pro- MMP-9), were measured by using a quantitative reverse transcriptase polymerase chain reaction procedure (11). Each sample was analyzed in triplicate. The optical density of the endogenous RNA was expressed in arbitrary units per unit of 28S ribosomal RNA. The respective levels of pro-MMP-2 and pro-MMP-9 proteins, MMP-2 and MMP-9 proteins, and mRNA were assessed by an experienced biologist (O.D.), who was blinded to the clinical and imaging data, by using a five-point scale: A score of 0 indicated null level; 1, low levels; 2, moderate levels; 3, high levels; and 4, very high levels.

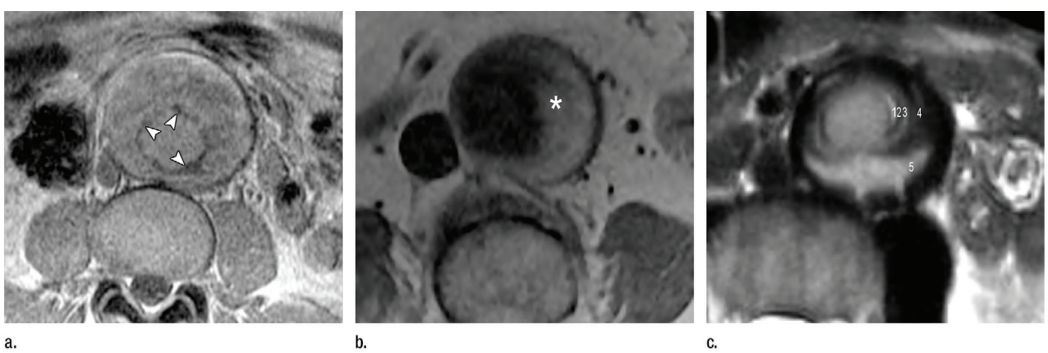

Figure 1: Representative in vivo baseline MR appearance of intraluminal thrombus (ILT) in three patients. (a) Preoperative axial T2*-weighted image in 73-year-old man with infrarenal AAA before SPIO injection. Luminal sublayer of ILT appeared as irregular low-SI rim delineating circulating blood (arrowheads). (b) Preoperative axial T1-weighted image in 60-year-old woman with infrarenal AAA shows ILT exhibited diffuse high SI (*). (c) Preoperative axial T2-weighted image in 74-year-old man with infrarenal AAA shows multilayer appearance of ILT, which refers to concentric apposition of layers exhibiting different SIs (1–5) .

Statistical Analysis

All the data were processed by using software (SPSS, version 14.0 for Windows; SPSS, Chicago, Ill). Continuous data were expressed as means ± standard deviations. Comparison of repeated measures was performed by using the Wilcoxon matched-pair signed-rank test; comparison of independent measures was performed with a multivariate analysis of variance. A P value of less than

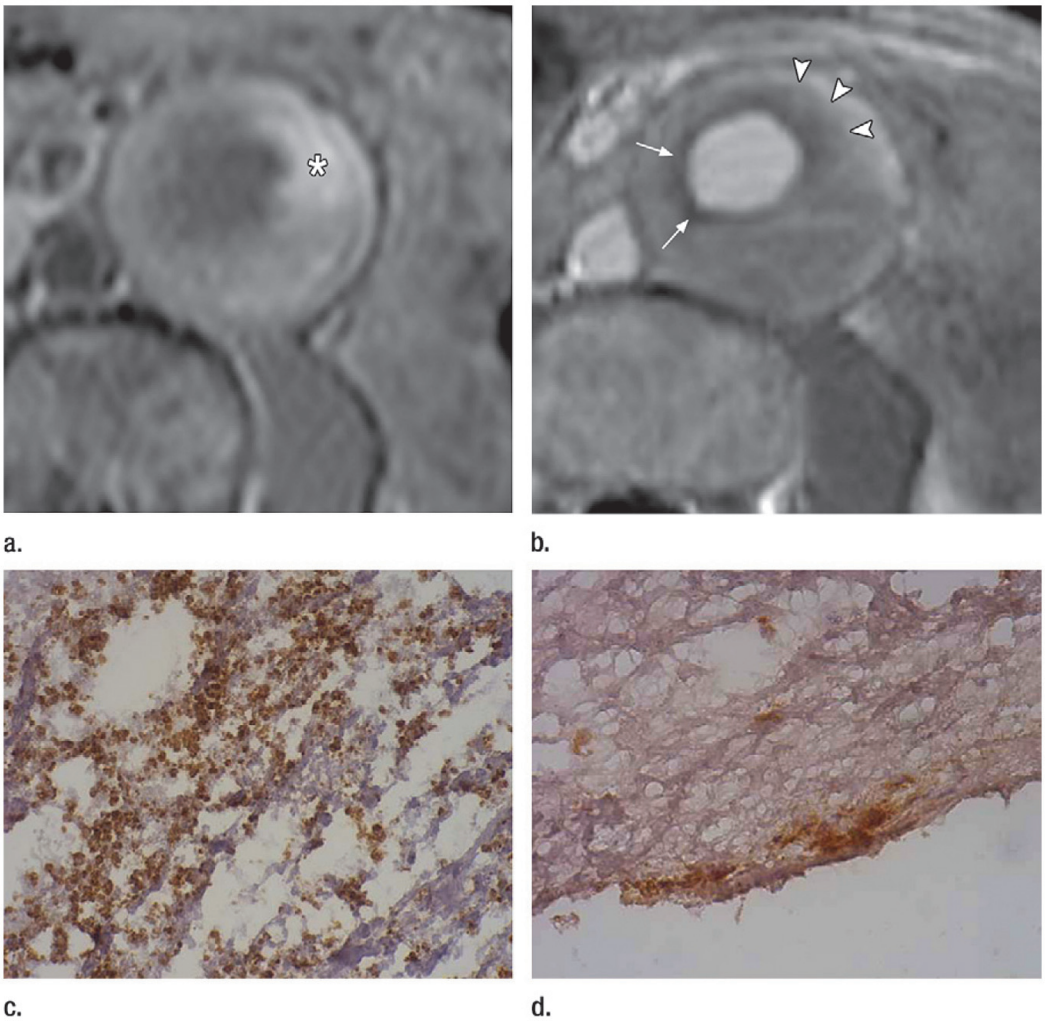

Figure 2: Effect of SPIO on MR imaging. (a) Preoperative axial T2*-weighted image at level of large aneurysm of infrarenal abdominal aorta before SPIO injection shows areas of high SI (*) . (b) T2*-weighted image 1 hour after SPIO at same level showed marked increase in SI of blood, owing to T1 effect of contrast agent, as well as areas of strong signal loss at levels of luminal sublayer (arrows) and deeper thrombus (arrowheads) resulting from T2* effect of contrast agent. Immunostaining of (c) neutrophils ($CD66b^+$ magnification, x 20) and (d) macrophages ($CD68^+$ magnification, x 20) show corresponding luminal infiltration of leukocytes containing cytopmlasmic brown iron deposits.

.05 was considered to indicate a signifi cant difference. When a significant difference was found at analysis of variance, multiple paired Bonferroni comparisons were performed. Nonparametric statistics were calculated by using the Spearman rank test to evaluate the linear correlations between the semiquantitative assessment of the thrombus SI decrease after SPIO and the semiquantitative levels of CD 68$^+$, CD 66b$^+$ cells, pro-MMP-2 and pro-MMP-9, MMP-2 and MMP-9 proteins, and MMP-9 mRNA.

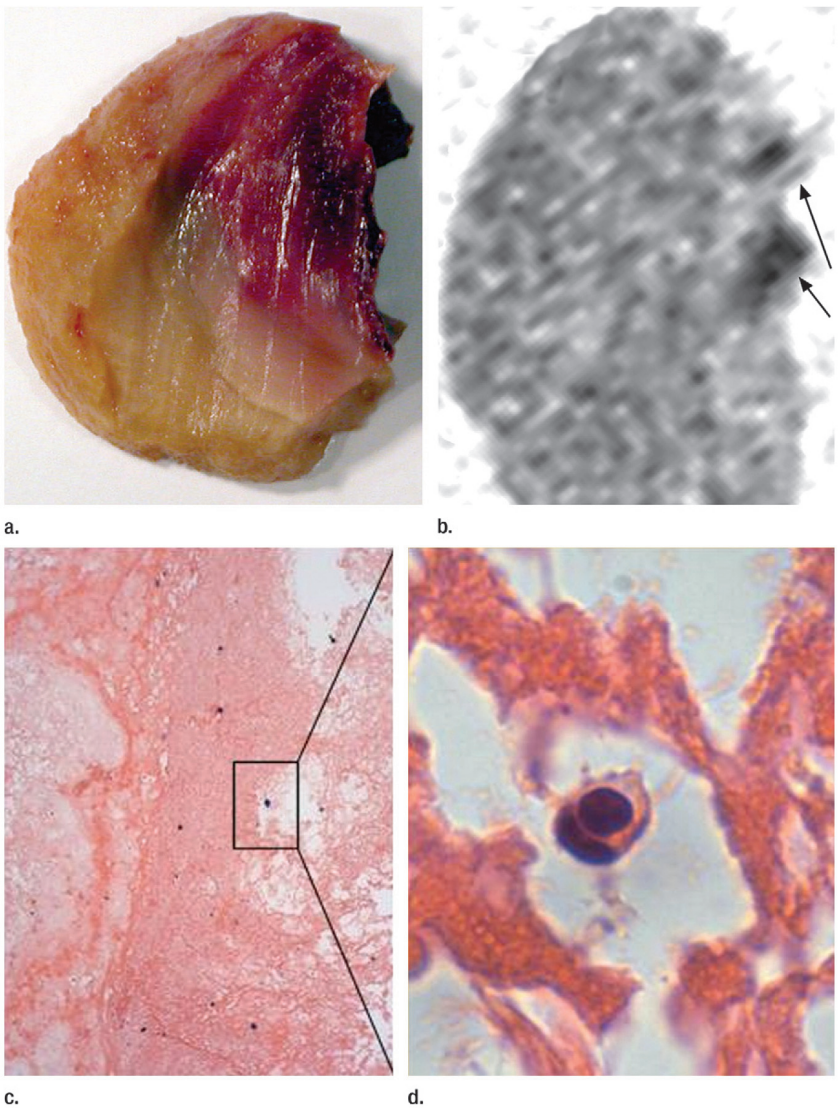

Figure 3: (a) Ex vivo appearance of intraluminal thrombus shows fragment of AAA thrombus that displays gross multilayered appearance, with successive layers representing different levels of blood iron concentration. (b) Ex vivo T2*-weighted section of thrombus fragment in a shows low-SI areas (arrows) at most luminal parts of thrombus, corresponding histologically to mononuclear infl ammatory infi ltration (c) Prussian blue staining (magnification, x 10) shows several neutrophils loaded by iron particles (d) Prussian blue staining magnifi ed from c (magnification, x 100).

Results

In Vivo MR Imaging

Clinical and imaging characteristics of the 15 AAAs are summarized online (Tables E1, E2) and in Table 2 and Figure 1 . Qualitatively, on pre-SPIO MR images, 12 (80%) of 15 thrombi had a multilayered appearance and three (20%) had a homogenous appearance on T2-weighted images, while seven (47%) thrombi exhibited a high-SI focus on T1-weighted images. In all patients, the luminal sublayer of the thrombus exhibited a lower SI compared with the deeper thrombus and the paravertebral muscle on T2*-weighted images. In all cases, the blood SI became higher while the thrombus SI became lower after SPIO injection (Fig 2).

At quantitative analysis on T2*-weighted images (Table 1), the mean pre-SPIO SNR was 28.60 ± 19.24 at the level of the luminal sublayer of the thrombus. SNRs were higher at the level of the deeper thrombus (37.10 ± 26.12) and the muscle (47.66 ± 21.94), but these differences were not significant (P = .081). After SPIO injection on T2*-weighted images, mean SNRs increased from the luminal sublayer (30.60 ± 16.07) to the deeper thrombus (40.18 ± 20.66) and the muscle (51.95 ± 22.39), with this difference being significant for the luminal sublayer of the thrombus versus the muscle (P = .016). The mean pre-SPIO CNRs of the luminal sublayer and the deeper thrombus were - 10.20 ± 12.69 and - 5.68 ± 10.38, respectively; mean post-SPIO CNRs were - 21.34 ± 13.07 and - 12.44 ± 14.56, respectively. The post-SPIO CNR decreases were significant for the luminal sublayer (P < .001) and the deeper thrombus (P < .012).

Ex Vivo MR Imaging

A low SI was observed at the level of the luminal face of the thrombus on T2*-weighted images, corresponding to areas where histologic analysis showed accumulation of leukocytes, including polymorphonuclears, which contain iron deposits seen at Prussian blue staining (Fig 3).

Correlation among Data from in Vivo MR, Histologic Analysis, Zymography, and Reverse Transcriptase Polymerase Chain Reaction

The postsurgical tissue samples were all obtained within 0–13 days after MR imaging (mean, 4.8 days ± 5.09). Figure 4 a is representative of MMP-2 and MMP-9 activity under latent or activated forms measured by using gelatin zymography, and Figure 4b shows the mean level of MMP-9 mRNA measured by using quantitative reverse transcriptase polymerase chain reaction for extracts of thrombus exhibiting three MR imaging appearances (ie, single-layer, multilayered, and high SI seen on T1-weighted images). The levels of MMP-9 and pro-MMP-9 protein, as well as MMP-9 mRNA, were higher in thrombi with a multilayered appearance or with high-SI foci on T1-weighted images, as compared with those with a single-layer appearance. The levels of MMP-2 and pro-MMP-2 protein remained relatively low and stable.

The respective correlations between semiquantitative assessment of the post-SPIO decrease in thrombus and the semiquantitative levels of CD 68⁺ and CD 66b⁺ cells (Figs 2c and 2d, respectively), pro-MMP-2/ and pro-MMP-9, MMP-2 and MMP-9, and MMP-9 mRNA are shown in Table 2. There was a significant linear correlation between the decrease in SI of the thrombus luminal sublayer and the levels of all markers ($P < .05$), except for MMP-2 ($P = .465$), pro-MMP-2 ($P = .144$), and MMP-9 ($P = .225$).

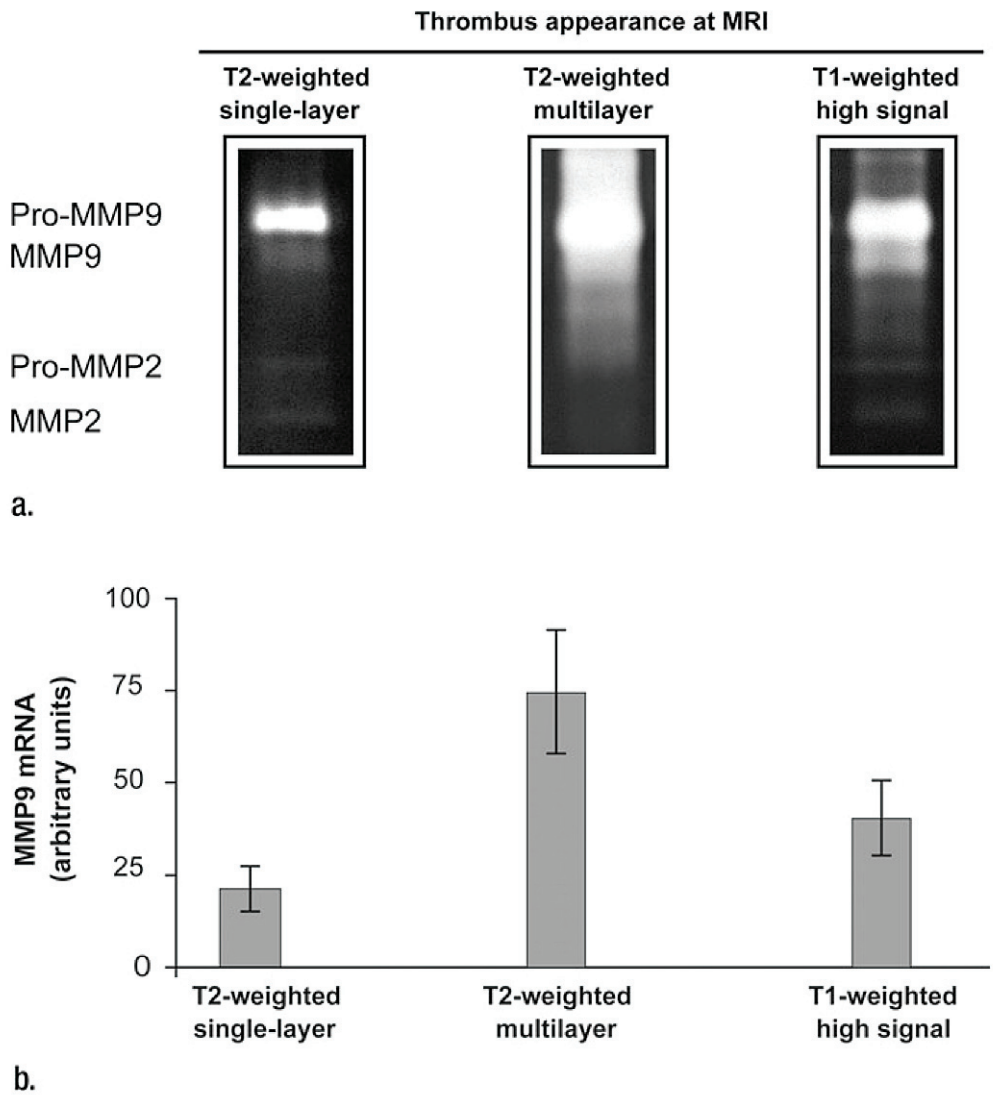

Figure 4: Relationship to MMP activities. (a) Maximum intensity projection zymograms of three AAA thrombi in patients with single-layer thrombi (left), 12 multilayered thrombi (center), and seven thrombi with areas of high SI on T1-weighted images (right) show high-intensity bands of pro-MMP-9 and MMP-9, especially in multilayered thrombi and thrombi with areas of high SI on T1-weighted images. (b) Levels of MMP-9 mRNA expression in three groups in relative arbitrary units (in same order as a) also showed increased expression in multilayered thrombi and those with areas of high SI on T1-weighted images.

Discussion

Our study shows in vivo evaluation of SPIO uptake at the level of the luminal and deeper layers of the thrombi of AAAs. Our study confirmed published in vivo and ex vivo data in which SPIO particles were successfully used to monitor phagocytic activities in nonaneurismal atherosclerotic plaques[16, 19-23]. It has been shown that the specific pathophysiologic processes in AAA thrombi include leukocyte retention[24], matrix destruction[25], and proteolytic activities[10]. MR imaging offers a twofold ability to monitor AAA, including morphologic assessment of the thrombus organization and visualization of phagocytic leukocytes by using SPIO as leukocyte-specific contrast agent.

MR imaging helps, to some degree, to evaluate tissue composition[26-27]. For example, given the absence of macroscopic fat accumulation in the thrombi, the high SI on T1-weighted images of thrombi suggest that either fibrinolysis or hemorrhage as their cause[28]. In our study, four of seven AAAs with high-SI foci seen on T1-weighted images were painful, whereas in the remaining eight patients, request for MR imaging was not related to a symptom. Such morphologic and clinical findings were also associated with high levels of MMP-9 and pro-MMP-9 (as well as its mRNA expression) that are known biomarkers of proteolysis.

On T2-weighted images, 12 (80%) of 15 high-risk AAAs evaluated in our study exhibited a multilayered thrombus consisting of successive layers with different SIs from the lumen to the adventitia. This finding correlates with the gross appearance of some AAA thrombi in which the most luminal sublayer of the thrombus is the most recent, while the most abluminal sublayer is the oldest[9-10, 29-30].

The relatively low SNR of the intimal sublayer of the thrombus compared with the deeper thrombus and the muscle on pre-SPIO T2*-weighted images, though not significant ($P < .081$), indicated that this part of the thrombus was particularly rich in SPIO particles. Similar findings were observed ex vivo and have been reported in rabbits in which provoked parietal thrombi were associated with hemosiderin deposition and signal loss on T2*-weighted images[31].

MR imaging can also demonstrate contrast agent uptake in the reticuloendothelial system[32]. In our study, the SPIO uptake resulted in significant signal reduction of both the luminal sublayer ($P < .001$) and deeper thrombus ($P < .012$). We also found a linear relationship between the thrombus SI reduction in and the abundance of iron-positive leukocytes, and the levels of MMP-9. These findings strongly link the thrombus trapping of leukocytes with the secretion of proteases in the thrombus, as suggested by previous reports[9, 13, 18].

Our study had a number of limitations. First, the use of SPIO particles was an important limitation, since only changes resulting from an early uptake could be visualized because of the massive liver clearance of the agent[32]. This might negatively affect the uptake sensitivity because such pharmacokinetics prevent uptake in poorly bloodaccessible areas. During the study, we abandoned scheduled imaging at 24 hours post-SPIO, as the images confirmed there provided no benefit. Second, we

did not semiquantitatively assess the levels of iron-containing infl ammatory cells. This was a result of the fact that we assumed an unknown leukocyte turnover at the luminal face of the thrombus. Indeed, the variable period between imaging and surgery resulted in some uncertainty regarding the localization of SPIO-loaded leukocytes.

Third, because of the small number of cases in our study and the recruitment mode, neither a precise relationship between MR imaging signal changes and the intensity of leukocyte infiltrates, nor a cutoff value of signal loss between normal and high-risk thrombus could be determined. Fourth, the pre-SPIO appearance of a relatively low SI on T2*-weighted images of the luminal sublayer of the thrombus compared with deeper layers account as a potential bias in imaging analysis. Indeed, the visual evaluation of SPIO uptake at the level of the luminal sublayer of the thrombus poses the challenge of evaluating a lowering of SI in a structure with an already low SI.

This challenge is further complicated by an increase of the circulating blood signal after SPIO injection, resulting from a T1 effect of the contrast agent. For similar reasons, ROI analysis at the level of the luminal sublayer is subject to a greater dispersion, although we averaged three different ROI for SI measurements to avoid this potential bias.

From a clinical point of view, the relevance of our study relies on the ability of MR imaging to help evaluate, in vivo, both morphologic and biologic changes at the luminal sublayer of the thrombus. These changes correlated with the level of proteolytic activities in the thrombus, which is the known cause of rupture. These changes may be realized in the future in the clinical environment if (a) there is further improvement in contrast agent pharmacokinetics to allow a better analysis of the deeper thrombus and the aortic wall by using ultrasmall SPIO particles instead of SPIO particles, and (b) there is documentation of the reproducibility of such findings in a larger series. Therefore, MR imaging could potentially provide crucial information in the assessment of risk rupture and surgical decision making.

MR imaging allows in vivo demonstration of SPIO uptake mainly localized at the luminal interface of the thrombus in high-risk AAAs. This uptake correlated with the abundance of leukocytes and may reflect the protease release in the thrombus.

Acknowledgments: The authors would like to thank Isabelle Mancini and Geneviève Peters for manuscript edition and management, and Samy Amir Aouchria, MD, for statistical advice.

Advances in Knowledge

- Phagocytosis, which is a specific leukocyte activity in abdominal aortic aneurysms (AAAs) in humans, can be demonstrated by using superparamagnetic iron oxide (SPIO)-enhanced MR imaging.
- Leukocyte phagocytic activity is mainly related to neutrophils and is seen at the luminal face of the parietal thrombus.
- The level of SPIO uptake—and therefore MR imaging changes— is not only correlated to the level of leukocyte infi ltrates, but also to the level of some parietal proteolytic enzymes, such as matrix metalloproteinase-9.

Implication for Patient Care

- MR imaging assessment of specific leukocyte activity at the luminal surface of an AAA thrombus may potentially result in better clinical risk stratification.

References

1. Law MR, Morris J, Wald NJ. Screening for abdominal aortic aneurysms. J Med Screen 1994; 1 (2): 110–115.
2. Wang DH, Makaroun MS, Webster MW, Vorp DA. Effect of intraluminal thrombus on wall stress in patient-specifi c models of abdominal aortic aneurysm. J Vasc Surg 2002 ; 36 (3): 598–604.
3. Hans SS, Jareunpoon O, Balasubramaniam M, Zelenock GB. Size and location of thrombus in intact and ruptured abdominal aortic aneurysms. J Vasc Surg 2005 ; 41 (4): 584–588.
4. Michel JB, Thaunat O, Houard X, Meilhac O, Caligiuri G, Nicoletti A. Topological determinants and consequences of adventitial responses to arterial wall injury. Arterioscler Thromb Vasc Biol 2007 ; 27 (6): 1259–1268.
5. Satta J, Läärä E, Juvonen T. Intraluminal thrombus predicts rupture of an abdominal aortic aneurysm. J Vasc Surg 1996 ; 23 (4): 737–739.
6. Stenbaek J, Kalin B, Swedenborg J. Growth of thrombus may be a better predictor of rupture than diameter in patients with abdominal aortic aneurysms. Eur J Vasc Endovasc Surg 2000 ; 20 (5): 466–469.
7. Touat Z, Lepage L, Ollivier V, et al. Dilationdependent activation of platelets and prothrombin in human thoracic ascending aortic aneurysm. Arterioscler Thromb Vasc Biol 2008 ; 28 (5): 940–946.
8. Sarda-Mantel L, Coutard M, Rouzet F, et al. 99mTc-annexin-V functional imaging of luminal thrombus activity in abdominal aortic aneurysms. Arterioscler Thromb Vasc Biol 2006 ; 26 (9): 2153–2159.
9. Fontaine V, Touat Z, Mtairag el M, et al. Role of leukocyte elastase in preventing cellular re-colonization of the mural thrombus. Am J Pathol 2004 ; 164 (6): 2077–2087.
10. Houard X, Rouzet F, Touat Z, et al. Topology of the fi brinolytic system within the mural thrombus of human abdominal aortic aneurysms. J Pathol 2007 ; 212 (1): 20–28.
11. Defawe OD, Colige A, Lambert CA, et al. TIMP-2 and PAI-1 mRNA levels are lower in aneurysmal as compared to atheroocclusive abdominal aortas. Cardiovasc Res 2003 ; 60 (1): 205–213.
12. Fontaine V, Jacob MP, Houard X, et al. Involvement of the mural thrombus as a site of protease release and activation in human aortic aneurysms. Am J Pathol 2002 ; 161 (5): 1701–1710.
13. Folkesson M, Kazi M, Zhu C, et al. Presence of NGAL/MMP-9 complexes in human abdominal aortic aneurysms. Thromb Haemost 2007 ; 98 (2): 427–433.
14. Hyafi I F, Laissy JP, Mazighi M, et al. Ferumoxtran- 10-enhanced MRI of the hypercholesterolemic rabbit aorta: relationship between signal loss and macrophage infi ltration. Arterioscler Thromb Vasc Biol 2006 ; 26 (1): 176–181.
15. Moreno PR, Purushothaman KR, Purushothaman M, et al. Haptoglobin genotype is a major determinant of the amount of iron in the human atherosclerotic plaque. J Am Coll Cardiol 2008 ; 52 (13): 1049–1051.
16. Schmitz SA, Coupland SE, Gust R, et al. Superparamagnetic iron oxide-enhanced MRI of atherosclerotic plaques in Watanabe hereditable hyperlipidemic rabbits. Invest Radiol 2000 ; 35 (8): 460–471.

17. Thurnher SA, Dorffner R, Thurnher MM, et al. Evaluation of abdominal aortic aneurysm for stent-graft placement: comparison of gadolinium-enhanced MR angiography versus helical CT angiography and digital subtraction angiography. Radiology 1997 ; 205 (2): 341–352.
18. Sakalihasan N, Delvenne P, Nusgens BV, Limet R, Lapière CM. Activated forms of MMP-2 and MMP-9 in abdominal aortic aneurysms. J Vasc Surg 1996 ; 24 (1): 127–133.
19. Reimer P, Allkemper T, Matuszewski L, Balzer T. Contrast-enhanced 3D-MRA of the upper abdomen with a bolus-injectable SPIO (SH U 555 A). J Magn Reson Imaging 1999 ; 10 (1): 65–7.
20. Kooi ME, Cappendijk VC, Cleutjens KB, et al. Accumulation of ultrasmall superparamagnetic particles of iron oxide in human atherosclerotic plaques can be detected by in vivo magnetic resonance imaging. Circulation 2003 ; 107 (19): 2453–2458.
21. Ruehm SG, Corot C, Vogt P, Kolb S, Debatin JF. Magnetic resonance imaging of atherosclerotic plaque with ultrasmall superparamagnetic particles of iron oxide in hyperlipidemic rabbits. Circulation 2001 ; 103 (3): 415–422.
22. Schmitz SA, Taupitz M, Wagner S, Wolf KJ, Beyersdorff D, Hamm B. Magnetic resonance imaging of atherosclerotic plaques using superparamagnetic iron oxide particles. J Magn Reson Imaging 2001 ; 14 (4): 355–361.
23. Litovsky S, Madjid M, Zarrabi A, Casscells SW, Willerson JT, Naghavi M. Superparamagnetic iron oxide-based method for quantifying recruitment of monocytes to mouse atherosclerotic lesions in vivo: enhancement by tissue necrosis factor-alpha, interleukin-1beta, and interferon-gamma. Circulation 2003 ; 107 (11): 1545–1549.
24. Houard X, Touat Z, Ollivier V, et al. Mediators of neutrophil recruitment in human abdominal aortic aneurysms. Cardiovasc Res 2009 ; 82 (3): 532–541.
25. Kazi M, Thyberg J, Religa P, et al. Infl uence of intraluminal thrombus on structural and cellular composition of abdominal aortic aneurysm wall. J Vasc Surg 2003 ; 38 (6): 1283–1292.
26. Toussaint JF, LaMuraglia GM, Southern JF, Fuster V, Kantor HL. Magnetic resonance images lipid, fi brous, calcifi ed, hemorrhagic, and thrombotic components of human atherosclerosis in vivo. Circulation 1996 ; 94 (5): 932–938.
27. Kramer CM, Cerilli LA, Hagspiel K, DiMaria JM, Epstein FH, Kern JA. Magnetic resonance imaging identifi es the fi brous cap in atherosclerotic abdominal aortic aneurysm. Circulation 2004; 109 (8): 1016–1021.
28. de Kerviler E, Cuenod CA, Clément O, Halimi P, Frija G, Frija J. What is bright on T1 MRI scans? [in French]. J Radiol 1998 ; 79 (2): 117–126.
29. Touat Z, Ollivier V, Dai J, et al. Renewal of mural thrombus releases plasma markers and is involved in aortic abdominal aneurysm evolution. Am J Pathol 2006 ; 168 (3): 1022–1030.
30. Carrell TW, Burnand KG, Booth NA, Humphries J, Smith A. Intraluminal thrombus enhances proteolysis in abdominal aortic aneurysms. Vascular 2006 ; 14 (1): 9–16.
31. Mani V, Briley-Saebo KC, Itskovich VV, Samber DD, Fayad ZA. Gradient echo acquisition for superparamagnetic particles with positive contrast (GRASP): sequence characterization in membrane and glass superparamagnetic iron oxide phantoms at 1.5T and 3T. Magn Reson Med 2006 ; 55 (1): 126–135.
32. Bulte JW, Kraitchman DL. Iron oxide MR contrast agents for molecular and cellular imaging. NMR Biomed 2004 ; 17 (7): 484–499.

Supplemental Tables

Patient No.	Sex	Age (y)	Aneurysm Size (mm)	Indication for surgery	Time for MR to surgery (d)	Included in Study	Reasons for Exlusion
1	M	80	Large, 59	Prophylaxis (uncertain follow-up compliance)	10	Y	Not applicable
2	M	76	Large, 67	Prophylaxis (critical size)	107	N	Delayed surgery
3	F	80	Small, 48	Expansion	2	Y	Not applicable
4	M	77	Large, 80	Prophylaxis (critical size)	13	Y	Not applicable
5	M	77	Large, 80	Expansion	Not applicable	N	MR imaging not completed (claustrophobia)
6	M	77	Large, 71	Prophylaxis (critical size)	0	Y	Not applicable
7	M	71	Large, 80	Prophylaxis (critical size)	0	Y	Not applicable
8	M	60	Small, 49	Expansion	4	Y	Not applicable
9	M	58	Small, 44	None	Not applicable	N	No surgery
10	F	66	Small, 48	Prophylaxis (uncertain follow-up compliance)	0	Y	Not applicable
11	F	68	Small, 32	Prophylaxis (severe underlying occlusive iliac disease)	2	Y	Not applicable
12	F	60	Large, 52	Expansion	12	Y	Not applicable
13	F	82	Large, 67	Pain relief	1	Y	Not applicable
14	M	74	Small, 52	Pain relief	4	Y	Not applicable
15	M	60	Large, 63	Prophylaxis (critical size)	0	Y	Not applicable
16	F	63	Large, 60	Prophylaxis (critical size)	Not applicable	N	MR imaging not completed (adverse reaction to contrast injection)
17	M	59	Small, 53	None	136	N	Delayed surgery (advanced colon cancer incidentally diagnosed)
18	M	74	Small, 45	Prophylaxis (large aneurysm of the left common iliac artery)	2	Y	Not applicable
19	M	79	Small, 33	Pain relief	9	Y	Not applicable
20	M	83	Large, 65	Pain relief	13	Y	Not applicable
21	M	45	Small, 51	Prophylaxis (Marfan disease with rapidity expanding aneurysm of thoracic aorta)	63	N	Delayed surgery

Table E1. Inclusion Status and Clinical Data of Patients

Patient No.	Clinical Indication for Imaging	Aneurysm Size (mm)	Whole Thrombus Thickness (mm)	Thickness of Luminal Sablayer of Thrombus (mm)*	Multilayered Appearance of Thrombus†	T1-weighted Focus of High SI
1	Evaluation of a recently diagnosed aneurysm	59	20	2	Y	N
3	Suspected expansion of a known aneurysm	48	20	2	Y	N
4	Evaluation of a recently diagnosed aneurysm	80	26	1	Y	N
6	Scheduled follow-up	71	30	2	Y	N
7	Scheduled follow-up	80	50	1	Y	N
8	Suspected expansion of a known aneurysm	49	20	1	N	N
10	Evaluation of a recently diagnosed aneurysm	48	15	1	N	N
11	Clinical suspicion of AAA in the setting of peripheral artery disease	32	7	1	N	N
12	Suspected expansion of a known aneurysm	52	25	3	Y	Y
13	Painful aneurysm	67	30	2	Y	Y
14	Painful aneurysm	52	35	2	Y	Y
15	Scheduled follow-up	63	18	2	Y	Y
18	Evaluation of a recently diagnosed aneurysm	45	15	2	Y	Y
19	Painful aneurysm	53	28	1	Y	Y
20	Painful aneurysm	65	35	2	Y	Y
All	Not applicable	56.47 ± 11.66‡	24.93 ± 10.46‡	1.6 ± 0.73‡	12/15 (80%)	7/15 (47%)

* Measured on T2*-weighted imaging.
† Seen on T2-weighted imaging.
‡ Data are the mean ± standard deviation.

Table E2. Morphologic MR Characteristics of AAAs

2. Publication N°5 (submitted). Assessment of the deleterious role of the intraluminal thrombus and its iron content with multi-modality imaging, in a rat model of abdominal aortic aneurysm

2.1. Introduction

The deleterious role of ILT in AAA is suggested by its biological activities. Inhibition of the ILT may therefore be a potential therapeutic option. TXA2 is one of the main mediators implicated in arterial thrombus formation. It has been shown that TXA2 receptor antagonists such as BM-573 can prevent the development of aortic atherosclerosis in different mice models. Though, inhibition of ILT growth has never been evaluated in a model that closely reproduces human AAA in terms of ILT composition, such as the rat model by aortic infusion of elastase.

This study was undertaken to evaluate imaging changes occurring with time in a rat model of unruptured AAA, with emphasis on the ILT. Further, MRI assessment of ILT appearance and its iron content was carried out after treatment by a TXA2 receptor antagonist, the BM-573. Growth curve of the elastase-induced AAA was characterized using daily ultrasound.

Then, growth curves and pre-sacrifice MRI assessment of AAA length, ILT signal intensity (SI), iron content, stratification, thickness and volume were evaluated in groups of 6 rats treated with the vehicle and a low- (10 mg/Kg) and high- (30 mg/Kg) dose of BM-573. Effects of BM-573 were evaluated using GLMM.

2.2. Findings summary

In our model, increased wall metabolic activity (glycolysis) and AAA growth occur after the appearance of a macroscopic ILT, approximately 6 days after elastase infusion. A significant decrease of the aneurysmal length and ILT thickness and volume over 2 weeks in animals treated preventively and continuously by high-dose BM-573, as compared to controls supported the concept emphasizing the role of the ILT in aneurysmal growth.

Since the relationship between imaging parameters and the dose were almost all quadratic, the BM-573 effect can therefore be considered as strongly dose-dependent. There was a good concordance between MRI and histology for the iron quantification.

2.3. Conclusions

Multimodality imaging confirmed the concept of the deleterious role of the ILT in AAA growth. Evaluating the iron content hold promises for monitoring ILT biological activities in AAA using MRI without exogenous contrast agent. Tackling ILT activities through effective platelet aggregation inhibition could be an option in the medical management of unruptured AAA.

Publication N° 5

This subchapter has been submitted as:

Assessment of the deleterious role of the intraluminal thrombus and its iron content with multimodality imaging, in a rat model of abdominal aortic aneurysm

A. Nchimi, A. Courtois, M. El Hachemi, Z. Touat, A. Arbesu Y Miar, P. Drion, N. Withofs, G. Warnock, M. Bahri, JP. Cheramy-Bien, L. Schoysman, J. Joskin, JM. Dogné, JB. Michel, JO. Defraigne, A. Plenevaux, N. Sakalihasan.

Submitted

Abstract

Objectives: To evaluate imaging changes occurring in a rat model of elastase-induced abdominal aortic aneurysm (AAA), with emphasis on the intraluminal thrombus (ILT) occurrence, with and without treatment by BM-573, a thromboxane receptor antagonist.

Methods: The growth the AAA was characterized using ultrasound. Then, growth curves and magnetic resonance imaging (MRI) assessment of AAA length, ILT thickness, volume, stratification and signal intensity (SI) properties, were retrieved from analysis of 3 groups of 6 rats treated with a vehicle, low- (10 mg/Kg) or high- (30 mg/Kg) dose BM-573.

Results: Aneurysm growth followed occurrence of ILT, approximately 6 days after elastase infusion. Using a threshold of < average ILT's SI -1.6 SE for iron detection on T2-weighted MRI, intraclass correlation (ICC) with histology were significant in all (ICC = 0.71) and in untreated rats (ICC = 0.65), but not in treated rats (ICC = 0.04) because of overestimation. Aortic growth, aneurysm length, ILT thickness, volume and scores of high SI on T1-weighted and low SI on T2-weighted images were reduced by BM-573 ($p < 0.05$).

Conclusion: Our model emphasizes that occurrence of ILT precedes AAA growth, which is partially inhibited by BM-573. Iron content relating to ILT's biological activities, is evaluated using MRI.

Key words: Aneurysm, Aorta, Thrombus, Iron, Imaging

Key points:

ILT triggers growth in a rat model of elastase-induced AAA.
MRI marks RBC trapping activities in AAA thrombus through iron content assessment.
Monitoring ILT activities using MRI may require no exogenous contrast agent.
Slowing down ILT activities could be a non-surgical management option for AAA.

Introduction

Aneurysm is characterized by excessive extra-cellular matrix (ECM) degradation, causing decreased vascular wall resilience and elasticity against luminal pressure[1]. This ultimately leads to unpredictable but irreversible vessel dilation and eventually rupture[2-3].

An intraluminal thrombus (ILT) is almost ubiquitously part of the wall remodeling in human abdominal aortic aneurysm (AAA). The deleterious role of the ILT in AAA is suggested by its ability to activate platelets[4-5]; initiate the fibrinolytic cascade[6-7]; activate the complement[8]; trap important amount of red blood cell (RBC)[9]; trap and activate leukocytes[10-12] that release serine proteases and matrix metalloproteases (MMPs). Inhibition of the ILT may therefore be a potential therapeutic option[13]. The binding of thromboxane A2 (TXA2), released by the activated platelets, to its receptor induces (amongst others) platelet aggregation[14]. TXA2 is indeed one of the main mediators involved in arterial thrombus formation[15]. It has been shown that TXA2 receptor antagonists such as BM-573 and terutroban (S-18886) can prevent the development of aortic atherosclerosis in different models through inhibition of platelet aggregation and other pro-inflammatory activities[16-19]. Abciximab, another inhibitor of platelet aggregation limited the evolution of AAA in a xenograft rat model[20]. Though, inhibition of ILT has never been evaluated in a model that closely reproduces human AAA in terms of ILT composition, such as the rat aorta after infusion of swine pancreatic elastase[21].

On the other hand, rupture risk assessment through endogenous iron released by trapped RBC in the ILT has received only little attention in the literature. Iron-dependent oxidative stress is potentially one of the biological mechanisms able to promote experimental AAA progression through smooth muscle cell injury, as recently shown[22]. Iron which is the core of the heme causes signal intensity (SI) disturbances on magnetic resonance imaging (MRI)[23-24], providing opportunities to assess noninvasively and without exogenous contrast agent the RBC-trapping, and therefore some of the oxidative activities of the ILT[9]. To date, heterogeneity of the ILT on T2-weighted MRI has only been noticed in human aneurysms[25], but iron content was not used as a potential monitoring tool.

This study aimed at evaluating imaging changes occurring in a rat model of abdominal aortic aneurysm (AAA), with emphasis on the intraluminal thrombus (ILT). To prove the biological concept relating aneurismal growth to ILT, MRI assessment of the ILT, including its iron content was carried out with and without treatment by a thromboxane receptor antagonist, the BM-573.

Materials and methods

Experimental model and study design

All experimental procedures and protocols used in this investigation were reviewed and approved by the Institutional Animal Care and Use Ethics Committee of the University of Liège (Belgium). The "Guide for the Care and Use of Laboratory Animals," prepared by the Institute of Laboratory Animal Resources, National Research Council, and published by the National Academy Press, was followed carefully as well as European and local legislations.

An experimental model of unruptured AAA, by infusion of porcine elastase into rat (Male Wistar rats aged of 6 to 7 weeks, 220 – 300g) aorta, modified from on a previous description[21] was used (see appendix). A total number of 40 consecutively operated rats were included. The study's first arm was the characterization of the aneurysm growth using multimodality imaging, with emphasis on the ILT occurrence and wall glycolysis. 22 rats underwent serial transabdominal US examinations daily from day 2 post-surgery, until sacrifice. In addition, 14 MRI and 18 ^{18}F-fluorodeoxyglucose (FDG) positron emission tomography (PET) examinations were performed respectively on 13 (average 10±5; 2-18 days post-surgery), and 10 rats (average 13±7; 2-27 days post-surgery) (see supplemental material for US, T1- and T2-weighted 3 Tesla MRI and material-enhanced PET-CT imaging parameters). We scheduled to sacrifice 3 rats every 3 days, from day 2 until day 17, then on the 28th day post-surgery for the remaining.

The study's second arm was designed to evaluate the effects of BM-573 on this model. BM-573 was synthesized as previously described[26]. Starting 10 days before elastase infusion until sacrifice, BM-573 was administered through drinking water after dissolution into a solution of 1M natrium hydroxide daily at the dose of 10 mg/kg body weight in 6 rats (low-dose (LD) group) and at the dose of 30 mg/kg/body weight in 6 rats (high-dose (HD) group), while 6 rats received a vehicle (V group). All 18 rats underwent serial transabdominal US examinations daily from day 2 post surgery, and MRI before sacrifice, in the range of 12-15 days after surgery.

Histology

At sacrifice AAAs were sampled and fixed in formaldehyde. Sections were stained with Perl's+DAB for sensitive iron detection and quantified by computer-assisted image analysis (see supplemental material for details).

Image analysis

Analyses were performed offline (Leonardo, Siemens Medical Solutions) by two reviewers with > 2-year experience in vascular imaging and blinded to the histological findings (ANc, MeH). All discordant measures were reviewed to reach a consensus. On all imaging methods, the maximal

aortic diameter was measured using calipers. ILT presence was defined as >100% thickening of the wall on at least 2 orthogonal planes, as its signaling properties are variable, often heterogeneous, and as it cannot be distinguished from the aortic wall on most imaging techniques. Otherwise, image analysis included assessment of: the aortic morphology, the ILT signal properties on MRI and the FDG uptake on PET as follows:

(i) On MRI, aortic aneurysm length was measured from the first transverse section of ≥ 2 mm in diameter to the next transverse section ≤ 2 mm in diameter. When applicable, ILT maximal thickness and volume were evaluated on T2-weighted images. Volumes were extrapolated from manual contouring on all transverse sections to obtain the total area, which was multiplied by the depth (slice thickness + interslice gap).

(ii) T1 and T2 properties of the ILT were evaluated on the largest aortic transverse section (see appendix Figure 1). Visually, SI characteristics of the ILT were semi-quantitatively graded on T1 and T2 weighted images as described on Tables 1 and 2. A circular region of interest (ROI) (~2 mm^2) was drawn into the paravertebral muscle, and a freehand ROI was drawn to include the whole aortic wall, from its outer limit (delineated by retroperitoneal fat) to the external limit of the blood which is typically dark on these pulse sequences. A special emphasis was placed into omission from the tracing of spurious high SI (inflow effect) along the luminal surface of the ILT, if applicable. ILT to muscle contrast-to-noise ratio (CNR) was then quantified as the difference between the mean SI in the ILT and the muscle divided by the standard deviation (SD) of the muscle's SI.

(iii) The PET images were evaluated visually for the presence of increased aortic FDG uptake, defined as abdominal aortic wall signaling higher than both the remote aortic segments and the vascular background. To quantify FDG uptake, standardized uptake values (SUV) were obtained from ROIs in the aortic wall and the ILT on PET images: SUV = [FDG uptake (MBq/g) x weight (g)] / injected activity (MBq).

Statistical analyses

All statistical analyses are performed using the statistical analysis software, SAS version 9.3 (SAS Institute, NC, USA). Continuous data are expressed as mean ± SD. Continuous data differences are tested, using two-tailed Student test or general linear mixed model (GLMM) to account for repeated measurements when applicable. Multiple threshold levels for iron detection on T2-weighted MRI (average SI of the ILT minus a multiple of the standard error (SE)) were tested to adjust the best intraclass correlation (ICC) with the iron content on Perl's-3,3' – diaminobenzidine (DAB) staining on histology.

Simple and quadratic ordinal regressions are performed to evaluate the relationship between the dose of BM-573 and MRI findings. The relationship between the dose of BM-573 and the diameter growth curve are assessed using GLMM. Differences are considered to be significant at the 5% critical level.

Results

Aneurysm model's growth characteristics

In the first study's arm, two rats developed no aneurysm. No spontaneous post-operative mortality was observed, but three rats died during or after contrast injection for PET/CT. The mean preoperative diameter of the abdominal aorta on ultrasound was 1.8 ± 0.09 mm. On day 2 after surgery, it became 2.10 ± 0.20 mm and it almost tripled (5.56 ± 0.18 mm) by day 16 (Figure 1). Evolution of the diameter was characterized by 4 phases, consisting of 2 phases of growth alternating with 2 plateaus. An early growth of 2-3 days was followed by a central quiescent phase. The second growth phase started approximately on day 6 after surgery, and was characterized by occurrence of ILT that progressively enlarged. A second plateau in the growth curve was observed after 12-14 days. CT images of the 18 PET/CT examinations exhibited no ILT on 7 examinations (average 7 ± 6; range 2-20 days), while ILT was present on the remaining (average 16 ± 6; range 7-27 days). In all examinations without ILT, no FDG uptake was noticed, unlike all those with ILT (Figure 2) (Table 3). The maximal diameter and the maximal SUV were both lower in aneurysms without ILT as compared to those with ILT ($p < 0.001$).

Correlation between histology and MRI

In the second study's arm, 5 rats were not analyzed because of early (<1 week) post-operative death (2 rats in the HD group and 3 rats in the LD group). Correlations between iron scores MRI and Perl's + DAB staining histology (Figure 3) were performed in the 6 rats of the V group and the 4 rats of the HD group. Iron-rich layers were visible as areas of dark signal on T2-weighted MRI (Figure 3D) and brown deposits on Perl's + DAB staining sections (Figure 3E), having variable intensity and depth into the thrombus and the aortic wall. On histology, the relative iron content of the ILT were respectively 15.06 ± 5.93 and 1.75 ± 1.52 in vehicle and treated rats ($p = 0.001$). These percentages on MRI were respectively 16.82 ± 3.20 and 8.72 ± 1.79 ($p < 0.001$). On T2-weighted MRI, the best correlation (ICC = 0.71; lower ICC limit = 0.18) with histology was obtained using the threshold of mean SI – 16SE. Separately, this correlation remained significant on untreated rats sections (ICC = 0.65; lower ICC limit = 0.04), but not when the iron score tended to be low (ie: in treated rats, Appendix Figure 2) (ICC = 0.04; lower ICC limit = -0.03).

Effect of BM-573

Table 4 summarizes the effect of low and high-dose BM-573 on MRI findings 12-15 days after surgery. ILT high SI score on T1-weighted images, low SI score on T2-weighted images, thickness, volume and aneurysm length decreased significantly with the treatment, with quadratic fits for the first four parameters (all p-values < 0.05). ILT stratification score and the aneurismal diameter also decreased, while the CNR-to-muscle on T2-weighted and T1-weighted images increased with the treatment, but these effects did not reach statistical significance. When specifically evaluating the effect of the treatment on the aortic diameter (Figure 4), there was a significant increase of the aortic diameter with time in all groups ($p < 0.001$). However, the aortic diameter rise was significantly lower in HD rats as compared to V and low LD ($p < 0.033$).

Discussion

The role played by ILT in AAA growth was emphasized in this study involving multimodality imaging to evaluate elastase-induced rat models of aortic aneurysms. The model exhibited a multiphasic curve of dilatation, indicating an intricate participation of several mechanisms. The main growth phase occurred shortly after the appearance of a macroscopic ILT, such as reported in human AAAs where despite a potentially protective biomechanical effect, ILT favors aneurismal development, as it is a significant source of protease activity and oxidation[27]. The intense biological activity associated with the ILT was supported by a systematic local increase of FDG uptake on PET.

The proof of the concept emphasizing the role of the ILT in aneurismal growth suffered two unexpected events including mortality and inhibition of the early dilatation which precedes ILT in BM-573 treated rats, which respectively reduced the statistical power of intergroup comparisons and pointed to platelet-independent effects of BM-573[16-18], even though a microscopic platelet-dependent mechanism causing this early dilatation in our model cannot be ruled out. As expected because of other thrombosis pathways[28-29], ILT was not fully prevented b y BM-573, but significantly slowed down, resulting in a significant decrease of the aneurismal length and the ILT thickness and volume over 2 weeks in animals treated preventively and continuously by high-dose BM-573 as compared to controls. Since these relationships were almost all quadratic, the BM-573 effect can be considered as strongly dose-dependent. In high-dose BM-573-treated rats, the aneurysm diameter grew significantly slower than in other groups, owing to the inhibition of the growth phases.

The heterogeneity induced in our model using BM-573 allowed to emphasize the role of MRI in the assessment of the biological activities of ILT, which may be crucial for risk-management in AAA. Indeed, several strategies have been developed to evaluate these activities, both in humans and in animal models, by various imaging techniques, of which nearly all necessitate an exogenous contrast agent[5, 25, 30-33]. The iron released from trapped RBC is: strongly oxidant by powerfully catalyzing Fenton and Haber-Weiss reactions, paramagnetic and plays a key role in atherothrombosis[33-34]. Iron is therefore a potential endogenous marker of biological activities of the ILT, such as RBC trapping, lysis and oxidative stress. In the present work, we found a significant correlation between the MRI signaling and the histological assessment of iron content, which supports the idea that unenhanced T2-weighted MRI could be used for ILT iron content assessment. Unenhanced high signaling on T1-weighted MRI, also related to its iron and related protein, has been reported in high-risk human AAA cohorts[25, 35].This finding was replicated in our model where the T1-weighted signaling decreased in high-dose BM-573-treated rats. In general however, the T2 or T2* shortening related to iron seems prevail over T1 shortening, making them more suitable for AAA assessment.

Some limitations apply to this study, including a definition of the ILT applicable to all imaging techniques. The differentiation of ILT from wall thickness, can lead to systematic errors, since wall thickening can occur without ILT and vice versa. Second, because of treatment and examinations side effects: (i) Neither a systematic correlation between histology, FDG PET and MRI nor a direct cor-

relation between both imaging techniques was provided; and (ii) The longitudinal data presented were extrapolations from discontinuous data; (iii) the decrease of[35] the number of rats reduced the statistical power of intergroup comparisons. Third, T2 mapping sequences using multiple echoes to obtain iron concentration on a voxel basis would have been more accurate but weren't available on our equipment. Finally, only a temporal relationship between ILT occurrence and aneurismal growth was established. The exact mechanism(s) behind this relationship fall(s) outside the scope of this study and warrant(s) further studies to investigate the participation of each of the known biological activities of the ILT in aneurismal growth.

In conclusion, the key role played by ILT in this experimental aneurysm model was evidenced using multimodality imaging. The endogenous iron content of the ILT can be quantified accurately using T2-weighted MRI, which can therefore serve to evaluate noninvasively its oxidative activities. Inhibition of platelet aggregation as a potential therapeutic in AAA warrants further studies targeting all thrombosis pathways.

Acknowledgements

The authors thank Mrs Cécile Wegria and Carmela La Mantia for manuscript handling, editing and management; Jacques Trentesaux, Jean-Marc Léonard and Jean-François Monville, M.D. for their kind assistance and advices in MRI.

References

1. Dobrin PB (1989) Pathophysiology and pathogenesis of aortic aneurysms. Current concepts. Surg Clin North Am 69:687-703.
2. Michel JB, Martin-Ventura JL, Egido J et al (2011) Novel aspects of the pathogenesis of aneurysms of the abdominal aorta in humans. Cardiovasc Res 90:18-27.
3. Sakalihasan N, Limet R, Defawe OD (2005) Abdominal aortic aneurysm. Lancet 365:1577-1589.
4. Touat Z, Lepage L, Ollivier V et al (2008) Dilation-dependent activation of platelets and prothrombin in human thoracic ascending aortic aneurysm. Arterioscler Thromb Vasc Biol 28:940-946.
5. Sarda-Mantel L, Coutard M, Rouzet F et al (2006) 99mTc-annexin-V functional imaging of luminal thrombus activity in abdominal aortic aneurysms. Arterioscler Thromb Vasc Biol 26:2153-2159.
6. Fontaine V, Touat Z, Mtairag el M et al (2004) Role of leukocyte elastase in preventing cellular re-colonization of the mural thrombus. Am J Pathol 164:2077-2087.
7. Houard X, Rouzet F, Touat Z et al (2007) Topology of the fibrinolytic system within the mural thrombus of human abdominal aortic aneurysms. J Pathol 212:20-28.
8. Martinez-Pinna R, Madrigal-Matute J, Tarin C et al (2013) Proteomic analysis of intraluminal thrombus highlights complement activation in human abdominal aortic aneurysms. Arterioscler Thromb Vasc Biol 33:2013-2020.
9. Martinez-Pinna R, Lindholt JS, Madrigal-Matute J et al (2014) From tissue iron retention to low systemic haemoglobin levels, new pathophysiological biomarkers of human abdominal aortic aneurysm. Thromb Haemost 112:87-95.
10. Defawe OD, Colige A, Lambert CA et al (2003) TIMP-2 and PAI-1 mRNA levels are lower in aneurysmal as compared to athero-occlusive abdominal aortas. Cardiovasc Res 60:205-213.
11. Fontaine V, Jacob MP, Houard X et al (2002) Involvement of the mural thrombus as a site of protease release and activation in human aortic aneurysms. Am J Pathol 161:1701-1710.
12. Folkesson M, Kazi M, Zhu C et al (2007) Presence of NGAL/MMP-9 complexes in human abdominal aortic aneurysms. Thromb Haemost 98:427-433.
13. Lindholt JS, Bjorck M, Michel JB (2013) Anti-platelet treatment of middle-sized abdominal aortic aneurysms. Curr Vasc Pharmacol 11:305-313.
14. Nakahata N (2008) Thromboxane A2: physiology/pathophysiology, cellular signal transduction and pharmacology. Pharmacol Ther 118:18-35.
15. Cheuk BL, Cheng SW (2007) Differential secretion of prostaglandin E(2), thromboxane A(2) and interleukin-6 in intact and ruptured abdominal aortic aneurysms. Int J Mol Med 20:391-395.
16. Cherdon C, Rolin S, Hanson J et al (2011) BM-573 inhibits the development of early atherosclerotic lesions in Apo E deficient mice by blocking TP receptors and thromboxane synthase. Prostaglandins Other Lipid Mediat 94:124-132.
17. Cyrus T, Yao Y, Ding T, Dogne JM, Pratico D (2007) A novel thromboxane receptor antagonist and synthase inhibitor, BM-573, reduces development and progression of atherosclerosis in LDL receptor deficient mice. Eur J Pharmacol 561:105-111.
18. Gelosa P, Sevin G, Pignieri A et al (2011) Terutroban, a thromboxane/prostaglandin endoperoxide receptor antagonist, prevents hypertensive vascular hypertrophy and fibrosis. Am J Physiol Heart Circ Physiol 300:H762-768.

19. Worth NF, Berry CL, Thomas AC, Campbell JH (2005) S18886, a selective TP receptor antagonist, inhibits development of atherosclerosis in rabbits. Atherosclerosis 183:65-73.
20. Touat Z, Ollivier V, Dai J et al (2006) Renewal of mural thrombus releases plasma markers and is involved in aortic abdominal aneurysm evolution. Am J Pathol 168:1022-1030.
21. Anidjar S, Salzmann JL, Gentric D, Lagneau P, Camilleri JP, Michel JB (1990) Elastase-induced experimental aneurysms in rats. Circulation 82:973-981.
22. Marbacher S, Marjamaa J, Bradacova K et al (2014) Loss of mural cells leads to wall degeneration, aneurysm growth, and eventual rupture in a rat aneurysm model. Stroke 45:248-254.
23. Mitchell DG, Burk DL, Jr., Vinitski S, Rifkin MD (1987) The biophysical basis of tissue contrast in extracranial MR imaging. AJR Am J Roentgenol 149:831-837.
24. Winner MW, 3rd, Sharkey-Toppen T, Zhang X et al (2014) Iron and noncontrast magnetic resonance T2* as a marker of intraplaque iron in human atherosclerosis. J Vasc Surg. 10.1016/j.jvs.2014.02.006.
25. Nchimi A, Defawe O, Brisbois D et al (2010) MR Imaging of Iron Phagocytosis in Intraluminal Thrombi of Abdominal Aortic Aneurysms in Humans. Radiology 254:973-981.
26. Rolin S, Dogne JM, Michaux C, Delarge J, Masereel B (2001) Activity of a novel dual thromboxane A(2)receptor antagonist and thromboxane synthase inhibitor (BM-573) on platelet function and isolated smooth muscles. Prostaglandins Leukot Essent Fatty Acids 65:67-72.
27. Coutard M, Touat Z, Houard X, Leclercq A, Michel JB (2010) Thrombus versus wall biological activities in experimental aortic aneurysms. J Vasc Res 47:355-366.
28. Fetkovska N (1992) Platelet activation by low-density lipoprotein and serotonin: effects of calcium antagonists. J Cardiovasc Pharmacol 19 Suppl 3:S25-28.29 Packham MA, Mustard JF (2005) Platelet aggregation and adenosine diphosphate/adenosine triphosphate receptors: a historical perspective. Semin Thromb Hemost 31:129-138.
30. Richards JM, Semple SI, MacGillivray TJ et al (2011) Abdominal aortic aneurysm growth predicted by uptake of ultrasmall superparamagnetic particles of iron oxide: a pilot study. Circ Cardiovasc Imaging 4:274-281
31. Klink A, Heynens J, Herranz B et al (2011) In vivo characterization of a new abdominal aortic aneurysm mouse model with conventional and molecular magnetic resonance imaging. J Am Coll Cardiol 58:2522-2530.
32. Rouzet F, Bachelet-Violette L, Alsac JM et al (2011) Radiolabeled fucoidan as a p-selectin targeting agent for in vivo imaging of platelet-rich thrombus and endothelial activation. J Nucl Med 52:1433-1440.
33. Nahrendorf M, Keliher E, Marinelli B et al (2011) Detection of macrophages in aortic aneurysms by nanoparticle positron emission tomography-computed tomography. Arterioscler Thromb Vasc Biol 31:750-757.
34. de Valk B, Marx JJ (1999) Iron, atherosclerosis, and ischemic heart disease. Arch Intern Med 159:1542-1548.
35. Nguyen VL, Leiner T, Hellenthal FA et al (2014) Abdominal Aortic Aneurysms with High Thrombus Signal Intensity on Magnetic Resonance Imaging are Associated with High Growth Rate. Eur J Vasc Endovasc Surg. doi: 10.1016/j.ejvs.2014.04.025.

Figures

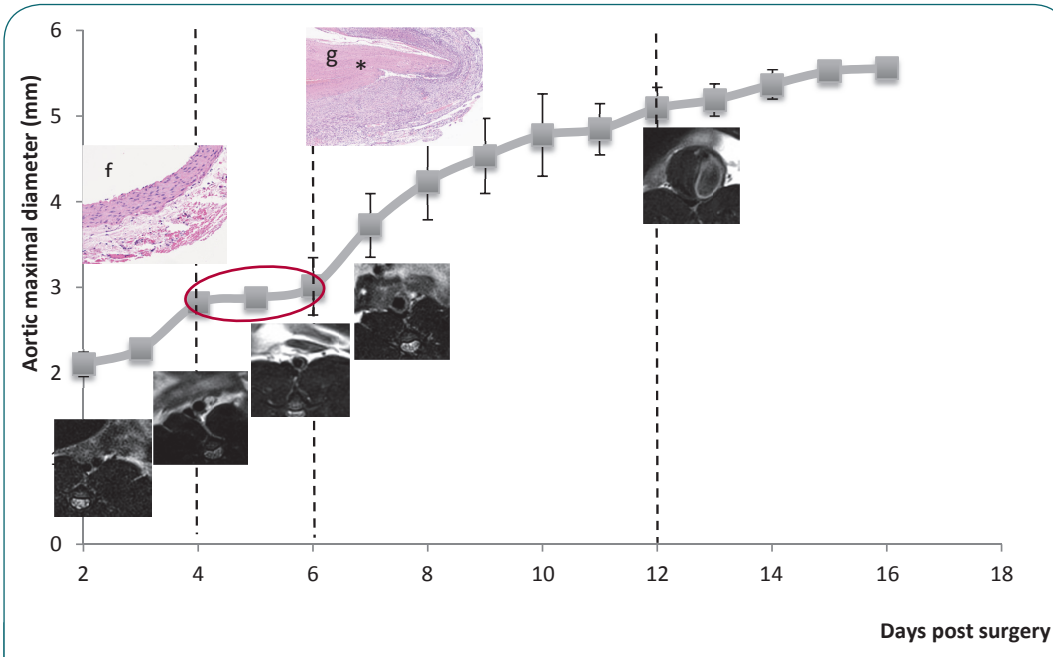

Figure 1: Post-surgical diameter growth curve of the aorta on Ultrasonography. Images (a-e) are time-line inserts of selected transverse T2-weighted MRI. The curve is characterized by 4 different phases separated by vertical dotted lines. There is a short central quiescent phase (red circle) in-between day 3-6 post surgery, where a macroscopic ILT appears on MRI (b). This phase is surrounded by two growth phases, the first of which is characterized by a subtle wall thickening and the remaining by progressive thickening and stratification of the ILT. Images (f-g) are inserts of x20 magnification hematoxylin-eosin histological views of the normal aortic wall (f) and the aneurismal wall after appearance of the ILT (g, asterisk), showing inflammatory infiltrates. Abbreviations as in the text.

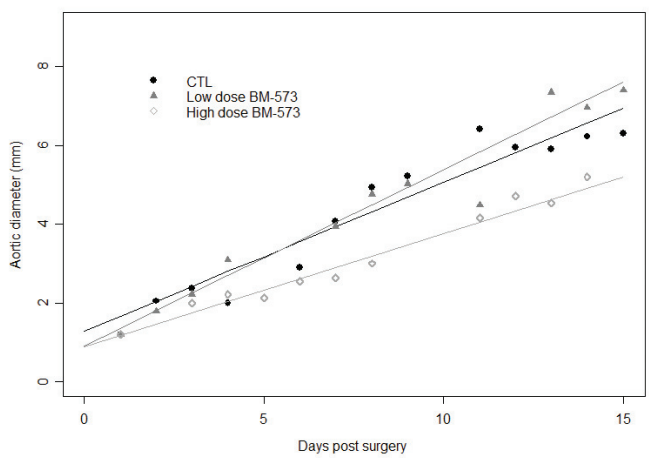

Figure 4: Regression lines of the aortic growth over 2 weeks post surgery in controls (black line, n = 6) low-dose (dark grey line, 10 mg/Kg BM-573, n = 3) and high-dose (30 mg/Kg BM-573, clear grey line, n = 4) BM-573-treated rats. Growth phases are delayed in high-dose BM-573-treated rats. Further, this group's curve slopes are reduced, resulting in an overall lower growth as compared to the others ($p < 0.001$).

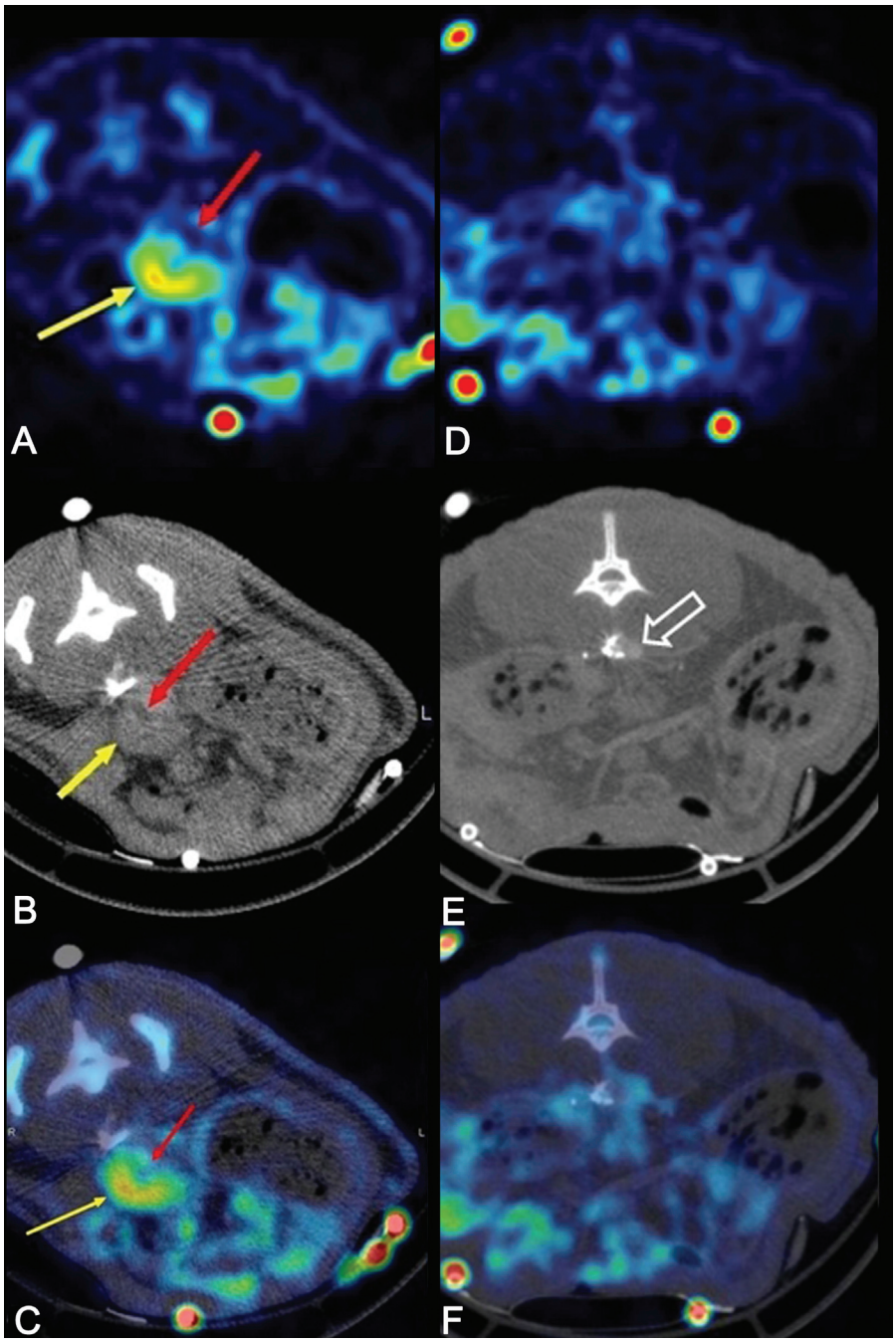

Figure 2: ILT positive (left panel) and ILT negative (right panel) prone transverse FDG PET (A and D), CT (B and E) and fused PET-CT (C and E) images of the aorta in rats, respectively 13 and 5 days after infusion of elastase. On the left panel, the aorta (arrow) is largely dilated. The ILT is seen as a ventral thickening of the aortic wall, containing two layers of different densities on CT. The luminal part of the ILT has a low density and exhibits low FDG uptake (red arrows), while the external part of the thrombus has a higher CT density and exhibits stronger FDG uptake (yellow arrows). On the right panel, the aorta (open arrow) is undilated, and neither intraluminal thrombus nor increased FDG uptake are seen. Abbreviations as in the text.

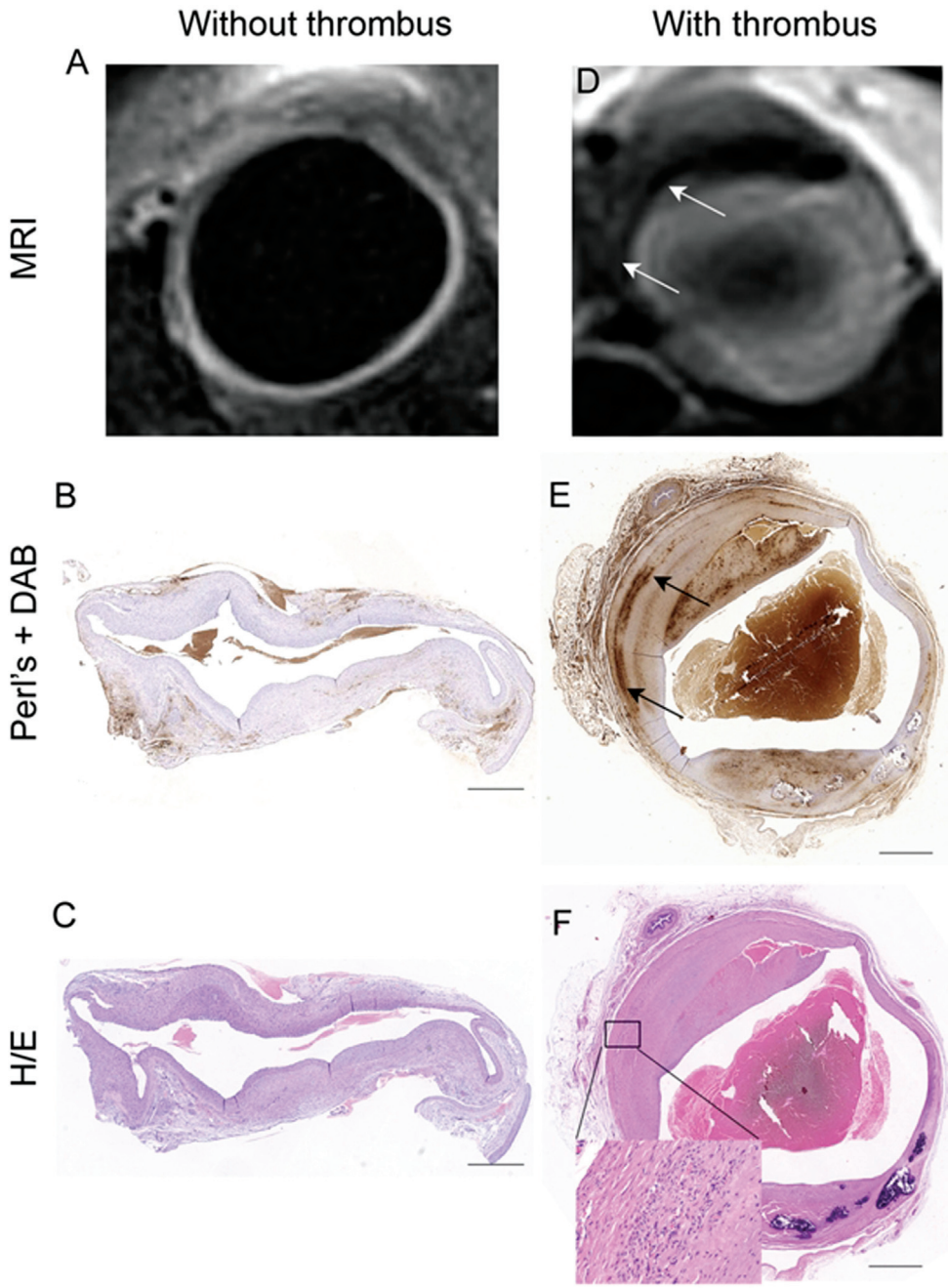

Figure 3: Correlation between aortic wall low signal intensity related to iron on T2-weighted MRI (A and D) and DAB-enhanced perl's staining in aneurysm sections (B and E) in a BM-573 treated rat with no ILT (A-C) and a vehicle with ILT (D-F). Arrows indicate layers of low signal intensity due to iron accumulation in the ILT and the aneurysm wall (D and E). Histology and MRI quantitative iron scores were respectively 1.38 and 8.65 on the treated rat section, and 21.86 and 20.92 on the vehicle rat section. Hematoxylin-eosin staining sections showed inflammatory cells with potential phagocytic activity associated with the ILT on the site of iron staining (F and higher magnification insert), whereas in aneurysm without ILT, no inflammatory cells were observed (C). Scale-bar = 1mm; abbreviations as in the text.

Tables

Score	Areas of the ILT with: SI > to the paravertebral muscle on T1-weighted images SI < to the cerebrospinal fluid on T2-weighed images
0	None
1	One linear area
2	One nodular area
3	> 1 area
4	Almost the whole ILT

Table 1: Semi-quantitative signal intensity (SI) scoring scale of the intraluminal thrombus (ILT) on T1- and T2-weighted MRI. Abbreviations as in the text.

Score	ILT layering appearance
0	None (homogenous SI)
1	Two distinct layers
2	Three distinct layers
3	Four distinct layers
4	> Four distinct layers

Table 2: Semi-quantitative intraluminal thrombus (ILT) signal intensity (SI) stratification scoring scale on T2-weighted MRI. Abbreviations as in the text.

	ILT (n = 11)	No ILT (n = 7)	p-value*
AAA diameter (mm)	6.51±1.17	2.66 ± 0.95	< 0.001
Visual FDG uptake	11	0	NA
Maximal SUV	2.65±1.07	0.98 ± 0.29	< 0.001

Table 3 : AAA findings on FDG PET/CT examinations with regard to the presence or absence of ILT. *p-values are corrected for repeated measurements. Abbreviations as in the text.

		V group (n = 6)	LD group (n = 3)	HD group (n = 4)	p-value*
ILT on T1-Weighted MRI	high SI score	1.33 ± 0.52	2.67 ±1.53	0.25 ± 0.50	L : 0.023 Q : 0.025
	CNR-to-muscle	1.99 ± 1.87	3.53 ± 0.11	2.19 ± 0.65	L : 0.61
ILT on T2-Weighted MRI	low SI score	1.50 ± 0.84	2.00 ± 1.73	0.25 ± 0.50	L : 0.017 Q : 0.024
	CNR-to-muscle	4.90 ± 1.68	6.74 ± 0.88	6.51 ± 2.25	L : 0.11
	stratification score	1.17 ± 0.75	2.67 ± 1.53	0.50 ± 0.58	L : 0.67
Morphometric aneurysm measurement	Maximum ILT thickness (mm)	3.10 ± 1.27	3.17 ± 1.52	0.88 ± 0.32	L : 0.025 Q : 0.032
	ILT volume (mL)	0.45 ± 0.17	0.58 ± 0.26	0.09 ± 0.07	L : 0.026 Q : 0.044
	Aneurysm length (mm)	17.5 ± 3.95	17.9 ± 4.45	6.75 ± 2.22	L : 0.022
	Aneurysm diameter (mm)	7.13 ± 1.19	9.23 ± 1.46	5.03 ± 2.44	L : 0.27

Aneurysm properties on MRI before sacrifice in the V, LD and HD groups of rats. Ordinal regression analyses were performed to evaluate the effect of the treatment on each variable. *L and Q respectively indicate p-values for linear and quadratic fits. Abbreviations as in the text.

Supplemental Material

Surgical procedures

All rats were treated with subcutaneous analgesic buprenorphine (Temgesic®, Reckitt Benckiser, Slough, UK) (0.05 mg/kg, SC), which was applied twice a day for 2 days, with the first injection administered 2 hours before anesthesia. All surgical procedures and euthanasia were performed under sterile conditions and general anesthesia induced by combination of buprenorphine SC and intraperitoneal injection of pentobarbital (Nembutal®, Boehringer Ingelheim, Brussels, Belgium) (50 mg/kg body-weight). A single dose of enrofloxacin (Baytril®, Bayer, Leverkusen, Germany) (10 mg/kg body-weight) was administered subcutaneously before surgical procedures. Anesthetized animals body temperature was controlled by intrarectal monitoring and maintained between 36 and 38°C with a heating lamp throughout the procedures.

After anesthesia and laparotomy, we isolated the abdominal aorta from vena cava by dissection under a binocular surgical microscope. We ligated (ETHICON® prolene® 8.0) all collateral arteries of the abdominal aorta in-between renal arteries and the iliac bifurcation. Then, this segment was clamped by using a Gilbert clamp. Aorta was incised near the iliac bifurcation to introduce a 24G polyethylene catheter (INTRAMEDIC® Polyethylene Tubing, Clay Adams®).

After catheter position check and ligation (ETHICON® ethilon® 7.0), a solution of 3 units of porcine pancreatic elastase at a rate of 700 µml/h (Sigma E1250-50MG Lot N.040M7017) was perfused through the catheter at the rate of 700 µml/h during 1h. The catheter was then removed and the aorta was sutured (ETHICON® ethilon® 8.0) and unclamped. Finally, the muscular fascia and the skin were sutured (respectively ETHICON prolene® 5.0 and ETHICON ethilon® 5.0). After surgery, rats were placed in a heating room with continuous monitoring until complete recovery. Operated rats were monitored 2 times per day.

Imaging parameters

Ultrasonography

After sedation by inhalation of isoflurane 2.5 % (FORENE® isoflurane ABBOTT-inhalator Ohmeda Isotec 3), rats were placed supine. Ultrasound gel at room temperature was applied on the abdomen and examinations were performed using a portable ultrasound scanner (LOGIC e, General Electrics, Milwaukee, USA). A linear 8 MHz transducer was used for gentle compression imaging of the abdominal aorta. Imaging depth (2 cm), zoom (maximal) and gain were set for appropriate evaluation of the aorta; and frames of the whole abdominal aorta in the transverse plane were acquired and stored.

Magnetic resonance imaging

Rats were placed into a single-element phased array coil and placed at the center of a 3 Tesla scanner unit (Magnetom Trio, Siemens Medical Solutions, Erlangen Germany) after isoflurane sedation, and scout images were acquired. Angiography was performed using 2mm-thick transverse phase-contrast images with venous inflow saturation preparation pulse. Others parameters were: repetition time (TR)/ echo time (TE)/flip angle/N° of averages/acceleration factor = 34ms/7.35ms/60°/1/2. The field of view (FOV) using a 256x256 base resolution was adjusted to the body size to avoid phase encoding direction aliasing and slice overlap was 33%. Three-dimensional angiographies served to place transverse 2mm-thick Turbo Spin Echo T2-weighted and Spin Echo T1-weighted images on the most dilated part of the aorta (Appendix Figure 1). The respective T2- and T1-weighted imaging TR/TE/flip angle/N° of averages/acceleration factor were 2380ms/60ms/160°/4/2 and 584ms/11ms/120°/4/2. Image FOVs were adjusted to the rat's body size, with a 320x320 base resolution.

Positron emission tomography

Prior to FDG PET/CT examinations (microCT) and Focus 120 (microPET), Siemens Medical Solutions Erlangen, Germany), rats underwent 12h fasting. 1h before image acquisition, a 24G peripheral venous catheter was placed in the lateral tail vein under isoflurane sedation, and 20-30 MBq of FDG in 0.5 mL were injected. Then, CT data were acquired in prone position, both without enhancement and during a continuous injection of 2 mL of Xenetix 300 (iobitridol, Guerbet, Aunay-sous-bois, France). All microCT images were reconstructed using Feldkamp's Filtered Back Projection (FBP) algorithm [1] with a cutoff at the Nyquist frequency and an isotropic voxel size of 0.1 mm.

Compressive micturition was induced to partially clear the bladder of excreted FDG and a 10 minute emission scan was acquired immediately after a 10 min transmission scan with Co-57 point source with single event acquisition mode using a 120-125 keV energy window. The abdomen was centered in the (8 cm axial) MicroPET FOV. PET raw data were corrected for attenuation using the data from the transmission scan. Emission data were acquired with an energy window of 350-650 keV and a coincidence-timing window of 6 ns. Images were reconstructed with all corrections except scatter [2] using

Fourier rebinning [3] and FBP with a ramp filter cutoff at the Nyquist frequency. A total of 95 transaxial slices was obtained in a 256 x 256 matrix. The slice thickness was 0.796 mm, and the in-slice pixel size was 0.43 mm. MicroCT and microPET images were co-registered using a landmark-based approach.

Histology

Aortic samples were fixed in 4% paraformaldehyde and embedded in paraffin. Sections of 5 mm were performed and stained with hematoxylin-eosin (HE) and Perl's reaction followed by 3,3'-diaminobenzidine (DAB) precipitation for sensitizing iron detection at optical microscopy [4]. For quantitative analyses, the largest aortic section was evaluated by a reader blinded to MRI findings. The iron content was evaluated by computer-assisted image analysis (ImageJ software, NIH) after manual tracing of the luminal and adventiceal limits of the aortic wall. The results were expressed in percentages of the delineated surface.

References

1. *Feldkamp L DL, Kress J (1984) Practical cone-beam algorithm. JOSA A 1:612-619.*
2. *Bahri MA, Plenevaux A, Warnock G, Luxen A, Seret A (2009) NEMA NU4-2008 image quality performance report for the microPET focus 120 and for various transmission and reconstruction methods. J Nucl Med 50:1730-1738.*
3. *Defrise M, Kinahan PE, Townsend DW, Michel C, Sibomana M, Newport DF (1997) Exact and approximate rebinning algorithms for 3-D PET data. IEEE Trans Med Imaging 16:145-158.*
4. *Nguyen-Legros J, Bizot J, Bolesse M, Pulicani JP (1980) [«Diaminobenzidine black» as a new histochemical demonstration of exogenous iron (author's transl)]. Histochemistry 66:239-244.*

Caption of the figures

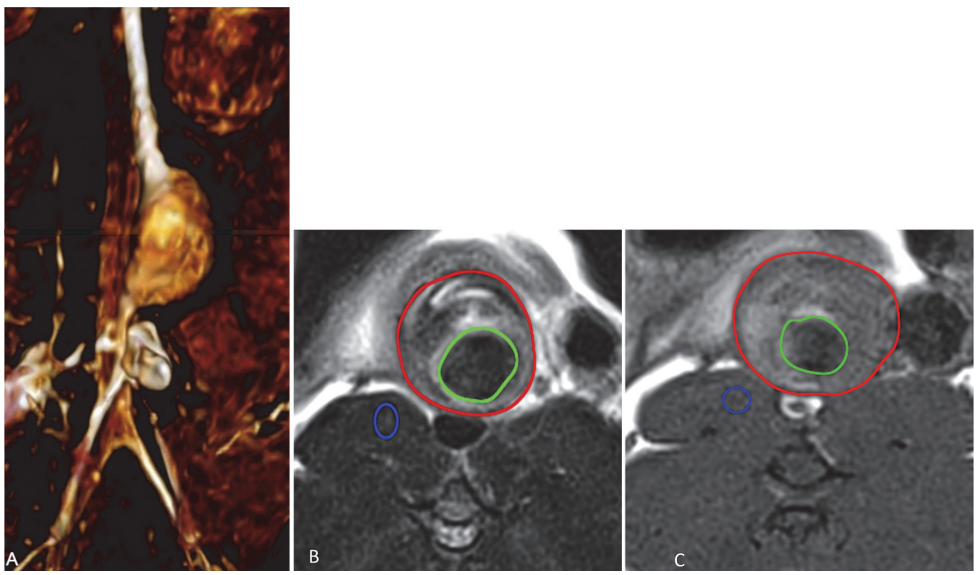

Figure 1: (A) representative tridimensional image of magnetic resonance angiography in a rat 21 days after aortic infusion of elastase, where the transverse line indicates the positioning of (B) T2-weighted and (C) T1-weighted images around the largest aneurismal section (where the regions of interest have been drawn on the muscle (blue) and the inner (green) and outer (red) limits of the artic wall including the thrombus). Note the stratification and the high signal intensities of the thrombus respectively on T2- and T1-weighted images.

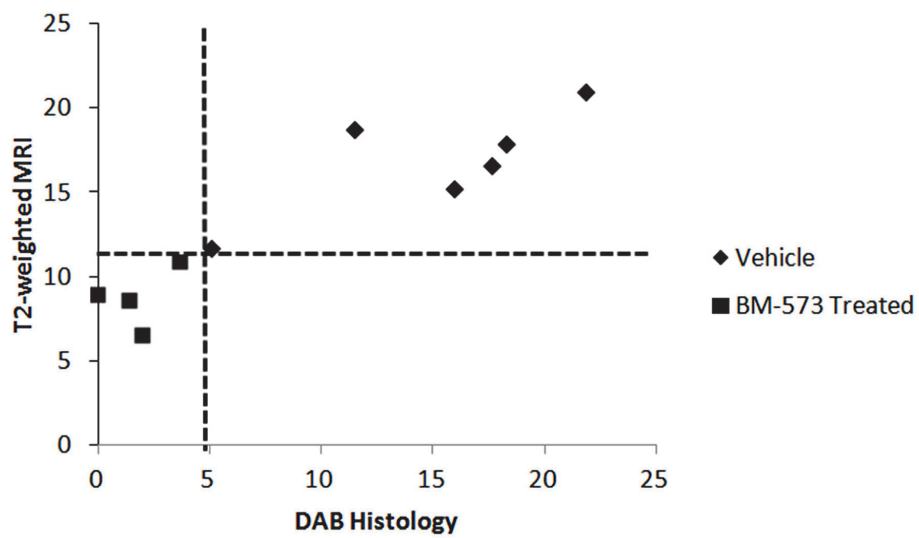

Figure 2: Scatterplot of relative intraluminal thrombus percentage of iron on T2-weighted imaging and histological sections in BM-573 treated rats and controls. The dotted lines represent the limits between treated and untreated rats on both imaging techniques. MRI = Magnetic Resonance Imaging; DAB = Diaminobenzidine.

GENERAL DISCUSSION

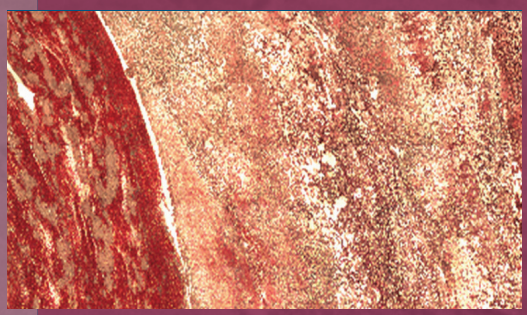
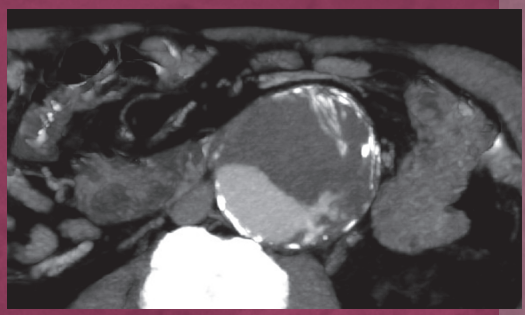
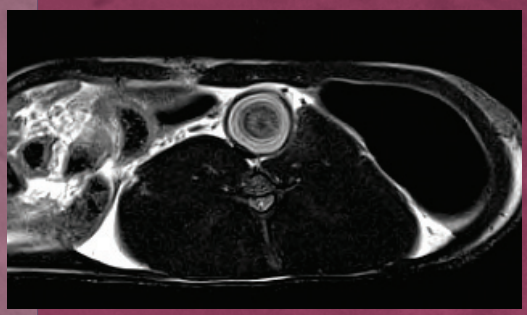
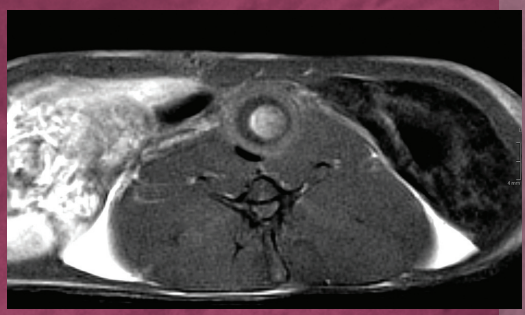

GENERAL DISCUSSION

The advances in knowledge and imaging techniques that took place in the past century offer prospects for a better AAA risk-stratification assessment using functional and metabolic imaging biomarkers that (unlike the diameter) provide information on the pathophysiological events taking place within the aneurysmal sac. FDG PET case-studies, including ours (Publication N°1), have shown that a given FDG PET examination can be intuitively reported as positive or negative for clinical purposes, according to the detection of one or several areas of increased signal. Aneurysm behavior with respect to this metabolic activation was so far unsolved, especially because of the lack of longitudinal data in broad ranges of aneurysms type, shape and diameter. We have evidenced that increased FDG uptake in aortic aneurysm is associated with a significantly higher risk of related events over 2 years (Publication N°3) (Figure 12). FDG uptake could therefore serve as an additional diameter-independent factor in the management of patients with aortic aneurysms. As others, we reported important intra- and inter-individual heterogeneity in the distribution of both wall stress and metabolic activity hot-spots that tend to co-localize, but were not precisely located on the maximal cross-sectional diameter of the aneurysm[109, 89]. This observation is also in accordance with the fact that aneurysm expansion and rupture are localized events that occur rarely if not never at the level of the maximal cross-sectional diameter[93]. Unfortunately, the clinical value of FES lacked of sound evidence partly since it was not thresholded in the same way as FDG PET.

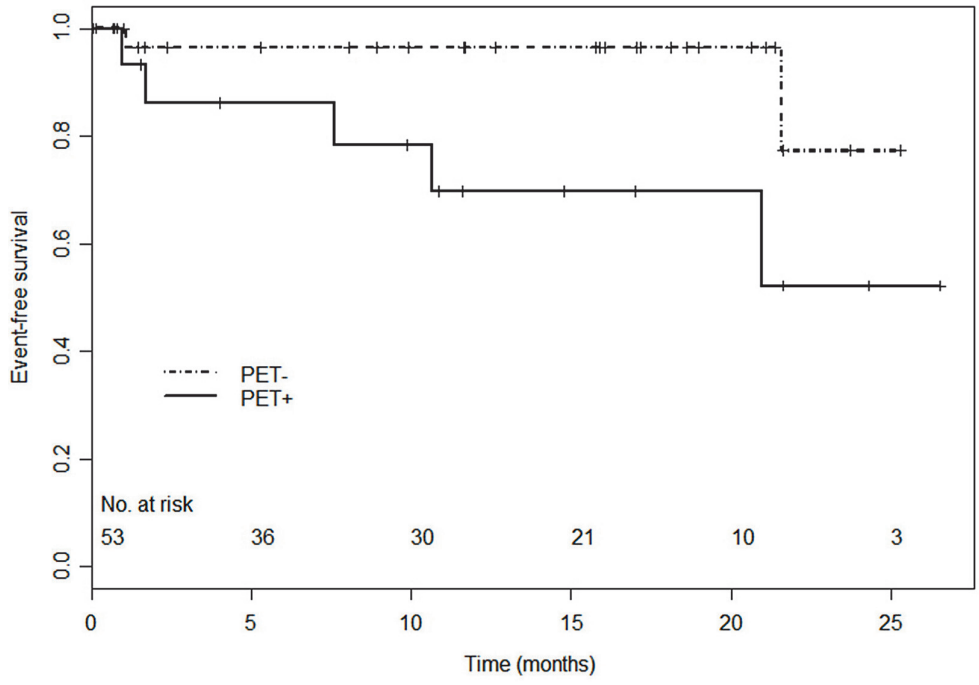

Figure 12 : Thirty-month event-free survival curves in PET–positive and PET-negative patients (p-value = 0.03) (110).

We therefore conducted a study to validate the translation of FES estimates into diameter-equivalent risk using data from a large multicenter trial (Publication N° 2). This study helped providing FES with a better clinical sense, and potentially a more widespread acceptance, although it responses remain non-dichotomous. Our data should not be regarded as showing no relationship between the aneurysm maximal diameter and biological activities or wall stress –while there are clearly some (Figure 13). All three quantities (ie: the maximal diameter, wall stress and biological activities) should be considered as elements of negative feedback loops that lead to aneurysm expansion, eventually rupture. Considering this concept, we only evaluated a time-point correlation between certain variables. The longitudinal relationship between imaging techniques should be addressed for pathophysiological purposes, to determine for example how far the biological events are the cause or the consequence of increased biomechanical stress at a given cross-sectional diameter.

On a clinical view, the predictive elements of our model interplay and probably have a complimentary value in evaluating the risk of AAA rupture. This is illustrated by the fact that wall metabolic activity and its correlation to wall stress were influenced by patient-specific factors such as the presence of other arterial aneurysms, a family history of aneurysm or a personal history of angina pectoris or peripheral arterial disease. This points to a potential alteration of the biological responses to wall stress in AAA and provide possible clues for the increased risk of rupture[111] and poor outcomes after endovascular repair[112] associated with a familial history of AAA. An integrated patient-specific risk-assessment including all available (imaging, clinical and history) data is therefore suitable. Such an approach is partially included into the PWRI provided FES, where estimation of the aortic wall strength accounts for ILT thickness and gender[113], so much so that within our cohort, a 50-mm diameter AAA in a female has the equivalent risk of rupture (ie: the risk that the wall stress overcomes wall strength) as a 63-mm AAA in a male.

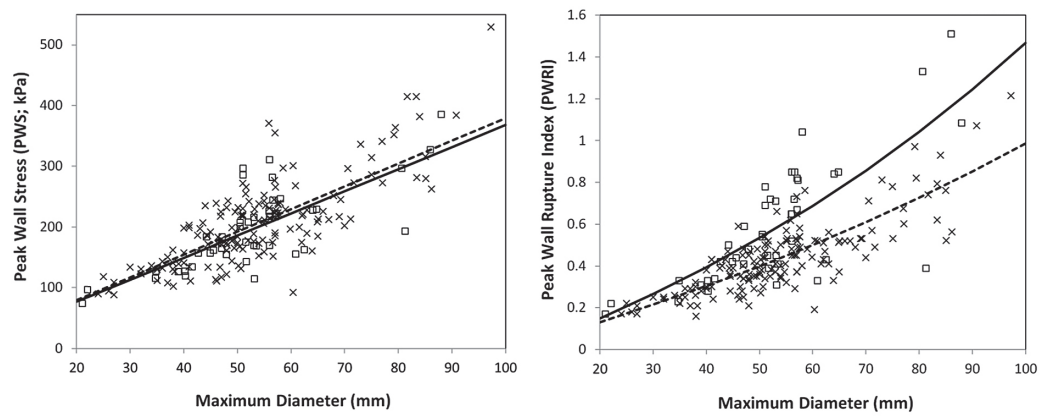

Figure 13 : Peak Wall Stress (PWS) and Peak Wall Rupture Index (PWRI) with respect to the maximum diameter of non-ruptured AAAs. Squares denote female and crosses male patients. Solid lines (female) and dashed lines (male) denote regression curves (117).

Inclusion of further variables with established effect on wall strength such as increased FDG uptake and smoking[66] will probably refine this model. However, the gain expected by this model refinement could be hampered by cost-effectiveness and epidemiological concerns, eventually limiting the clinical usefulness of biological activities or wall stress imaging. Indeed, it is questionable in how far sophisticated risk-stratification investigations could be applied to all individuals with significant outcome- and cost-effective differences as compared to the current guidelines, especially with regard to the declining incidence of AAA in economically developed countries[114-116]. Nevertheless, a certain number of diameter-based clinical scenarios could be improved by the impact of both FDG PET and FES in AAA risk of rupture assessment, including for example decision making in an old patient in poor condition with a large AAA, for whom operative or endovascular repair risks has to account for co-morbidity.

Throughout our data, a certain difference between TAA and AAA was noticed in the incidence of aneurysms with increased FDG uptake and correlations with wall stress, towards higher values in TAA. We failed to show any significant effect of ILT thickness behind these differences, although the two types of aortic aneurysms are characterized by a difference in ILT amount. It has therefore to be stressed that ILT thickness is probably a poor marker of its biological activities that include phagocytosis. With regard to the radiation dose burden related to CT and PET, our clinical data indicate that safer and widely available concepts for imaging biological activities in AAAs are needed. Our pilot study including 15 patients was the first in which iron-based RES MRI contrast agents were evaluated in AAAs (publication N°4). This study demonstrated two important findings, including firstly a gradient of signaling in ILT on unenhanced T2*W sequences, with the lowest SI just beneath the aortic lumen. This SI gradient reflects the decreasing concentration of iron from the lumen towards the adventitial ILT. The presence of iron, as demonstrated in vivo, may also impact the level of oxidative stress, as iron is an important oxidant through the Fenton's reaction. Other MRI appearances of ILT included a high T1W SI caused by certain derivatives of methemoglobin, and a multilayered T2W appearance related to apposition of successive layers with different iron and water contents during ILT growth.

These two appearances were associated with an upregulation of activated MMP9, confirming a relationship between the biological activities of the ILT and its appearances on MRI. The second main finding of this study was a T2*W signal decrease at the luminal surface of ILT after injection of SPIO, as the result of phagocytosis. These changes correlated well to the density of phagocytic cells (macrophages and neutrophils) identified by histology. A similar correlation with the expression of MMP thus suggests a link between phagocytic cells in ILT and its proteolytic activity. Because of the important role of ILT and its iron content, we conducted a validation study using a rat model of AAA after infusion of elastase which shares the human AAA propensity for large ILT (Submitted Publication N°5). We characterized the aneurysm growth using multimodality imaging and evidenced that ILT occurrence is associated with major changes in the AAA behavior, including mainly increased FDG uptake and diameter growth. ILT activities monitored through iron content assessment using MRI was well correlated with histology in this model. As a proof of concept emphasizing the role of

ILT in the aneurysmal growth, we demonstrated a dose-dependent effect BM-573, a TXA2 antagonist, on aneurysm growth, length and ILT volume. Our results indicate that phenotyping ILT and assessing its iron content using MRI are feasible and could be both used as novel imaging biomarkers of aneurysm (in)stability. Further, inhibiting or slowing down ILT formation could be a potential therapeutic option in patients with AAA.

Independent assessment of our work is mandatory to address large scale reproducibility and cost-effectiveness before launching the randomized trials required for changes in clinical practice. First, numerous technical issues regarding imaging techniques and pathophysiological interpretation should be properly addressed. These include both a low spatial resolution of PET scanners causing partial volume effects[118], and a lack of sensitivity of FDG uptake[119-120] on a patient basis, appealing to improvement in PET scanners hard- and software. Current tracers and contrast agents remain relatively unspecific, as they track many biological processes occurring in the aneurysmal sac including reparative processes (eg: calcification). The diameter of the SPIO agents we used (> 50 μm) causes a massive capture by the hepatic reticuloendothelial system (RES) (Kupffer cells), and therefore a poor bioavailability for the assessment of AAA walls. This is not the case for ultrasmall iron oxide particles (USPIO)[121].

This remark could be anecdotic because the research trying to evaluate iron phagocytosis by MRI was closed recently by the withdrawn from the market of all iron oxide-based contrast agents, but it illustrates that the lack of proper evaluation of the periadventitial area is the main pathophysiological weakness of our research. Although intra-thrombus flow channels can be seen (Figure 5), most of the molecular signaling in the AAA wall probably depends on the inside-out and outside-in pathways. FDG uptake which was the only imaging biomarker statistically associated with a poor clinical outcome in patients with AAA, can be theoretically detected on both ends of ILT, provided its thickness and spatial resolution are sufficient to allow the discrimination between both areas. In general, the vascular background prevents the detection of subtle luminal infiltrates. Yet, those considered here address undefined area. Another imaging biomarker of the periadventitial activities is neoangiogenesis, which can be evaluated more specifically using ^{18}F-FPRGD2 for PET imaging [100], a tracer which was not available at the beginning of our investigations, or Fucoidan-labelled radionuclide for SPECT[122]. Alternatively, DW-MRI[123] and either CT or MR perfusion imaging[124-125] can be used, but too few AAA patients were enrolled for MRI, while radiation issues largely prevented the use of CT perfusion. Whatsoever, there is to our knowledge, currently no single tracer or imaging technique that could address satisfactorily biological activities at both ends of ILT.

CONCLUSION AND PERSPECTIVES

Our research evidenced findings that lie at the frontiers between translational and clinical research. MRI and FDG PET are capable of capturing and quantifying in vivo some of the notoriously deleterious biological processes taking place into the aneurysmal sac, including blood cells trapping at the luminal interface of ILT and the periadventitial inflammatory response. Further, increased wall metabolic activity is associated to a significant diameter-independent increased risk of AAA-related events at 2 years, although this important clinical value should be weighted by scanning availability, cost and radiation doses. Further, potentially important pathophysiological links in AAA progression were shown in vivo using imaging, with significant correlations between biological activities and wall stress and the central role played by the ILT in AAA behavior.

With regard to our findings, there are four main perspectives for further research. First, FDG PET assessment of AAAs promoted significant steps forward in the use of metabolic imaging as biomarker for risk stratification in AAA thanks to close collaborations between the departments of vascular surgery of the Liège University Hospital (Prof. Jean-Olivier Defraigne) and nuclear medicine of both the Liège University Hospital (Prof. Roland Hustinx) and the Centre Hospitalier Chrétien of Liège (Dr. Pierre Gomez), under the umbrella and fundings of the 7th European Union framework project "Fighting Aneurysmal Disease" (FAD). Nevertheless, certain specific developments are still needed. These mainly include two components: the first relating to data acquisition analysis, processing, filtering and quantification, while the second relates to the synthesis of contrast agents and tracers with specific affinity to overexpressed or activated molecules. Second, the evaluation of AAA wall stress by FES was performed in collaboration with the Royal Institute of Technology University of Stockholm (Dr Christian Gasser). This expertise is to be improved and implemented locally. Integration of FES imaging to available commercial multimodality imaging platforms, so that the simulation maps could overlay other morphological and metabolic data, will represent a major milestone in the development of this technique. On the other hand, we have developed and reported a landmark-based fusion between PET and FES imaging that needs refinement and a less rigid approach, along with a better management of the discrepancies in spatial resolution and partial volume effects between the two techniques. Third, randomized trials should be launched to determine the importance of these imaging parameters, as well as the MRI assessment of the endogenous iron content of the ILT on clinical decision-making. More translational research needs to be performed to specifically evaluate: (i) the robustness of the T2* mapping of the ILT and its correlations with the levels of oxidative stress in humans; (ii) and the pathways specifically associated with the inherited and acquired biological responses alteration to wall stress. Lastly, we characterized a rat model AAA by infusion of elastase, modified from the model initially described in the vascular biology laboratory of the INSERM at Hospital Bichat in Paris (Prof. Jean-Baptiste Michel), using multimodality imaging, which required collaborations between the Cyclotron Research Center facilities (Dr Alain Plenevaux) and several research entities grouped in the GIGA translational Research platform, including the "Center of experimental surgery (Prof. Natzi Sakalihasan) and animal facilities of the university hospital of Liège (Prof. Pierre Drion) . This model characterization by imaging is a critical step ahead of new cardiovascular disease drugs testing which we started using a TXA2 antagonist (BM 573), developed at the University Hospital Notre Dame de Namur (Prof. Jean-Michel Dogné).

EPILOGUE

Advanced imaging methods remain somewhat subject to concerns regarding performance, interpretation and cost analysis, notably because of the poor availability of scanning technologies, contrast agents and tracers with high sensitivity and specificity. Despite this, using imaging to monitor biological processes remains one of our best assets in the fight to prevent death from known AAA.

There is little doubt that further studies and technical advances will eventually compensate the shortcomings of the current AAA risk-assessment strategy, by allowing new imaging biomarkers to enter the clinical armamentarium. We introduced the promises of iron imaging, but many other research paths awaits in the pursuit of a diagnostic holy grail that does not hurt patients, help saving lives and unnecessary interventions, and that can be repeated to assess future non-surgical treatment options for AAA.

BIBLIOGRAPHY

1. Maurel E, Shuttleworth CA, Bouissou H. Interstitial collagens and ageing in human aorta. Virchows Archiv. 1987;410(5):383-90.
2. Ghorpade A, Baxter BT. Biochemistry and molecular regulation of matrix macromolecules in abdominal aortic aneurysms. Annals of the New York Academy of Sciences. 1996 Nov 18;800:138-50.
3. Sonesson B, Lanne T, Hansen F, Sandgren T. Infrarenal aortic diameter in the healthy person. European Journal of Vascular Surgery. 1994 Jan;8(1):89-95.
4. Collin J, Araujo L, Walton J, Lindsell D. Oxford screening programme for abdominal aortic aneurysm in men aged 65 to 74 years. Lancet. 1988 Sep 10;2(8611):613-5.
5. Johnston KW, Rutherford RB, Tilson MD, Shah DM, Hollier L, Stanley JC. Suggested standards for reporting on arterial aneurysms. Subcommittee on Reporting Standards for Arterial Aneurysms, Ad Hoc Committee on Reporting Standards, Society for Vascular Surgery and North American Chapter, International Society for Cardiovascular Surgery. Journal of Vascular Surgery. 1991 Mar;13(3):452-8.
6. Wanhainen A, Themudo R, Ahlstrom H, Lind L, Johansson L. Thoracic and abdominal aortic dimension in 70-year-old men and women--a population-based whole-body magnetic resonance imaging (MRI) study. Journal of Vascular Surgery. 2008 Mar;47(3):504-12.
7. Brown LC, Powell JT. Risk factors for aneurysm rupture in patients kept under ultrasound surveillance. UK Small Aneurysm Trial Participants. Annals of Surgery. 1999 Sep;230(3):289-96.
8. Guo W, Zhang T. Abdominal aortic aneurysm prevalence in china. Endovascular Today 2014;2(2):76-82.
9. Webster MW, Ferrell RE, St Jean PL, Majumder PP, Fogel SR, Steed DL. Ultrasound screening of first-degree relatives of patients with an abdominal aortic aneurysm. Journal of Vascular Surgery. 1991 Jan;13(1):9-13.
10. McGregor JC, Pollock JG, Anton HC. The value of ultrasonography in the diagnosis of abdominal aortic aneurysm. Scottish Medical Journal. 1975 May;20(3):133-7.
11. Sterpetti AV, Schultz RD, Feldhaus RJ, Cheng SE, Peetz DJ, Jr. Factors influencing enlargement rate of small abdominal aortic aneurysms. The Journal of Surgical Research. 1987 Sep;43(3):211-9.
12. Crawford ES. Thoracoabdominal aortic aneurysm. In: Rutherford R, Ed. Vascular Surgery: WB Saunders Co; 1989. p. 927.
13. Larsson E, Vishnevskaya L, Kalin B, Granath F, Swedenborg J, Hultgren R. High frequency of thoracic aneurysms in patients with abdominal aortic aneurysms. Annals of Surgery. 2011 Jan;253(1):180-4.
14. Isselbacher EM. Thoracic and abdominal aortic aneurysms. Circulation. 2005 Feb 15;111(6):816-28.
15. Brown RD, Jr., Broderick JP. Unruptured intracranial aneurysms: epidemiology, natural history, management options, and familial screening. Lancet Neurology. 2014 Apr;13(4):393-404.
16. Lawrence PF, Lorenzo-Rivero S, Lyon JL. The incidence of iliac, femoral, and popliteal artery aneurysms in hospitalized patients. Journal of Vascular Surgery. 1995 Oct;22(4):409-15.

17. Lederle FA, Johnson GR, Wilson SE, Chute EP, Littooy FN, Bandyk D, et al. Prevalence and associations of abdominal aortic aneurysm detected through screening. Aneurysm Detection and Management (ADAM) Veterans Affairs Cooperative Study Group. Annals of Internal Medicine. 1997 Mar 15;126(6):441-9.
18. Chichester Aneurysm Screening Group, Viborg Aneurysm Screening Group, Western Australian Abdominal Aortic Aneurysm Program, Multicentre Aneurysm Screening Study. A comparative study of the prevalence of abdominal aortic aneurysms in the United Kingdom, Denmark, and Australia. Journal of Medical Screening. 2001;8(1):46-50.
19. Sakalihasan N, Limet R, Defawe OD. Abdominal aortic aneurysm. Lancet. 2005 Apr 30-May 6;365(9470):1577-89.
20. Nicholls SC, Gardner JB, Meissner MH, Johansen HK. Rupture in small abdominal aortic aneurysms. Journal of Vascular Surgery. 1998 Nov;28(5):884-8.
21. Mortality results for randomised controlled trial of early elective surgery or ultrasonographic surveillance for small abdominal aortic aneurysms. The UK Small Aneurysm Trial Participants. Lancet. 1998 Nov 21;352(9141):1649-55.
22. Lederle FA, Johnson GR, Wilson SE, Ballard DJ, Jordan WD, Jr., Blebea J, et al. Rupture rate of large abdominal aortic aneurysms in patients refusing or unfit for elective repair. JAMA. 2002 Jun 12;287(22):2968-72.
23. Stonebridge PA, Draper T, Kelman J, Howlett J, Allan PL, Prescott R, et al. Growth rate of infrarenal aortic aneurysms. European Journal of Vascular and Endovascular Surgery. 1996 Jan;11(1):70-3.
24. Vardulaki KA, Prevost TC, Walker NM, Day NE, Wilmink AB, Quick CR, et al. Growth rates and risk of rupture of abdominal aortic aneurysms. The British Journal of Surgery. 1998 Dec;85(12):1674-80.
25. Santilli SM, Littooy FN, Cambria RA, Rapp JH, Tretinyak AS, d'Audiffret AC, et al. Expansion rates and outcomes for the 3.0-cm to the 3.9-cm infrarenal abdominal aortic aneurysm. Journal of Vascular Surgery. 2002 Apr;35(4):666-71.
26. Stenbaek J, Kalin B, Swedenborg J. Growth of thrombus may be a better predictor of rupture than diameter in patients with abdominal aortic aneurysms. European Journal of Vascular and Endovascular Surgery. 2000 Nov;20(5):466-9.
27. Limet R, Sakalihassan N, Albert A. Determination of the expansion rate and incidence of rupture of abdominal aortic aneurysms. Journal of Vascular Surgery. 1991 Oct;14(4):540-8.
28. Kurvers H, Veith FJ, Lipsitz EC, Ohki T, Gargiulo NJ, Cayne NS, et al. Discontinuous, staccato growth of abdominal aortic aneurysms. Journal of the American College of Surgeons. 2004 Nov;199(5):709-15.
29. Darling RC, Messina CR, Brewster DC, Ottinger LW. Autopsy study of unoperated abdominal aortic aneurysms. The case for early resection. Circulation. 1977 Sep;56(3 Suppl):II161-4.
30. Brady AR, Thompson SG, Fowkes FG, Greenhalgh RM, Powell JT, Participants UKSAT. Abdominal aortic aneurysm expansion: risk factors and time intervals for surveillance. Circulation. 2004 Jul 6;110(1):16-21.
31. Michel JB, Martin-Ventura JL, Egido J, Sakalihasan N, Treska V, Lindholt J, et al. Novel aspects of the pathogenesis of aneurysms of the abdominal aorta in humans. Cardiovascular Research. 2011 Apr 1;90(1):18-27.

32. Busuttil RW, Abou-Zamzam AM, Machleder HI. Collagenase activity of the human aorta. A comparison of patients with and without abdominal aortic aneurysms. Archives of Surgery. 1980 Nov;115(11):1373-8.
33. Dobrin PB, Schwarcz TH, Baker WH. Mechanisms of arterial and aneurysmal tortuosity. Surgery. 1988 Sep;104(3):568-71.
34. Sakalihasan N, Heyeres A, Nusgens BV, Limet R, Lapiere CM. Modifications of the extracellular matrix of aneurysmal abdominal aortas as a function of their size. European Journal of Vascular Surgery. 1993 Nov;7(6):633-7.
35. Aimes RT, Quigley JP. Matrix metalloproteinase-2 is an interstitial collagenase. Inhibitor-free enzyme catalyzes the cleavage of collagen fibrils and soluble native type I collagen generating the specific 3/4- and 1/4-length fragments. The Journal of Biological Chemistry. 1995 Mar 17;270(11):5872-6.
36. Egeblad M, Werb Z. New functions for the matrix metalloproteinases in cancer progression. Nature Reviews Cancer. 2002 Mar;2(3):161-74.
37. Busti C, Falcinelli E, Momi S, Gresele P. Matrix metalloproteinases and peripheral arterial disease. Internal and emergency medicine. 2010 Feb;5(1):13-25.
38. Thompson RW, Parks WC. Role of matrix metalloproteinases in abdominal aortic aneurysms. Annals of the New York Academy of Sciences. 1996 Nov 18;800:157-74.
39. Kent KC, Zwolak RM, Egorova NN, Riles TS, Manganaro A, Moskowitz AJ, et al. Analysis of risk factors for abdominal aortic aneurysm in a cohort of more than 3 million individuals. Journal of Vascular Surgery. 2010 Sep;52(3):539-48.
40. Remus EW, O'Donnell RE, Jr., Rafferty K, Weiss D, Joseph G, Csiszar K, et al. The role of lysyl oxidase family members in the stabilization of abdominal aortic aneurysms. American Journal of Physiology Heart and Circulatory Physiology. 2012 Oct 15;303(8):H1067-75.
41. Abedin M, Tintut Y, Demer LL. Vascular calcification: mechanisms and clinical ramifications. Arteriosclerosis, Thrombosis, and Vascular Biology. 2004 Jul;24(7):1161-70.
42. Tintut Y, Parhami F, Bostrom K, Jackson SM, Demer LL. cAMP stimulates osteoblast-like differentiation of calcifying vascular cells. Potential signaling pathway for vascular calcification. The Journal of Biological Chemistry. 1998 Mar 27;273(13):7547-53.
43. Tintut Y, Demer LL. Recent advances in multifactorial regulation of vascular calcification. Current Opinion in Lipidology. 2001 Oct;12(5):555-60.
44. Iijima K, Hashimoto H, Hashimoto M, Son BK, Ota H, Ogawa S, et al. Aortic arch calcification detectable on chest X-ray is a strong independent predictor of cardiovascular events beyond traditional risk factors. Atherosclerosis. 2010 May;210(1):137-44.
45. Lindholt JS. Aneurysmal wall calcification predicts natural history of small abdominal aortic aneurysms. Atherosclerosis. 2008 Apr;197(2):673-8.
46. Buijs RV, Willems TP, Tio RA, Boersma HH, Tielliu IF, Slart RH, et al. Calcification as a risk factor for rupture of abdominal aortic aneurysm. European Journal of Vascular and Endovascular Surgery . 2013 Nov;46(5):542-8.
47. Ehara S, Kobayashi Y, Yoshiyama M, Shimada K, Shimada Y, Fukuda D, et al. Spotty calcification typifies the culprit plaque in patients with acute myocardial infarction: an intravascular ultrasound study. Circulation. 2004 Nov 30;110(22):3424-9.

48. Shroff RC, Shanahan CM. The vascular biology of calcification. Seminars in Dialysis. 2007 Mar-Apr;20(2):103-9.
49. Heilmaier C, Koester A, Moysidis T, Weishaupt D, Kroger K. Abdominal aortic calcification and its distribution in normal-sized and aneurysmatic abdominal aortas. VASA. 2014 Mar;43(2):132-40.
50. Takagi H, Umemoto T. A contemporary meta-analysis of the association of diabetes with abdominal aortic aneurysm. International angiology. 2014 In press.
51. Raghavan ML, Kratzberg JA, Golzarian J. Introduction to biomechanics related to endovascular repair of abdominal aortic aneurysm. Techniques in Vascular and Interventional Radiology. 2005 Mar;8(1):50-5.
52. Vorp DA, Raghavan ML, Webster MW. Mechanical wall stress in abdominal aortic aneurysm: influence of diameter and asymmetry. Journal of Vascular Surgery. 1998 Apr;27(4):632-9.
53. Kazi M, Thyberg J, Religa P, Roy J, Eriksson P, Hedin U, et al. Influence of intraluminal thrombus on structural and cellular composition of abdominal aortic aneurysm wall. Journal of Vascular Surgery. 2003 Dec;38(6):1283-92.
54. Vollmar JF, Paes E, Pauschinger P, Henze E, Friesch A. Aortic aneurysms as late sequelae of above-knee amputation. Lancet. 1989 Oct 7;2(8667):834-5.
55. Biasetti J, Hussain F, Gasser TC. Blood flow and coherent vortices in the normal and aneurysmatic aortas: a fluid dynamical approach to intra-luminal thrombus formation. Journal of the Royal Society Interface. 2011 Oct 7;8(63):1449-61.
56. Touat Z, Lepage L, Ollivier V, Nataf P, Hvass U, Labreuche J, et al. Dilation-dependent activation of platelets and prothrombin in human thoracic ascending aortic aneurysm. Arteriosclerosis, Thrombosis, and Vascular Biology. 2008 May;28(5):940-6.
57. Sarda-Mantel L, Coutard M, Rouzet F, Raguin O, Vrigneaud JM, Hervatin F, et al. 99mTc-annexin-V functional imaging of luminal thrombus activity in abdominal aortic aneurysms. Arteriosclerosis, Thrombosis, and Vascular Biology. 2006 Sep;26(9):2153-9.
58. Houard X, Rouzet F, Touat Z, Philippe M, Dominguez M, Fontaine V, et al. Topology of the fibrinolytic system within the mural thrombus of human abdominal aortic aneurysms. The Journal of Pathology. 2007 May;212(1):20-8.
59. Martinez-Pinna R, Madrigal-Matute J, Tarin C, Burillo E, Esteban-Salan M, Pastor-Vargas C, et al. Proteomic analysis of intraluminal thrombus highlights complement activation in human abdominal aortic aneurysms. Arteriosclerosis, Thrombosis, and Vascular Biology. 2013 Aug;33(8):2013-20.
60. Defawe OD, Colige A, Lambert CA, Munaut C, Delvenne P, Lapiere CM, et al. TIMP-2 and PAI-1 mRNA levels are lower in aneurysmal as compared to athero-occlusive abdominal aortas. Cardiovascular Research. 2003 Oct 15;60(1):205-13.
61. Fontaine V, Jacob MP, Houard X, Rossignol P, Plissonnier D, Angles-Cano E, et al. Involvement of the mural thrombus as a site of protease release and activation in human aortic aneurysms. The American Journal of Pathology. 2002 Nov;161(5):1701-10.
62. Vorp DA, Lee PC, Wang DH, Makaroun MS, Nemoto EM, Ogawa S, et al. Association of intraluminal thrombus in abdominal aortic aneurysm with local hypoxia and wall weakening. Journal of Vascular Surgery. 2001 Aug;34(2):291-9.

63. Hans SS, Jareunpoon O, Balasubramaniam M, Zelenock GB. Size and location of thrombus in intact and ruptured abdominal aortic aneurysms. Journal of Vascular Surgery. 2005 Apr;41(4):584-8.
64. Behr-Rasmussen C, Grondal N, Bramsen MB, Thomsen MD, Lindholt JS. Mural thrombus and the progression of abdominal aortic aneurysms: a large population-based prospective cohort study. European Journal of Vascular and Endovascular Surgery. 2014 Sep;48(3):301-7.
65. Pincemail J, Defraigne JO, Cheramy-Bien JP, Dardenne N, Donneau AF, Albert A, et al. On the potential increase of the oxidative stress status in patients with abdominal aortic aneurysm. Redox Report : communications in free radical research. 2012;17(4):139-44.
66. Powell JT, Worrell P, MacSweeney ST, Franks PJ, Greenhalgh RM. Smoking as a risk factor for abdominal aortic aneurysm. Annals of the New York Academy of Sciences. 1996 Nov 18;800:246-8.
67. Lindeman JH, Abdul-Hussien H, van Bockel JH, Wolterbeek R, Kleemann R. Clinical trial of doxycycline for matrix metalloproteinase-9 inhibition in patients with an abdominal aneurysm: doxycycline selectively depletes aortic wall neutrophils and cytotoxic T cells. Circulation. 2009 Apr 28;119(16):2209-16.
68. Nyberg A, Skagius E, Englund E, Nilsson I, Ljungh A, Henriksson AE. Abdominal aortic aneurysm and the impact of infectious burden. European Journal of Vascular and Endovascular Surgery . 2008 Sep;36(3):292-6.
69. Cheuk BL, Ting AC, Cheng SW. Detection of C. pneumoniae by polymerase chain reaction-enzyme immunoassay in abdominal aortic aneurysm walls and its association with rupture. European Journal of Vascular and Endovascular Surgery. 2005 Feb;29(2):150-5.
70. Marques da Silva R, Caugant DA, Lingaas PS, Geiran O, Tronstad L, Olsen I. Detection of Actinobacillus actinomycetemcomitans but not bacteria of the red complex in aortic aneurysms by multiplex polymerase chain reaction. Journal of Periodontology. 2005 Apr;76(4):590-4.
71. Nakano K, Nemoto H, Nomura R, Inaba H, Yoshioka H, Taniguchi K, et al. Detection of oral bacteria in cardiovascular specimens. Oral Microbiology and Immunology. 2009 Feb;24(1):64-8.
72. Choke E, Cockerill GW, Dawson J, Wilson RW, Jones A, Loftus IM, et al. Increased angiogenesis at the site of abdominal aortic aneurysm rupture. Annals of the New York Academy of Sciences. 2006 Nov;1085:315-9.
73. Holmes DR, Liao S, Parks WC, Thompson RW. Medial neovascularization in abdominal aortic aneurysms: a histopathologic marker of aneurysmal degeneration with pathophysiologic implications. Journal of Vascular Surgery. 1995 May;21(5):761-71.
74. Paik DC, Fu C, Bhattacharya J, Tilson MD. Ongoing angiogenesis in blood vessels of the abdominal aortic aneurysm. Experimental & Molecular Medicine. 2004 Dec 31;36(6):524-33.
75. Reeps C, Pelisek J, Seidl S, Schuster T, Zimmermann A, Kuehnl A, et al. Inflammatory infiltrates and neovessels are relevant sources of MMPs in abdominal aortic aneurysm wall. Pathobiology : Journal of Immunopathology, Molecular and Cellular Biology. 2009;76(5):243-52.
76. Darling RC, 3rd, Brewster DC, Darling RC, LaMuraglia GM, Moncure AC, Cambria RP, et al. Are familial abdominal aortic aneurysms different? Journal of Vascular Surgery. 1989 Jul;10(1):39-43.

77. Derubertis BG, Trocciola SM, Ryer EJ, Pieracci FM, McKinsey JF, Faries PL, et al. Abdominal aortic aneurysm in women: prevalence, risk factors, and implications for screening. Journal of Vascular Surgery. 2007 Oct;46(4):630-5.
78. Brown PM, Zelt DT, Sobolev B. The risk of rupture in untreated aneurysms: the impact of size, gender, and expansion rate. Journal of Vascular Surgery. 2003 Feb;37(2):280-4.
79. Tanaka H, Zaima N, Sasaki T, Hayasaka T, Goto-Inoue N, Onoue K, et al. Adventitial vasa vasorum arteriosclerosis in abdominal aortic aneurysm. PloS One. 2013;8(2):e57398.
80. Feng Y, Chen F, Xie Y, Wang H, Cona MM, Yu J, et al. Lipomatous metaplasia identified in rabbits with reperfused myocardial infarction by 3.0 T magnetic resonance imaging and histopathology. BMC Medical Imaging. 2013;13(1):18.
81. Roy J, Labruto F, Beckman MO, Danielson J, Johansson G, Swedenborg J. Bleeding into the intraluminal thrombus in abdominal aortic aneurysms is associated with rupture. Journal of Vascular Surgery. 2008 Nov;48(5):1108-13.
82. Mehard WB, Heiken JP, Sicard GA. High-attenuating crescent in abdominal aortic aneurysm wall at CT: a sign of acute or impending rupture. Radiology. 1994 Aug;192(2):359-62.
83. Hellenthal FA, Geenen IL, Teijink JA, Heeneman S, Schurink GW. Histological features of human abdominal aortic aneurysm are not related to clinical characteristics. Cardiovascular Pathology. 2009 Sep-Oct;18(5):286-93.
84. Mitchell DG, Burk DL, Jr., Vinitski S, Rifkin MD. The biophysical basis of tissue contrast in extracranial MR imaging. AJR 1987 Oct;149(4):831-7.
85. Fenton HJH. Oxidation of tartaric acid in presence of iron J Chem Soc, Trans. 1894;65:899-910.
86. Hamacher K, Coenen HH, Stocklin G. Efficient stereospecific synthesis of no-carrier-added 2-[18F]-fluoro-2-deoxy-D-glucose using aminopolyether supported nucleophilic substitution. Journal of Nuclear Medicine. 1986 Feb;27(2):235-8.
87. Reivich M, Kuhl D, Wolf A, Greenberg J, Phelps M, Ido T, et al. The [18F]fluorodeoxyglucose method for the measurement of local cerebral glucose utilization in man. Circulation Research. 1979 Jan;44(1):127-37.
88. Rudd JH. The role of 18F-FDG PET in aortic dissection. Journal of Nuclear Medicine. 2010 May;51(5):667-8.
89. Truijers M, Kurvers HA, Bredie SJ, Oyen WJ, Blankensteijn JD. In vivo imaging of abdominal aortic aneurysms: increased FDG uptake suggests inflammation in the aneurysm wall. Journal of Endovascular Therapy. 2008 Aug;15(4):462-7.
90. Kotze CW, Menezes LJ, Endozo R, Groves AM, Ell PJ, Yusuf SW. Increased metabolic activity in abdominal aortic aneurysm detected by 18F-fluorodeoxyglucose (18F-FDG) positron emission tomography/computed tomography (PET/CT). European Journal of Vascular and Endovascular Surgery. 2009 Jul;38(1):93-9.
91. Marini C, Morbelli S, Armonino R, Spinella G, Riondato M, Massollo M, et al. Direct relationship between cell density and FDG uptake in asymptomatic aortic aneurysm close to surgical threshold: an in vivo and in vitro study. European Journal of Nuclear Medicine and Molecular Imaging. 2012 Jan;39(1):91-101.

92. Sarda-Mantel L, Alsac JM, Boisgard R, Hervatin F, Montravers F, Tavitian B, et al. Comparison of 18F-fluoro-deoxy-glucose, 18F-fluoro-methyl-choline, and 18F-DPA714 for positron-emission tomography imaging of leukocyte accumulation in the aortic wall of experimental abdominal aneurysms. Journal of Vascular Surgery. 2012 Sep;56(3):765-73.
93. Defawe OD, Hustinx R, Defraigne JO, Limet R, Sakalihasan N. Distribution of F-18 fluorodeoxyglucose (F-18 FDG) in abdominal aortic aneurysm: high accumulation in macrophages seen on PET imaging and immunohistology. Clinical Nuclear Medicine. 2005 May;30(5):340-1.
94. Sakalihasan N, Hustinx R, Limet R. Contribution of PET scanning to the evaluation of abdominal aortic aneurysm. Seminars in Vascular Surgery. 2004 Jun;17(2):144-53.
95. Courtois A, Nusgens BV, Hustinx R, Namur G, Gomez P, Somja J, et al. 18F-FDG uptake assessed by PET/CT in abdominal aortic aneurysms is associated with cellular and molecular alterations prefacing wall deterioration and rupture. Journal of Nuclear Medicine. 2013 Oct;54(10):1740-7.
96. Buvat I. Les limites du SUV. Médecine Nucléaire. 2007;21:165-72.
97. Le Bihan D, Breton E, Lallemand D, Grenier P, Cabanis E, Laval-Jeantet M. MR imaging of intravoxel incoherent motions: application to diffusion and perfusion in neurologic disorders. Radiology. 1986 Nov;161(2):401-7.
98. Padhani AR, Koh DM, Collins DJ. Whole-body diffusion-weighted MR imaging in cancer: current status and research directions. Radiology. 2011 Dec;261(3):700-18.
99. Jacobs MA, Ibrahim TS, Ouwerkerk R. AAPM/RSNA physics tutorials for residents: MR imaging: brief overview and emerging applications. Radiographics. 2007 Jul-Aug;27(4):1213-29.
100. Kitagawa T, Kosuge H, Chang E, James ML, Yamamoto T, Shen B, et al. Integrin-targeted molecular imaging of experimental abdominal aortic aneurysms by (18)F-labeled Arg-Gly-Asp positron-emission tomography. Circulation Cardiovascular Imaging. 2013 Nov;6(6):950-6.
101. Tegler G, Estrada S, Hall H, Wanhainen A, Bjorck M, Sorensen J, et al. Autoradiography screening of potential positron emission tomography tracers for asymptomatic abdominal aortic aneurysms. Upsala Journal of Medical Sciences. 2014 Aug;119(3):229-35.
102. Zienkiewicz OC. The Finite Elements Method. The Basis. 5th edition ed. Oxford:Butterworth Heinemann; n°1. 2000.
103. Auer M, Gasser TC. Reconstruction and finite element mesh generation of abdominal aortic aneurysms from computerized tomography angiography data with minimal user interactions. IEEE Transactions on Medical Imaging. 2010 Apr;29(4):1022-8.
104. Caro CG. Discovery of the role of wall shear in atherosclerosis. Arteriosclerosis, Thrombosis, and Vascular Biology. 2009 Feb;29(2):158-61.
105. Zhang Z, Deng X, Fan Y, Guidoin R. The effects of recirculation flows on mass transfer from the arterial wall to flowing blood. ASAIO Journal. 2008 Jan-Feb;54(1):37-43.
106. Martinez-Pinna R, Lindholt JS, Madrigal-Matute J, Blanco-Colio LM, Esteban-Salan M, Torres-Fonseca MM, et al. From tissue iron retention to low systemic haemoglobin levels, new pathophysiological biomarkers of human abdominal aortic aneurysm. Thrombosis and Haemostasis. 2014 Jul 3;112(1):87-95.

107. Coutard M, Touat Z, Houard X, Leclercq A, Michel JB. Thrombus versus wall biological activities in experimental aortic aneurysms. Journal of Vascular Research. 2010;47(4):355-66.
108. Folkesson M, Kazi M, Zhu C, Silveira A, Hemdahl AL, Hamsten A, et al. Presence of NGAL/MMP-9 complexes in human abdominal aortic aneurysms. Thrombosis and Haemostasis. 2007 Aug;98(2):427-33.
109. Sakalihasan N, Van Damme H, Gomez P, Rigo P, Lapiere CM, Nusgens B, et al. Positron emission tomography (PET) evaluation of abdominal aortic aneurysm (AAA). European Journal of Vascular and Endovascular Surgery. 2002 May;23(5):431-6.
110. Nchimi A, Cheramy-Bien JP, Gasser TC, Namur G, Gomez P, Seidel L, et al. Multifactorial relationship between 18F-fluoro-deoxy-glucose positron emission tomography signaling and biomechanical properties in unruptured aortic aneurysms. Circulation Cardiovascular Imaging. 2014 Jan;7(1):82-91.
111. Sakalihasan N, Defraigne JO, Kerstenne MA, Cheramy-Bien JP, Smelser DT, Tromp G, et al. Family members of patients with abdominal aortic aneurysms are at increased risk for aneurysms: analysis of 618 probands and their families from the Liege AAA Family Study. Annals of Vascular Surgery. 2014 May;28(4):787-97.
112. van de Luijtgaarden KM, Bastos Goncalves F, Hoeks SE, Valentijn TM, Stolker RJ, Majoor-Krakauer D, et al. Lower atherosclerotic burden in familial abdominal aortic aneurysm. Journal of Vascular Surgery. 2014 Mar;59(3):589-93.
113. Vande Geest JP, Wang DH, Wisniewski SR, Makaroun MS, Vorp DA. Towards a noninvasive method for determination of patient-specific wall strength distribution in abdominal aortic aneurysms. Annals of Biomedical Engineering. 2006 Jul;34(7):1098-106.
114. Svensjo S, Bjorck M, Gurtelschmid M, Djavani Gidlund K, Hellberg A, Wanhainen A. Low prevalence of abdominal aortic aneurysm among 65-year-old Swedish men indicates a change in the epidemiology of the disease. Circulation. 2011 Sep 6;124(10):1118-23.
115. Anjum A, Powell JT. Is the incidence of abdominal aortic aneurysm declining in the 21st century? Mortality and hospital admissions for England & Wales and Scotland. European Journal of Vascular and Endovascular Surgery. 2012 Feb;43(2):161-6.
116. Sandiford P, Mosquera D, Bramley D. Trends in incidence and mortality from abdominal aortic aneurysm in New Zealand. The British Journal of Surgery. 2011 May;98(5):645-51.
117. Gasser TC, Nchimi A, Swedenborg J, Roy J, Sakalihasan N, Bockler D, et al. A novel strategy to translate the biomechanical rupture risk of abdominal aortic aneurysms to their equivalent diameter risk: method and retrospective validation. European Journal of Vascular and Endovascular Surgery. 2014 Mar;47(3):288-95.
118. Reeps C, Bundschuh RA, Pellisek J, Herz M, van Marwick S, Schwaiger M, et al. Quantitative assessment of glucose metabolism in the vessel wall of abdominal aortic aneurysms: correlation with histology and role of partial volume correction. The International Journal of Cardiovascular Imaging. 2013 Feb;29(2):505-12.
119. Palombo D, Morbelli S, Spinella G, Pane B, Marini C, Rousas N, et al. A positron emission tomography/computed tomography (PET/CT) evaluation of asymptomatic abdominal aortic aneurysms: another point of view. Annals of Vascular Surgery. 2012 May;26(4):491-9.

120. Tegler G, Ericson K, Sorensen J, Bjorck M, Wanhainen A. Inflammation in the walls of asymptomatic abdominal aortic aneurysms is not associated with increased metabolic activity detectable by 18-fluorodeoxglucose positron-emission tomography. Journal of Vascular Surgery. 2012 Sep;56(3):802-7.
121. Richards JM, Semple SI, MacGillivray TJ, Gray C, Langrish JP, Williams M, et al. Abdominal aortic aneurysm growth predicted by uptake of ultrasmall superparamagnetic particles of iron oxide: a pilot study. Circulation Cardiovascular Imaging. 2011 May;4(3):274-81.
122. Rouzet F, Bachelet-Violette L, Alsac JM, Suzuki M, Meulemans A, Louedec L, et al. Radiolabeled fucoidan as a p-selectin targeting agent for in vivo imaging of platelet-rich thrombus and endothelial activation. Journal of Nuclear Medicine. 2011 Sep;52(9):1433-40.
123. Couvreur TL, Györgyi; Nchimi, Alain. Imaging Assessment of Periaortic Inflammation in Erdheim-Chester Disease. AORTA. 2013;Volume 1, Number 2:146-8.
124. Nguyen VL, Backes WH, Kooi ME, Wishaupt MC, Hellenthal FA, Bosboom EM, et al. Quantification of abdominal aortic aneurysm wall enhancement with dynamic contrast-enhanced MRI: feasibility, reproducibility, and initial experience. Journal of Magnetic Resonance Imaging. 2014 Jun;39(6):1449-56.
125. Nguyen VL, Kooi ME, Backes WH, van Hoof RH, Saris AE, Wishaupt MC, et al. Suitability of pharmacokinetic models for dynamic contrast-enhanced MRI of abdominal aortic aneurysm vessel wall: a comparison. PloS One. 2013;8(10):e75173.

ANNEXES

Additional publication N°1

A. Nchimi. Imaging in aortic aneurysms.
In Aortic Aneurysms. New insights into an old problem. Eds N. Sakalihasan, H. Kuivaniemi, J.B. Michel. Les Editions de l'Université de Liège, Snel, Vottem, Belgique, 2008.

Additional publication N° 2

A. Nchimi, T. Couvreur, B. Meunier, N. Sakalihasan. Magnetic resonance Imaging findings in a positron emission tomography-positive thoracic aortic aneurysm. Aorta, 2013 (3) : 198-201.

Additional figure 1

Summary in French- Résumé (FR)

Curriculum vitae

Additional publication N°1

This book chapter has been published as:

Imaging in aortic aneurysm

A. Nchimi

In Aortic Aneurysms. New insights into an old problem.
Eds: N. Sakalihasan, H. Kuivaniemi, J.B. Michel.
Les Editions de l'Université de Liège, Snel, Vottem, Belgique, 2008, p85-100.

Natzi Sakalihasan
Helena Kuivaniemi
Jean-Baptiste Michel

Aortic Aneurysms

New insights into an old problem

Les Éditions de l'Université de Liège

4

Imaging in aortic aneurysms

Alain Nchimi

Introduction

Virtually every vascular structure can become aneurysmal, with aorta being by far the most common location in humans. Aneurysm can be defined as a persistent localized dilatation of a vessel, exceeding 50% of the expected normal diameter and causing loss of the borders parallelism [1]. This differentiates aneurysms from ectasia which is a localized dilatation of less than 50%, and arteriomegaly defined as non localized dilatation [2]. Histologically, aneurysms wall contains the vessels' three layers, in contrast to pseudoaneurysms in which at least one of the layers is missing.

Knowledge of the pathophysiology of human aneurysm has evolved, allowing some independent risk factors to be identified. Currently, markers of aneurysms behavior, such as parietal compliance and stress, inflammation and leukocyte trapping are being investigated by novel imaging abilities [3-5]. The natural history of aneurysms remains incompletely elucidated, but large cohort studies have validated that the risk of a catastrophic outcome is related to: (i) the size by the time of the diagnosis, (ii) the rate of expansion [6-8]. Size of an aneurysm is currently the sole validated criteria indicating preventive surgical intervention in asymptomatic aneurysms [9-11]. As the result, imaging should provide the most precise and reproducible measurements of aortic aneurysms. Progresses in imaging speed currently enable high quality 3-dimensionnal (3D) and nearly 4-dimensionnal (4D) cross sectional angiography imaging of the whole aorta that fulfill these criteria. Dedicated computer workstations are capable of producing multiplanar reformatted images that show true aortic cross sections. Some systems are sophisticated enough to perform automatic segmentation, 3D volume rendering, and a variety of calculations. Aneurysm features can therefore be digitized, quantified, and stored as numeric information.

Properties of the different imaging modalities

Table 1 reviews the main imaging modalities advantages and disadvantages in evaluating aortic aneurysms. Diagnostic catheter angiography is invasive and inaccurate in evaluating aortic wall. It remains indicated only before endovascular repair, or to identify preoperatively spinal arteries. Similarly, chest radiography (CRX) has a very low diagnostic accuracy and should be used only in case of extreme emergency.

Ultrasonography (US) is the most available technique for aortic aneurysm evaluation. Computed tomography (CT) angiography is accurate and fast in evaluating both abdominal and thoracic aorta aneurysms. Both speed and availability make of CT the examination of choice in the setting of acute symptoms. Data from CT angiography can be used for wall stress evaluation. Coupling CT scanners with emission positron cameras allows combining the morphologic study of aneurysms with

Table 1: Imaging modalities properties in evaluating aortic aneurysms.

Imaging modality	Advantages	Disadvantages
Computed tomography (CT) angiography	- Assess the whole aorta - Fast, specific and sensitive - Accurate measurements - Broadly accessible - Assess aneurysm complications, and associated major risk factors - Can be combined with PET - Can be used for wall stress imaging	- Ionizing radiation - Nephrotoxic contrast agent
Chest radiography (CRX)	- Fast, portable in case of emergency, exclude non aortic causes - Can demonstrate aortic enlargement, pleural fluid	- Poor specificity and sensitivity - Can't visualize abdominal aorta
Transoesophageal ultrasonography (US)	- Highly sensitive and specific - Portable	- Blind areas - Can't explore abdominal aorta - Invasive
Transabdominal US	- Highly sensitive and specific - Portable - Can be used for plaque composition and parietal compliance imaging	- Can't explore thoracic aorta
Magnetic resonance (MR) angiography	- Assess the whole aorta - Sensitive and specific - Accurate measurements - Assess aneurysm complications, and associated major risk factors - Can be used for plaque composition, parietal compliance, wall stress and metabolic imaging	- Slow (not for unstable patients) - Poorly accessible - Risks of nephrogenic systemic fibrosis in cases of severe renal insufficiency

metabolic information of positron emission tomography (PET) in a single examination. Nonetheless, both PET and CT are responsible of considerable administration of ionizing radiation to the patients.

Among all imaging techniques, magnetic resonance (MR) has the greater ability in tissue characterization. MR angiography is as accurate as CT in evaluation of aneurysms, and the data can be used for wall stress and compliance imaging. However, since MR imaging is slow and poorly accessible, it should never be performed in case of emergency.

Ultrasonography

In contrast to CT and MR, US cannot image the whole aorta within a single imaging session. The thoracic aorta is evaluated via transesophageal approach. For such exploration, no preparation is required and the patients undergo light intravenous benzodiazepine sedation. In most cases, both ascending and descending thoracic aorta are superbly evaluated, but the aortic arch may be difficult to assess [12]. Because of its high spatial resolution, the measurements performed at US correlated well with those obtained by other imaging techniques. The temporal resolution of US is also better than any other imaging technique and allows real-time imaging. Coupling US with Doppler help to detect and quantify valvular abnormalities and flow direction. Lastly, data from tissue Doppler US showed promise in evaluating wall compliance.

Abdominal aorta is accessible from diaphragmatic hiatus through the carefour via transabdominal approach, without specific preparation. US requires operators' expertise and patient collaboration, but has the advantages to be: (i) harmless, (ii) performed without intravenous contrast agent, and (iii) portable and if necessary performed quickly at patient's bed.

Three-dimensional angiography

Which scanning limits?

Ideally, imaging protocols must be adapted to the specific clinical question to be answered, anatomic coverage and the technique used for 3D angiography (CT versus MR), and the type of scanner available. Ascending thoracic aortic aneurysms are not uncommonly isolated. While the aneurysms of the infrarenal abdominal aorta are much more commonly associated with iliac (aneurysmal or occlusive) than thoracic diseases, those of the descending and suprarenal aorta are commonly associated to another aortic abnormality. Therefore, we advise to include the whole aorta in case of descending thoracic and suprarenal aorta aneurysm, and to limit 3D angiography coverage to; (i) the chest (from the sternal notch through the diaphragmatic crus) in case of ascending thoracic aneurysm, (ii) the abdominal aorta (from the diaphragmatic dome through the pubic symphysis) in case of infrarenal abdominal aortic aneurysm.

How the patients should be prepared?

Prior to examination, the medical history of the patient should be checked for contraindications to CT or MR imaging. Allergy to iodized contrast agents used for CT angiography is more common than to gadolinium-based agents used for MR angiography. The renal function should be scrutinized carefully before injection of a contrast agent. In patients under oral antidiabetics and those with mild to moderate renal impairment (i.e.: creatinine clearance > 30 ml/min), MR angiography should be preferred. When CT angiography can not be avoided, patients should be prepared by intravenous hyperhydratation and homocysteine prior to examination; oral antidia-

betics should be stopped 48 hours around the examination. Patients with severe renal impairment (i.e.: creatinine clearance ≤ 30 ml/min) are at risk to develop nephrogenic systemic fibrosis after intravenous injection of a gadolinium-based contrast agent [13]. In these patients, only non contrast 3D MR angiography applies.

CT angiography

How the data are acquired?

Scanning is performed in the axial plane during maximal arterial enhancement, with minimal venous enhancement. Depending on the balance between signal-to-noise ratio and radiation dose, slice thickness varies between 1.5 and 3mm, tube current between 80 and 140 kVp and intensity between 50 and 400mA [14]. Arterial enhancement is obtained via intravenous injection of 2ml/kg of an iodine contrast agent, via a power injector, flushed by 20-50ml of saline fluid, at the rate of 3-6 ml/s. The following equation represents the relationships between the volume, the contrast medium flow rate and the scan duration:

Contrast volume (ml) = contrast material flow rate (ml/s) x scan duration (s).

With recent multidetector scanners, scanning duration is proportional to the pitch (ie: ratio between scanning table speed and collimation configuration of the tube) and coverage. The whole aorta can be scanned in less than 10s, with benefits on both the renal function (via reduction of contrast agent volumes) and the image quality, since the patients are instructed to hold breath during acquisitions.

Table 2 : MR image weighting and signal intensity appearances of some aneurysm wall findings.

	T1-Weighted imaging	T2-Weighted imaging	Proton density imaging
Repetition time	Short (<600ms*)	Long (>1000ms*)	Intermediate
Echo time	Short (<20ms*)	Long (> 50ms*)	
Flip angle**	Very low	High	
Hemorrhage or fibrinolysis	High SI	Variable SI	High SI
Multilayer thrombus	Homogeneous	Superimposed layers of different SI	Homogenous
Diamagnetic particles accumulation (iron, calcium…)	Variable SI	Variable SI	Low SI

* Indicative values are given for spin echo sequences. These values are proportionally very low for gradient echo sequences.

** is used for gradient sequences echo weighting.

Reference for the signal intensity values is the signal intensity of the blood pool.

SI = Signal Intensity. Table 3 : Risk factors for acute aortic syndrome

Acquisition can be synchronized to patients' electrocardiogram in order to minimize artifacts related heartbeats. Although an increased recognition of normal and abnormal can be anticipated from such image quality [15], electrocardiographic triggering causes significant increase in ionizing radiation dose to the patients.

Table 3 : Riskfactors for acute aortic syndrome

Acquired and congenital disorders of the aortic wall
Bicuspid aortic valve
Coarctation
Connective tissue disorders
Ehlers-Danlos syndrome
Familial annulaortic ectasia
Familial aortic dissection
Marfan syndrome
Turner syndrome
Vascular inflammation
Behçet disease
Giant celle arteritis
Syphilitic aortitis
Takayasu arteritis
Multifactorial complex acquired conditions
Atherosclerosis
Diabetes
Dyslipidemia
Hypertension
Renal disease
Iatrogenic factors
Endovascular instrument
Valvular or aortic surgery
Modifiable risk factor
Cocaine or other illicit drug use
Smoking

Modified from Smith and Schoenhagen [6].

In patients with normal cardiac output, an enhancement of the aorta of at least 100 Hounsfield units is usually obtained 20-30s after the beginning of the injection. Using systematically this time delay may result in time/bolus inadequacy in patients with aneurysms, as they may have low cardiac output, reduced flow rates in the aorta or both (figure 1). To avoid such occurrence, performing a single slice every 2s at the level of the diaphragmatic hiatus could be useful for either calculate the appropriate time delay during a test bolus (1/10 of the contrast agent volume to administrate) injection, or triggering directly acquisition to the arterial enhancement peak during the injection of the main bolus.

After angiography, the same scanning range should be repeated at a delayed or parenchymal phase, in certain specific indications, such as dissection and prosthetic grafts follow-up [16, 17].

How the data are displayed?

Scanning the whole aorta with thin overlapping slices result in a considerable amount of slices that are commonly displayed using 3D imaging softwares. The 3D imaging modes include multiplanar reformation (MPR), rendering techniques, maximum intensity projection (MIP) and virtual endoscopy (figure 2).

MPR is a fast and simple technique that enables simultaneous visualization of complex anatomy, in axial, sagittal, coronal, oblique and curved planes [18]. This technique is the most effective for evaluation of: (i) vessel diameter or stenosis, (ii) parietal thrombus (contours, thickness and appearance), (iii) parietal ulcers, (iv) dissection, (v) perivascular fat planes.

In the rendering mode, thresholds are used to color display the surface of struc-

tures according to their respective range of densities [19]. Virtual angioscopy represents a variation from the rendering techniques; in which threshold selection enables navigation from inside the vessel. Little diagnosis yield is provided by rendering mode, but the display commonly summarizes all information requested by clinicians in an impressive manner.

MIP proceeds with extraction and projection in a given plane of the voxels exhibiting the highest density within a ray. This technique is the better suited for CT angiography, since the voxels representing the contrast filled vessels are the most likely to be the highest values [20].

MR angiography

Basically, MR image weighting is related to: (i) repetition time (TR), (ii) echo time (TE), and (iii) flip angle. Depending on these parameters, three major types of weighting can be obtained. Examination starts with scouting and axial 5-8mm slices in T1, T2 and proton density weightings, covering the region of interest. On all sequences, pre-pulses can be added to suppress the signal corresponding to some particular structures such as fat or the blood pool. Characteristics of these sequences are given on table 2 with corresponding appearances of some aneurysm features.

Some MR pulse sequences are sensitized to moving protons and therefore have the ability to image arteries without contrast agent injection. Such techniques require long acquisition times and should be limited to patients with contraindication to intravenous contrast.

In most cases, aorta angiography is performed using very fast 3D gradient echo T1-weighted sequence during intravenous injection of a T1 shortening contrast agent. The main advantage of gradient echo compared to spin echo sequences is that both TE and TR (therefore acquisition times) can be substantially reduced. This enables MR angiography to be performed quickly within a breathhold. The contrast agent is a gadolinium chelate, administered at the dose of 1-2mmol/kg patient weight, flushed by 10-20ml saline, at the rate of 2-3ml/s. MR has the ability to acquire images in every plane. Thus, the whole aorta can be imaged in its long axis (coronal oblique plane) that lowers the number of slices needed for coverage as compared to axial acquisitions. To acquire a 3D dataset, the same technical rules and data display as for CT angiography apply to MR.

With increasing scanner abilities, a 3D dataset can be acquired within very few seconds and therefore repeated through-

Figure 1 : CT angiography performed in the setting of an acute chest syndrome showed inadequate scanning time/bolus enhancement. Although scanning was performed 20 s after injection of the contrast agent, aortic enhancement was weak because of the cardiac tamponade caused by hemopericardium (a, arrows). The patient eventually died few minutes after the scanner and necropsy found a ruptured aneurysm of the ascending aorta with a Stanford A dissection. In retrospect, only very subtle signs of this diagnosis could be identified at CT (b, arrowheads).

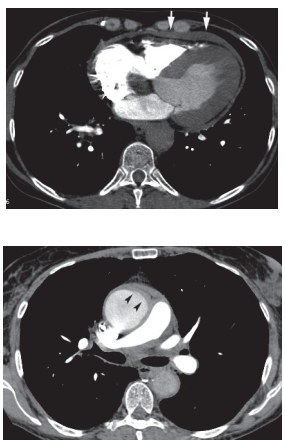

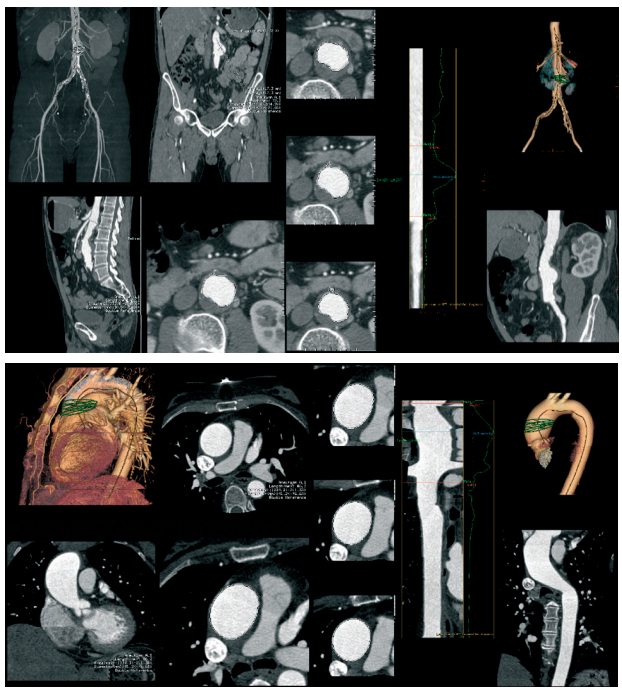

Figure 2 : Analysis of CT angiographies in subjects with isolated aneurysms of the infrarenal (a) and ascending thoracic aorta (b). Computer analysis shows the data in all planes in the MPR mode, allowing operator to indicate precisely all the necessary landmarks. Then, the data displayed in MIP or volume rendering modes with superimposed features of the aneurysm.

out the circulation of the bolus of contrast agent, since there is no additional hazard to the patient. The resulting imaging can be used to create 4D (3D x time) imaging (figure 3).

Emerging techniques

Over the past two decades, progresses in technologies have progressively made possible imaging of some of the physiological events that occur in aortic aneurysms. These approaches showed promises in risk stratification of aortic aneurysms [21, 22]. For example, imaging now enables precise determination of plaques or thrombus components, arterial flow pattern and parietal compliance as well as the level of metabolism attributable to different cell types populated in unstable aneurysms.

Plaque composition

The first attempts to plaque composition study by imaging were performed to detect calcifications by CT. Such finding is associated with an increased atherosclerosis burden in the coronary arteries [21]. However, there are no relevant data indicating that calcifications are associated to increased risks of complications in aortic aneurysms. MR has the ability to recognize aortic wall layers and evaluate their respective composition [12]. Areas of fat accumulation within the thrombus are bright on both T1- and T2-weighted images, while recent hemorrhagic or fibrinolytic areas that have a superior protein content are bright only on T1-weighted images (figure 4). The signal intensity of the thrombus on both proton density and T2-weighted images vary according to the amount of water and diamagnetic particles such as iron or calcium: the more water the higher signal and the more particles the lower signal. Intravascular US can also be used for plaque characterization, but remains invasive [23].

Figure 3 : MR angiography of the throracoabdominal aorta in a subject with a small aneurysm of the abdominal aorta. Several 3D datasets (a-f), displayed as MIPs are acquired. The contrast agent first flows through the pulmonary circulation, then progressively into different parts of the aorta.

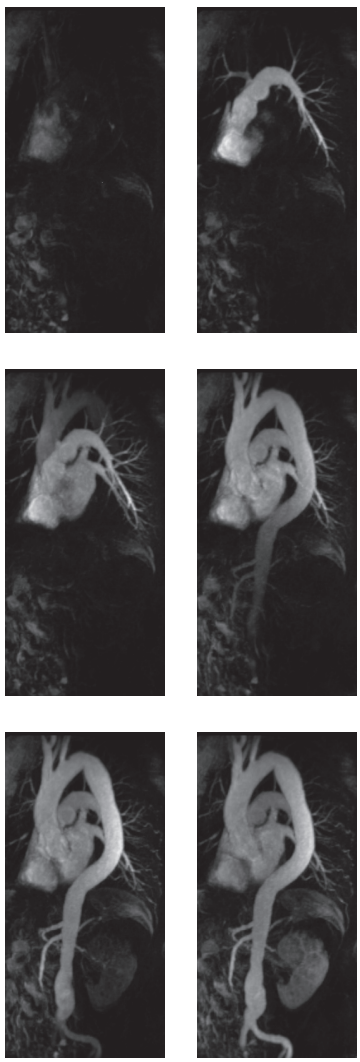

Parietal compliance and wall stress imaging

Elastic properties or compliance of the aortic wall is decreased in patients with aneurysm. This property has been studied with tissue Doppler velocity imaging [3, 24] and MR imaging [25]. The blood flow turbulence within the aorta itself generates parietal inhomogeneous tension. Experimental models of flow can identify areas of high parietal tension, using the volumetric data of CT or MR angiography. Loss of compliance and increased wall stress are both involved in aneurysm formation and rupture [26, 27]. Nonetheless, clinical relevance of these measurements is yet to be established since: (i) only a limited number of aneurysms has been studied, and (ii) the algorithms used for these measurements are numerous and provide significantly heterogeneous results [28].

Metabolic imaging

Expanding or high-risk aneurysms are linked with increased inflammatory infiltrates and metabolism. The process can be monitored non-invasively by targeting the cells involved, via phagocytosis or endocytosis of paramagnetic MR contrast agents [29-31]. Administering for energy supply, 18-fluoro-deoxyglucose –a radiotracer analog of the glucose, that can be detected by positron emission tomography– also provide an elegant approach for non invasive monitoring of plaques and aneurysms and risk stratification [32, 33].

Role of imaging in regard to the patient status

The patient is asymptomatic

In subjects to screening, US should be privileged [34]. Most aneurysms are discov-

ered incidentally as shown by systematic CT examinations performed to detect lung or colorectal cancer [35].

How the measurements are performed?

When an aneurysm is first discovered, 3D imaging should be performed via CT or MR angiography. The measurements provided at this time will serve for treatment planning and expansion rate calculation. These measurements can be performed manually on reformatted images that enable identification of the largest aortic section using calipers from an outer limit to the opposed. The neck and the end of the aneurysm should be identified and localized via a landmark and measured as well. Computerized software enables to segment and extract the aorta from the whole volumetric data, and perform automatically the measurements after the operator has indicate these landmarks (figure 2). Obtaining 3D imaging is also necessary to assess: (i) the relationships of the aorta with the surrounding organs, and (ii) the curvatures of both normal and aneurysmal aorta that are independent risk factors [36].

Figure 4 : T1- (a) and T2-weighted (b) MR imaging in a subject with aneurysm of the aortic arch. The first pulse sequence showed an eccentric thick thrombus as bright, while the second displayed multiple layers of different signal intensity (arrows). These findings suggest an area of hemorrhage, since the initial T2-weighted MR imaging examination performed one year earlier at the same level (c) showed a thin homogenous thrombus.

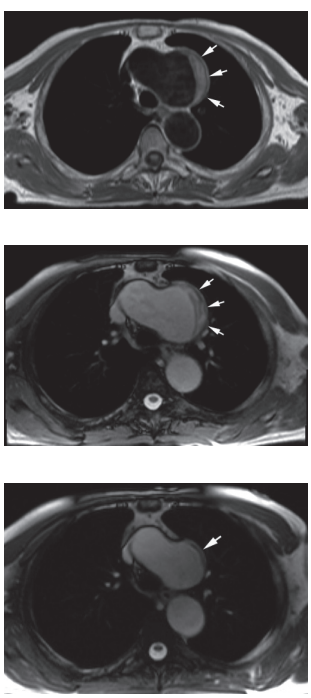

After an initial evaluation, follow-up should be performed every 3 or 6 months according to aneurysm size, location and specific patient risk. If abnormal expansion is suspected, another 3D angiography of the aorta should be performed. When the data are subject to expansion rates evaluation, the most recent examination should confront not only to the previous, but also the less recent, since the rate of expansion of aneurysm is not constant.

In subjects to follow-up after open surgical or endovascular aneurysm repair, 3D CT angiography should be preferred, since the current endovascular prostheses causes magnetic disturbances that are not suitable at MR angiography. The main complications from grafting is the failure to isolate aneurysm from the circulating blood which is seen on CT angiography as opacification of the thrombus and may cause persisting expansion and eventually rupture. Such complication have been classified as :

- direct leakage of the contrast agent from the aortic lumen (type I), resulting from tiny migration at the graft neck (figure 5)
- reverse side-branch circulation (type II)
- perforation of the graft (type III)
- diffuse leakage (type IV)

Other complications include side-branch occlusion or dissection and kinking [37].

Infrarenal aortic aneurysms

Risks of severe complications outpass morbidity repair for a maximal diameter of 5.5 cm. This diameter is decreased by 0.5 cm for women. New imaging modalities will probably appear in different schemes with time, in order to extend or reduce periods between imaging referrals. For example, PET has recently been included for risk stratification in abdominal aortic aneurysms by Sakalihassan et al [38].

Figure 5 : Immediate (a) and 1-year post-procedural (b) CT angiographies on volume rendering display in a patient with isolated aneurysm of the abdominal aorta treated by stent grafting. The 1-year post procedural CT angiography showed a type I leakage into the thrombus (asterisk).

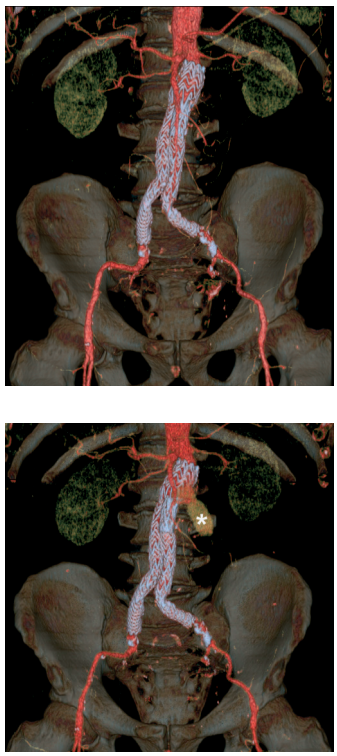

Thoracic aortic and thoracoabdominal aneurysms

With ascending thoracic aorta aneurysm, repair is indicated when the diameter exceeds 5.5 cm. Familial cases, Marfan's disease, aortic bicuspidy and cloverleaf appearance of the aortic arch represent additional risk factors indicating repair for lower diameters. The descending thoracic and thoracoabdominal aortic aneurysms share similar risk factors, but should be repaired when their diameter reach 6.5 cm.

The patient suffers acute syndrome

Acute aortic syndrome is defined as chest pain due to an aortic condition [39]. The risk factors for such a syndrome are given on table 3. Abdominal aortic diseases also cause pain and shock. These syndromes result of various causes including rupture, fistulization, infection and fibrosis of an aneurysm, as well as the following conditions that may occur with and without aneurysm: (i) dissection, (ii) mural hematoma, and (iii) penetrating ulcer. In some cases, only abdominal or chest radiography US performed at patients' bed may be allowed by patient's hemodynamic instability. In cases of thoracic aortic aneurysm rupture, chest radiograph may show aortic enlargement and with pleural fluid (figure 6). US signs of ruptured abdominal aortic aneurysms include: (i) disruption of aortic wall, (ii) hyperechoic periaortic and retroperitoneal collection, poorly delineated and displacing the adjacent organs (figure 7).

When patients are hemodynamically stable enough to undergo another examination, CT angiography should be performed without further delay. In these patients, the main question to answer is to determine in how far they can escape emergency surgery. A temporarily conservative approach is preferred in certain cases of complicated aneurysms (figure 8). These include a spectrum of injuries involving dissection,

Figure 6 : A subject with a known small aneurysm of the aortic arch was admitted with acute chest syndrome. An antero-posterior chest radiography performed showed enlarged aortic arch (asterisk) and a large left pleural effusion, suggesting rupture, which was confirmed during subsequent emergency thoracotomy.

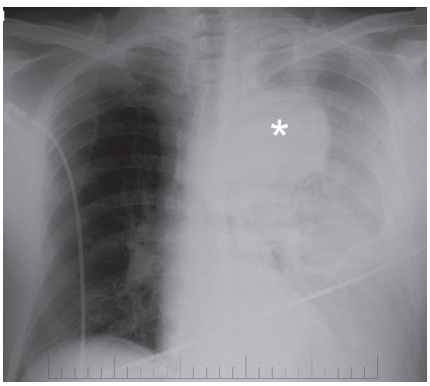

penetrating ulcer and mural hematoma. In all cases, blood start to flow within aortic wall and collects as hematoma. The flow originates either from the vasa vasorum, or the aortic lumen. In the latter case, the flow joins the aortic wall through a penetrating ulcer. If the parietal flow is driven by a sufficiently high pressure, a false blood flow channel dissecting the aortic wall can be created.

Signs of rupture

The signs of rupture at CT are similar to US. In addition, direct leakage from the aortic lumen to the retroperitoneum or adjacent organs can be visualized (figure 9). Before disruption of the external limit of the aneurysm and retroperitoneal collection become visible, leakage of the luminal contrast into the thrombus and a high attenuation crescent opacity in the thrombus are both signs of instability and impending rupture [40]. When rupture occurs into adjacent organs, the connection between both organs

Figure 7 : A patient admitted for acute abdominal pain and shock underwent transabdominal US. A large ruptured aneurysm of the abdominal aorta was found, displacing the adjacent organs. External thrombus was largely hyperechoic (asterisk) and the contours of the aorta were poorly defined.

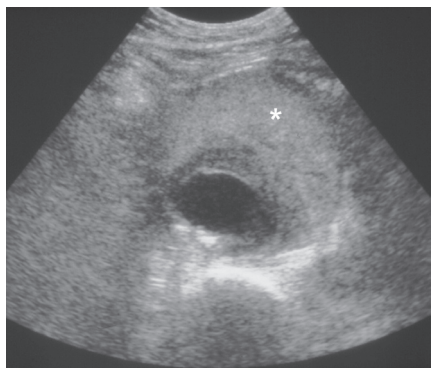

can be seen. Occasionally, parietal gas bubbles can be detected when aneurysm fistulizes into the gastrointestinal tract.

Other complications of aortic aneurysms

Inflammatory aneurysms

Inflammatory aneurysms are characterized by periaortic fat planes hyperattenuation and enhancement after contrast injection (figure 10). When inflammation extends to the retroperitoneum, the resulting fibrosis may lead to hydronephrosis and/or venous obstruction.

Penetrating ulcers

Penetrating ulcer appears as a discontinuity of the blood pool limits, commonly at the level of an atherosclerotic plaque. Pseudoaneurysms in which blood content crosses at least two of the three aortic wall layers represents an extreme form of a penetrating ulcer (figure 11).

Wall hematoma and dissection

At CT, dissection can occur from the level of the aortic valves (Stanford A) or

Figure 8 : Proposed patient flow chart in case of acute symptomatic aneurysm.

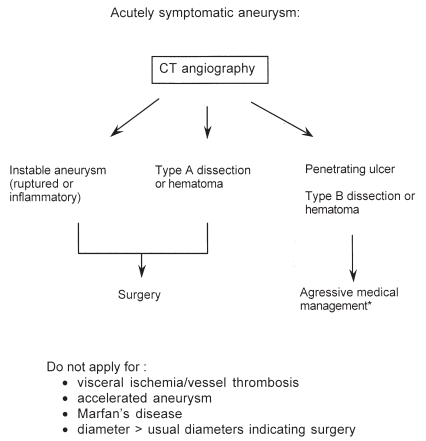

from any other part of the aorta (Stanford B). 3D cross-sectional angiography displays both flow channels in the aorta, separated by the intimal layer. In such cases, a special attention should be paid to the branches of the aorta and vascularization of different organs supplied by these branches (figure 12). Wall hematoma is visible as a localized non-enhancing high attenuation thickening of the aortic wall. In most cases, the periaortic fat planes are also of high attenuation. MR imaging allow to identify hematomas as knight on T1-weighted images. The false lumen can be recognized as it connections with the true lumen exhibit acute angles : the so-called "beak sign" [41]. Another sign of dissection is the displacement of intimal calcifications (figure 12).

Although in most cases there can be overlapping between aneurysms complications, CT angiography accurately allows triage between the patients requiring emergency surgery and those who could benefit a conservative approach [26]. In these cases, a close (i.e.: every 3 months) MR imaging follow-up should be performed.

Figure 9 : A patient admitted for acute back pain and a pulsatile abdominal mass underwent CT angiography of the whole aorta. Chest CT angiography shows aneurysms of the right coronary artery (a) (arrowheads). At the abdominal level, arterial (b) and parenchymal (c) post contrast phases in the axial plane showed a ruptured aortic aneurysm, associated with a left retroperotoneal hematoma (asterisks) and a leakage of the blood pool toward this hematoma best seen on the oblique reformations (d, arrows).

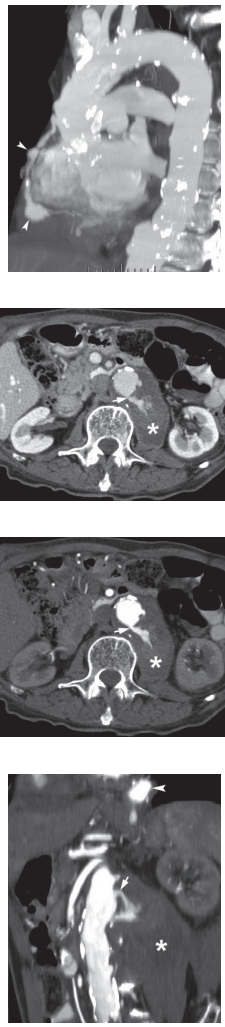

Conclusion

Aortic aneurysms are common causes of decease in elder subjects. Currently, imaging plays a major role in both secondary prevention and treatment planning. In the near future, new approaches in imaging allowing a better risk stratification will be included in the work-up algorithms.

Figure 10 : A subject with several weeks back pain, irradiating to both groins underwent triphasic CT of the abdominal aorta. A small inflammatory aneurysm was found, associated with an anterior crescent of tissue obliterating periaortic fat planes (arrows), isodense on non-enhanced scan (a) and progressively enhancing during arterial (b) and parenchymal (c) post-contrast phases.

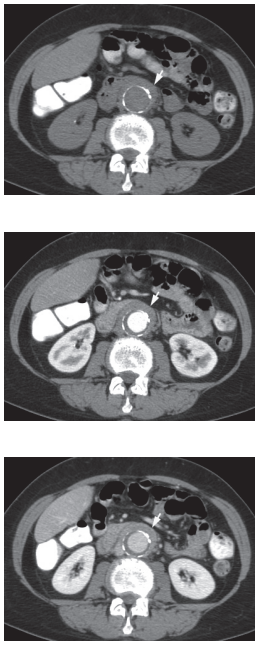

Figure 11 : MR angiography of the thoraco-abdominal aorta, performed in a patient with severe epigastric pain since 2 weeks, in whom abdominal CT incidentally showed a "thickened" wall of the throracoabdominal aorta (not shown). Penetrating ulcer (arrow) of the aortic arch with a pseudoaneurysm, causing hematoma of the descending aorta (arrowheads) was found on volume rendering (a) and parasagittal reformatted slices (b).

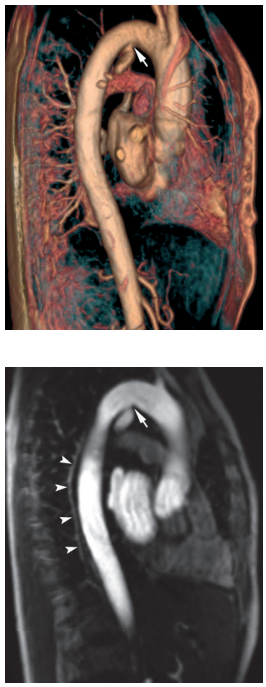

References

1. Johnston KW, Rutherford RB, Tilson MD, Shah DM, Hollier L, Stanley JC. Suggested standards for reporting on arterial aneurysms. Subcommittee on Reporting Standards for Arterial Aneurysms, Ad Hoc Committee on Reporting Standards, Society for Vascular Surgery and North American Chapter, International Society for Cardiovascular Surgery. J Vasc Surg 1991;13:452-8.
2. Izzillo R, Cassagnes L, Boutekadjirt R, Garcier JM, Cluzel P, Boyer L. Imaging of abdominal

Figure 12 : Thoraco-abdominal CT angiography of a patient with history of thoracotomy and abdominal aneurysm repair. Reformatted parasagittal (a) and successive axial slices through the aorta (b-d) showed both the false lumen (asterisk), beaking in the true lumen (arrowheads). Both lumens are separated by the intimal flap (white arrows). Dissection displaces intimal calcifications (black arrow) and extends through the celiac trunk (d).

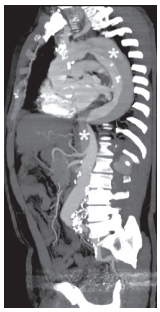

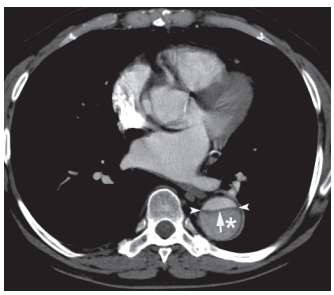

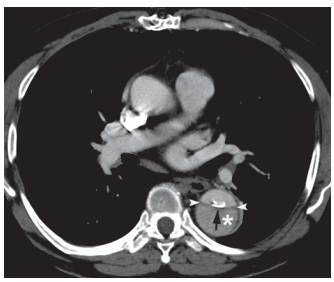

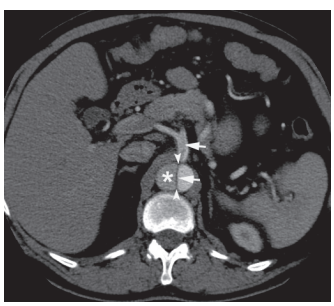

aortic aneurysms: when, how and why? J Radiol 2004;85:870-82.

3. Long A, Rouet L, Bissery A, Rossignol P, Mouradian D, Sapoval M. Compliance of abdominal aortic aneurysms evaluated by tissue Doppler imaging: correlation with aneurysm size. J Vasc Surg 2005;42:18-26.
4. Fillinger MF, Raghavan ML, Marra SP, Cronenwett JL, Kennedy FE. In vivo analysis of mechanical wall stress and abdominal aortic aneurysm rupture risk. J Vasc Surg 2002;36:589-97.
5. Takahashi K, Ohyanagi M, Ikeoka K, Masai M, Naruse H, Iwasaki T, Fukuchi M, Miyamoto T. Detection of inflammation in aortic aneurysms with indium 111-oxine--labeled leukocyte imaging. J Nucl Cardiol 2001;8:165-70.
6. Vardulaki KA, Prevost TC, Walker NM, Day NE, Wilmink AB, Quick CR, Ashton HA, Scott RA. Growth rates and risk of rupture of abdominal aortic aneurysms. Br J Surg. 1998;85:1674-80.
7. Hirose Y, Takamiya MGrowth curve of ruptured aortic aneurysm. J Cardiovasc Surg 1998;39:9-13.
8. Lobato AC, Puech-Leão P. Predictive factors for rupture of thoracoabdominal aortic aneurysm. J Vasc Surg. 1998;27:446-53.
9. Brady AR, Thompson SG, Fowkes FG, Greenhalgh RM, Powell JT; UK Small Aneurysm Trial Participants. Abdominal aortic aneurysm expansion: risk factors and time intervals for surveillance. Circulation 2004;110:16-21.
10. Elefteriades JA. Natural history of thoracic aortic aneurysms: indications for surgery, and surgical versus nonsurgical risks. Ann Thorac Surg 2002;74:S1877-80.
11. Davies RR, Goldstein LJ, Coady MA, Tittle SL, Rizzo JA, Kopf GS, Elefteriades JA. Yearly rupture or dissection rates for thoracic aortic aneurysms: simple prediction based on size. Ann Thorac Surg 2002;73:17-27.
12. Fayad ZA, Nahar T, Fallon JT, Goldman M, Aguinaldo JG, Badimon JJ, Shinnar M, Chesebro JH, Fuster V. In vivo magnetic resonance evaluation of atherosclerotic plaques in the human thoracic aorta: a comparison with transesophageal echocardiography. Circulation 2000;101:2503-9.
13. Bongartz G, Mayr M, Bilecen D. Magnetic resonance angiography (MRA) in renally impaired patients: When and how. Eur J Radiol. 2008;66:213-9.
14. Coulam CH, Rubin GD. Acute aortic abnormalities. Semin Roentgenol. 2001;36:148-64.
15. Smith AD, Schoenhagen P. CT imaging for acute aortic syndrome. Cleve Clin J Med. 2008;75:7-9, 12, 15-7 passim.

16. Rozenblit AM, Patlas M, Rosenbaum AT, Okhi T, Veith FJ, Laks MP, Ricci ZJ. Detection of endoleaks after endovascular repair of abdominal aortic aneurysm: value of unenhanced and delayed helical CT acquisitions. Radiology 2003;227:426-33.
17. Hayter RG, Rhea JT, Small A, Tafazoli FS, Novelline RA. Suspected aortic dissection and other aortic disorders: multi-detector row CT in 373 cases in the emergency setting. Radiology 2006;238:841-52.
18. Quint LE, Francis IR, Williams DM, Bass JC, Shea MJ, Frayer DL, Monaghan HM, Deeb GM. Evaluation of thoracic aortic disease with the use of helical CT and multiplanar reconstructions: comparison with surgical findings. Radiology 1996;201:37-41.
19. Remy-Jardin M, Remy J, Artaud D, Fribourg M, Naili A. Tracheobronchial tree: assessment with volume rendering--technical aspects. Radiology 1998;208:393-8.
20. Takahashi K, Stanford W. Multidetector CT of the thoracic aorta. Int J Cardiovasc Imaging 2005;21:141-53.
21. Kramer CM, Cerilli LA, Hagspiel K, DiMaria JM, Epstein FH, Kern JA. Magnetic resonance imaging identifies the fibrous cap in atherosclerotic abdominal aortic aneurysm. Circulation 2004;109:1016-21.
22. Mitsuoka H, Unno N, Takei Y, Saito T, Ishimaru K, Miki K, Nakamura S. Videodensitometric blood flow analysis of abdominal aortic aneurysm and intravascular coagulation. J Vasc Surg. 2003;38:340-5.
23. Nicholls SJ, Andrews J, Moon KW. Exploring the natural history of atherosclerosis with intravascular ultrasound. Expert Rev Cardiovasc Ther 2007;5:295-306.
24. Huang Y, Hu B, Huang PT, Sun HY, Zhu JA. Abdominal aortic wall motion of healthy and hypertensive subjects: evaluation of tissue Doppler velocity imaging. J Clin Ultrasound 2008;36:218-25.
25. Metafratzi ZM, Efremidis SC, Skopelitou AS, De Roos A. The clinical significance of aortic compliance and its assessment with magnetic resonance imaging. J Cardiovasc Magn Reson 2002;4:481-91.
26. Vorp DA, Raghavan ML, Webster MW. Mechanical wall stress in abdominal aortic aneurysm: influence of diameter and asymmetry. J Vasc Surg 1998;27:632-9.
27. Vorp DA, Lee PC, Wang DH, Makaroun MS, Nemoto EM, Ogawa S, Webster MW. Association of intraluminal thrombus in abdominal aortic aneurysm with local hypoxia and wall weakening. J Vasc Surg. 2001;34:291-9.
28. Doyle BJ, Callanan A, McGloughlin TM. A comparison of modelling techniques for computing wall stress in abdominal aortic aneurysms. Biomed Eng Online 2007;6:38.
29. Ruehm SG, Corot C, Vogt P, Kolb S, Debatin JF. Magnetic resonance imaging of atherosclerotic plaque with ultrasmall superparamagnetic particles of iron oxide in hyperlipidemic rabbits. Circulation 2001;103:415-22.
30. Howarth SP, Tang TY, Trivedi R, Weerakkody R, U-King-Im J, Gaunt ME, Boyle JR, Li ZY, Miller SR, Graves MJ, Gillard JH. Utility of USPIO-enhanced MR imaging to identify inflammation and the fibrous cap: A comparison of symptomatic and asymptomatic individuals. Eur J Radiol 2008;18.
31. Tang TY, Howarth SP, Li ZY, Miller SR, Graves MJ, U-King-Im JM, Trivedi RA, Walsh SR, Brown AP, Kirkpatrick PJ, Gaunt ME, Gillard JH. Correlation of carotid atheromatous plaque inflammation with biomechanical stress: utility of USPIO enhanced MR imaging and finite element analysis. Atherosclerosis 2008;196:879-87.
32. Kuehl H, Eggebrecht H, Boes T, Antoch G, Rosenbaum-Krumme S, Ladd S, Bockisch A, Barkhausen J, Erbel R. Detection of inflammation in patients with acute aortic syndrome: comparison of FDG-PET/CT imaging and serologic markers of inflammation. Heart 2007.
33. Sakalihasan N, Van Damme H, Gomez P, Rigo P, Lapiere CM, Nusgens B, Limet R. Positron emission tomography (PET) evaluation of abdominal aortic aneurysm (AAA). Eur J Vasc Endovasc Surg 2002;23:431-6.
34. Dehlin JM, Upchurch GR. Management of Abdominal Aortic Aneurysms. Curr Treat Options Cardiovasc Med. 2005 Jun;7:119-130.
35. Hassan C, Pickhardt P, Laghi A, Kim D, Zullo A, Iafrate F, Di Giulio L, Morini S. Computed tomographic colonography to screen for colorectal cancer, extracolonic cancer, and aortic aneurysm: model simulation with cost-effectiveness analysis. Arch Intern Med 2008;168:696-705.
36. Poullis MP, Warwick R, Oo A, Poole RJ. Ascending aortic curvature as an independent risk factor for type A dissection, and ascending aortic aneurysm formation: a mathematical model. Eur J Cardiothorac Surg 2008;33:995-1001.
37. Tillich M, Hausegger KA, Tiesenhausen K, Tauss J, Groell R, Szolar DH. Helical CT angiography of stent-grafts in abdominal aortic aneurysms: morphologic changes and complications. Radiographics 1999;19:1573-83.
38. Sakalihasan N, Hustinx R, Limet R. Contribution of PET scanning to the evaluation of abdominal aortic aneurysm. Semin Vasc Surg 2004;17:144-53.

39. Vilacosta I, Román JA. Acute aortic syndrome. Heart 2001 Apr;85:365-8.
40. Coulam CH, Rubin GD. Acute aortic abnormalities. Semin Roentgenol 2001;36:148-64.
41. Castañer E, Andreu M, Gallardo X, Mata JM, Cabezuelo MA, Pallardó Y. CT in nontraumatic acute thoracic aortic disease: typical and atypical features and complications. Radiographics 2003;23:S93-110.
42. Sakalihasan N, Limet R, Defawe OD. Abdominal aortic aneurysm. Lancet 2005;365:1577-89.

Additional publication N°2

This paper has been published as:

Magnetic resonance Imaging findings in a positron emission tomography-positive thoracic aortic aneurysm

A. Nchimi, T. Couvreur, B. Meunier, N. Sakalihasan

Aorta, 2013 (3) : 198-201
DOI: http://dx.doi.org/10.12945/j.aorta.2013.13-022

Images in Aortic Disease

AORTA

Aorta, August 2013, Volume 1, Issue 3: 198–201
DOI: http://dx.doi.org/10.12945/j.aorta.2013.13-022

Received: April 9, 2013
Accepted: August 21, 2013
Published online: August 2013

Magnetic Resonance Imaging Findings in a Positron Emission Tomography-Positive Thoracic Aortic Aneurysm

Alain Nchimi, MD[1]*, Thierry Couvreur, MD[1], Benoit Meunier, MD[1], Natzi Sakalihasan, MD, PhD[2]

[1]Department of Cardiovascular and Thoracic Imaging, University Hospital, Liège, Belgium; [2]Department of Cardiovascular Surgery, University Hospital, Liège, Belgium

Abstract

Diffusion-weighted MRI (DW-MRI) and ^{18}F-fluorodeoxyglucose positron emission tomography (FDG-PET) findings are described in a patient with a thoracic aortic aneurysm. Both examinations have the ability to noninvasively assess biological processes associated with aneurysm instability and therefore to potentially impact clinical decision-making regardless of the vessel size. Despite similarities between images on both techniques, FDG-PET evaluates glycolysis, while DW-MRI evaluates cell density, edema, and perfusion. Longitudinal studies including larger patient numbers are needed to investigate the temporal continuum and clinical significance of these findings.

Key Words

Magnetic resonance imaging · Positron emission tomography · Aortic aneurysm

Introduction

Atherosclerotic and inflammatory aortic diseases may cause complications at all ages, including aneurysmal dilatation and rupture, which is the 13th leading cause of death in the United States [1]. Evidence that most of these complications result from biological processes led to the emergence of imaging techniques with the capacity to evaluate these processes [2]. Using ^{18}F-fluorodeoxyglucose (FDG) (a glucose analog) positron emission tomography (PET) allows imaging of glycolysis and, therefore, tissue metabolism. FDG uptake in the aortic aneurysm wall is an important parameter, positively correlated to the magnitude of inflammatory cell infiltrates, matrix metalloprotease activation, and risk of rupture [3]. Diffusion-weighted MRI (DW-MRI), which evaluates the water motion within a milieu, has established clinical value in early stroke detection and cancer staging [4,5]. DW-MRI has, to our knowledge, never been evaluated in aortic aneurysms. In this board-approved report, we present the DW-MRI findings and clinical outcome in a patient with an FDG-avid aneurysm of the aortic arch.

Case Presentation

The patient was a 68-year-old male smoker (30 pack/years) with a history of lower limb artery claudication and a saccular aneurysm of the aortic arch, for which he was included in a large trial aiming to determine the role of FDG-PET and MRI in aortic aneurysm rupture-risk assessment (http://www.fighting-aneurysm.org).

After a nightlong fast, he underwent clinical follow-up showing normal blood cell count and levels of C-reactive protein and sedimentation rate. There-

Fax +1 203 785 3346
E-Mail: aorta@scienceinternational.org
http://aorta.scienceinternational.org

ISSN 2325-4637

Accessible online at:
http://aorta.scienceinternational.org

*Corresponding author:
Alain Nchimi, MD
Department of Cardiovascular and Thoracic Imaging
University Hospital
Domaine Universitaire du Sart-Tilman B 35
B-4000 Liege, Belgium
Tel: +32 4 366 77 67, Fax: +32 4 366 77 72, E-Mail: anchimi@chu.ulg.ac.be

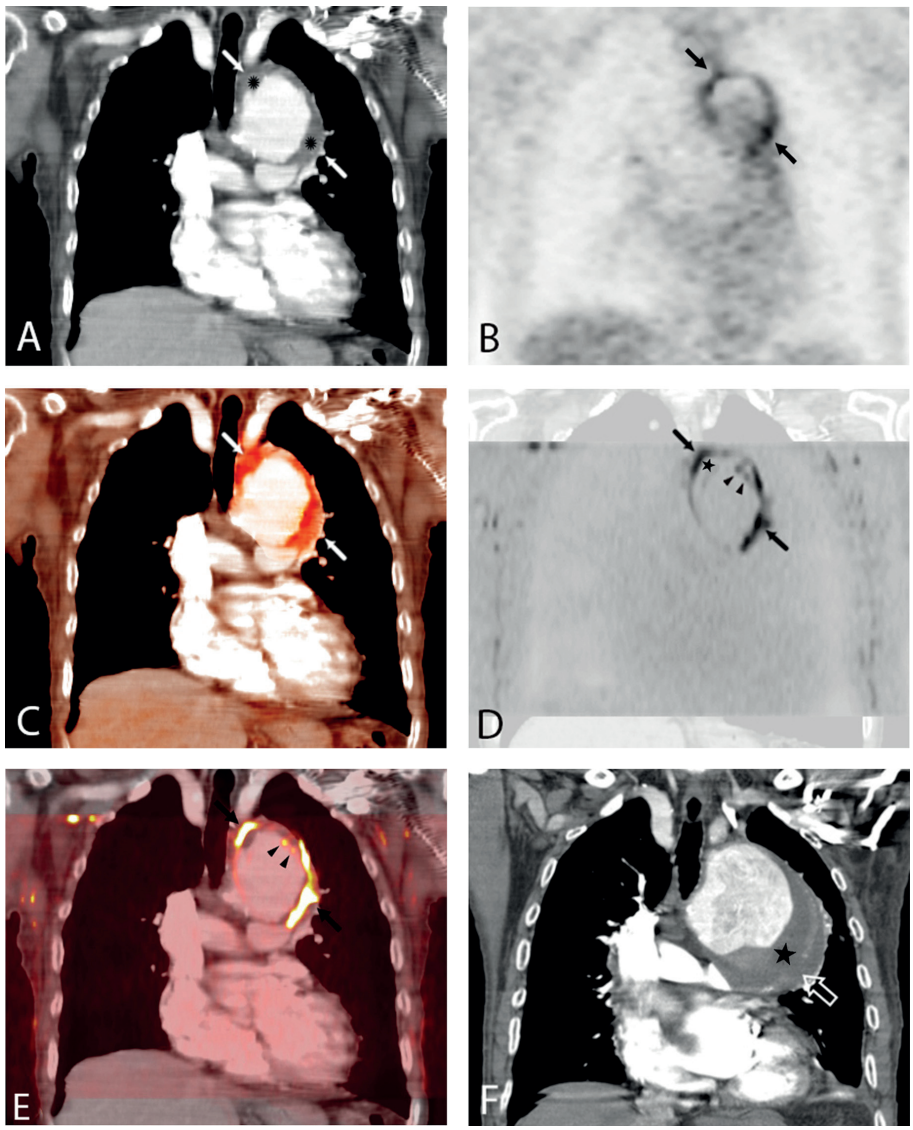

Figure 1. A. Coronal reformatted contrast-enhanced computed tomography (CT) of the chest demonstrates a large aortic arch aneurysm, with an intraluminal thrombus (ILT) (stars). ^{18}F-Fluorodeoxyglucose positron emission tomography (FDG-PET) (B) and color intensity maps fused with CT (C) showed FDG uptake on the aneurysm wall (**arrows**, D). E. Coronal reformats of transverse diffusion-weighted magnetic resonance images with a diffusion factor value of 800 s/mm^2 were fused to CT images in a similar plane and showed restricted diffusion on the aneurysm wall (**arrows**), but differed from FDG-PET by increased signaling on the luminal surface of the ILT (**arrowheads**). The patient died three months later. F. Admission CT showed aortic enlargement and rupture on thrombus-covered aneurysm wall (**open arrow**).

after, combined whole-body (neck to pelvis) computed tomography (CT) and PET (Discovery LS, GE Healthcare, Milwaukee, WI) was performed 1 h after injection of 3.7 MBq FDG/kg body weight. PET data were corrected for attenuation using CT tissue density values. The patient's aneurysm was evaluated the same day in a separate 3T MRI unit (Achieva, Philips, Best, The Netherlands), using tridirectional diffusion gradients.

DW-MRI Technique

In short, the principle of DW-MRI is that the signal change between two opposed gradient pulses of similar intensity and duration is related to the movement (diffusion) of water protons. Because MRI voxel size is much larger than water molecules, there are several sources of intravoxel incoherent motion such as closed spaces, tortuosity, and microvasculature. Rather than absolute diffusion, DW-MRI therefore refers to an apparent diffusion coefficient (ADC) whereof the tridimensional components are defined in the equation: $ADC(x,y,z) = \ln[S2(x,y,z)/S1(x,y,z)]/(b1 - b2)$; where $b1$ and $b2$ are acquisition-dependent factors, and S1 and S2 the respective image signal intensity [5]. Two b-values (0 and 800 s/mm^2) were used for 7-mm-thick cross-sections; the other MRI parameters were: repetition time/echo time: 1300/67 ms; matrix, 144 × 192; number of slices adjusted to the area of interest; intersection gap, 1.4 mm; and field of view adjusted to the body size. Both FDG-PET and $b = 800$ s/mm^2 diffusion images (where the signal intensity is inversely proportional to ADC) were matched to CT images using anatomical landmarks (Osirix, Pixmeo, Geneva, Switzerland).

Findings on both imaging modalities disclosed an aortic arch aneurysm containing a large intraluminal thrombus (ILT). The aneurysm diameter was 69 mm (65 mm six months earlier) and the aneurysm wall exhibited diffuse FGD uptake; the maximal standardized FDG uptake value was 4.8 g/mL. On DW-MRI, in a roughly similar distribution, ADC was strongly reduced. There was also an area of restriction at the luminal surface of the ILT (Fig. 1). The patient was informed of the increased risks related to such findings and declined any repair despite surgical insistence, but eventually died three months later from aortic rupture.

Discussion

The case presented illustrates the usefulness of a local assessment of biological processes in aortic aneurysms. Despite the fact that this patient was asymptomatic and his systemic inflammatory blood tests were normal, there was increased aneurysm glycolysis (on PET imaging), suggesting a poor outcome. DW-MRI necessitates no ionizing radiation, and the actual causes of signaling differ from that of FDG-PET but similarly address tissue cellularity at high b-values, as shown. Because DW-MRI has a lower vascular background signal, beyond just replicating findings from other modalities, DW-MRI surpasses FDG-PET in the detection of cellular infiltrates at the luminal surface of the ILT. The same characteristic was shown previously using MRI to assess superparamagnetic iron oxide phagocytosis at the luminal surface of the ILT [6], which has pivotal implications in aneurysm destabilization through proteases released by inflammatory cells and conveyed through the thrombus [7]. As observed, aneurysm rupture often occurs on the ILT-covered area.

The composite nature of DW-MRI signaling may be another important asset. T2-relaxation and perfusion effects that are prominent at very low b-values reflect other important biological processes like edema and perfusion (angiogenesis) that were not evaluated in this report. Further investigating the temporal correlations between DW-MRI and FDG-PET signaling, biological activities, and clinical outcomes may therefore help elucidate interactions and eventually improve treatment and clinical decision-making in aortic aneurysms.

Acknowledgments

Alain Nchimi and Natzi Sakalihasan are supported by the "Fighting Aneurysmal Disease" grant from the European Union (http://www.fighting-aneurysm.org).

Conflict of interest

None

References

1. Patel MI, Hardman DT, Fisher CM, Appleberg M. Current views on the pathogenesis of abdominal aortic aneurysms. J Am Coll Surg. 1995;181:371–382.
2. Sakalihasan N, Limet R, Defawe O. Abdominal aortic aneurysm. Lancet. 2005;365:1577–1589. 10.1016/S0140-6736(05)66459-8
3. Reeps C, Essler M, Pelisek J, Seidl S, Eckstein HH, Krause BJ. Increased 18F-fluorodeoxyglucose uptake in abdominal aortic aneurysms in positron emission/computed tomography is associated with inflammation, aortic wall instability, and acute symptoms. J Vasc Surg. 2008;48:417–423. 10.1016/j.jvs.2008.03.059
4. Padhani AR, Koh DM, Collins DJ. Whole-body diffusion-weighted MR imaging in cancer: current status and research directions. Radiology. 2011;261:700–718. 10.1148/radiol.11110474
5. Jacobs MA, Ibrahim TS, Ouwerkerk R. AAPM/RSNA physics tutorials for residents: MR imaging: brief overview and emerging applications. Radiographics. 2007;27:1213–1229. 10.1148/rg.274065115
6. Nchimi A, Defawe O, Brisbois D, Broussaud TKY, Defraigne JO, Magotteaux P, et al. MR imaging of iron phagocytosis in intraluminal thrombi of abdominal aortic aneurysms in humans. Radiology. 2010;254:973–981. 10.1148/radiol.09090657
7. Fontaine V, Jacob MP, Houard X, Rossignol P, Plissonnier D, Angles-Cano E, et al. Involvement of the mural thrombus as a site of protease release and activation in human aortic aneurysms. Am J Pathol. 2002;161:1701–1710. 10.1016/S0002-9440(10)64447-1

Cite this article as: Nchimi A, Couvreur T, Meunier B, Sakalihasan N, Magnetic Resonance Imaging Findings in a Positron Emission Tomography-Positive Thoracic Aortic Aneurysm. Aorta 2013;1(3):198–201. DOI: http://dx.doi.org/10.12945/j.aorta.2013.13-022

Additonal figure

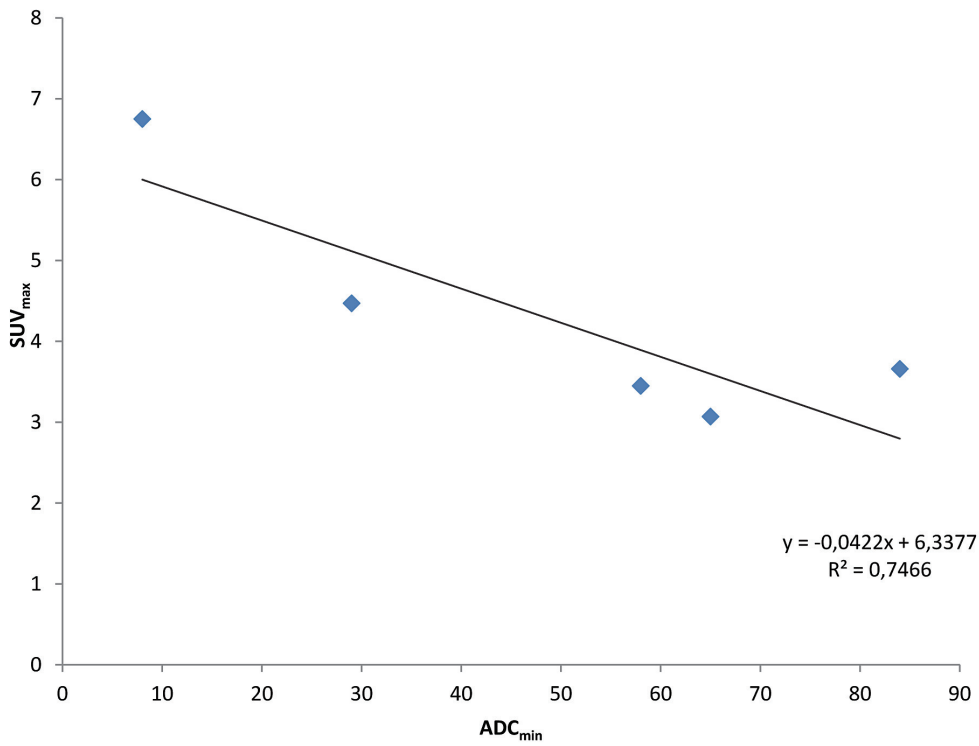

Figure 14 : Scatter-plot correlation between volume-analysis minimal values of ADC and maximal values of SUV in 5 AAAs (mean age 67 years; mean aortic diameter 68 mm) (Unpublished data).

RÉSUMÉ (FR)

Introduction

Le contexte général de cette thèse est d'évaluer les risques de rupture de l'anévrisme de l'aorte abdominale (AAA), en utilisant des techniques d'imagerie ayant la capacité d'évaluer les processus biologiques.

Après une description approfondie des techniques d'imagerie disponibles, notre travail a été divisé en deux principaux objectifs, à savoir : (i) fournir une plus grande valeur clinique à des concepts d'imagerie existants mais non prouvées, et (ii) proposer de nouveaux concepts d'imagerie pour l'amélioration de l'évaluation du risque de rupture des AAAs.

Méthodes

Le stress pariétal et les activités biologiques sont des acteurs importants de la progression des AAAs, pouvant être évalués respectivement par simulations par éléments finis (SEF) et tomographie par émission de positons (TEP) au 18F-Fluorodéoxyglucose (FDG). Le premier objectif de recherche était d'évaluer à quel point ce(s) mode(s) d'imagerie peu(ven)t aider à la prise de décision clinique chez les patients porteurs d'un AAA, et quelle(s) serai(en)t leur(s) valeur incrémentale(s) par rapport aux décisions prises en fonction du diamètre maximal de l'anévrysme. L'évolution maximal du diamètre des AAAs et des patients ont donc été évalués, eu égard aux signaux recueillis en TEP et en SEF.

En outre, la notion de diamètre-ajusté par le risque de rupture déterminé par SEF a été décrite et validée a posteriori en utilisant les données de grandes études multicentriques. Le deuxième objectif de la recherche comprenait l'évaluation des activités biologiques du thrombus intraluminal (TIL) et la preuve par l'imagerie de son rôle délétère dans l'AAA, en utilisant plusieurs techniques. L'accent y était mis sur les propriétés de l'imagerie par résonance magnétique (IRM) pour le suivi des activités biologiques du TIL sans contraste exogène, simplement par l'évaluation de sa teneur en fer.

Résultats

Publication N° 1

Cinq anévrismes de l'aorte (3 TAA et 2 AAA) avec des foyers d'hyperfixation du FDG en TEP ont été évalués par la SEF. Les points chauds sur les imageries par TEP et SEF avaient tendance à se superposer, et être associés à une mauvaise évolution de l'anévrysme, justifiant d'autres études portant sur des échantillons plus importants.

Publication N° 2

En utilisant 203 et 40 scanographies de patients avec AAAs respectivement non-rompus et rompus, nous avons évalué le concept de diamètre-ajusté. Dans ce concept, les estimations biomécaniques du risque de rupture sont converties en un diamètre maximal correspondant à celui d'un anévrysme avec le même risque chez un sujet moyen de notre cohorte d'anévrysmes non-rompus, pondéré par le rapport entre les sexes observés dans une large cohorte d'anévrismes au Royaume-Uni.

Le concept de diamètre-ajusté fait le lien entre les estimations biomécaniques et les conclusions tirées d'essais clinique à large échelle sur la gestion du risque de rupture des AAA en fonction du diamètre maximal. Notre validation rétrospective du diamètre-ajusté a vérifié que les indicateurs biomécaniques sont plus élevés en cas de rupture que dans les AAAs non rompus.

Publication N° 3

Un total de 68 examens TEP combinés à un scanner utilisé pour SEF ont été réalisées chez 53 patients (45 hommes) de 72 ans d'âge moyen. Des analyses visuelle et semi-quantitative de la captation du FDG ont été réalisées et corrélées avec les estimations du stress pariétal. Un suivi moyen de 11 mois a été observé. L'augmentation de la captation du FDG par un AAA était un facteur de mauvais pronostic à deux ans, indépendamment du diamètre. Un tel résultat n'a pu être obtenu pour l'augmentation du stress pariétal par absence de seuil de dichotomisation, mais la corrélation entre stress pariétal et glycolyse indique une valeur potentiellement comparable en termes de pronostic.

Enfin, nous avons évalué l'effet de plusieurs variables sur la fixation du FDG et le stress pariétal. La captation du FDG est influencée par des facteurs héritables ou acquis spécifiques à chaque patient, indiquant une l'implication d'une altération acquise ou héréditaire des réponses biologiques au stress pariétal chez certains patients.

Publication N° 4

Les leucocytes présents dans le TIL et impliqués dans la glycolyse sont capables d'endocy ter plusieurs particules telles que des oxydes de fer superparamagnétiques (OFSP). Nous avons mené une étude pour évaluer la faisabilité d'une telle perspective chez 15 patients qui ont subi une IRM avec séquences T1, T2 ; T2* pré et post-OFSP dans les 2 semaines avant réparation d'un AAA. Les changements de signal T2* du TIL après OFSP ont été quantifiés et corrélés à l'analyse histologique et immunohistochimique des fragments recueillis, ainsi que la l'analyse de leur richesse en enzymes protéolytiques. Enfin, les résultats in vivo ont été validés par imagerie des fragments de TIL ex-vivo, avant et après incubation dans des solutions d'OFSP.

L'IRM a ainsi permis la démonstration de la phagocytose à la face luminale du TIL, à la fois ex vivo et in vivo. Cette activité biologique du TIL qui est associée à la glycolyse (FDG) est également corré-

Iée avec l'abondance des leucocytes et l'activité protéolytique. De plus, les apparences IRM relatives au contenu en fer du TIL se rapportent également à ces activités biologiques.

Dans un dernier travail soumis récemment, l'imagerie multimodale a été utilisée pour confirmer le concept du rôle nocif de l'ILT en croissance dans un modèle d'AAA par infusion d'élastase chez le rat.

Conclusion

IRM et la TEP sont capables de démontrer et de quantifier in vivo certains des processus biologiques notoirement délétères qui se déroulent dans le sac anévrismal, incluant le piégeage à l'interface luminal du TIL des cellules sanguines et la réponse inflammatoire periadventitielle.

Le rôle central joué par le TIL et ses activités biologiques a également été démontré in vivo en utilisant plusieurs techniques d'imagerie. La valeur clinique de l'imagerie de ces activités biologiques est incarnée par le fait que l'augmentation de la captation du FDG (glycolyse) dans les AAA est associée à un risque accru d'événements péjoratifs dans les 2 ans, indépendamment du diamètre.

CURRICULUM VITAE

Alain Nchimi was born may 25th 1972.
He is Married to Carole and father of three boys: Bruno Patrick, Jeremy Alan and David Alexandre.
He currently heads the CardioVascular & Thoracic Imaging clinic of the Department of Medical Physics at the University Hospital of liege Sart Tilman, Belgium.

His full list of publications can be found at the address: http://orbi.ulg.ac.be/orbi-report?query=%28%28uid%3Ac054447%29%29&model=a&format=apa&data=metric&data=pr&sort_by0=1&order0=DESC&sort_by1=3&order1=ASC&sort_by2=2&order2=ASC&output=pdf&language=fr&title=Publications+et+communications+de+Alain+NCHIMI+LONGANG+%5Bc054447%5D.

Contributions in relation to this dissertation:

Invited lectures

Nchimi A. Thoracic aortic dilatation and aneurysm CT/CMR approaches, EUROECHO & Other Imaging Modalities 2013, Istanbul, Turkey.

Nchimi A. Thoracic aortic dilatation and aneurysm CT/CMR approaches, EUROECHO & Other Imaging Modalities 2012, Athens, Greece.

Nchimi A. Imaging in aortic aneurysms. 1st International Meeting on Aortic Diseases (IMAD) congress, Liège, October 2008, Belgium.

Scientific papers and poster abstracts

Nchimi A. Multifatorial relationship between 18F-FDG PET signaling and biomechanical properties in unruptured aortic aneurysms. 3rd IMAD meeting October 2012, Liège, Belgium.

Roy J, Swedenborg J, Sakalihasan N, Nchimi A, Boeckler D, Hyhlik-Duerr A, Gasser TC. Biomechanical rupture risk assessment in patients with abdominal aortic aneurysms: Introducing rupture risk equivalent diameter. Arterioscl Thromb Vasc Biol. 32:A103, ATVB 2012, Chicago, USA.

Nchimi A. MR imaging of iron phagocytosis in intraluminal thrombi of abdominal aortic aneurysm in humans. 2011 FAD meeting, Istanbul, Turkey.

Nchimi A. Relationship between signalling in PET-CT and biomechanical stress in untreated aneurysmal aortic wall. 2010 FAD meeting, Prague, Czech republic.

Nchimi A, Brisbois D, Grayet B, Gomez P, Sakalihasan N, Magotteaux P. Metabolic Assessment of Abdominal Aortic Aneurysms. Exhibit presented at the RSNA meeting, Chicago 2004, USA.

Peer-reviewed papers

Gasser TC, Nchimi A, Swedenborg J, Roy J, Sakalihasan N, Bockler D, Hyhlik-Durr A. A novel strategy to translate the biomechanical rupture risk of abdominal aortic aneurysms to their equivalent diameter risk: Method and retrospective validation. European journal of vascular and endovascular surgery. 2014;47:288-295.

Nchimi A, Cheramy-Bien JP, Gasser TC, Namur G, Gomez P, Seidel L, Albert A, Defraigne JO, Labropoulos N, Sakalihasan N. Multifactorial relationship between 18f-fluoro-deoxy-glucose positron emission tomography signaling and biomechanical properties in unruptured aortic aneurysms. Circulation. Cardiovascular imaging. 2014;7:82-91.

Nchimi A, Couvreur T, Meunier B, Sakalihasan N. Magnetic resonance Imaging findings in a positron emission tomography-positive thoracic aortic aneurysm. Aorta, 2013; 3 : 198-201.

Nchimi A, Defawe O, Brisbois D, Broussaud T, Defraigne JO, Magotteaux P, Massart B, Serfaty JM, Houard X, Michel JB, Sakalihasan N. Magnetic resonance imaging of iron phagogocytosis in intraluminal thrombi of abdominal aortic aneurysms in humans. Radiology, 2010; 254: 973-981.

Xu XY, Borghi A, Nchimi A, Leung J, Gomez P, Cheng Z, Defraigne JO, Sakalihasan N. High levels of 18F-FDG uptake in aortic aneurysm wall are associated with high wall stress. European Journal of Vascular and Endovascular Surgery, 2010;39:295-301.

Book chapters

Nchimi A. Imaging in aortic aneurysms. Aortic Aneurysms. New insights into an old problem. Sakalihasan N, Kuivaniemi H, Michel JB. Les Editions de l'Université de Liège, Snel, Vottem, Belgique, 2008.

Sakalihassan N, Hustinx R, Gomez P, Nchimi A, Limet R. Can positron emission tomography (PET) predict the risk of rupture of abdominal aortic aneurysm (AAA)? Controversies and updates in vascular surgery. Editors Becquemin JP, Alimi YS, Gerard JL, Edizioni Minerva Medica, Torino 2008.